



National Library
of Canada

Bibliothèque nationale
du Canada

Canadian Theses Service Services des thèses canadiennes

Ottawa, Canada
K1A 0N4

CANADIAN THESES

NOTICE

The quality of this microfiche is heavily dependent upon the quality of the original thesis submitted for microfilming. Every effort has been made to ensure the highest quality of reproduction possible.

If pages are missing, contact the university which granted the degree.

Some pages may have indistinct print especially if the original pages were typed with a poor typewriter ribbon or if the university sent us an inferior photocopy.

Previously copyrighted materials (journal articles, published tests, etc.) are not filmed.

Reproduction in full or in part of this film is governed by the Canadian Copyright Act, R.S.C. 1970, c. C-30. Please read the authorization forms which accompany this thesis.

**THIS DISSERTATION
HAS BEEN MICROFILMED
EXACTLY AS RECEIVED**

THÈSES CANADIENNES

AVIS

La qualité de cette microfiche dépend grandement de la qualité de la thèse soumise au microfilmage. Nous avons tout fait pour assurer une qualité supérieure de reproduction.

S'il manque des pages, veuillez communiquer avec l'université qui a conféré le grade.

La qualité d'impression de certaines pages peut laisser à désirer, surtout si les pages originales ont été dactylographiées à l'aide d'un ruban usé ou si l'université nous a fait parvenir une photocopie de qualité inférieure.

Les documents qui font déjà l'objet d'un droit d'auteur (articles de revue, examens publiés, etc.) ne sont pas microfilmés.

La reproduction, même partielle, de ce microfilm est soumise à la Loi canadienne sur le droit d'auteur, SRC 1970, c. C-30. Veuillez prendre connaissance des formules d'autorisation qui accompagnent cette thèse.

**LA THÈSE A ÉTÉ
MICROFILMÉE TELLE QUE
NOUS L'AVONS REÇUE**



National Library
of Canada

Bibliothèque nationale
du Canada

0-315-26855-7

Canadian Theses Division Division des thèses canadiennes

Ottawa, Canada
K1A 0N4

PERMISSION TO MICROFILM — AUTORISATION DE MICROFILMER

• Please print or type — Écrire en lettres moulées ou dactylographier

Full Name of Author — Nom complet de l'auteur

SEAN MICHAEL MALONEY

Date of Birth — Date de naissance

AUGUST 18, 1950

Country of Birth — Lieu de naissance

CANADA

Permanent Address — Residence fixe

209-11135-83 AVE
EDMONTON, ALBERTA
T6G 2C6

Title of Thesis — Titre de la these

AN ASSESSMENT OF DEFORMATION MONITORING
IN UNDERGROUND EXCAVATIONS IN WEAK ROCK
BY MODEL TESTS

University — Université

UNIVERSITY OF ALBERTA

Degree for which thesis was presented — Grade pour lequel cette these fut presentee

M.Sc.

Year this degree conferred — Année d'obtention de ce grade

1984

Name of Supervisor — Nom du directeur de these

DR. P.K. KAISER

Permission is hereby granted to the NATIONAL LIBRARY OF CANADA to microfilm this thesis and to lend or sell copies of the film.

The author reserves other publication rights and neither the thesis nor extensive extracts from it may be printed or otherwise reproduced without the author's written permission.

L'autorisation est par la presente, accordee a la BIBLIOTHEQUE NATIONALE DU CANADA de microfilmer cette these et de prêter ou de vendre des exemplaires du film.

L'auteur se reserve les autres droits de publication, ni la these ni de longs extraits de celle-ci ne doivent être imprimés ou autrement reproduits sans l'autorisation écrite de l'auteur.

Date

April 18, 1984

Signature

THE UNIVERSITY OF ALBERTA

AN ASSESSMENT OF DEFORMATION MONITORING PRACTICE IN
UNDERGROUND EXCAVATIONS IN WEAK ROCK BY MODEL TESTS

by

C

SEAN MICHAEL MALONEY

A THESIS

SUBMITTED TO THE FACULTY OF GRADUATE STUDIES AND RESEARCH
IN PARTIAL FULFILMENT OF THE REQUIREMENTS FOR THE DEGREE
OF MASTER OF SCIENCE

IN
CIVIL ENGINEERING

DEPARTMENT OF CIVIL ENGINEERING

EDMONTON, ALBERTA

SPRING 1984

THE UNIVERSITY OF ALBERTA

RELEASE FORM

NAME OF AUTHOR SEAN MICHAEL MALONEY
TITLE OF THESIS AN ASSESSMENT OF DEFORMATION MONITORING
PRACTICE IN UNDERGROUND EXCAVATIONS IN
WEAK ROCK BY MODEL TESTS
DEGREE FOR WHICH THESIS WAS PRESENTED MASTER OF SCIENCE
YEAR THIS DEGREE GRANTED SPRING 1984

Permission is hereby granted to THE UNIVERSITY OF ALBERTA LIBRARY to reproduce single copies of this thesis and to lend or sell such copies for private, scholarly or scientific research purposes only.

The author reserves other publication rights, and neither the thesis nor extensive extracts from it may be printed or otherwise reproduced without the author's written permission.

(SIGNED) *S. M. Maloney*.....

PERMANENT ADDRESS:

...209-11135-83 AVE.....
...EDMONTON, ALBERTA..
...T66 2C6.....

DATED ...MARCH 21... 1984

THE UNIVERSITY OF ALBERTA
FACULTY OF GRADUATE STUDIES AND RESEARCH

The undersigned certify that they have read, and recommend to the Faculty of Graduate Studies and Research, for acceptance, a thesis entitled AN ASSESSMENT OF DEFORMATION MONITORING PRACTICE IN UNDERGROUND EXCAVATIONS IN WEAK ROCK BY MODEL TESTS submitted by SEAN MICHAEL MALONEY in partial fulfilment of the requirements for the degree of MASTER OF SCIENCE in CIVIL ENGINEERING.

Dr. P. K. Kaiser

.....
P. Kaiser

Supervisor

Dr. N. R. Morgenstern

.....
N. R. Morgenstern

Dr. B. Stimpson

.....
B. Stimpson

Date. *MARCH 21 1984*

ABSTRACT

The monitoring of the deformation response of the rock mass upon excavation of a tunnel is the most commonly applied means of evaluating the design and stability of the opening. Because of the importance attached to this monitoring operation, a critical assessment of current practice, with particular regard to excavations in highly stressed or overstressed rock, was undertaken.

Laboratory model tests were employed to determine the rock mass response to the excavation of a tunnel under controlled environmental conditions. These tests were classified as either excavation simulation or external loading. In the former, a tunnel is excavated or enlarged in a pre-stressed sample while in the latter, the sample containing a pre-excavated tunnel is loaded at its boundaries. Plane strain conditions were maintained along the the tunnel axis in all tests. In excavation simulation testing, the development of radial strain around the opening was recorded during and following excavation. The convergence of the tunnel walls could only be monitored in the post-excavation period. In external loading tests, both convergence and radial strains were measured throughout. Coal was chosen as the model material because of its small scale, regular joint pattern, low strength and time-dependent deformation properties.

As a result of the model tests, a rational procedure for the evaluation of tunnel behaviour, based on the rate of

tunnel convergence, was developed. The appropriate rate criteria for this evaluation require field determination and their application requires separation of the convergence due to face advance from that due to the creep of the rock mass. Expressions for the determination of the convergence and radial strain rates due to the advancing face were developed for this purpose.

The limitations of current deformation monitoring practice in tunnels constructed at great depth were identified. It was determined that the interpretation of the results can be significantly influenced by the location and time of installation of the instrumentation, particularly where the material exhibits time-dependent behaviour. To evaluate the design and stability of the excavation requires multi-directional instrumentation installed as close to the face as practically possible (preferably ahead of the face, although this is generally not possible at depth) with frequent reading and consideration of the face advance effect. It was further determined that there is a need for instrumentation capable of displacement detection ahead of the face.

ACKNOWLEDGEMENTS

This research was conducted at the University of Alberta under the supervision of Dr. Peter K. Kaiser. His guidance and assistance are greatly appreciated. Thanks are also extended to all the professors in the Geotechnical Group for their dedication to both the student and subject. I am particularly grateful to Dr. J.D. Scott for directing me to this field of engineering, Dr. M.B. Dusseault for his assistance during my first two years at the university and Dr. D. Cruden for his review of Chapter 4 of this thesis. I also wish to thank Dr. N. R. Morgenstern for the inspiration he provides to all students of geotechnique.

The financial support of the Alberta-Canada Energy Resources Research Fund, a joint program of the Federal and Alberta governments, and administered by Alberta Energy and Natural Resources is gratefully acknowledged. Support by the Alberta Oil Sands Technology and Research Authority during my second year of study is also gratefully acknowledged.

I would like to express my gratitude to the technical staff of the Department of Civil Engineering, Geotechnical Group under the direction of G. Cyre as well as A. Muir, H. Friedrich and K. Ellis of the Civil Engineering Machine Shop. Their assistance throughout this project is appreciated.

I am especially grateful to my fellow graduate students for their fellowship and guidance throughout my time of study. Special thanks are extended to S. Dufour, E. Evgin,

A. Gale, D. Sargent, H. Soderberg, R. Sterne, R. Stewart, B. Watts, and R. Wittebolle for their friendship and encouragement. I would also like to thank T. Schulz for typing this thesis.

I wish to thank my parents for their continuing love and support. I feel very fortunate to be their son. I am also grateful for the support and understanding of my brothers and sisters.

Finally, I wish to express my sincere gratitude to my wife, Sandra. Without her love, patience, support and encouragement, I could not have achieved this goal. To her then, I dedicate this thesis.

Table of Contents

Chapter		Page
1.	INTRODUCTION	1
	1.1 Thesis Objective	2
	1.2 Scope of the Thesis	3
2.	REVIEW OF CURRENT DEFORMATION MONITORING PRACTICE	5
	2.1 Introduction	5
	2.2 Role of Monitoring in Underground Excavations in Rock	7
	2.3 Deformation Monitoring	10
	2.3.1 Optical Surveying	11
	2.3.2 Convergence Measurement	12
	2.3.3 Borehole Extensometers	14
	2.4 Instrument Location and Monitoring Schedule	15
	2.5 Stability Criteria	19
	2.6 Limitations of Current Deformation Monitoring Practice	21
3.	SAMPLE DESCRIPTION AND TEST METHODOLOGY	24
	3.1 Sample Description	24
	3.1.1 Description of Coal	24
	3.1.2 Sample Preparation	24
	3.1.3 Description of Individual Specimens	26
	3.1.3.1 Sample MC-5	26
	3.1.3.2 Sample MC-6	26
	3.1.3.3 Sample MC-7	29
	3.2 Deformation Instrumentation	29
	3.2.1 Boundary Displacements	31
	3.2.2 Radial Strain	31

3.2.3	Tunnel Closure	33
3.2.4	Sample Instrumentation	33
3.2.4.1	Sample MC-5	35
3.2.4.2	Sample MC-6	35
3.2.4.3	Sample MC-7	38
3.3	Description of the Test Facility	40
3.4	Loading Sequence	44
4.	DETERMINATION OF MATERIAL PROPERTIES	49
4.1	Strength Properties	49
4.2	Deformation Properties	50
4.2.1	Time-Independent Behavior	51
4.2.2	Material Properties for Isotropic Elastic Formulation	53
4.2.3	Material Properties for Transverse Isotropic Formulation	64
4.2.4	Time-Dependent Behavior	65
4.2.4.1	Hydrostatic Creep	70
4.2.4.2	Stress Relief Creep	75
4.2.4.3	Deviatoric Creep	79
4.2.4.4	Multi-Stage Testing	83
4.2.5	Verification of Time Dependent Relationships	85
5.	RESULTS OF LABORATORY INVESTIGATION	95
5.1	Introduction	95
5.2	Behaviour During External Loading Tests	96
5.2.1	Time-Independent Behaviour	96
5.2.2	Time-Dependent Behaviour	106
5.2.2.1	Critical Closure Rates	107

5.2.2.2	Evaluation of Test Results	116
5.3	Behaviour During Excavation Simulation Tests ..	126
5.3.1	Behaviour Near the Tunnel Face	127
5.3.2	Development of Radial Strains Near the Tunnel Face	157
6.	CONCLUSIONS AND RECOMMENDATIONS	174
6.1	Introduction	174
6.2	Conclusions from Model Tests	177
6.3	Recommendations	182
7.	REFERENCES	184
8.	APPENDIX A - DETERMINATION OF TIME-DEPENDENT PROPERTIES	190
9.	APPENDIX B - RADIAL STRAIN AND TUNNEL CLOSURE RATES MEASURED DURING CREEP TESTS PERFORMED ON THREE SAMPLES	196
10.	APPENDIX C - TUNNEL CLOSURE AND RADIAL CREEP STRAIN INCREMENT PATTERNS OBSERVED DURING TESTING OF THE THREE SAMPLES	216
11.	APPENDIX D - DEVELOPMENT OF RADIAL STRAINS NEAR THE TUNNEL FACE - SAMPLE MC-7	256

List of Tables

Table		Page
3.1	Composition of Coal.....	25
4.1	Orientation Dependence of Extensometer Response....	54
4.2	Elastic Properties of Coal.....	63
4.3	Parameters from Linear Elastic, Transverse Isotropic Formulation.....	66
5.1	Predicted Stress Level for CCR(20) and PCR(20) and Observed Stress Level where Propogation Clearly Observed from Extensometers - Samples MC-5 and MC-6.....	117
5.2	Predicted Stress Level for CCR(20) and PCR(20) and Observed Stress Level Where Propogation Clearly Observed from Extensometers - Sample MC-7.....	118
5.3	Near Face Radial Strain Behavior.....	167

List of Figures

Figure	Page
2.1 Tunnel Design Sequence.....	6
2.2 Deformation Monitoring Instrumentation Layout.....	18
3.1 Plan View of the Top Surface of Sample MC-5.....	27
3.2 Plan Views of the Top and Side Surfaces of Sample MC-6.....	28
3.3 Plan Views of the Top and Side Surfaces of Sample MC-7.....	30
3.4 Typical Extensometer Set-up (to scale).....	32
3.5 Tunnel Convergence Measurement Device (electrical wires omitted for clarity).....	34
3.6 Internal Instrumentation Layout - Sample MC-5.....	36
3.7 Internal Instrumentation Layout - Sample MC-6.....	37
3.8 Internal Instrumentation Layout - Sample MC-7.....	39
3.9 Side View of Test Frame.....	42
3.10 Tunnel Excavation Equipment.....	43
3.11 Loading History of Sample MC-5.....	45
3.12 Loading History of Sample MC-6.....	46
3.13 Loading History of Sample MC-7.....	47
4.1 Average Extensometer Response During Hydrostatic (N=1) Loading of the Intact Specimen - Sample MC-7.....	52
4.2 Spatial Distribution of Young's Modulus : a) Sample MC-5 b) Sample MC-6 and c) Sample MC-7.....	55
4.3 Variation in Elastic Parameters with Stress - Sample MC-5, Method 1.....	57
4.4 Variation in Elastic Parameters with Stress - Sample MC-6, Method 1.....	58
4.5 Variation in Elastic Parameters with Stress - Sample MC-7, Method 1.....	59

Figure	Page
4.6	Variation in Elastic Parameters with Stress - Sample MC-7, Method 2.....60
4.7	Development of Strain with Time.....67
4.8	Idealized Double Logarithmic Plot of Strain Rate vs Time.....69
4.9	Determination of Representative Time-Dependent Parameters.....71
4.10	Variation in 'm' Parameter with Increasing Stress.....73
4.11	Variation in 'a' Parameter with Increasing Stress.....74
4.12	Variation in 'm' Parameter with Decreasing Stress.....76
4.13	Variation in 'a' Parameter with Decreasing Stress.....78
4.14	Mean and Range of Measured Creep Rates in Test MC-7.05.....81
4.15	Deviatoric Creep Rates - Test MC-7.05.....82
4.16	Comparison of Near Tunnel Predicted and Observed Radial Strain Rates.....87
4.17	Comparison of Observed and Predicted Radial Strain Rates Under Multi-Stage Hydrostatic Loading - Sample MC-5.....89
4.18	Comparison of Observed and Predicted Radial Strain Rates Under Multi-Stage Hydrostatic Loading - Sample MC-7.....90
4.19	Comparison of Observed and Predicted Radial Strain Rates Parallel to the Maximum Field Stress - Sample MC-7.....91
4.20	Comparison of Observed and Predicted Radial Strain Rates Perpendicular to the Maximum Field Stress - Sample MC-7.....92
5.1	Extensometer Response : Test MC-7.02.....98

Figure	Page
5.2 Tunnel Closure and Extensometer Response : Test MC-5.04.....	99
5.3 Tunnel Closure and Extensometer Response : Test MC-5.05.....	101
5.4 Tunnel Closure and Extensometer Response : Test MC-7.11.....	102
5.5 Tunnel Closure and Extensometer Response : Test MC-7.15.....	104
5.6 Tunnel Closure and Extensometer Response : Test MC-7.16.....	105
5.7 Schematic Representation of the Critical Rate Functions : a)uniaxial compression test; b)tunnel.....	108
5.8 Typical Tunnel Closure Rates During Test MC-4.2...	111
5.9 Compressional Strain Rates for Intact Samples and Ranges of Tunnel Closure Rates for Samples MC-5 to MC-7.....	113
5.10 Comparison of Observed Tunnel Closure Rates under Excavation (Test MC-7.10) and External Loading (Test MC-7.11) Conditions....	114
5.11 Observed Tunnel Closure Rates : a) Test MC-7.13 pre-widening; b) Test MC-7.14.....	121
5.12 Observed Tunnel Closure Rates - Test MC-7.15.....	122
5.13 Observed Tunnel Closure Rates - Test MC-7.17.....	124
5.14 Observed Stress Changes in Tunnel Widening.....	132
5.15 Predicted Radial Strain Rate Components - Tunnel Excavation (Test MC-7.08).....	133
5.16 Comparison of Observed and Predicted Radial Strain Rates - Test MC-6.02, Parallel to Principal Stress Directions.....	134
5.17 Comparison to Observed and Predicted Radial Strain Rates - Test MC-6.02, 45° to Principal Stress Direction.....	135

Figure	Page
5.18	Comparison of Observed and Predicted Radial Strain Rates - Test MC-7.08, Parallel to Principal Stress Directions.....137
5.19	Comparison of Observed and Predicted Radial Strain Rates - Test MC-7.08, 45° to Principal Stress Directions.....138
5.2	Comparison of Observed and Predicted Radial Strain Rates - Test MC-7.10, Parallel to Principal Stress Directions.....140
5.21	Comparison of Observed and Predicted Radial Strain Rates - Test MC-7.10, 45° to Principal Stress Directions.....141
5.22	Comparison of Observed and Predicted Radial Strain Rates - Test MC-7.13, Parallel to Principal Stress Directions.....142
5.23	Comparison of Observed and Predicted Radial Strain Rates - Test MC-7.13, 45° to Principal Stress Directions.....143
5.24	Comparison of Radial Strain Rates: Observed and Predicted Face Advance - Test MC-7.10 ($r/a=1.77, \theta=135^\circ$).....147
5.25	Comparison of Radial Strain Rates: Observed and Predicted Face Advance - Test MC-7.10 ($r/a=2.12, \theta=135^\circ$).....148
5.26	Comparison of Radial Strain Rates: Observed and Predicted Face Advance - Test MC-7.13 ($r/a=1.36, \theta=135^\circ$).....149
5.27	Comparison of Radial Strain Rates: Observed and Predicted Face Advance - Test MC-7.13 ($r/a=1.61, \theta=135^\circ$).....150
5.28	Comparison of Predicted Radial Strain Rates Assuming Various Tunnel Advance Rates in Wabamun Coal.....153
5.29	Comparison of Predicted Radial Strains Assuming Various Tunnel Advance Rates in Wabamun Coal.....155
5.30	Variation in Tunnel Closure Rate with Radius of Yield Zone.....158

Figure	Page
5.31	Variation of Radial Strain Rate with Radius of Yield Zone.....159
5.32	Predicted Tunnel Convergence as a Function of the Distance from the Tunnel Face and the Extent of the Yield Zone.....160
5.33	Development of Radial Strain - 108mm Tunnel Excavation, Sample MC-6 (parallel to the principal stress directions).....162
5.34	Development of Radial Strain - 108mm Tunnel Excavation, Sample MC-6 (45° to the principal stress directions).....163
5.35	Development of Radial Strain - Widening to 152mm, Sample MC-6 (parallel to the principal stress directions).....164
5.36	Development of Radial Strain - Widening to 152mm, Sample MC-6 (45° to the principal stress directions).....165
5.37	Development of Radial Strain - 42mm Tunnel Excavation, Sample MC-7.....168
5.38	Development of Radial Strain - Widening to 108mm, Sample MC-7.....169
5.39	Development of Radial Strain - Widening to 152mm, Sample MC-7.....170
6.1	Confinement-Convergence Curve.....175
9.1	Strain Rates: MC-5.02 and 5.03.....197
9.2	Closure Rates: MC-5.05.....198
9.3	Closure Rates: MC-5.07.....199
9.4	Closure Rates: MC-5.09.....200
9.5	Closure Rates: MC-5.11.....201
9.6	Closure Rates: MC-5.13.....202
9.7	Strain Rates: MC6.01S and 6.02.....203
9.8	Closure Rates: MC-6.02, 6.03, 6.05 (108mm tunnel).....204

Figure	Page
9.9	Closure Rates: MC-6.05 (152mm tunnel), 6.06 and 6.08.....205
9.10	Closure Rates: MC-6.09.....206
9.11	Closure Rates: MC-6.10 and 6.11.....207
9.12	Strain Rates: MC-7.02, 7.03, 7.04, 7.05 and 7.08.....208
9.13	Strain Rates: MC-7.06.....209
9.14	Strain Rates: MC-7.07.....210
9.15	Closure Rates: MC-7.10, 7.11 and 7.13.....211
9.16	Closure Rates: MC-7.12.....212
9.17	Closure Rates: MC-7.15.....213
9.18	Closure Rates: MC-7.17.....214
9.19	Closure Rates: MC-7.13, 7.14 and 7.16.....215
10.1	Creep Closure and Contours of Creep Strain - MC-5.05 at 12.8 MPa.....217
10.2	Creep Closure and Contours of Creep Strain - MC-5.07 at 12.9 MPa.....218
10.3	Creep Closure and Contours of Creep Strain - MC-5.09 at 13.4 MPa.....219
10.4	Creep Closure and Contours of Creep Strain - MC-5.11 at 11.1 MPa.....220
10.5	Creep Closure and Contours of Creep Strain - MC-5.11 at 13.8 MPa.....221
10.6	Creep Closure and Contours of Creep Strain - MC-5.13 at 11.0 MPa.....222
10.7	Creep Closure and Contours of Creep Strain - MC-6.02 at 12.6 MPa (t=28.8).....223
10.8	Creep Closure and Contours of Creep Strain - MC-6.02 at 12.6 MPa (t=29.9).....224
10.9	Creep Closure and Contours of Creep Strain - MC-6.03 at 12.4 MPa.....225

Figure	Page
10.10 Creep Closure and Contours of Creep Strain - MC-6.04 at 14.9 MPa.....	226
10.11 Creep Closure and Contours of Creep Strain - MC-6.05 (108mm) at 12.4 MPa.....	227
10.12 Creep Closure and Contours of Creep Strain - MC-6.05 (152mm) at 12.4 MPa.....	228
10.13 Creep Closure and Contours of Creep Strain - MC-6.06 at 12.4 MPa.....	229
10.14 Creep Closure and Contours of Creep Strain - MC-6.07 at 12.4 MPa.....	230
10.15 Creep Closure and Contours of Creep Strain - MC-6.07 at 14.8 MPa.....	231
10.16 Creep Closure and Contours of Creep Strain - MC-6.08 at 12.5 MPa.....	232
10.17 Creep Closure and Contours of Creep Strain - MC-6.08 at 15.0 MPa.....	233
10.18 Creep Closure and Contours of Creep Strain - MC-6.09 at 12.4 MPa.....	234
10.19 Creep Closure and Contours of Creep Strain - MC-6.09 at 15.0 MPa.....	235
10.20 Creep Closure and Contours of Creep Strain - MC-6.10 at 12.1 MPa.....	236
10.21 Creep Closure and Contours of Creep Strain - MC-6.11 at 12.1 MPa.....	237
10.22 Creep Closure and Contours of Creep Strain - MC-6.11 at 14.5 MPa.....	238
10.23 Creep Closure and Contours of Creep Strain - MC-7.10 at 12.5 MPa (t=31.5).....	239
10.24 Creep Closure and Contours of Creep Strain - MC-7.10 at 12.5 MPa (t=91.5).....	240
10.25 Creep Closure and Contours of Creep Strain - MC-7.11 at 12.5 MPa.....	241
10.26 Creep Closure and Contours of Creep Strain - MC-7.12 at 12.5 MPa.....	242

Figure	Page
10.27 Creep Closure and Contours of Creep Strain - MC-7.12 at 14.3 MPa.....	243
10.28 Creep Closure and Contours of Creep Strain - MC-7.13 at 12.5 MPa (t=20.0).....	244
10.29 Creep Closure and Contours of Creep Strain - MC-7.13 at 12.5 MPa (t=29.7).....	245
10.30 Creep Closure and Contours of Creep Strain - MC-7.13 at 12.8 MPa (t=89.7).....	246
10.31 Creep Closure and Contours of Creep Strain - MC-7.14 at 12.5 MPa.....	247
10.32 Creep Closure and Contours of Creep Strain - MC-7.15 at 7.5 MPa.....	248
10.33 Creep Closure and Contours of Creep Strain - MC-7.15 at 10.0 MPa.....	249
10.34 Creep Closure and Contours of Creep Strain - MC-7.15 at 12.5 MPa.....	250
10.35 Creep Closure and Contours of Creep Strain - MC-7.15 at 14.0 MPa.....	251
10.36 Creep Closure and Contours of Creep Strain - MC-7.16 at 12.5 MPa.....	252
10.37 Creep Closure and Contours of Creep Strain - MC-7.17 at 7.5 MPa.....	253
10.38 Creep Closure and Contours of Creep Strain - MC-7.17 at 10.0 MPa.....	254
10.39 Creep Closure and Contours of Creep Strain - MC-7.17 at 12.5 MPa.....	255
11.1 Tunnel Advance Test MC-7.08 Excavation.....	259
11.2 Development of Radial Strain - Test MC-7.08 Sta. 56.....	260
11.3 Development of Radial Strain - Test MC-7.08 Sta. 81 (parallel).....	261
11.4 Development of Radial Strain - Test MC-7.08 Sta. 81 (45°).....	262

Figure	Page
11.5 Development of Radial Strain - Test MC-7.08 Sta. 106 (parallel).....	263
11.6 Development of Radial Strain - Test MC-7.08 Sta. 106 (45°).....	264
11.7 Development of Radial Strain - Test MC-7.08 Sta. 131.....	265
11.8 Development of Radial Strain - Test MC-7.08 Sta. 156.....	266
11.9 Tunnel Advance - Test MC-7.10, First Widening.....	267
11.10 Development of Radial Strain - Test MC-7.10 Sta. 56.....	268
11.11 Development of Radial Strain - Test MC-7.10 Sta. 81 (parallel).....	269
11.12 Development of Radial Strain - Test MC-7.10 Sta. 81 (45°).....	270
11.13 Development of Radial Strain - Test MC-7.10 Sta. 106 (parallel).....	271
11.14 Development of Radial Strain - Test MC-7.10 Sta. 106 (45°).....	272
11.15 Development of Radial Strain - Test MC-7.10 Sta. 131.....	273
11.16 Development of Radial Strain - Test MC-7.10 Sta. 156.....	274
11.17 Tunnel Advance - Test MC-7.13, Final Widening.....	275
11.18 Development of Radial Strain - Test MC-7.13 Sta. 56.....	276
11.19 Development of Radial Strain - Test MC-7.13 Sta. 81 (parallel).....	277
11.20 Development of Radial Strain - Test MC-7.13 Sta. 81 (45°).....	278
11.21 Development of Radial Strain - Test MC-7.13 Sta. 106 (parallel).....	279

Figure	Page
11.22 Development of Radial Strain - Test MC-7.13 Sta. 106 (45°).....	280
11.23 Development of Radial Strain - Test MC-7.13 Sta. 131.....	281
11.24 Development of Radial Strain - Test MC-7.13 Sta. 156.....	282

1. INTRODUCTION

The greatest demands of modern societies are the same as those of ancient societies; resources and accommodation. While past generations were able to avail themselves in a relatively easy manner (though not necessarily easy given the technological level) the increased demands of a growing world have caused 'modern' men to foray in further fields. Past exploitation of surficial resources have forced man deeper beneath the earth's surface for the required commodity. Land and energy costs have halted the post-war urban sprawl and forced man into vertical accommodation, his living space upwards and storage space downwards. These resource and storage requirements, along with their support measures are the catalyst for the field of underground excavation (tunnelling) technology.

While underground excavations have been constructed throughout recorded history, it is only recently that both the scale and economics of tunnelling have undergone dramatic change. Prior to this current, cost-conscious efficiency, tunnelling was considered an 'art' practiced by a few 'artists' who could cope with the existing demand. Present demand, however, requires that the behavior of underground excavations be understood so that less experienced engineers or contractors may undertake these endeavours, in essence the transformation from an art to a science.

Current tunnelling technology, while far advanced, is still in this transition stage. Because of this, underground excavations, whether they be in soil or rock, and independent of their intended use, require monitoring. Unfortunately, field monitoring in itself is not sufficient for the development of a predictive capability. In the field, there are a multitude of influences on tunnel performance which complicate analysis. Controlled environmental conditions are essential for a rational analysis. One means by which this may be achieved is the simulation of field conditions in laboratory scale models. In this manner, the response of an excavation to pre-determined stimuli may be observed and a clearer picture of the overall behavior of underground excavations emerge, especially when coupled with field observations.

1.1 Thesis Objective

The monitoring of underground excavations is crucial to the further development of tunnelling technology. Because of this importance, it is essential that a proper framework for data interpretation be devised, the limitations to the instrumentation employed for monitoring be understood and that their application be appropriate for their purpose.

Most tunnel excavation monitoring schemes employ deformation instrumentation as the primary mode of investigation. This is particularly true in excavations where large deformations are anticipated, such as in weak

rock or rock exhibiting time-dependent deformation. It is therefore essential that the use of current deformation instrumentation in this type of environment be critically reviewed. That is the objective of this thesis.

In order that this objective be realized, it was decided to forego field analysis, due to its inherent ambiguities, and instead, concentrate on laboratory model studies. Particular attention was paid to the evaluation of opening stability by deformation measurements and the instrumentation response to tunnelling activity.

1.2 Scope of the Thesis

The first step in any investigative research is the review of the current knowledge on the subject. The results of a review of current tunnel monitoring as practiced by both the civil engineering and mining engineering (particularly coal mining) professions are presented in Chapter 2. Areas of particular interest included the monitoring objectives, the means by which these objectives are achieved, the selection of the type of monitoring, the type of instrumentation, the selection of appropriate design and performance criteria and the limitations as presently understood.

Descriptions of the test apparatus employed in this research are presented in Chapter 3. Also included in this chapter are physical descriptions of each sample along with a description of the type, installation and layout of

instrumentation and a summary of the adopted loading sequence. Coal was used as a test material because of its time-dependent strength and deformation properties.

In order to analyze the observed behavior of the tunnels during process simulation testing it was necessary to determine the material properties of the test specimen. Both the time-dependent and time-independent properties were obtained from the response of large intact blocks (600x600x200mm) to a variety of loading conditions. The results of these investigations, presented in Chapter 4, allowed formulation of numerical expressions for the prediction of the deformation response of the test material under given stress conditions. The analysis of the test results, with particular emphasis on the implications towards deformation monitoring in underground excavations in weak rock subject to time-dependent deformation, are presented in Chapter 5. Attention was focused on the limitations of deformation monitoring for stability evaluation and the verification of design assumptions under both advancing tunnel and long-term conditions.

Conclusions regarding the application of deformation monitoring instrumentation in weak rock at depth are presented in Chapter 6. Also included are recommendations for the implementation of deformation instrumentation and suggestions for further research in this area.

2. REVIEW OF CURRENT DEFORMATION MONITORING PRACTICE

2.1 Introduction

The 'art' of tunnelling is becoming more of a science as a result of the application of recent advances in design, construction and monitoring of underground openings. These three components are no longer discrete elements of the tunnelling process but are interrelated as shown in Figure 2.1. In the site characterization phase, the geology along the alignment is determined as are the engineering properties of the rock mass required for its description. Once these are known, the excavation sequence, construction method and support system are often selected on the basis of simple empirical classification systems. Detailed design is then derived from empirical methods, more refined classification systems or an analytical approach. After commencement of construction, monitoring of tunnel performance permits critical evaluation and possible revision of the design or construction procedure. Because of the importance of this final phase to modern tunnelling technology, it was decided to critically review the means by which the performance is presently evaluated.

The above tunnelling process is generally limited to civil engineering works. In mining, the most common design concept is the duplication of previous support and geometry from existing operations under similar conditions [Dahl(1978)]. Monitoring of underground excavations,

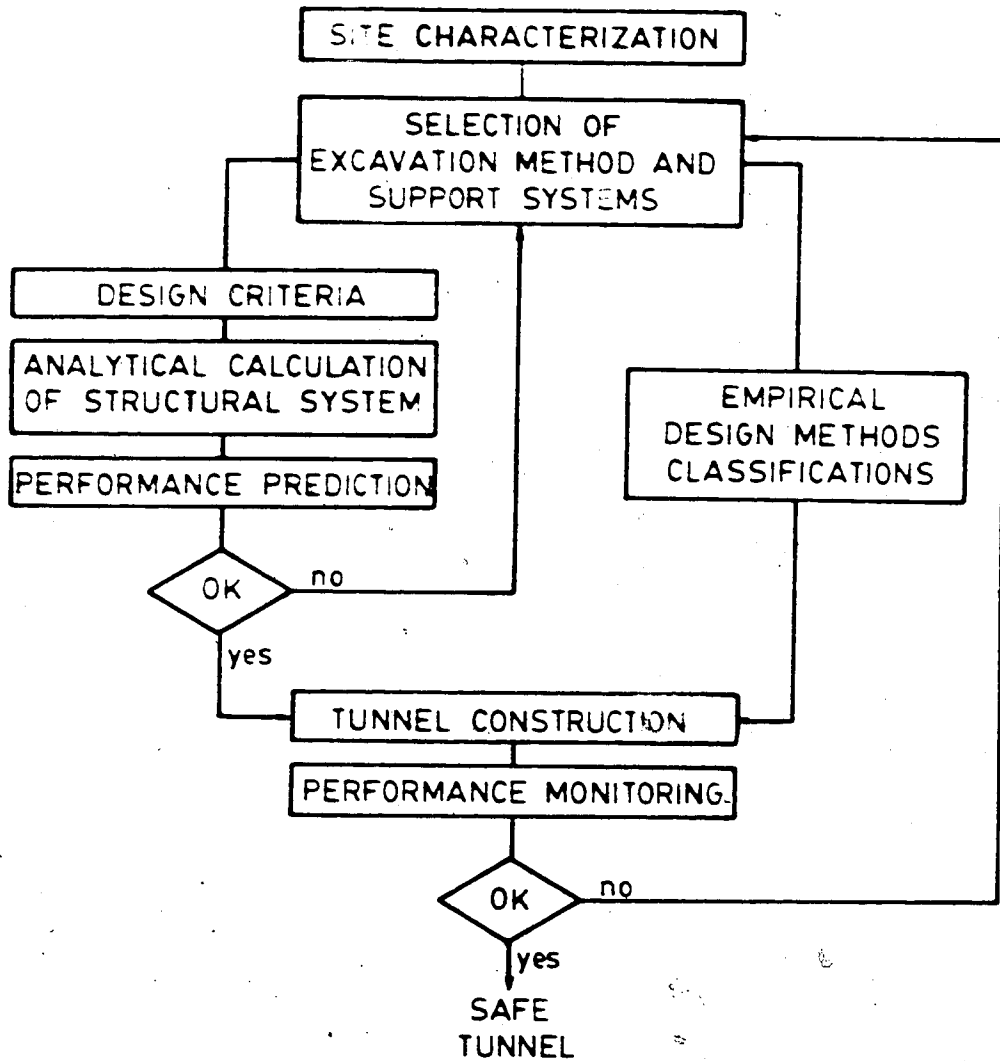


Figure 2.1 Tunnel Design Sequence

however, has been actively pursued by the mining industry and valuable contributions in this field have resulted from their efforts. While the purposes of the underground excavations for civil and mining works may be very different, the rock mass is unaware of it, and will react in a similar manner to similar stimuli. The advances in the monitoring of underground excavations in rock are equally applicable to both.

2.2 Role of Monitoring in Underground Excavations in Rock

The monitoring of an underground excavation in rock is simply the measurement of the rock mass response to the changes imposed. These measurements may then be employed to satisfy the objectives of the monitoring program. Paramount amongst these objectives are the determination of the opening stability and the verification of the design [Kaiser (1981d), Franklin (1977)]. Additional objectives have been defined by Lane (1977), Londe (1977) and Dunnicliff *et al* (1981). These are outlined below along with those previously mentioned.

Stability Evaluation

The primary role of monitoring is to ensure the safety of the underground environment during both construction and operation. Current monitoring technology, if applied correctly, permits determination of incipient tunnel instability with sufficient time for excavation or remedial

action if the process leading to instability is gradual.

Design Validation

The design of the tunnel support is made with gross assumptions as to the geology and rock mass properties. To ensure that the design is appropriate requires verification of the assumed conditions and predicted performance by in-situ measurement.

The validity of a new design approach may also require the performance monitoring of a prototype for comparison with the new and proven design methods. Advancement of the state-of-the-art requires hard evidence which can only be achieved by in-situ measurements.

Construction Assessment

The adequacy and suitability of a given or new construction method is best assessed by monitoring the performance of the excavation during these endeavours and then comparing with measurements made in excavations with similar geologic conditions but where different construction methods were employed.

As tunnels become more expensive to construct, the avoidance of overdesign is of increasing importance. In situ instrumentation allows the designer to implement a 'minimal support design with provision for additional support where measurements dictate.

Problem Diagnosis

The remedy of an incipient instability requires a prior knowledge of the nature of the instability (i.e., the mechanism, location and extent). This can only be achieved by insitu measurements.

Performance Documentation

Records of the performance of the underground excavation provide documentation of 'as built' conditions and structural response. These may then be employed to check for compliance with contract requirements and to assist in the design of future works.

Public Reassurance

Use of current tunnel monitoring technology serves to reassure the workers and the public in general of the owner's and contractor's concern with their safety as well as with the long term integrity of the excavation.

The objectives pursued by the monitoring program at any given site will depend on the nature and difficulty of the project, the owner's habits, the designer's style and the contractor's experience [Londe (1977)]. The means by which the monitoring is performed are discussed in the following section.

2.3 Deformation Monitoring

In addition to visual observation of the excavation, monitoring is performed by in-situ measurement of stress changes and displacements. The environment in which these measurements are made is particularly harsh. Therefore, it is necessary that any instrumentation be of simple and rugged design yet yielding reliability and accuracy. Readings must be easily interpreted so that the necessary action may be taken and neither the instrument nor its reading should duly interfere in the construction or operation of the opening. Given these operating criteria, the most commonly employed monitoring system is that of displacement measurement. Londe (1977) considered stress change measurements the most difficult to interpret as the instrument itself alters the local stress field and the discontinuities inherent in the rock mass cause an unacceptable degree of scatter in results. Kaiser (1981d) considered displacement measurements as the most important indicator in ground control as did Cording *et al* (1975) because of the ability of deformation measurements to yield information as to the depth and magnitude of the movement. Lemcoe *et al* (1980) in their state-of-the-art review of measurement techniques found displacement measurements more direct, easier and less costly to perform and hence more commonly employed than stress measurements. The 'observational method' of tunnel design as exemplified by the New Austrian Tunneling Method (NATM) depends heavily on

interactive deformation instrumentation [Kuesel (1983), Amberg (1983)]. In the mining environment deformation measurements are employed in the design of roof and face supports and roof or floor bolting [Lu (1982)] or in assessing stability [Whittaker (1974)].

Due to the dominance of displacement or deformation measurements in the performance monitoring of underground excavations it was decided to forego any detailed consideration of stress measurements in monitoring. This does not imply that stress measurements are not of value in monitoring. Indeed, stress change measurements can greatly enhance the value of deformation measurements [Kaiser and Mackay (1982)].

The monitoring of deformations in underground excavations is achieved by optical surveying, convergence measurements and borehole extensometer measurements. Generally no single means of monitoring is employed on a given project as the three methods complement each other.

2.3.1 Optical Surveying

Optical surveying methods such as levelling and triangulation are widely employed to monitor movements of the rock surface or tunnel lining [Londe (1977)]. Where accessible and where the measurements can be related to a remote stable base the absolute displacements of the tunnel wall can be determined. The advantages of this system are that the personnel and equipment are generally on site (for

alignment control) however, these are outweighed by the disadvantages of interference with the construction procedure and the considerable time required for computation and interpretation. This latter point is particularly important where monitoring is employed to detect incipient instability.

Electro-optical distance measuring instruments employing a modulated light or laser beam projected onto reflective targets on the surface of the excavation are superseding the optical instruments [Franklin (1977), Hoek and Brown (1980)]. Their principal advantage over the optical system is that many measurements, including those in highly inaccessible regions can be made from a single instrument location in a short period of time.

Elaboration on this form of instrumentation will not be undertaken as laboratory simulation is not possible. However, the results of the laboratory investigation reported in Chapter 5 have significance with regard to this form of monitoring as well.

2.3.2 Convergence Measurement

One of the most common and easily performed deformation monitoring methods undertaken in underground excavations is the measurement of the change in diameter or convergence between reference points. Convergence is measured by either a tape or rod extensometer with the tape being the more widely used because of its range (50 m versus 8 m for the

rod type) and handling ease [Lemcoe *et al* (1980)].

The tape extensometer consists of a stainless steel tape with a tensioning spring and a mechanical measuring device such as a dial indicator gauge. The rod extensometer employs a rod in the place of the tape, thereby removing the need for a tensioning device. The rod can be of fixed length or telescopic (possibly spring loaded) and is fitted with a micrometer or dial gauge [Franklin (1977)]. Lu (1982) describes an automated rod type convergence meter where, upon convergence, a lever arm on the device causes a scribe point to trace a path on a pressure sensitive chart or rotating drum giving a complete time-convergence record. Rod type extensometers employing electric readout devices and their application to mining are described by McVey and Howie (1981).

Convergence targets for both systems generally consist of steel or aluminum anchor bolts secured in the rock by an expanding shell anchor or by grouting. The target ends are designed to mate with the appropriate convergence meter [Franklin (1977)].

The accuracy of these instruments is highly dependent on the care employed in making the reading (temperature compensation, spring tension, etc.) and in installing and providing protection for the reference target [Lemcoe *et al* (1980)].

2.3.3 Borehole Extensometers

The previously described deformation measurement systems give only surface displacements of the opening walls. For 'in-depth' measurement of the rock mass deformation, borehole extensometers are required. As the name implies this type of instrumentation requires the drilling of boreholes either from the excavation or from outside the excavation if conditions are favourable (shallow cover or parallel adit). Two types of borehole extensometers, probe and fixed, are commonly employed [Lemcoe *et al* (1980)]. In both systems the differential movement of anchor points installed at various depths is measured.

Probe Type

The probe type extensometer system measures the change in location along the borehole axis of pre-set anchors with respect to each other or some datum (furthest anchor or borehole collar) by means of a moving sensor. The most popular of this type employs magnetized anchors and a probe capable of sensing the magnetic field [Lemcoe *et al* (1980)]. The major disadvantage of this system is that it is labour and time intensive and not suitable for automated or continuous recording.

Fixed Type

For increased precision or where continuous or remote readout is required extensometers of the fixed type are used. The displacement along the borehole axis of selected

points is determined by measuring the displacement at the borehole collar of rods or tensioned wires extending from anchors located at those points [Franklin (1977)].

Measurements are commonly made with a dial indicator gauge, however for continuous or remote monitoring electric displacement transducers are employed [Amberg (1983), Lu (1982)]. Rod type extensometers yield more reliable and accurate results as the wire type are prone to kinking and creep. In single hole, multi-point installations, wire extensometers are more often used because of their reduced space requirements [Franklin (1977)].

Because of the ability of the borehole extensometer to provide information regarding the extent and depth of rock movement they are generally used in conjunction with convergence measurements to monitor underground excavations during the construction and operation phases. Selection of the monitoring instrumentation is only the first phase of the monitoring process. When and where to monitor and what criteria to employ are of equal if not more importance.

2.4 Instrument Location and Monitoring Schedule

The general principle governing the selection, location and recording schedule of deformation measuring instruments is that of working from the general to the particular [Franklin (1977)]. The intended role of the monitoring system will also influence the selection as will the type of excavation and support method [Cording et al (1975)].

Franklin (1977) suggests that when monitoring is performed to ensure the safety of the excavation, there should be extensive coverage with low precision, low frequency monitoring supplemented with more frequent, more accurate monitoring where conditions dictate. If design verification is the objective, he suggests selecting 'representative profiles' corresponding to various geologies and geometries for monitoring. Borehole extensometers are required in addition to convergence measuring devices at these profile locations. Other design principles presented by Franklin include:

1. Adoption of redundancy in the instrumentation to accommodate instances of damage to an installation or malfunction of an instrument;
2. Employment of a large number of low precision instruments rather than fewer, high precision instruments. With more instrumentation, anomalies in readings are more readily ascertained;
3. Adjustment of the monitoring frequency to suit the situation. After installation monitoring should be frequent to identify trends in ground behavior. Afterwards the frequency of readings will depend on the activity of the specific site; and
4. Proper installation and calibration of the instrument so that it functions as intended.

Both Franklin (1977) and John (1977) recommend convergence measurements spaced at 50 to 100 metre intervals along the

tunnel axis and at geological changes under good rock conditions. John also suggests a reduction in this interval to between 10 and 20 metres when fracture processes are occurring. At each measuring station the convergence is measured at the springline and from the crown to the invert. Supplementary measurements across oblique diameters are performed when considered necessary. At selected monitoring stations borehole extensometers are also installed, principally to verify support design. Cording *et al* (1975) recommend installation as close to the face as possible so measurements can be made before tunnel advance. They further recommend that the anchors be placed at a minimum of two depths; one close to the tunnel wall (1-2 m) to record near surface movement and the other deeper to give evidence of deep seated movements. Extensometers are generally situated in the crown and at the springline with occasional installation in the invert and at oblique angles. A typical deformation instrumentation array is shown in Figure 2.2.

This array demonstrates the basic needs of the instrumentation system for a full face, circular excavation. Horizontal and vertical convergence determine the deformed shape of the excavation. Extensometers in the crown and invert as well as convergence measurements from the springline to the crown allow separation of the convergence components (i.e., bed separation, floor heave, etc.). Ideally all deformation measurements are tied together and then referenced to a remote datum (by tunnel survey) in

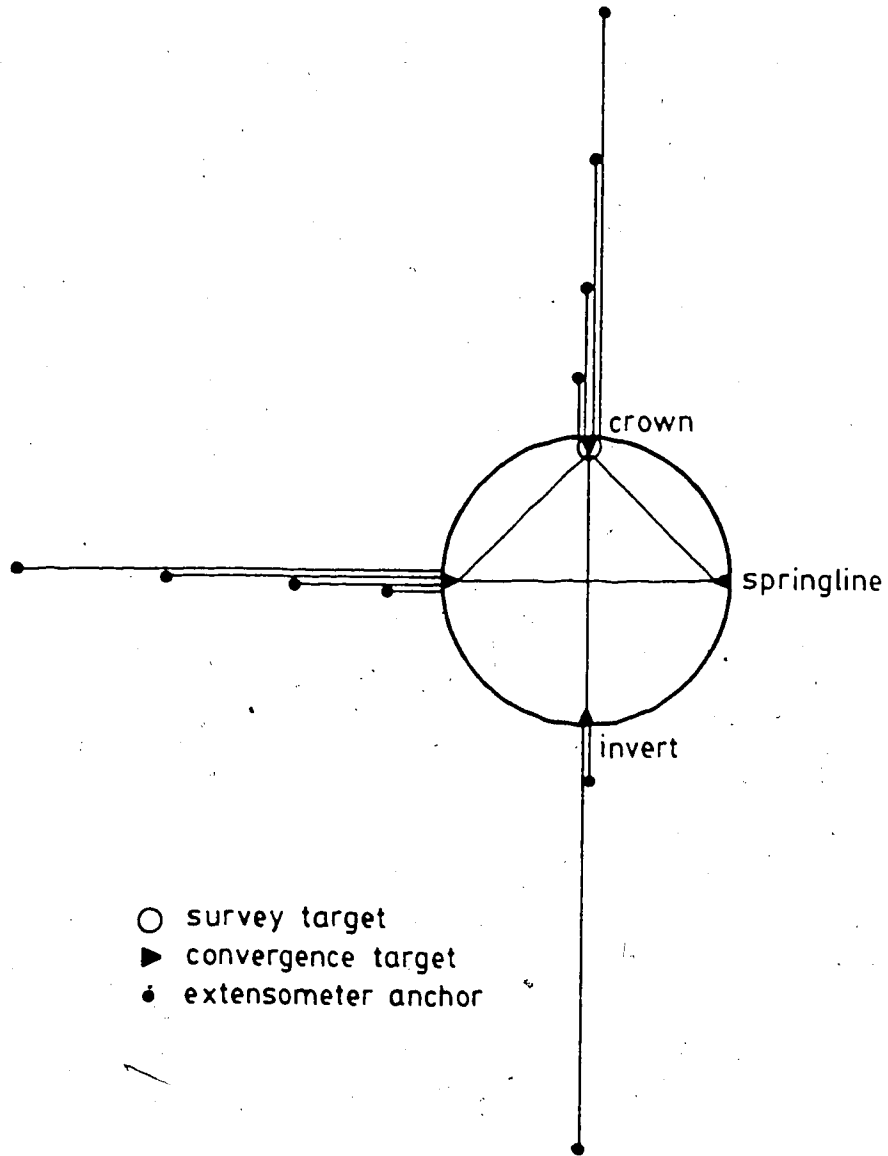


Figure 2.2 Deformation Monitoring Instrumentation Layout

order to fix the displacement field in space. In multiple heading excavations the same principles are employed, however, the location of the instruments will depend on the particular excavation sequence and the anticipated behaviour as discussed by Cording *et al* (1975).

Deformation monitoring in mining applications is not as rigorously applied as in civil engineering projects due mainly to the short life span of the majority of mine works. Where monitoring is employed it generally consists of roof to floor convergence measurements. Occasionally the convergence is further defined by separation into floor heave and roof sag [Hargraves and Martin (1977)]. Stability monitoring by microseismic methods has been undertaken by the mining industry [Blake (1982)] but is not considered in this research.

2.5 Stability Criteria

When deformation monitoring is being employed to ascertain the stability of an underground excavation, the recorded measurements must be compared to design criteria in order that an assessment be made. Both Franklin (1977) and Londe (1977) consider absolute values of displacement as insufficient for stability assessment. They along with John (1977) and Cording *et al* (1975), however, consider the use of displacement rate as a sufficient, suitable criterion. Indeed this is the most frequently employed means of stability assessment in tunnelling [Lane (1977)].

In mining, closure rate measurements are commonly employed in the determination of opening stability [McVey and Howie (1981), Hams (1978) and Wieselmann (1968)]. Lu (1982) and Pothini and von Schonfeldt (1978) recommend both the cumulative convergence and the rate of convergence be used in establishing stability. Pothini and von Schonfeldt also consider the change in the convergence rate in their assessment of opening stability. Serata *et al* (1976) suggest that the determination of opening stability can best be determined by plotting the closure rate versus the excavation age in a double log diagram. The degree of current stability is indicated by the magnitude of the creep rate with that of future stability by the slope of the "creep rate curve. This point will be discussed later.

Selection of an appropriate critical deformation rate for stability assessment is not an easy task. The range of convergence rates encountered in underground excavations is quite large. John (1977) found that rates less than 10 mm per month (in an 11 m dia. tunnel) resulted in low lining loads while McVey and Howie (1981) found rates of 5 mm per minute to indicate impending roof fall in a specific coal mine. Criteria such as these indicate the range of rates which may be encountered. They are not directly transferable to other sites.

As an early indication of instability, in the absence of predetermined values, high rates of movement unrelated to excavation advance or sudden rate increases may be used

[Cording *et al* (1975)]. To determine the site specific critical rate requires observation of rates, under similar conditions, where stability and instability of the excavation were encountered. These can be determined from other projects but care must be exercised in any extrapolations needed due to changes in support or geometry. The best method of selection is the observation of deformation rates in pilot headings or test sections of the same project.

In mining, special care is required to separate the effects of headings at other levels or in parallel advances. The excavation sequence (i.e., leading, trailing or simultaneous gateroad excavation) is also relevant.

2.6 Limitations of Current Deformation Monitoring Practice

Current deformation monitoring practice in underground excavations suffers limitations in both concept and application. The former relates to the inadequacy of the program as discussed by Kaiser (1981d) while the latter relates to field problems presented by Dunnicliff *et al* (1981) and others.

Kaiser (1981d) points out that most monitoring systems concentrate on the determination of the stress or displacement field while neglecting or inadequately handling the determination of the material property distribution and the mode of behaviour of the system. Based on the results of model studies, Kaiser concludes that interpretation of field

behaviour' is not possible without a knowledge of all three. While acknowledging that it is often necessary and indeed permissible to make assumptions for some of the components described above, he suggests that this is not the case with the mode of behaviour. The monitoring system should be designed to ascertain the deformation process rather than to record the response to an unknown process.

Applications problems related to deformation monitoring are of both procedural and mechanical origin. Procedural problems identified by Dunnicliff *et al* (1981) include:

1. Failure to identify the need for instrumentation at a given location;
2. Inflexibility in the instrumentation layout and recording schedule (ie. failure to adapt to changing requirements); and
3. Dilatory collection and interpretation of measurements.

An additional procedural problem relates to the reduced deformations measured by instrumentation installed behind the face as noted by Lo and Lukajic (1984). Mechanical problems are generally related to instrument reliability particularly where anomolous measurements are recorded. In situations such as this the experience of the instrumentation engineer is usually relied upon [Cording *et al* (1975)]. Minor mechanical problems occur due to improper installation or post installation damage.

Additional concerns regarding the monitoring of underground excavations were identified by Wieselmann (1968)

and Muir Wood (1979). Wieselmann in an investigation into the use of closure rates as a monitor in potash mines found that the rates were dependent on the opening shape and the method of excavation. Muir Wood indicated that, in materials exhibiting time dependent behavior, separation of the deformation into that resulting from the variation of the stress field due to face advance and the creep under constant shear stress is necessary.

In an attempt to assess the implications of these influences on the deformation monitoring of underground excavations, particularly those in weak rock, a series of simulation tests were performed on laboratory specimens. The results of this investigation are presented in Chapter 5.

3. SAMPLE DESCRIPTION AND TEST METHODOLOGY

3.1 Sample Description

3.1.1 Description of Coal

The coal employed as the model material in this testing program was obtained from the Highvale Mine in the Wabamun Lake District near Edmonton, Alberta. This coal was graded by Standsfield and Lang (1944) as subbituminous B according to the Canadian Classification and its composition determined by Pearson (1959) as presented in Table 3.1. A detailed structural survey conducted by Noonan (1972) concluded that the coal is horizontally bedded with two orthogonal cleat systems perpendicular to bedding. The major system is oriented N45°E and has an average joint spacing of approximately 20 mm. Jointing is essentially planar but discontinuous.

3.1.2 Sample Preparation

Test specimens of approximately 600 x 600 x 200 mm were prepared from large block sample as described by Kaiser (1979). The major joint set was oriented parallel to the main diagonal of the specimen and the bedding planes parallel to the larger surface. In this manner, the bedding plane was perpendicular to the tunnel axis and the major jointing at approximately 45° to the principal stress direction when installed in the test frame.

Table 3.1 Composition of Coal

Moisture	18.4 - 21.8	} % by weight
Ash	8.0 - 14.9	
Volatile Matter	24.4 - 28.3	
Fixed Carbon	38.9 - 42.3	
Fuel Ratio	1.50 - 1.59	
Gross kJ per N	1898 - 2116	

3.1.3 Description of Individual Specimens

3.1.3.1 Sample MC-5

Sample MC-5 was prepared in the prescribed manner to final dimensions of 620 x 615 x 210 mm. The major joint set was inclined at approximately 49° to the major principal stress direction. Joint spacing varied from approximately 10 to 20 mm. A plan view of the top surface of this sample is shown in Figure 3.1.

A fracture running linearly across the sample from Side 2 to Side 4 was noted during pre-test mapping, however it was located outside the tunnel area and thought to be of minimal significance. Associated with this fracture was a large depression caused by removal of loose material. The depression was filled with high strength grout which may have influenced the stiffness in this region.

3.1.3.2 Sample MC-6

Sample MC-6 was prepared in the same manner as MC-5 to final dimensions of 620 x 620 x 206 mm. The major joint set was distinctly non-planar with inclinations of 21° to 68° from the major principal stress direction. Joint spacing was generally in the range of 10 to 20 mm with spacing of less than 5 mm in the heavily jointed region surrounding a clay shale inclusion. Plan views of the top and side surfaces are presented in Figure 3.2.

A clay inclusion, elliptic in section, is evident in the plan view of Side 3. This inclusion dipped at

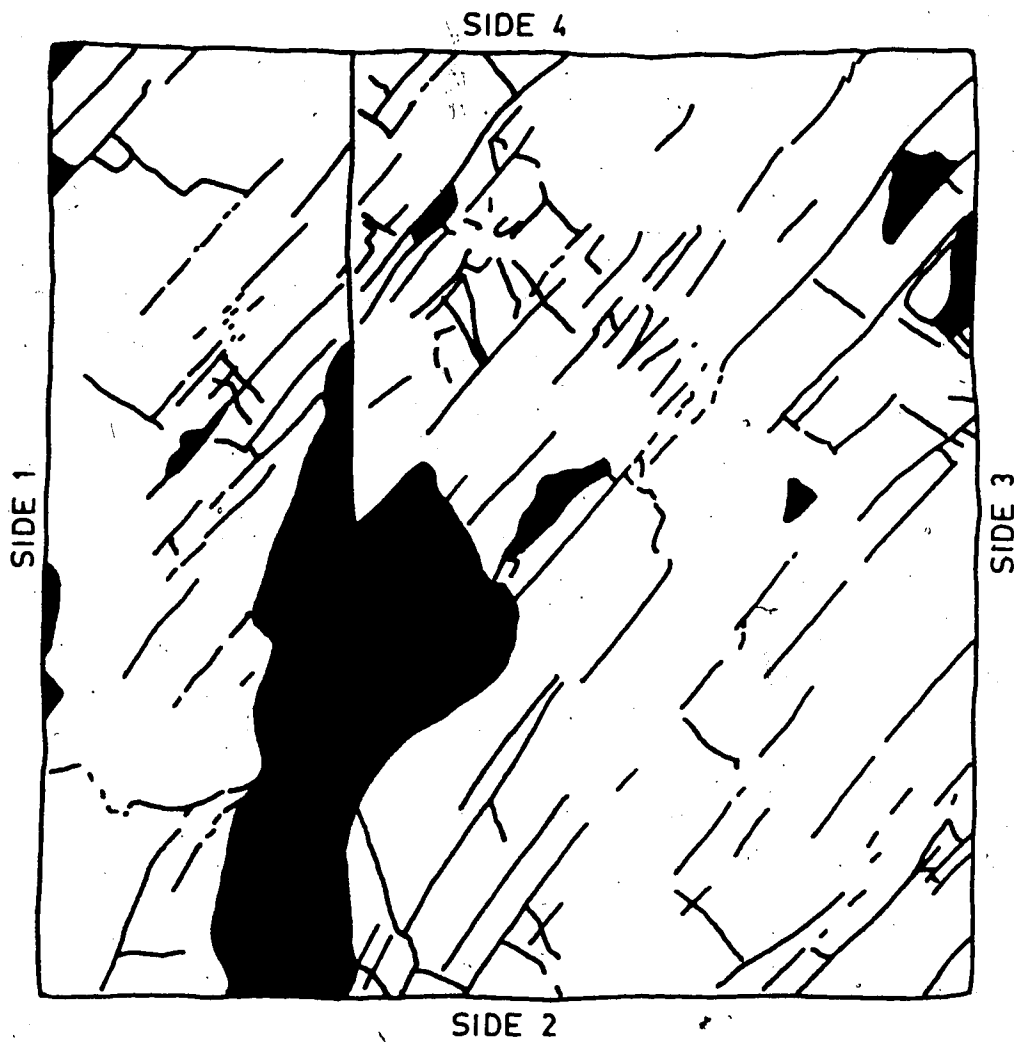


Figure 3.1 Plan View of the Top Surface of Sample MC-5

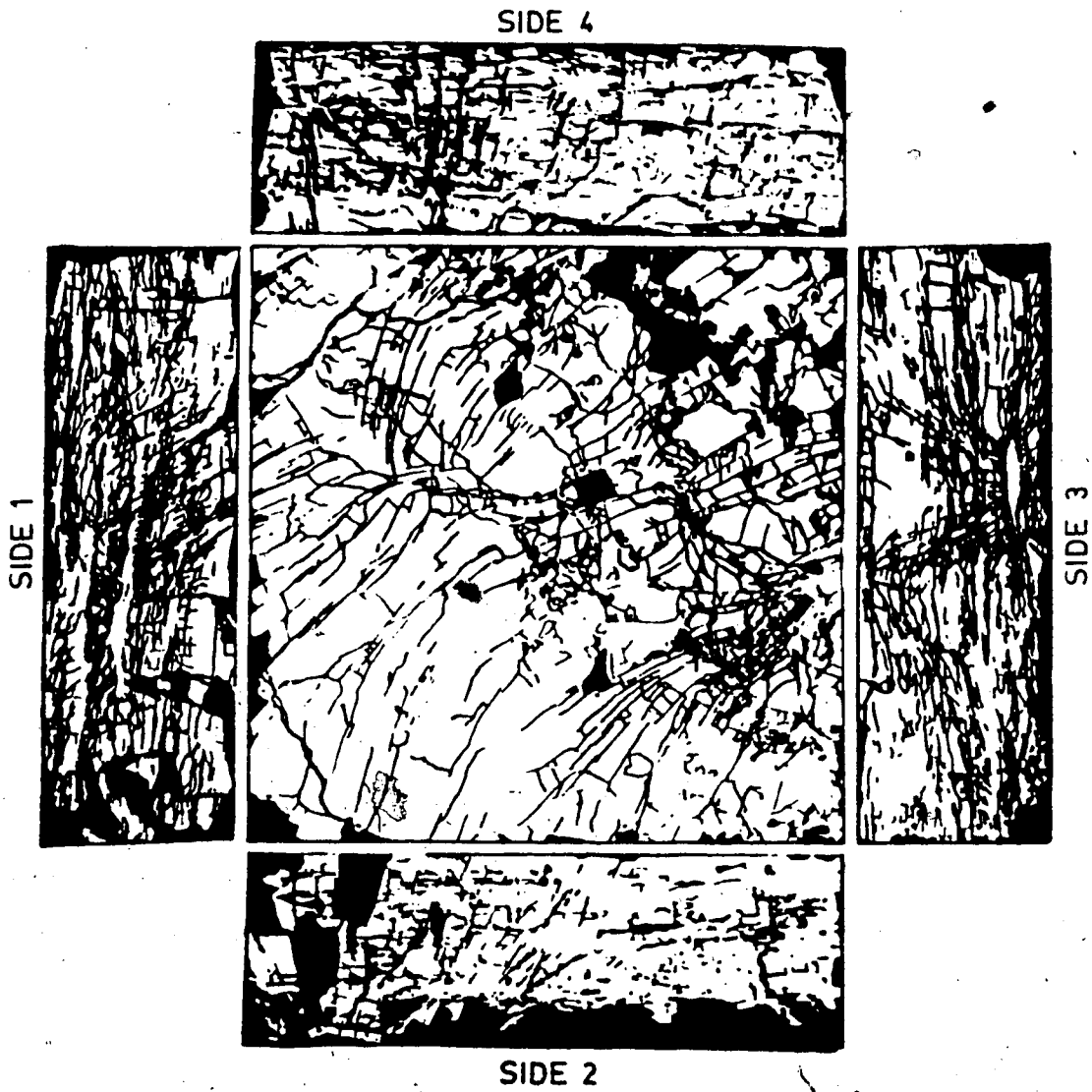


Figure 3.2 Plan Views of the Top and Side Surfaces of Sample MC-6

approximately 7.5° towards Side 1 and increased in width down dip. Jointing, which in the remainder of the sample was essentially vertical, inclined in the vicinity of the inclusion; the joints radiated from the inclusion. The inclusion had a dominant effect on the structure of the sample and will thus have a considerable influence on the sample performance. Side 2 and, to a lesser extent, Sides 1 and 3 required a high strength grout infilling of depressions caused by removal of loosened material. As these infillings were concentrated around the sample periphery, their effect on near tunnel performance should be negligible.

3.1.3.3 Sample MC-7

Sample MC-7 was prepared in the required manner to final dimensions of 625 x 625 x 212 mm. The major joint set was non-planar and non-uniform. The strike of this joint set, referenced to the major principal stress direction, varied from 20° to 70° with a mean value of approximately 40° . The dip angle varied from 70° to 90° . The joint spacing varied from 5 to 25 mm. Plan views of the top and side surfaces of this sample are presented in Figure 3.3.

3.2 Deformation Instrumentation

During the testing of a given specimen the following deformation measurements were recorded:

1. boundary displacements;
2. radial strain; and



Figure 3.3 Plan Views of the Top and Side Surfaces of Sample MC-7

3. tunnel closure.

The means by which these measurements were obtained are briefly described below. More detailed descriptions of the deformation monitoring instruments are presented by Kaiser (1979) and Guenot (1979).

3.2.1 Boundary Displacements

The boundary displacements in the principal stress directions were measured by displacements transducers (LVDTs) mounted on metal stands attached to the base plate of the specimen. In the lateral direction, the LVDT cores were spring forced against teflon discs fixed to steel pins grouted at an average depth of 35 mm into the specimen. These discs were located midway along the length of the sides at a height dependent upon the location of the radial extensometers.

In the longitudinal direction, displacements were measured by LVDTs located at each corner of the loading head. In addition, dial gauges were also located at each corner to provide quick visual monitoring during testing.

3.2.2 Radial Strain

The relative radial displacement was measured by LVDTs connected to extensometers located in small diameter drill holes adjacent to the tunnel. Each extensometer consisted of a coaxial rod and tube grouted at their ends in a hole within the rock mass as shown in Figure 3.4. The relative

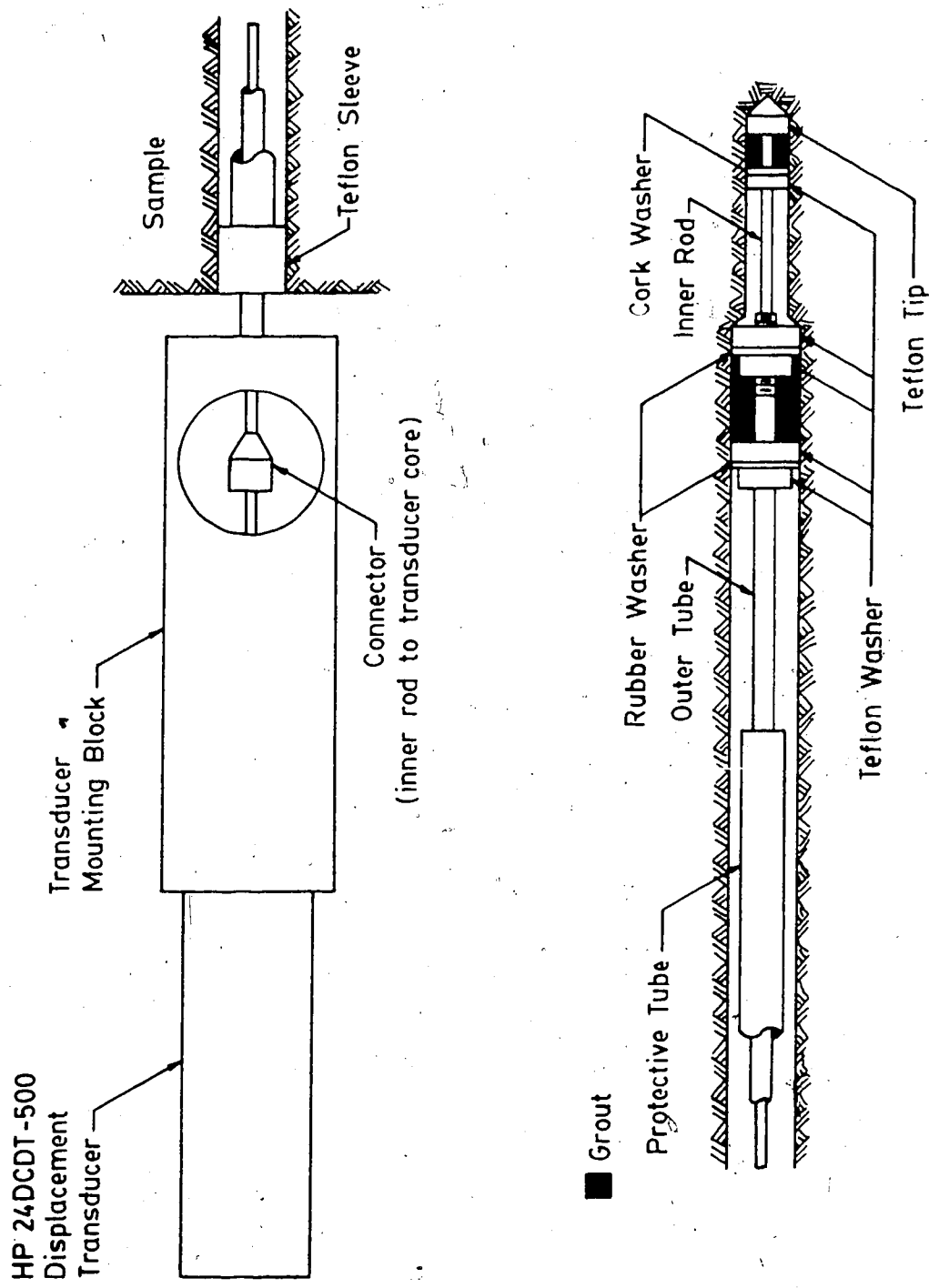


Figure 3.4 Typical Extensometer Set-up (to scale)

displacement of these two anchor points is measured by an LVDT fixed to the outer ends of the coaxial rods; the inner rod is fixed to the core and the outer tube to the body of the LVDT. The average radial strain for each extensometer was calculated as the relative displacement divided by the gauge length (ie. the length between anchor center points).

3.2.3 Tunnel Closure

Tunnel closure measurements (i.e., the ratio of the change in tunnel diameter to the original diameter) were made along four diameters spaced 25 mm apart along the tunnel axis and 45° apart in the plane perpendicular to the tunnel axis. Measurements were made by LVDTs mounted inside the tunnel on a stand secured to the sample base plate as shown in Figure 3.5. Two LVDTs are mounted on the same axis, their cores pressed to the tunnel wall by a spring, to measure the closure of opposite points on the tunnel wall.

3.2.4 Sample Instrumentation

Deformation measuring instruments within the sample are located by reference to a cylindrical coordinate system. The vertical axis corresponds with the tunnel axis and the polar axis with the principal field stress direction. The top surface of the specimen represents Station 0.0 on the tunnel axis. Station numbers correspond to the vertical distance from the top surface in millimetres. The mid point of the gauge length is used in locating radial extensometers.

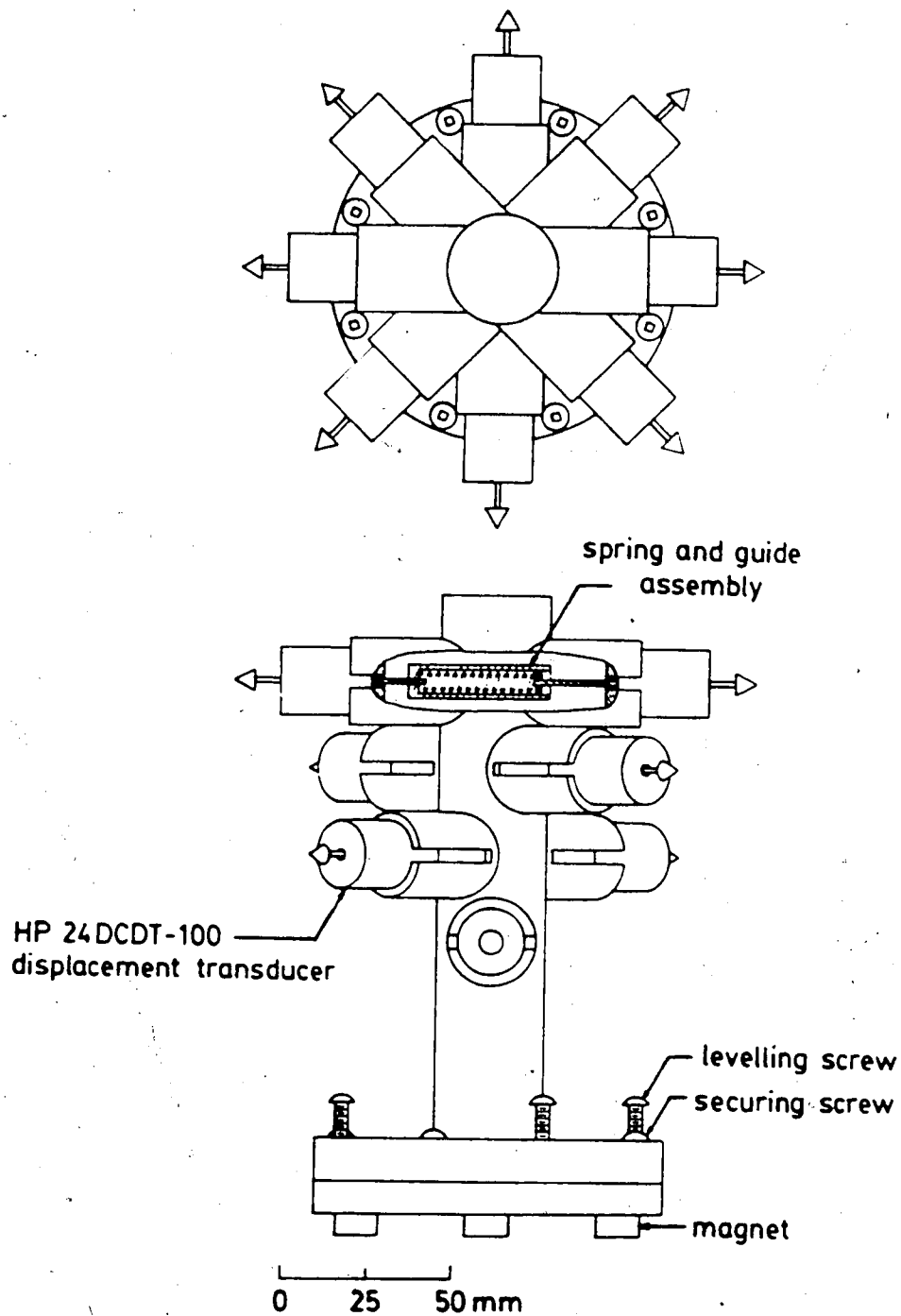


Figure 3.5 Tunnel Convergence Measurement Device (electrical wires omitted for clarity)

3.2.4.1 Sample MC-5

Plan and sectional views of the instrumentation layout employed in Sample MC-5 are presented in Figure 3.6.

Lateral boundary displacements were measured at a radius of approximately 270 mm from the tunnel axis at Station 142.5 (L1 to L4 on Figure 3.6).

Radial strain measurements were made by a total of 16 extensometers located in two rings concentric with the tunnel axis. The first ring (R1) was located at a radius of 103.6 ± 1.5 mm from the tunnel axis at Station 92.5 while the second ring (R2) was located at a radius of 140.9 ± 2.3 mm at Station 117.5. Average gauge lengths were 32 and 47 mm respectively.

For Tests MC-5.04 and MC-5.05 and from MC-5.10 on, tunnel closures parallel and perpendicular to the major joint set were measured at Station 120.6 and 44.4 respectively. Closures parallel and perpendicular to the major principal stress direction were measured at Stations 95.2 and 69.8 respectively. For tests MC-5.06 to MC5.09 closures parallel and perpendicular to the major joint set were measured at Stations 44.4 and 120.6 respectively while closures parallel and perpendicular to the major principal stress direction were measured at Stations 69.8 and 95.2 respectively.

3.2.4.2 Sample MC-6

Plan and sectional views of the instrumentation layout employed in Sample MC-6 are presented in Figure 3.7.

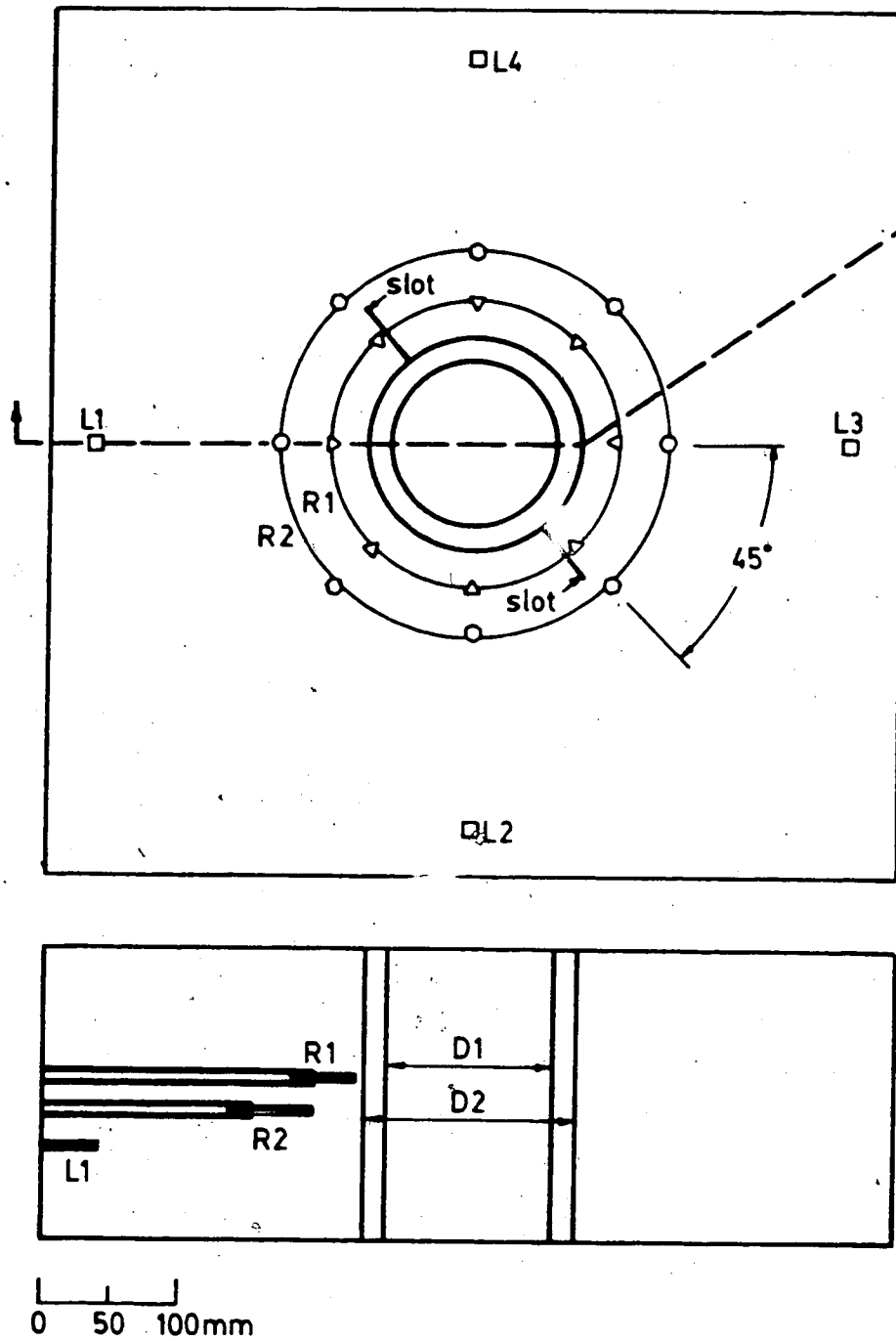
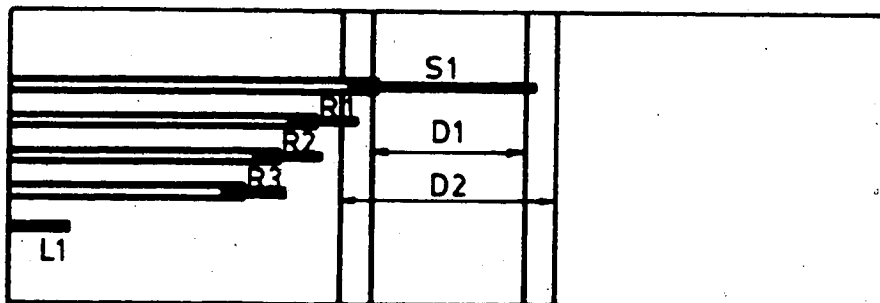
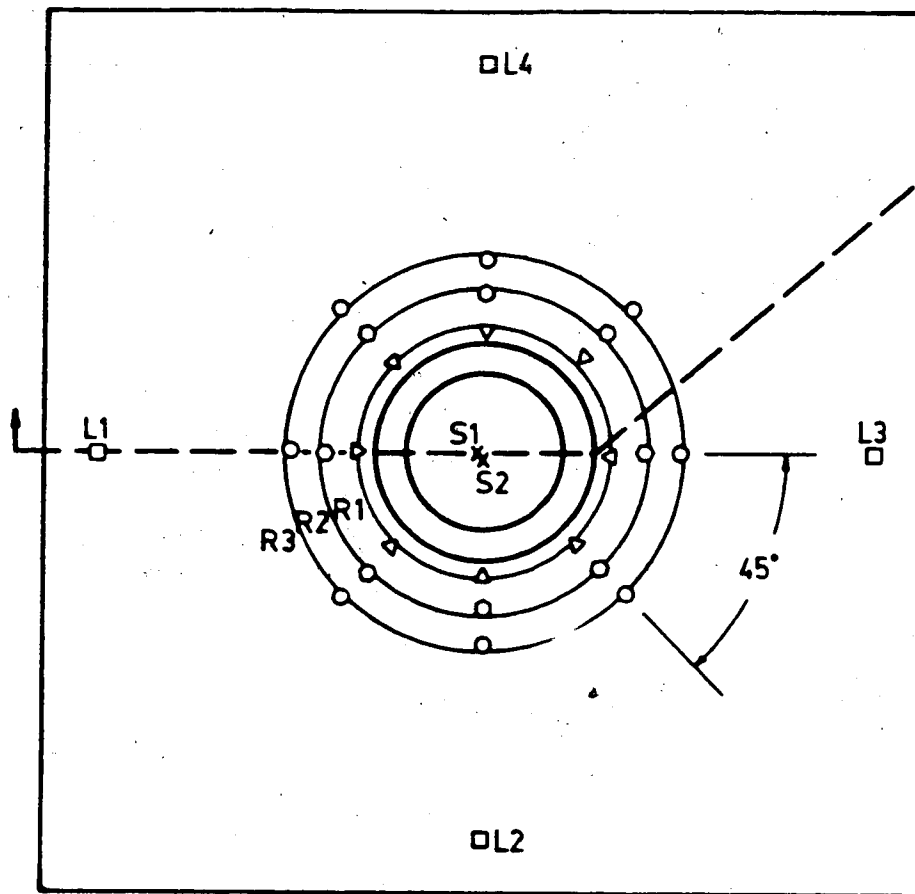


Figure 3.6 Internal Instrumentation Layout - Sample MC-5



0 50 100mm

Figure 3.7 Internal Instrumentation Layout - Sample MC-6

Lateral boundary displacements were measured at a radius of approximately 275 mm from the tunnel axis at Station 153.0 (L1 to L4 on Figure 3.7).

Radial strain measurements were made by a total of 24 extensometers located in three rings around the tunnel axis. The first ring (R1) of eight extensometers was located at a radius of 90.0 ± 2.7 mm at Station 78.0, the second ring (R2) at a radius of 115.3 ± 2.8 mm at Station 103.0, and the third ring (R3) at a radius of 139.9 ± 3.1 mm at Station 128.0. Average gauge lengths were 34, 33 and 33 mm respectively. Rings R1 and R2 were monitored through Test MC-6.04. From Test MC-6.05 on, rings R2 and R3 were monitored as ring R1 had been excavated during tunnel widening. Two special extensometers (S1 and S2) were installed at Stations 55.0 and 67.5 with gauge lengths corresponding to the initial tunnel diameter. These instruments were monitored until cut through during the drilling operation of Test MC-6.02.

Closure measurements were made at Stations 63.5 and 83.9 parallel and perpendicular to the major joint set and at Stations 114.3 and 38.1 parallel and perpendicular to the major principal stress direction for all tests.

3.2.4.3 Sample MC-7

Plan and sectional views of the instrumentation layout employed in Sample MC-7 are presented in Figure 3.8.

Lateral boundary displacements were measured at a radius of approximately 257 mm from the sample centre at Station 131 for Sides 1 and 4 (L1 and L4), at Station 181

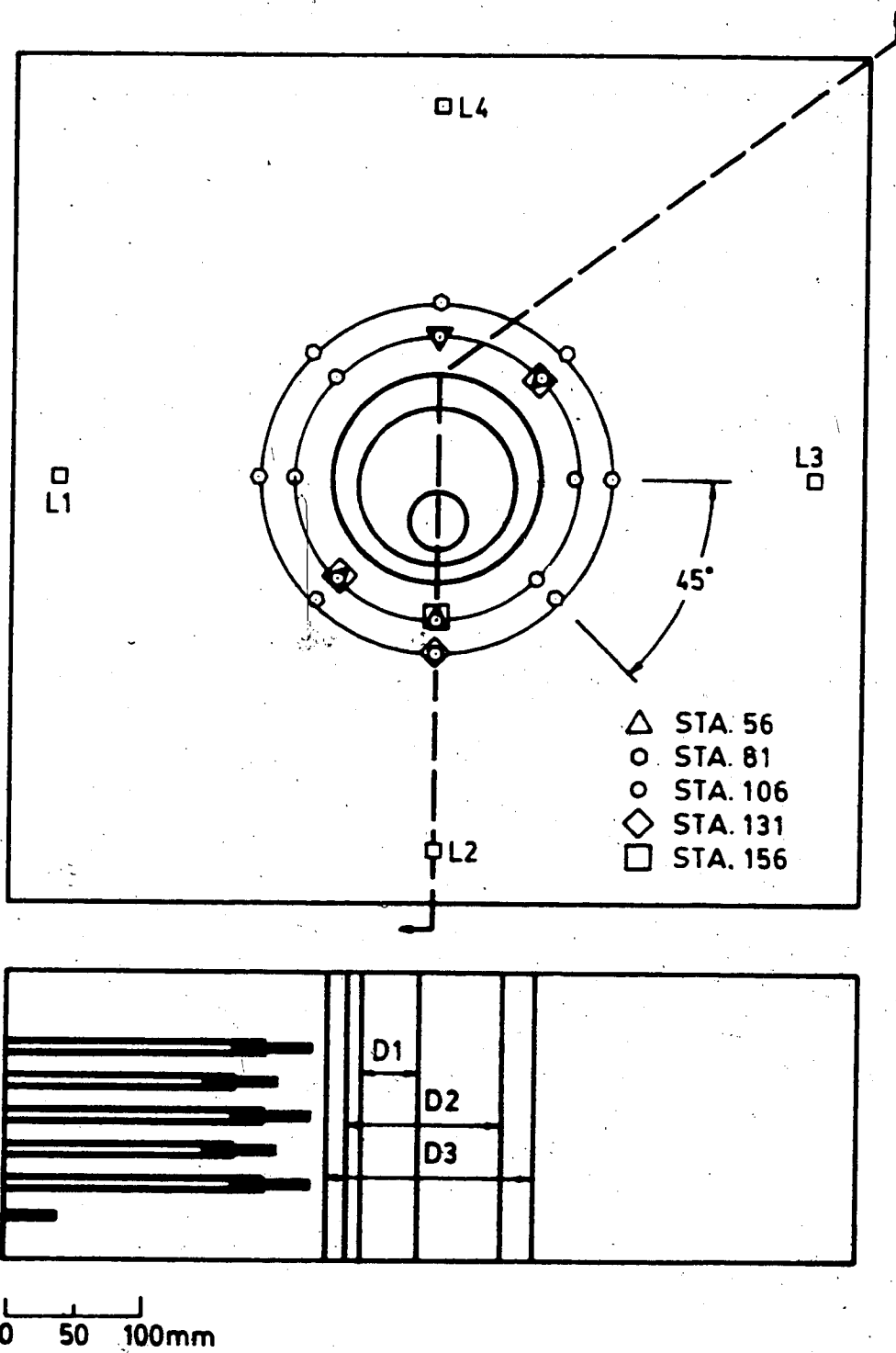


Figure 3.8 Internal Instrumentation Layout - Sample MC-7

for Side 2 (L2) and at Station 136 for Side 3 (L3).

Radial strain measurements were made by a total of 24 extensometers arranged in the following manner:

Station 56: $r = 104.1 \pm 1.2$ mm at orientations of $\theta = 45^\circ$, 90° , 225° and 270° ;

Station 81: $r = 128.6 \pm 3.0$ mm at 45° intervals from $\theta = 0^\circ$ to 315° inclusive;

Station 106: $r = 104.2 \pm 1.6$ mm at 45° intervals from $\theta = 0^\circ$ to 315° inclusive;

Station 131: $r = 128.0$ mm at an orientation of $\theta = 90^\circ$;
and

Station 156: $r = 103.7 \pm 1.9$ mm at orientations of $\theta = 45^\circ$, 90° and 225° ,

where r is the distance from the centre of the sample to the mid point of the gauge length. The average gauge length was 35 mm.

Tunnel closures parallel and perpendicular to the major joint set were measured at Stations 113 and 88 and parallel and perpendicular to the major principal stress direction at Stations 139 and 62 respectively from Test MC-7.10 on. Prior to this the opening was not of sufficient diameter to allow closure measurements.

3.3 Description of the Test Facility

The equipment and methodology employed in this test program are essentially the same as used by Kaiser (1979), Guenot (1979) and Sargent (1981) with the exception of the

tunnel excavation procedure. The test facility was designed by Kaiser based on a similar facility developed by Heuer and Hendron (1971). A detailed description of the test facility is presented by Kaiser and Morgenstern (1981a). Only a brief description is repeated here.

The test frame shown in Figure 3.9 was designed to permit long term testing of large specimens (up to approximately 600 x 600 x 200 mm) under plane strain conditions. In the lateral directions loads of up to 1300 kN are transferred from the hydraulic rams through load cells and load distribution triangles to the sample. Longitudinal expansion is nulled (thereby maintaining plane strain conditions) by applying load to the longitudinal loading head through 4 hydraulic rams. The hydraulic pressure system can maintain pressures over a period of several days with fluctuations of less than one percent.

The advancement of a tunnel under stress was performed by full face drilling of the tunnel employing the equipment shown in Figure 3.10. Tunnels were advanced using diamond bit core barrels attached to a heavy duty Milwaukee Dymodrill operating at 750 rpm. Air at 100 to 150 kPa was used to remove cuttings and to cool the bit. During the excavations performed on Sample MC-6 the drill was mechanically advanced. To provide better control over the rate of advance, the advance mechanism was fitted with a Drayton RQ motor and appropriate gearing prior to drilling of Sample MC-7. Reaction for the drill was provided by rigid

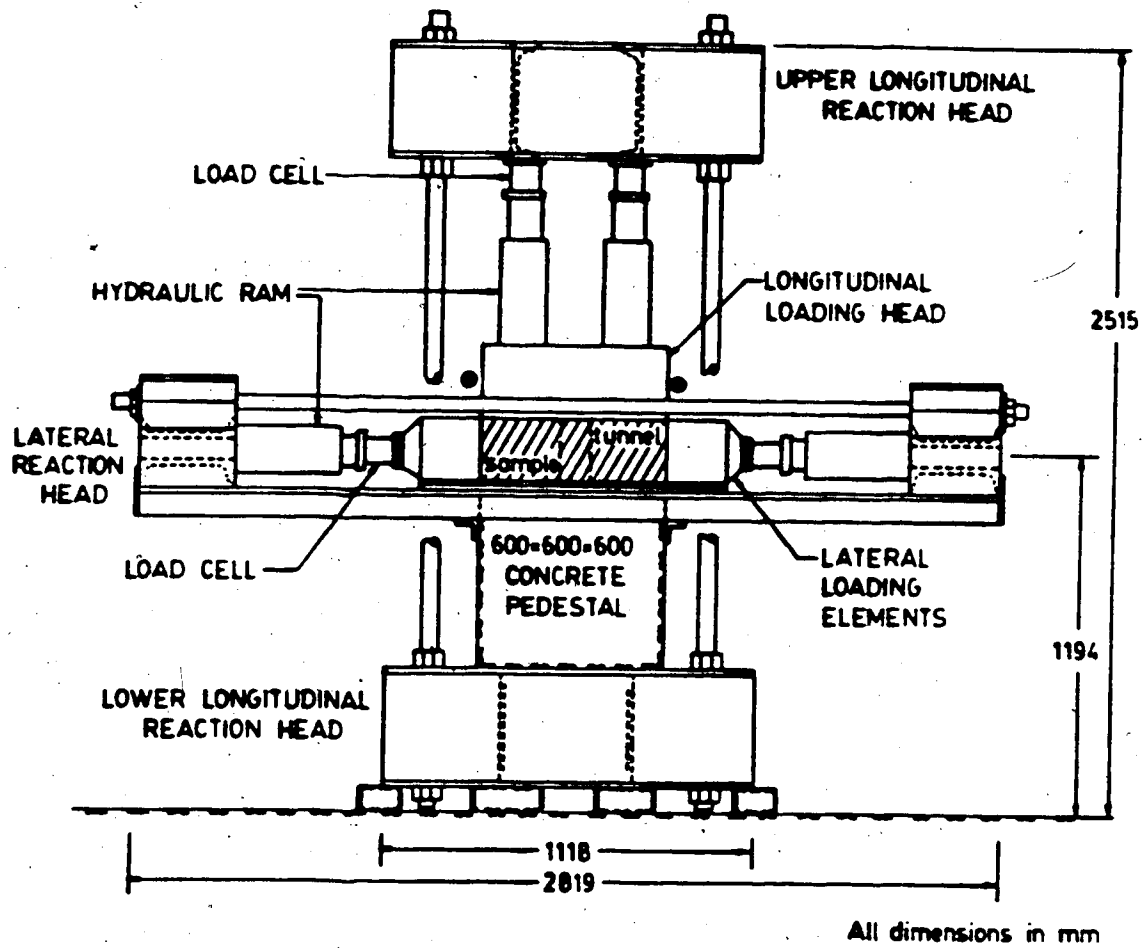


Figure 3.9 Side View of Test Frame

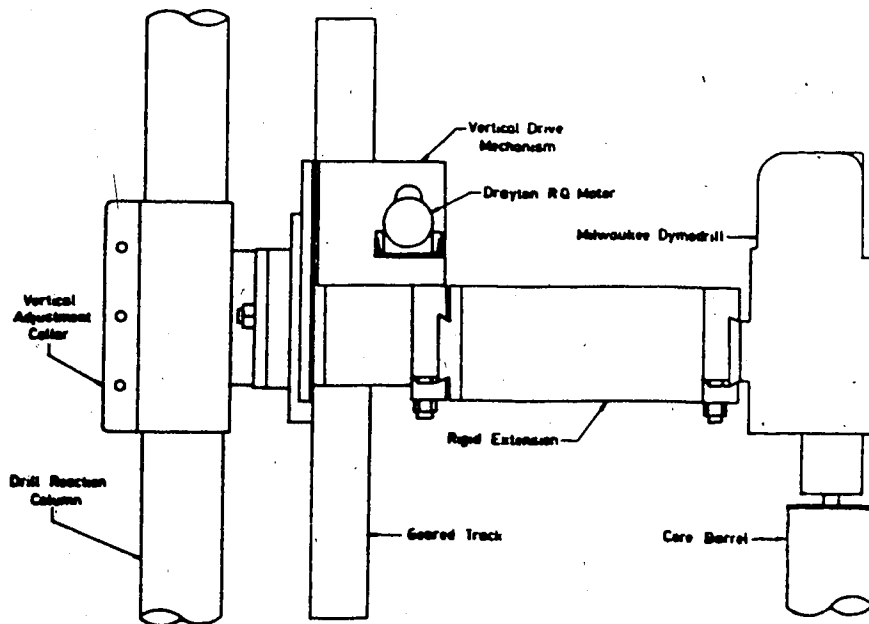
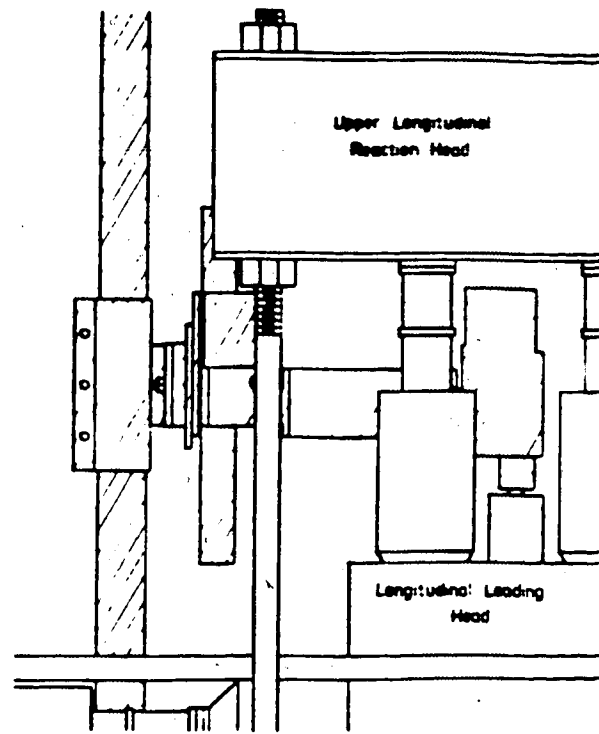


Figure 3.10 Tunnel Excavation Equipment

connections between the drill and support shaft which was in turn hydraulically jacked against the concrete ceiling. Industrial vacuum cleaners were employed to collect the dust from the drilling operations and to clean the excavation.

The data from all load cells and deformation recording devices are recorded automatically on magnetic tape and then transferred to the central computer. The data is then processed and the results plotted. The original test results are kept on file at the Department of Civil Engineering, Geotechnical Division, the University of Alberta by P.K. Kaiser.

3.4 Loading Sequence

The loading sequence of a given specimen consists of two distinct phases. During the first phase, a series of tests is performed on the intact specimen to determine the deformation properties of the material and their spatial distribution. In the second phase the behaviour of the loaded specimens during the excavation or widening of a tunnel or the response of the specimen containing a tunnel to a change in load is monitored.

The loading history of Samples MC-5, MC-6 and MC-7 are presented in Figures 3.11 to 3.13 respectively. In these figures the average vertical (i.e., major) field stress, the field stress ratio (ratio of horizontal to vertical field stress), the Poisson's ratio in the longitudinal direction (ratio of the stress in the longitudinal direction to the

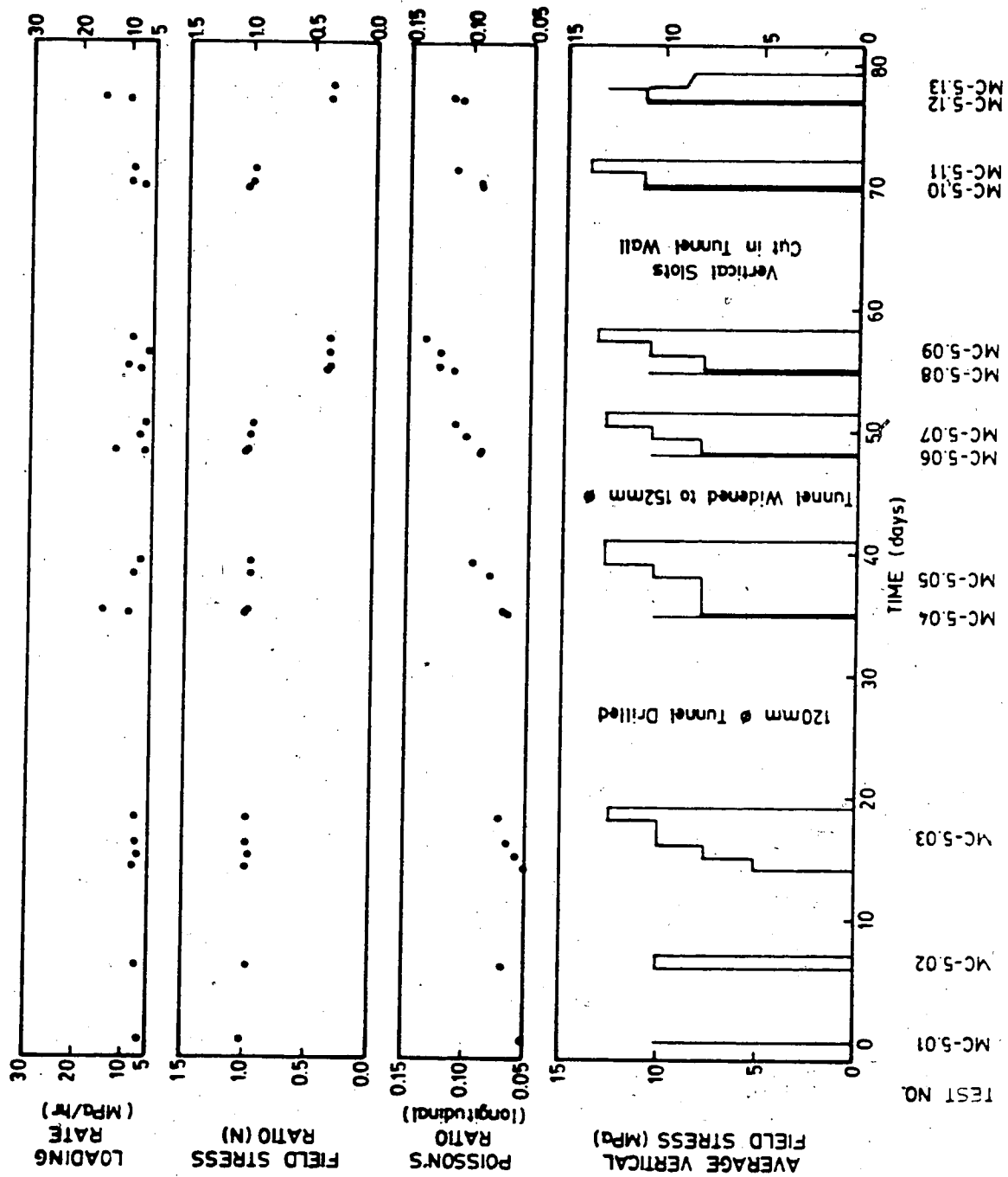


Figure 3.11 Loading History of Sample MC-5

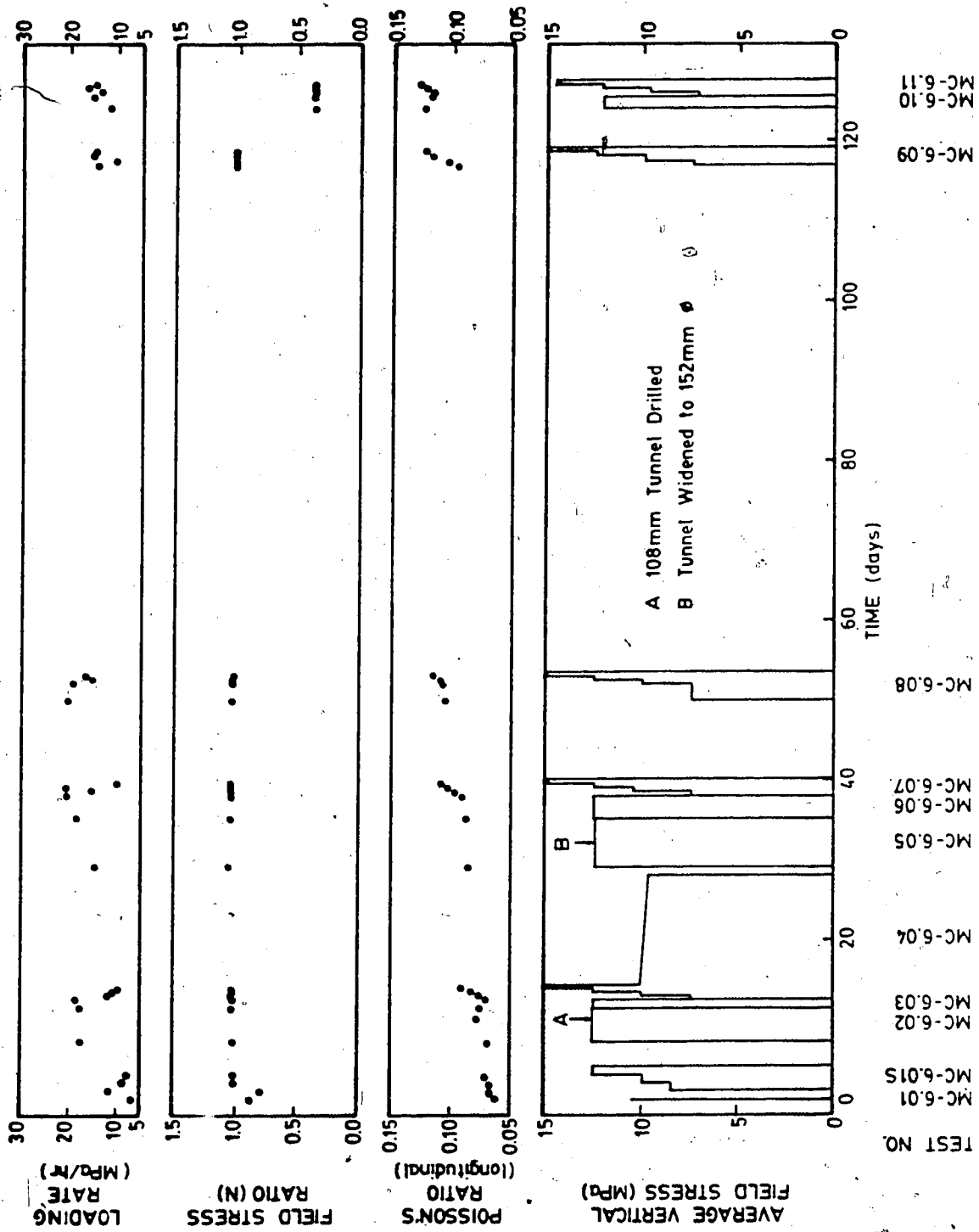


Figure 3.12 Loading History of Sample MC-6

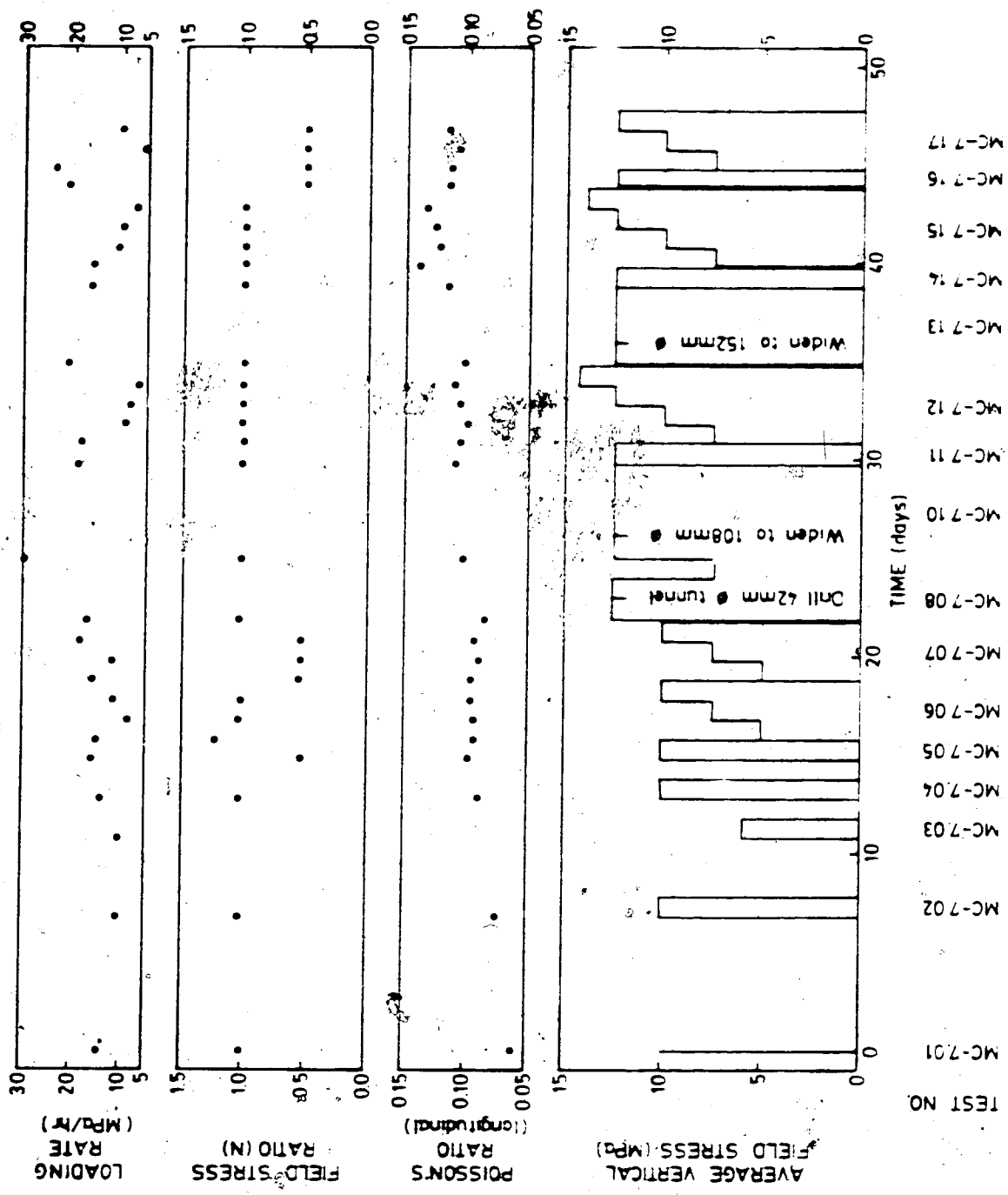


Figure 3.13 Loading History of Sample MC-7

sum of the other two stresses) and the loading rate during each single loading stage are given as functions of time.

4. DETERMINATION OF MATERIAL PROPERTIES

Coal is the product of the physical and chemical alteration of vegetal matter accumulated in low energy non-marine to mixed marine environments. Because of the depositional environment coals commonly include layers or lenses of sandstones, siltstones or shales. The coal itself contains a variety of plant tissue (macerals) in different stages of preservation. This heterogeneity of the coal material will therefore result in non-uniform responses to stress change and thereby complicate the selection of representative properties.

In the following sections the parameters were selected to describe the material property representing the average response; significant local deviations from this mean response were observed. This particular investigation was concerned with the deformation properties. The strength properties reported summarize the work of earlier investigators.

4.1 Strength Properties

Investigations of the strength of the coal were conducted by Noonan (1972), Kaiser (1979) and Guenet (1979). Both direct shear and triaxial compression tests were employed. The unconfined compression strength of the coal was found to lie between 8 and 12 MPa. A bi-linear Coulomb failure criterion best described the strength under a multi-axial stress state. At normal stresses below 1 MPa,

the strength parameters, c , the cohesion intercept, and ϕ , the angle of internal friction were approximately 0 MPa and 60-70° respectively. For normal stresses above 1 MPa, a cohesion intercept of 2-3 MPa and an angle of internal friction of 30° were found to best fit the experimental results. The cohesion intercept varied inversely with the continuity of jointing (i.e., the ratio of the area of the open joint surface to the total area of the plane containing the joint). The ultimate friction angle was found to be 30°.

The axial strain at the yield point was 0.1-0.2 % at confining stresses less than 1 MPa rising to 0.5 % at higher confining pressures. Axial failure strains varied from 0.5 to 1.6 % at low confining stresses. Under higher confinement failure strains up to 3.75 % were recorded. The strain values presented above were obtained from triaxial compression tests conducted at constant strain rates of 0.3 to 0.8 %/hr.

4.2 Deformation Properties

In order to ascertain the constitutive relationship between applied stress and resultant strain for this coal, a series of tests were performed on each sample prior to tunnel excavation. Parameters describing both the time-independent behavior and time-dependent deformation behavior were thus determined.

4.2.1 Time-Independent Behavior

The observed instantaneous or time-independent response of the intact sample to an applied increment of stress was typical of a fissured rock. The stress-strain curves showed an initial upward concavity at low stresses (below 3 MPa on average) becoming linear at higher stresses (maximum applied stress: 12.5 MPa). First loading produced appreciable strains as a result of joint and crack closure. Subsequent loadings produced significantly less straining and more repeatable stress-strain responses. These phenomena, as observed in the testing of Sample MC-7 are demonstrated in Figure 4.1.

Triaxial compression tests at confining pressures up to 10 MPa conducted by Kaiser (1979) and Guenot (1979) have shown that the coal is an elastic, brittle plastic material with a strain weakening stress-strain curve. Non-linearity, aside from the initial, is only observed at stresses approaching the peak strength of the coal or if the strain rate is changed. The linear portion of the stress-strain curve was employed in the determination of the elastic parameters.

In order to determine representative parameters, a procedure such as that outlined by Ko and Gerstle (1976) in which all the coefficients of the compliance matrix are determined, should be followed. However, such an investigation was beyond the scope of this research. In its place, the form of the constitutive elastic relationship was

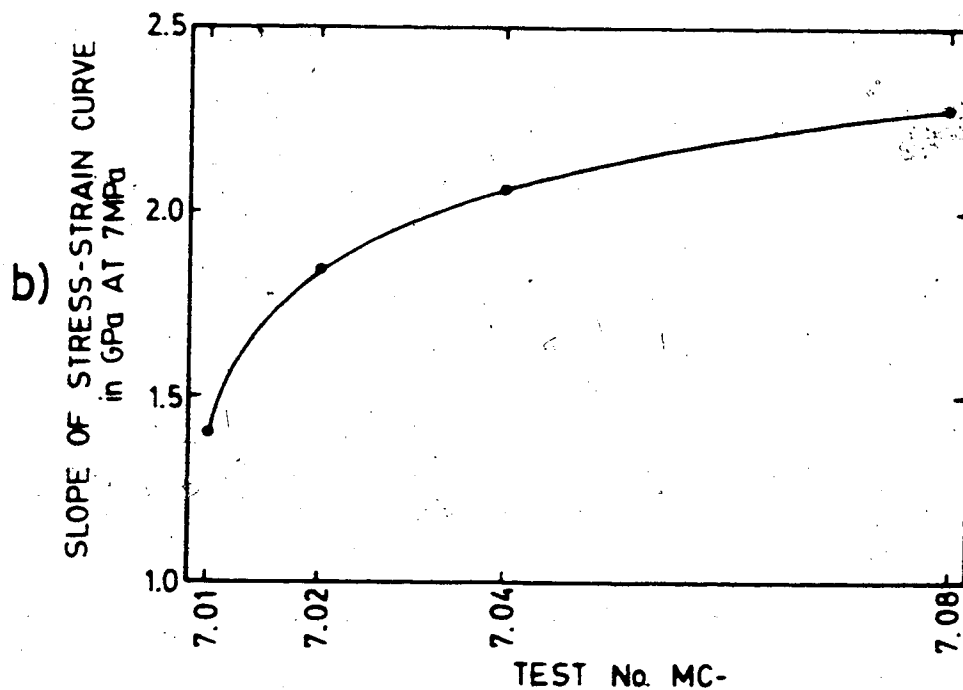
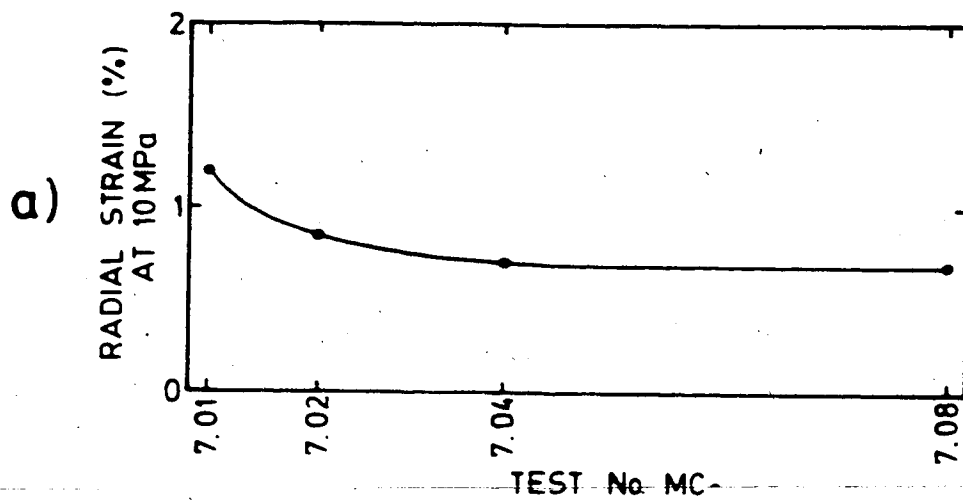


Figure 4.1 Average Extensometer Response During Hydrostatic (N=1) Loading of the Intact Specimen - Sample MC-7

inferred from the sample response and appropriate parameters determined.

The spatial arrangement of the radial extensometers allowed for the determination of any directional dependence of the deformation properties in the plane of bedding. Under conditions of equal lateral stress, no significant variation in extensometer response was observed in Samples MC-5 and MC-7 as shown in Table 4.1. Sample MC-6, however, demonstrated a marked orientation dependence being much stiffer in the $0^\circ - 180^\circ$ orientation. This higher stiffness was caused, most probably, by the clay-shale inclusion previously noted and as such did not reflect an inherent anisotropy in the bedding plane of the coal. Hence, for the purposes of this research, it was decided to consider the sample to be isotropic in the plane of bedding. This allowed simplification of the analysis of the time-independent response to isotropic or transverse-isotropic elastic formulations.

4.2.2 Material Properties for Isotropic Elastic Formulation

Describing the linear elastic, isotropic behavior of the coal required the determination of two parameters: Young's modulus, E , and Poisson's ratio, ν . Formulae for their determination are presented in Appendix A.

Figure 4.2 shows the spatial distribution of Young's modulus, normalized to the mean value, as determined by Method 1 of Appendix A at a field stress of 7 MPa for

Table 4.1 Orientation Dependence of Extensometer Response

ORIENTATION	SLOPE RATIO(1)		
	Test MC-5.03(2)	Test MC-6.02(3)	Test MC-7.08(3)
0 - 180	0.99	1.81	0.97
45 - 225	1.07	0.81	1.03
90 - 270	1.05	0.63	0.94
135 - 315	0.89	0.75	1.11

- (1) Average slope of stress-strain curve for that orientation divided by the average slope of all orientations
- (2) Slopes determined from linear regression of stress-strain coordinates at the beginning of each creep stage in multi-stage creep tests
- (3) Slopes determined from tangent to stress-strain curves at a field stress of 7 MPa

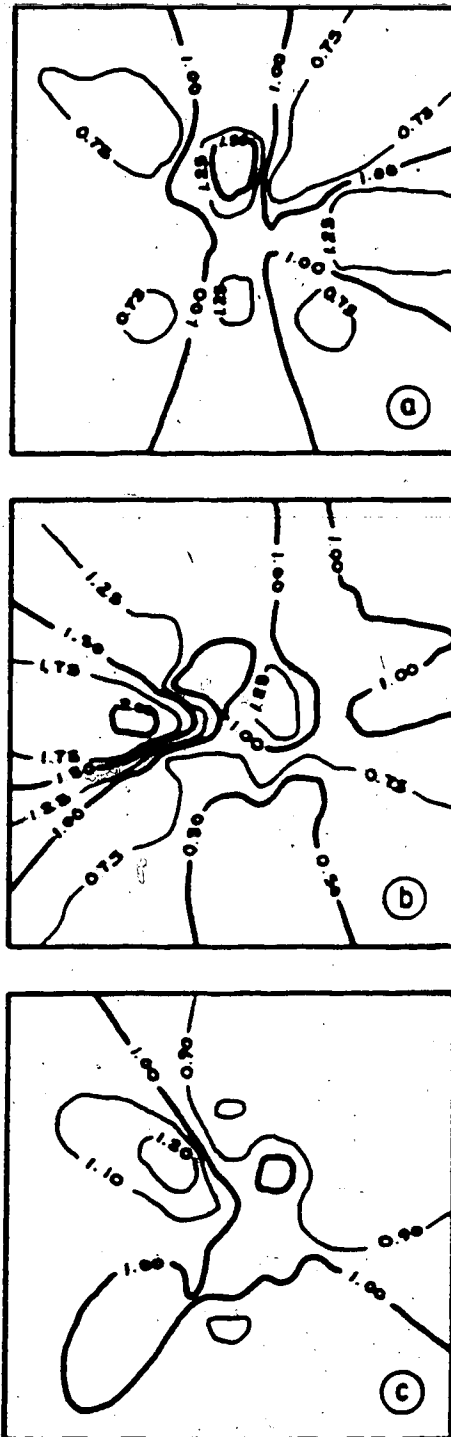


Figure 4.2 Spatial Distribution of Young's Modulus :
a) Sample MC-5 b) Sample MC-6 and c) Sample MC-7

Samples MC-5 to MC-7. Mean values for Young's modulus and Poisson's ratio for these specimens were 1.73 GPa, 0.34, 1.40 GPa, 0.29 and 1.50 GPa, 0.23 respectively. Application of Method 2 to Sample MC-7 (only intact specimen tested at different N values) yielded values of Young's modulus and Poisson's ratio of 1.46 GPa and 0.23 which were very similar to those obtained by Method 1. The spatial variation in deformation properties can be related to material heterogeneities as mentioned previously.

The shape of the stress-strain curve and hence the derived elastic parameters depends, under isothermal conditions, on the combined effects of stress level and loading rate. In an attempt to ascertain the relative influence of the stress level, the elastic parameters were determined at stress increments of 1 MPa from an initial value of 3 MPa.

Figures 4.3 to 4.5 show the mean and range of values for the elastic parameters determined by Method 1 for Samples MC-5 to MC-7 respectively. All specimens exhibit an increase in Poisson's ratio with increased stress. This phenomenon may be associated with widening of the joint space [Lama and Vutukuri (1978)] or dilatancy [Goodman and Dubois (1972)]. The opposite effect was noted when Method 2 was applied for Sample MC-7 as shown in Figure 4.6. The effects of joint spacing and dilatancy are more suppressed during testing of an intact specimen. Increased stress may result in compression of the pores and increased crack

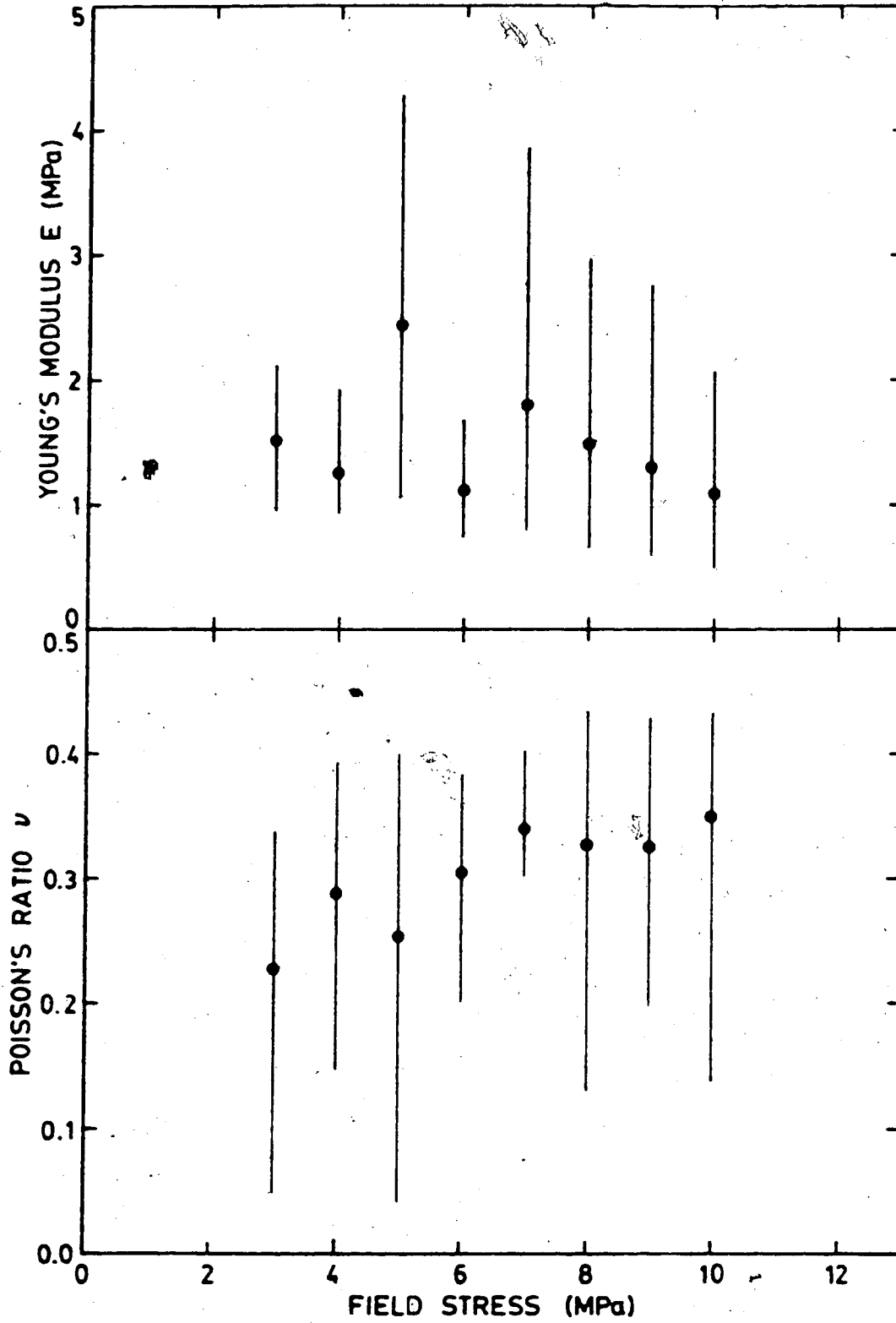


Figure 4.3 Variation in Elastic Parameters with Stress -
Sample MC-5, Method 1

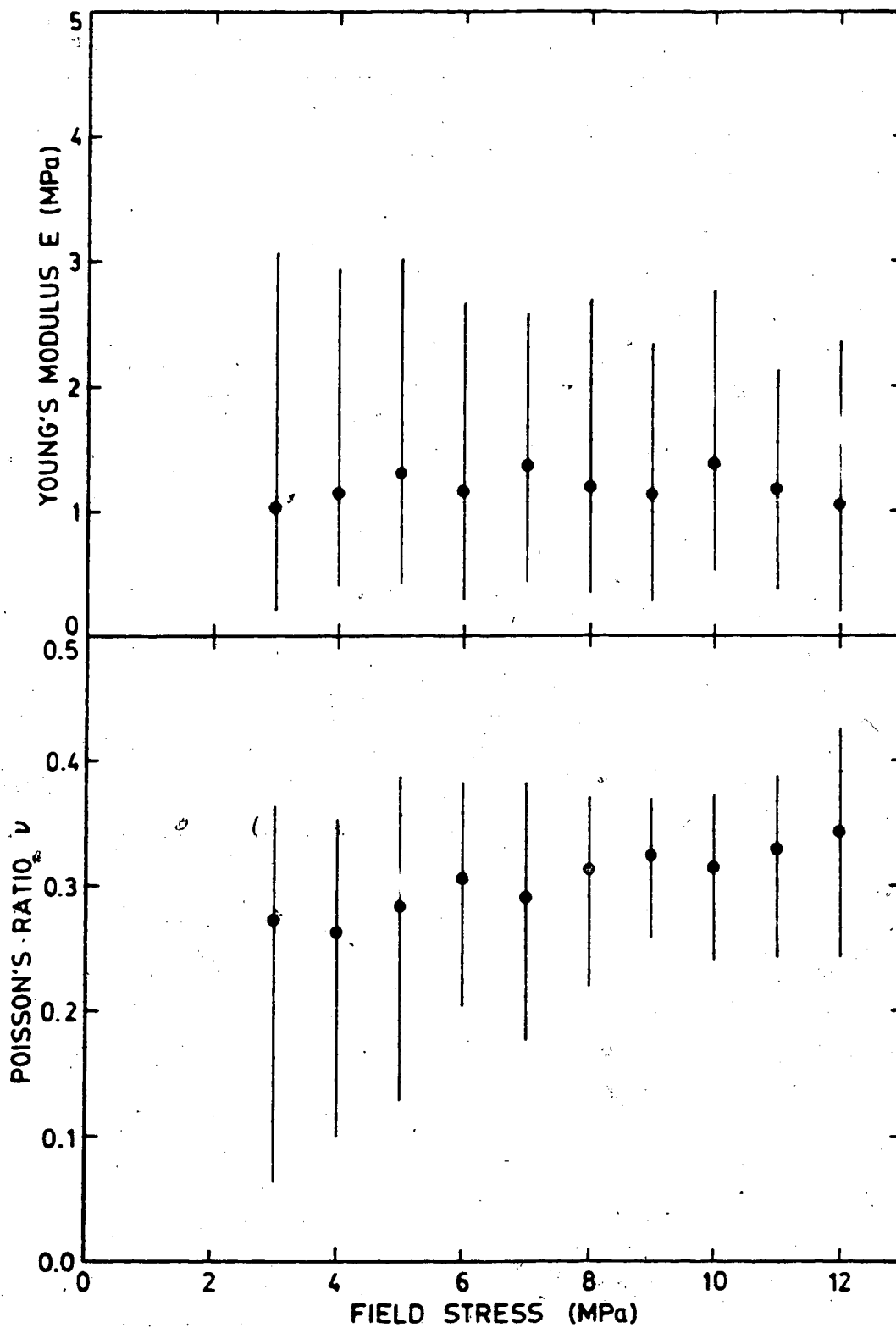


Figure 4.4 Variation in Elastic Parameters with Stress - Sample MC-6, Method 1

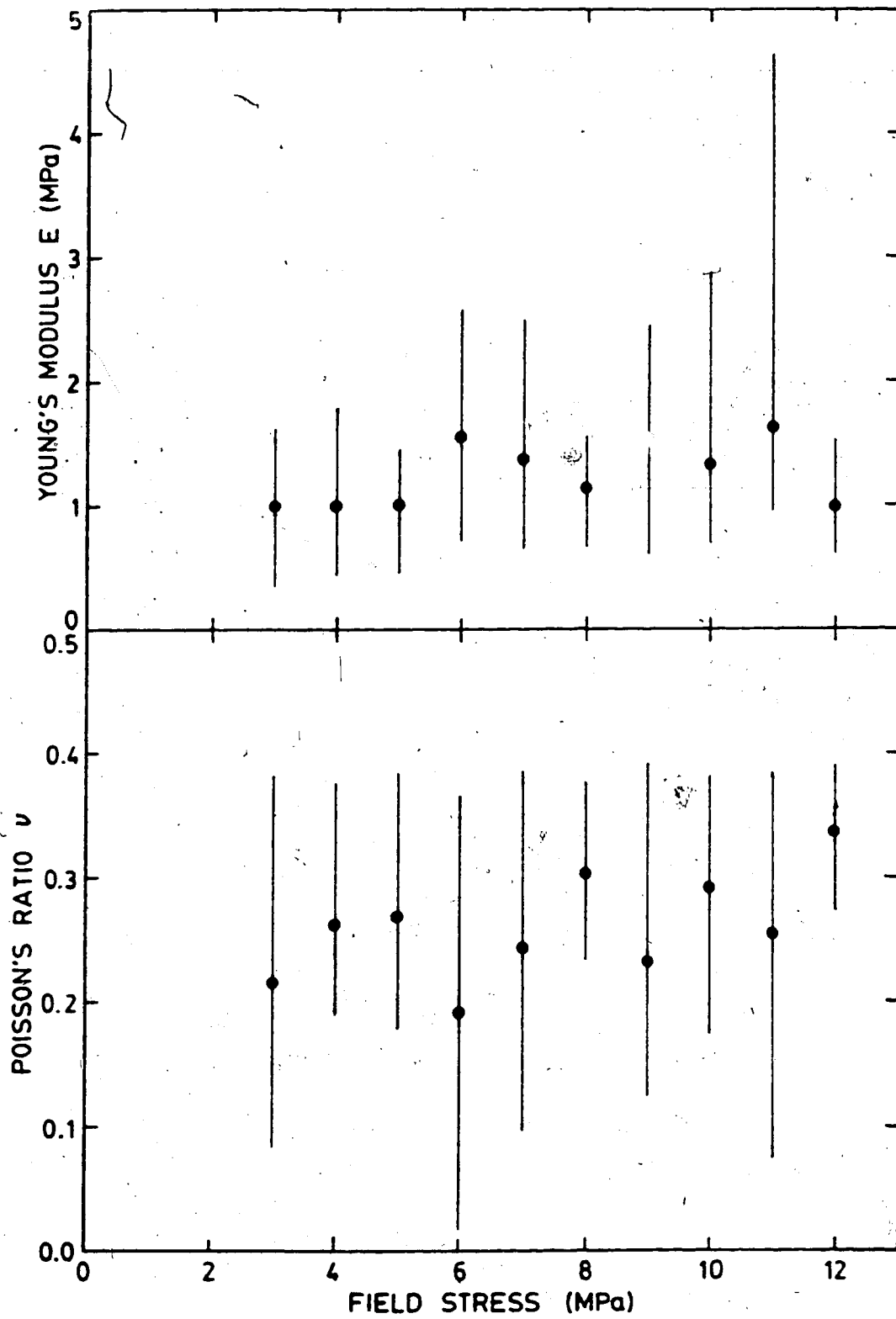


Figure 4.5 Variation in Elastic Parameters with Stress -
Sample MC-7, Method 1

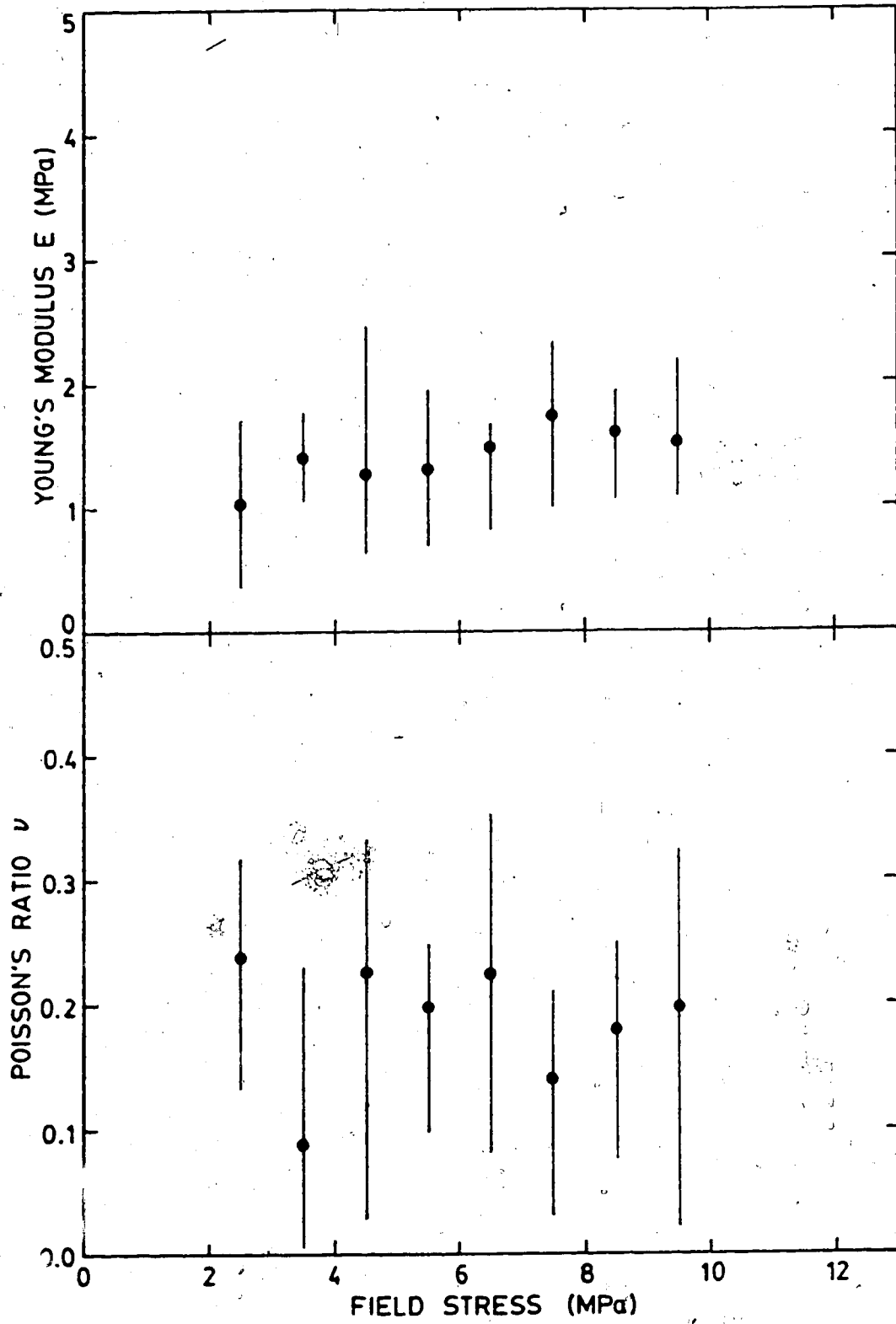


Figure 4.6 Variation in Elastic Parameters with Stress - Sample MC-7, Method 2

closure thereby resulting in the lower values for Poisson's ratio noted.

The influence of stress level on Poisson's ratio is inconsistent. Sample MC-5 (Figure 4.3) exhibited a decrease in modulus with increasing stress while Samples MC-6 and MC-7 (Figures 4.4 and 4.5) exhibited little change (employing Method 1). Application of Method 2 to the results from Sample MC-7 showed a direct correlation between modulus and stress as would normally be expected (Figure 4.6).

While the results of this investigation regarding the influence of stress level on the elastic parameters are somewhat inconclusive it is most probable that the effects observed in Figure 4.6 are representative. This is due to the uncertainty of the assumed elastic stress distribution around the opening in Figures 4.3 to 4.5. Yielding of the near tunnel material, a distinct possibility, will certainly also influence the results presented in these figures.

Results from investigations of the time-dependent response of the coal have shown that the magnitude of the creep rate increases rapidly at high stress levels (see Section 4.2.2). Mechanical constraints as well as test requirements restrict stress application to a maximum of approximately 0.005 MPa/sec. This is significantly below the rate of 0.07 - 0.7 MPa/sec commonly applied in static testing [Obert and Duvall (1967)]. Because of this slow loading rate, the strains recorded at higher stress levels will have increasing creep components which can result in a

non-linear, concave downwards stress-strain curve. This in turn results in reduced values of Young's modulus and possibly an increase in Poisson's ratio as the ratio of lateral to longitudinal creep strains may be greater than the ratio of elastic strains. Quantification of this effect was not possible given the test constraints, however, it is not expected to be any more significant than that due to the stress level for the given rate of stress application.

The effects of loading rate and stress level upon the elastic properties of the coal are to a certain extent counterbalancing. It is therefore probable that the parameters presented are representative of the material. This assumption is verified by two observations:

1. The sample to sample variation in material properties is of the same order as those effects due to stress level and loading rate.
2. The parameters determined for this coal are similar to those determined by others for various coals using standard methods (see Table 4.2).

Based on the above results, it may be concluded that under the assumption of linear elastic, isotropic behaviour, the coal has a Young's modulus of approximately 1.6 GPa and a Poisson's ratio of 0.3. However, in the longitudinal direction the stress required to maintain plane strain conditions is much less than predicted based on these parameters. For this reason, a linear elastic, transverse isotropic formulation is more probable.

Table 4.2 Elastic Properties of Coal

COAL NO.	ELASTIC FORMULATION	YOUNG'S MODULUS			POISSON'S RATIO						SHEAR MODULUS		
		E _x	E _y	E _z	xy	yx	xz	zx	yz	zy	yz	xz	xy
1	Transverse	13.3		6.6	0.03		0.68	0.31			3.96		6.46
	Transverse	8.7		4.8	0.10		0.65	0.34			2.62		3.97
	Transverse	5.7		4.9	0.33		0.41	0.35			1.90		2.14
	Isotropic	5.2			0.34						1.93		
	Isotropic	4.6			0.35						1.72		
	Isotropic	4.5			0.34						1.68		
	Isotropic	5.3			0.35						1.96		
	Isotropic	4.5			0.34						1.67		
2	Transverse	4.0		3.3	0.26		0.43	0.35			1.36		
3	Transverse	4.1		3.8	0.37		0.44	0.41					1.8
4	Transverse	4.4		4.6	0.44		0.50	0.48					
5	Transverse	3.4		2.7									
6	Transverse	4.0		3.8									
7	Isotropic	4.6			0.41								
	Isotropic	4.9			0.43								
8	Isotropic	6.1			0.29								
9	Isotropic	4.6			0.35								
10	Isotropic	5.0			0.22								
11	Isotropic	4.3			0.21								
12	Isotropic	4.4			0.25								
13	Isotropic	2.9			0.29								
14	Orthotropic	3.2	3.2	2.6	0.34	0.33	0.53	0.42	0.37	0.34	0.67	0.33	0.77
15	Orthotropic	2.7	2.7	2.8	0.33	0.29	0.58	0.28	0.37	0.27	0.56	0.65	0.58
16	Orthotropic	2.4	2.4	2.4	0.43	0.38	0.36	0.17	0.27	0.22	1.00	0.85	1.00
17	Orthotropic	3.0	3.8	4.7	0.25	0.40	0.30	0.44	0.38	0.41	0.93	0.87	0.70
18	Orthotropic	3.5	3.1	2.9	0.27	0.30	0.33	0.27	0.30	0.27	0.78	0.87	0.74

NOTE: ALL MODULI IN GPa

- 1 Dynamic, plane parallel plates 5x40 mm in X-section. Terms 3 to 8, 10 and 11 Coalification Series of Vitrain Schuyer et al (1954)
- 2 Dynamic; 3.2x3.2x20-30 mm, Barnsley Hards, Morgans & Terry (1958)
- 3 Static, 12.7 mm cube, Barnsley Hards, Morgans & Terry (1958)
- 4 Static, 12.7 mm cube, Anthracite, Morgans & Terry (1958)
- 5 Static, 38.1 mm cube, Barnsley Hards, Morgans & Terry (1958)
- 6 Static, 38.1 mm cube, Anthracite, Morgans & Terry (1958)
- 7 Static, 25 mm dia. core, Bieniawski (1967)
- 8 Static, 41 mm dia. core, Bieniawski (1967)
- 9 Static, 50 mm cube, Bieniawski (1967)
- 10 Static, 600x600x600-1200 mm, Bieniawski (1967)
- 11 Static, 900x900x600-900 mm, Bieniawski (1967)
- 12 Static, 1200x1200x600-1200 mm, Bieniawski (1967)
- 13 Static, 1500x1500x600-1500 mm, Bieniawski (1967)
- 14 Static, 100 mm cube, Pittsburg, Hawk & Ko (1980)
- 15 Static, 100 mm cube, Old Ben, Hawk & Ko (1980)
- 16 Static, 100 mm cube, York Canyon, Hawk & Ko (1980)
- 17 Static, 100 mm cube, Beehive, Hawk & Ko (1980)
- 18 Static, 100 mm cube, Paonia, Hawk & Ko (1980)

4.2.3 Material Properties for Transverse Isotropic Formulation

A total of five parameters are required to fully describe the linear elastic, transverse isotropic behaviour of a material:

1. Young's modulus in the plane of isotropy (E_z);
2. Young's modulus normal to the plane of isotropy (E_r);
3. Poisson's ratio relating strains in the plane of isotropy (ν_{rz});
4. Poisson's ratio relating the strain in the plane of isotropy to the strain normal to it (ν_{zr});
5. Shear modulus relating shear stresses to shear strains out of the plane of isotropy (G_{rz}).

The full constitutive relationship and the method of determining the five constants are presented in Appendix A. Data sufficient for the determination of these parameters was only available from the results of the tests performed on Sample MC-7.

A hydrostatic compression test (all three principal stresses equal; Test MC-7.03) enabled determination of E_z as 0.314 GPa. This most probably constitutes a lower bound for this modulus because it was essentially an initial loading modulus. The reloading modulus could be significantly higher, as previously demonstrated (see Figure 4.1). Poisson's ratio relating the in-plane strain to the normal strain, ν_{zr} , was found to be 0.082 ± 0.015 . The above two values were then employed to calculate the remaining constants presented in

Table 4.3. Insufficient data was available to enable calculation of G .

Finite element simulation of a tunnel in a medium with the above properties (assumed shear modulus equivalent to that in an isotropic medium) has shown that under plane strain conditions, the stresses and displacements around the opening are not significantly different from those in an isotropic medium with the properties as given in the previous section. For this reason, subsequent analyses of test results assume linear elastic, isotropic behavior.

4.2.4 Time-Dependent Behavior

The time-dependent deformation of a material under a constant stress (creep) is a major engineering concern, particularly in underground works. In order to address this concern it is necessary to determine 'a priori' the time-dependent behaviour of the material. This is very difficult as the long term response of the material may not be predictable from the short term laboratory response.

An idealized strain versus time curve for a material with time dependent strength and deformation properties at a constant stress is shown in Figure 4.7. This curve can be divided into four regions:

1. Elastic response of medium to change in stress;
2. Primary creep stage characterized by a continual decrease in the rate of straining;
3. Secondary creep stage characterized by a constant strain

Table 4.3 Parameters from Linear Elastic, Transverse Isotropic Formulation

Tests Employed	Poisson's Ratio		Young's Modulus Er
	ν_{re}	ν_{rz}	
7.02 & 7.05	0.226	0.352	1.416
7.04 & 7.05	0.260	0.361	1.486
7.08 & 7.05	0.332	0.368	1.541
7.06 & 7.07	0.269	0.372	1.567

$$\nu_{zr} = 0.082$$

$$E_z = 0.314 \text{ GPa}$$

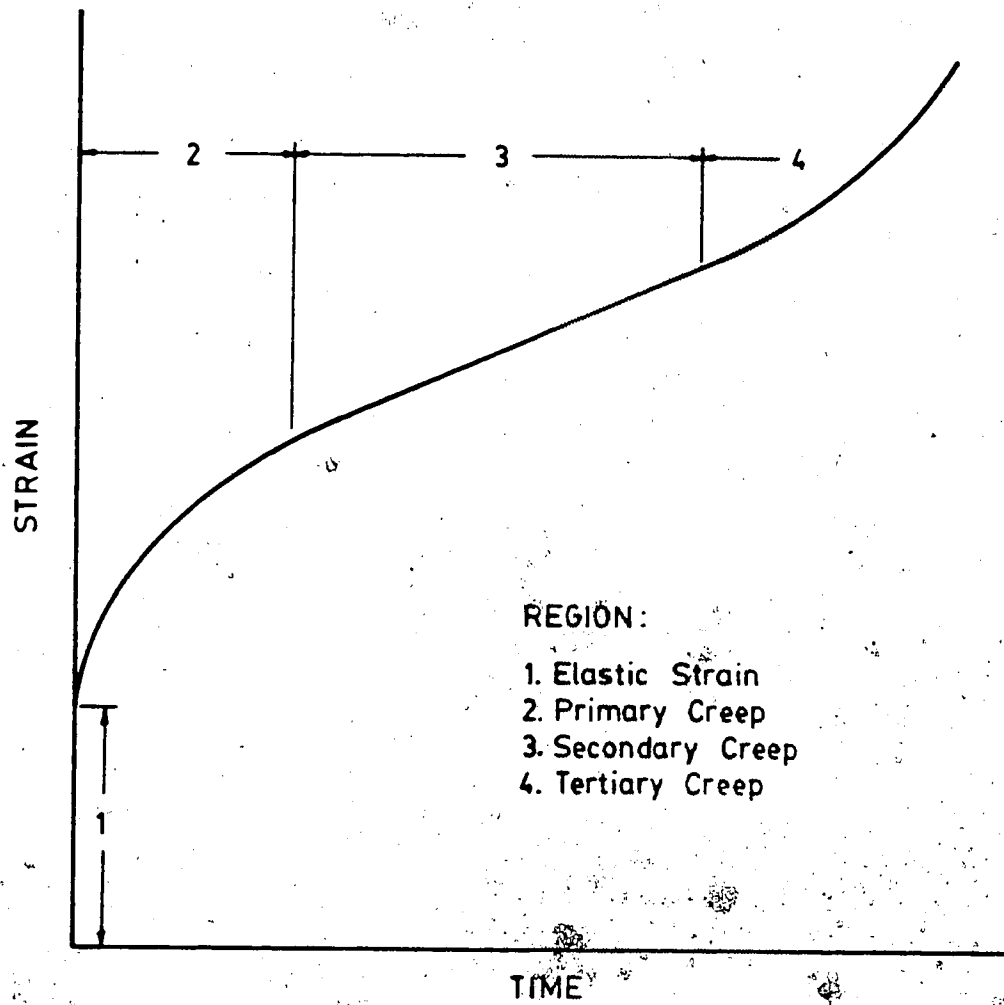


Figure 4.7 Development of Strain with Time

rate. This secondary creep stage may be very short in duration or may not exist at all in a brittle rock like coal; and

4. Tertiary creep stage characterized by an increasing strain rate resulting in the ultimate failure of the specimen.

The same three creep stages (Regions 2 - 4) as characterized above are also shown in a double logarithmic diagram of strain rate versus time in Figure 4.8. The primary and tertiary creep stages are shown as linear, however, this need not be the case.

In order to define the creep response of the material in a simple manner, an empirical approach, based upon curve fitting of experimental data, is generally employed. In most rock engineering problems the applied loads are sufficiently low that the tertiary stage doesn't develop and hence, is neglected [Schwartz and Kolluru (1987)]. The existence of a secondary creep stage has not been rigorously proven [da Fontoura (1980)], although recent studies by Tocher and Ko (1980) on coal have shown that a region of constant strain rate is achieved after approximately 2000 hours. No evidence of a secondary creep stage was found for the coal of this study under testing of up to 120 hours duration [da Fontoura and Morgenstern (1981)]. As no testing performed during this study was of longer duration expressions for the primary creep of this coal will be sufficient.

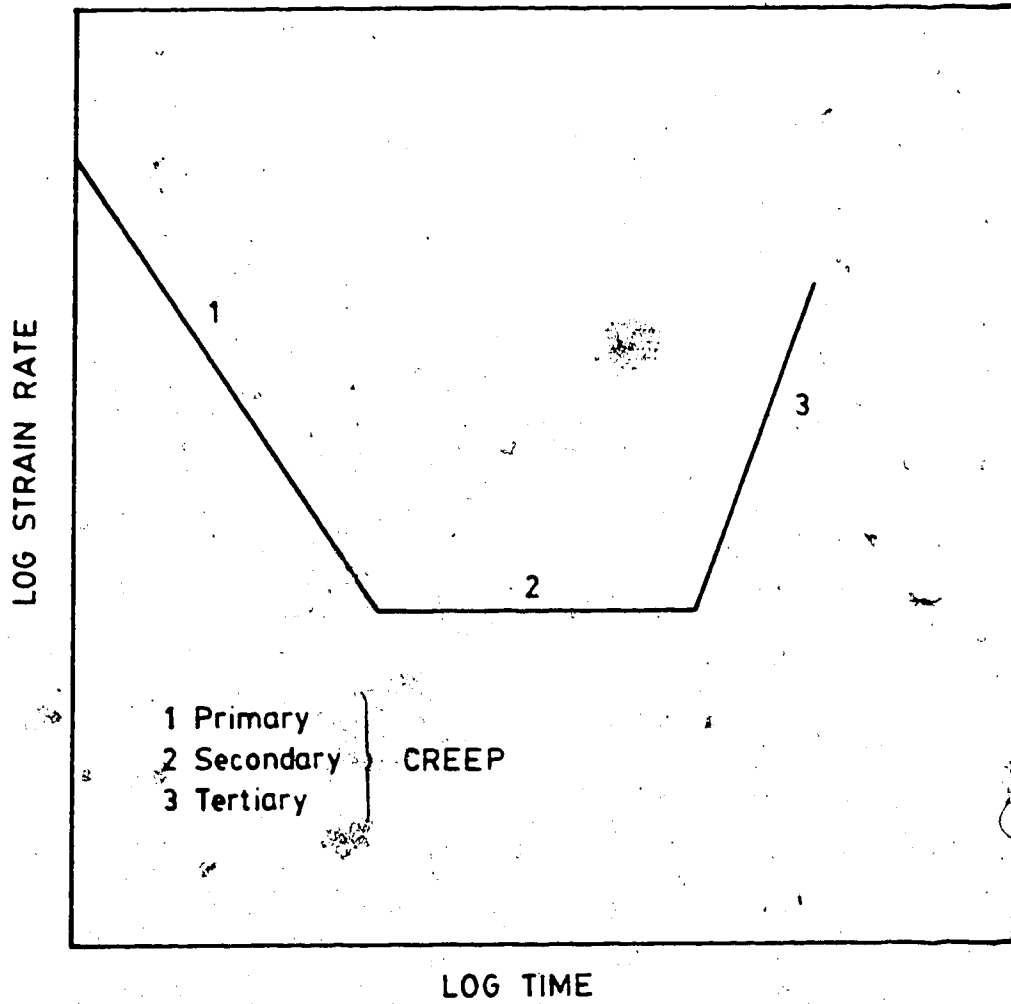


Figure 4.8 Idealized Double Logarithmic Plot of Strain Rate vs Time

The time laws describing primary creep are generally of the exponential or power law form. Cruden (1971a) demonstrated the superiority of the power law for primary creep in rock and da Fontoura (1980) showed its suitability for this coal. The parameters required for this formulation are easily obtained from a log strain rate versus log time plot as shown in Figure 4.9. Expressions obtained from strain rate vs. time data are inherently better than those obtained from strain vs. time data [Cruden (1970)] and therefore this procedure was employed in the determination of the appropriate parameters.

Most studies into the creep of materials under constant stress have been concerned with the creep resulting from a deviatoric stress condition (deviatoric creep). However, in this study, in order to describe the time dependent deformations observed in the laboratory it was necessary to develop expressions for the creep resulting from a decrease in stress (stress relief creep or relaxation) and that resulting from the uniform compressive stress (hydrostatic creep). For the purposes of this research it was assumed that direct superposition of all components was admissible.

4.2.4.1 Hydrostatic Creep

The term 'hydrostatic creep' in this study refers to those time-dependent deformations resulting from an equal lateral stress, no longitudinal strain condition and not a true hydrostatic stress condition. A linear relationship between the log of the strain rate and the log of time was

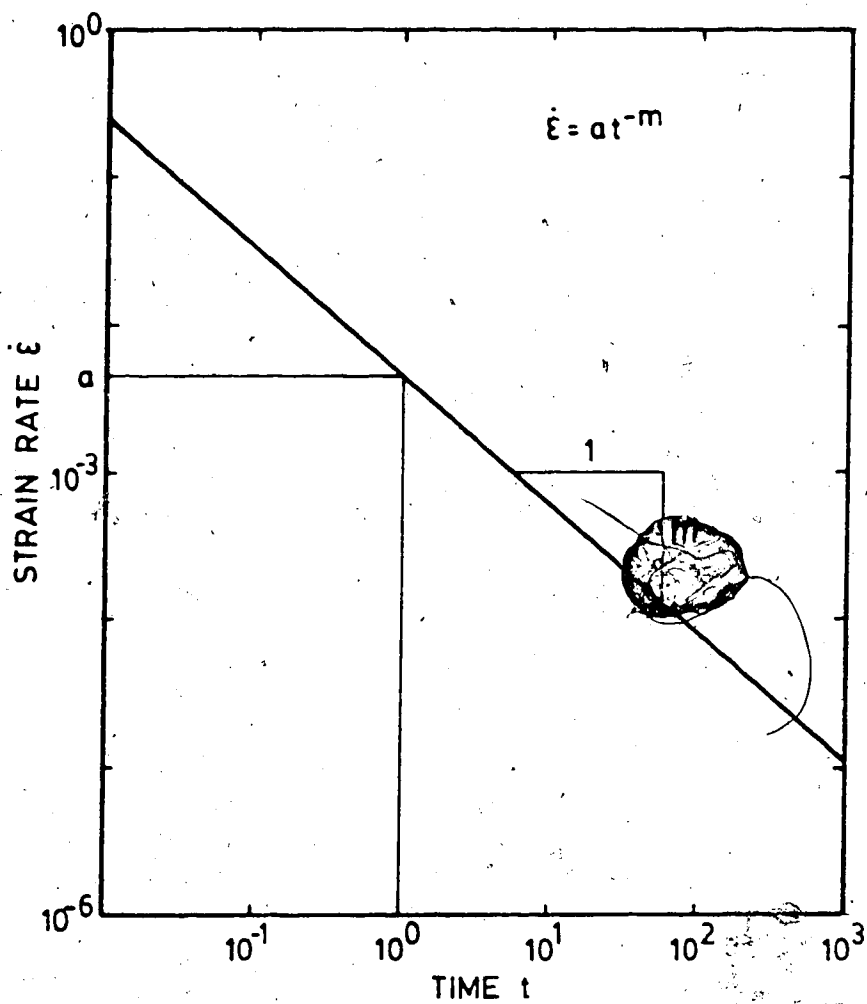


Figure 4.9 Determination of Representative Time-Dependent Parameters

observed for each extensometer during single increment or the initial stage of multi-stage creep tests performed on the intact specimen under these conditions. Because of this a power law form of the 'hydrostatic' creep expression was adopted.

Each of the extensometer responses was analyzed and a set of 'a' and 'm' parameters, representing the mean of the values, selected for a particular test. The hardening parameter 'm' which represents the rate of dissipation of strain rate with time was found to be relatively invariant of the 'hydrostatic' stress level as shown in Figure 4.10. A value of 'm'=0.83 would seem appropriate for this material.

The magnitude of the strain rate at unit time (one hour in this study) is defined as the parameter 'a' and it represents the strain potential. This parameter exhibited a strong stress dependency as shown in Figure 4.11. Least square regression analysis of the data resulted in the three expressions for the 'a' parameter shown. All had very similar correlation coefficients ($r^2=0.68$) and would yield similar results in the range of interest (3 to 12.5 MPa). However, it was decided to adopt the power law relationship for the following reasons:

1. The exponential relationship would tend to overestimate the parameter in both the low and high stress ranges. Indeed its use would result in predictions of hydrostatic creep at zero stress which is a physical impossibility under conditions of constant temperature.

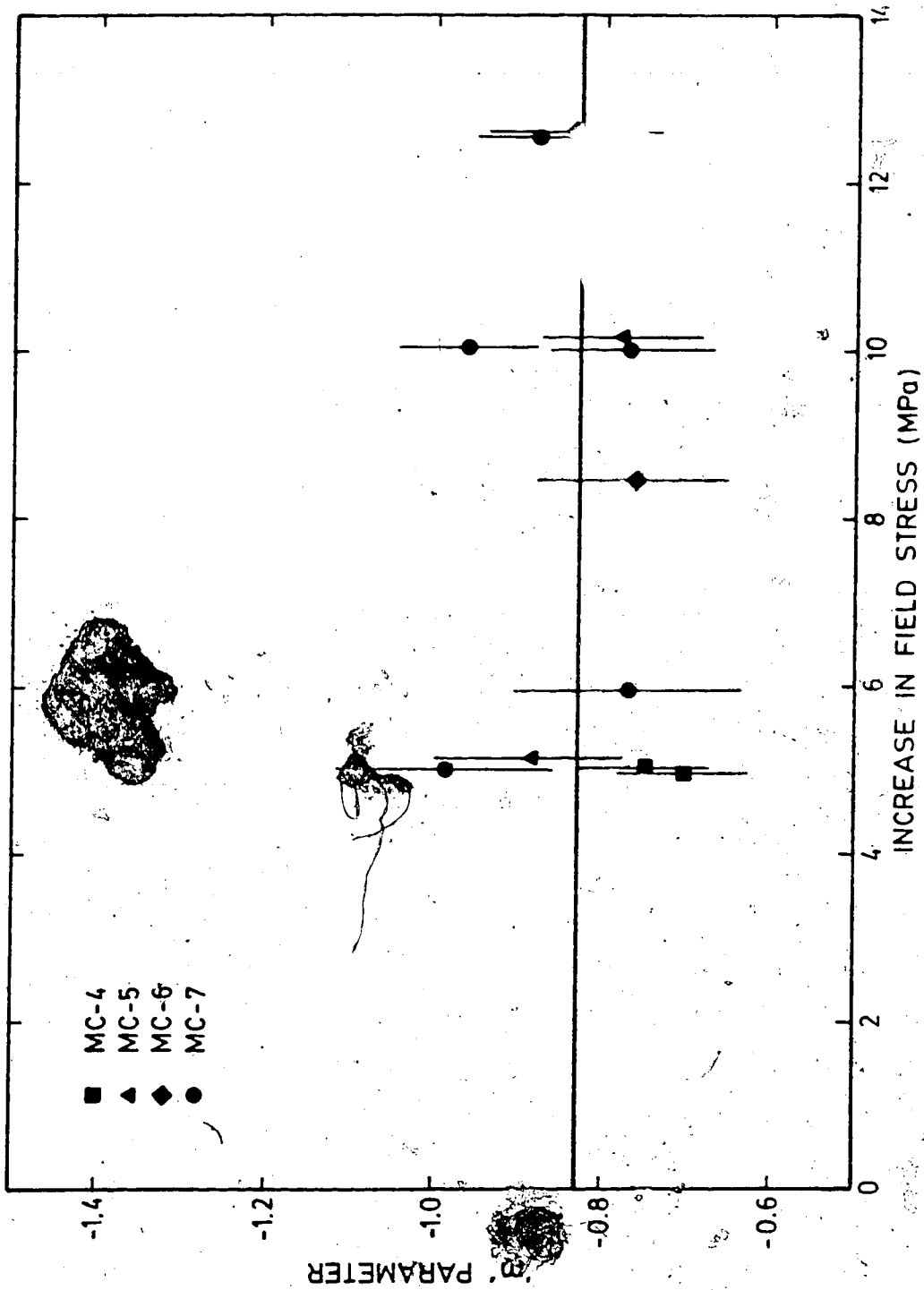


Figure 4.10 Variation in 'm' Parameter with Increasing Stress

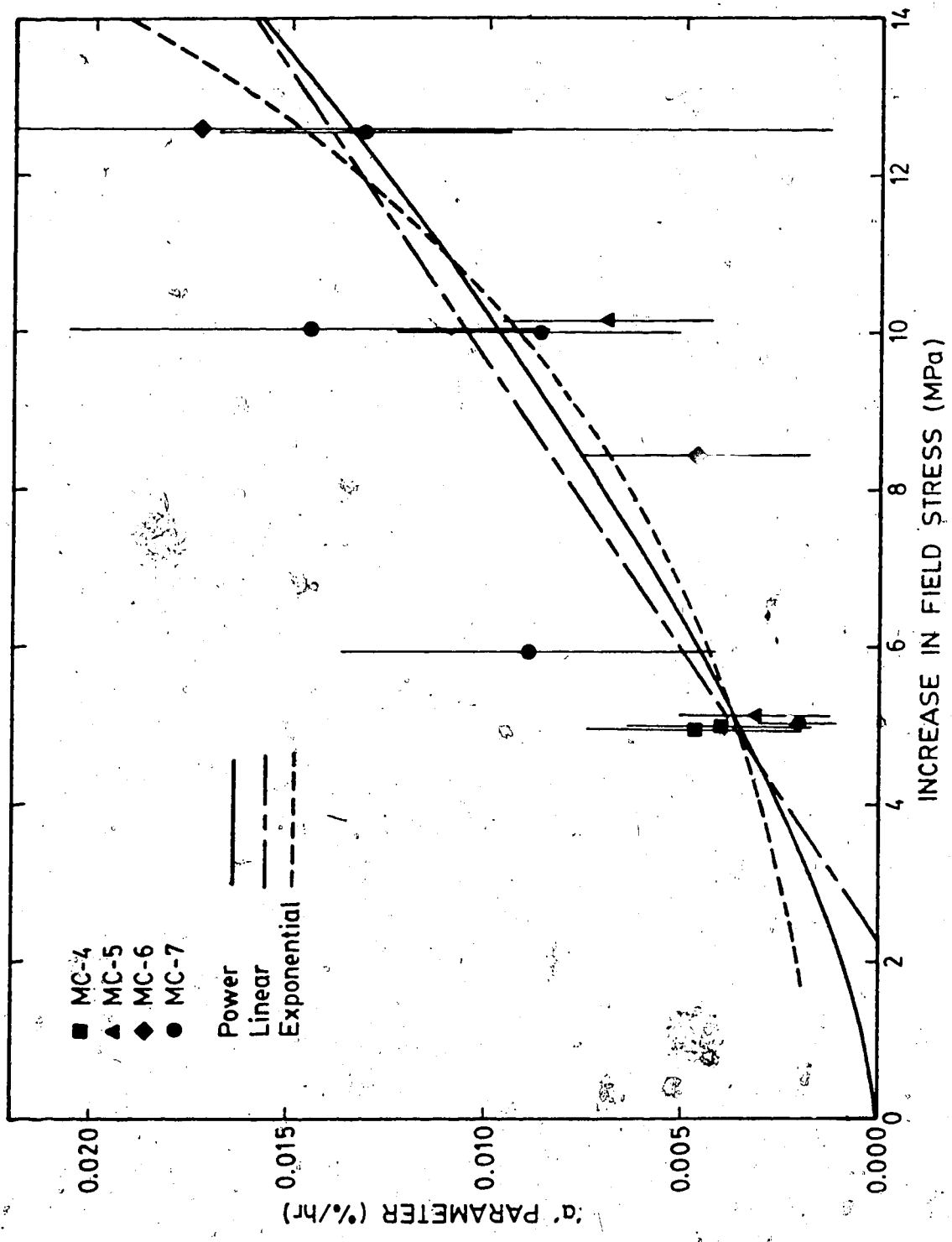


Figure 4.11 Variation in 'a' Parameter with Increasing Stress

and humidity.

2. The linear relationship suggested the existence of a threshold stress level beneath which no hydrostatic creep would occur. The existence of such a level is subject to question.

Based on the above results the expression selected to describe the hydrostatic creep rate component was:

$$\dot{\epsilon}'(t) = \frac{B \Delta \sigma}{h} t^{r-n} \quad \text{Eqn. 4.1}$$

where $B = 3.53 \times 10^{-6}$

$\Delta \sigma$ = hydrostatic stress increment in MPa

$r = 1.439$

t = time in hours

$n = 0.83$.

4.2.4.2 Stress Relief Creep

The recovery of the sample upon removal of load was utilized to determine an appropriate expression for the stress relief creep. Again a linear relationship was observed in the double logarithmic plots of strain rate versus time allowing determination of representative 'a' and 'm' parameters.

The 'm' parameter was again relatively constant at a value of 1.05 as shown in Figure 4.12. Schwartz and Kolluru (1981) reasoned that values for 'm' greater than 1 are physical impossibilities as the integration of such an expression would result in a creep function in which total

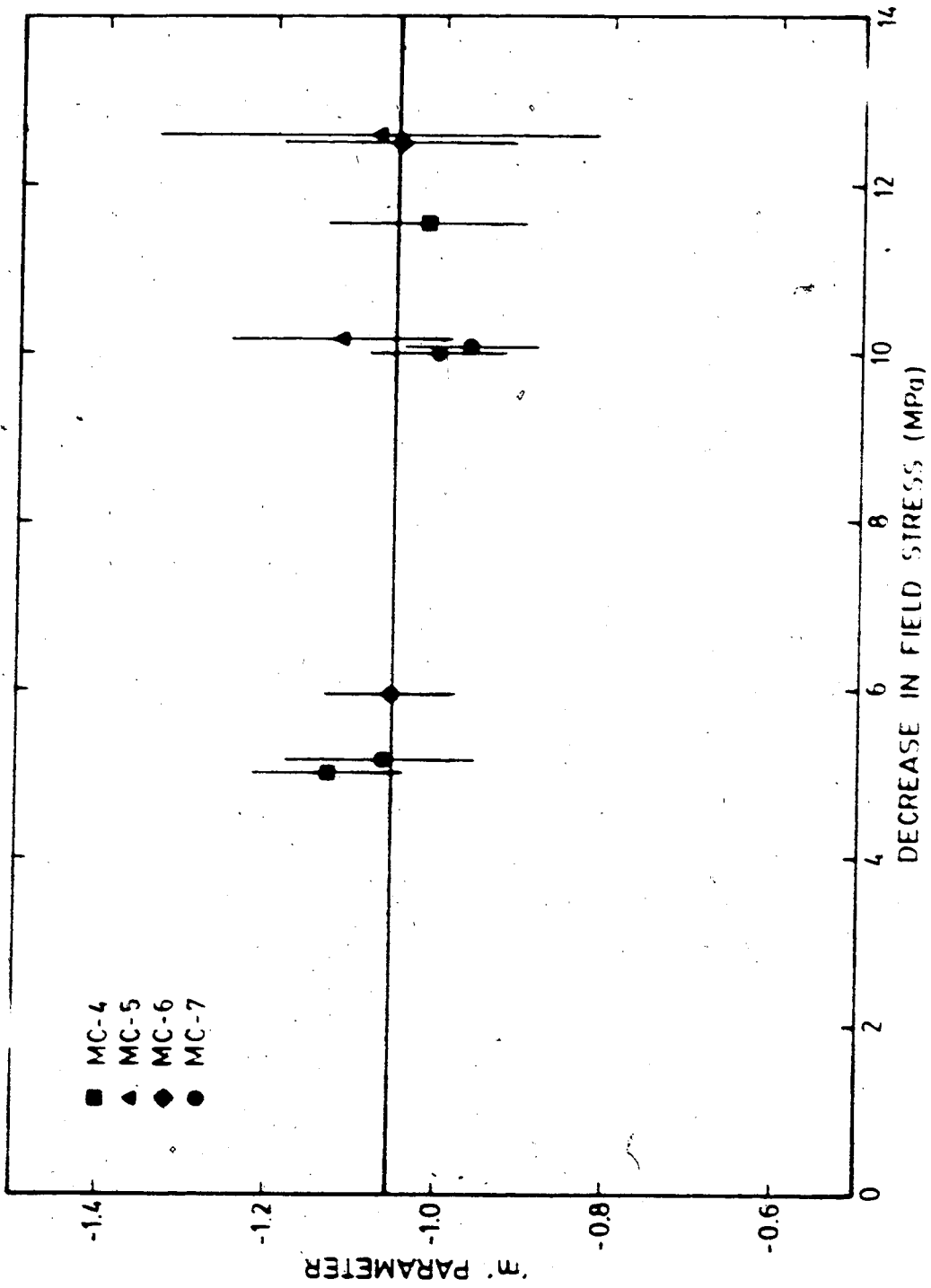


Figure 4.12 Variation in 'm' Parameter with Decreasing Stress

strains decrease with time. However, this only is true if one considers the limits of integration as being from $t_1=0$ to some time t_2 . Cruden (1971b) suggests that the least value of t_2 is the time taken for the stress wave to travel through the specimen (approximately equal to 2×10^{-4} hours if the stress wave travels at about the speed of sound). Use of this lower limit for t_2 results in an expression in which creep strains increase with time.

The 'a' parameter exhibited a dependence on the magnitude of the stress relief as shown in Figure 4.13. Least square regression analysis of the data resulted in three expressions with similar but poor correlation coefficients ($r^2=0.14$). Cruden (1971b) in a study of the recovery of Pennant Sandstone from uniaxial compressive load found the recovery rates to be stress independent. He surmised that normal recovery results from motion along cracks where the friction has been reduced with time due to corrosion aided failure of asperities. As the load on the specimen during recovery was much less than the applied loads the recovery rate would only depend on the cracks closed at this low load and hence be independent of the maximum load (cracks closed at higher loads would only open upon load reduction). While Cruden's results and rationale are compelling, the data presented in Figure 4.13 do indicate a slight stress dependency. Hence, it was decided to adopt the power law relationship (more reasonable at low magnitudes of stress relief).

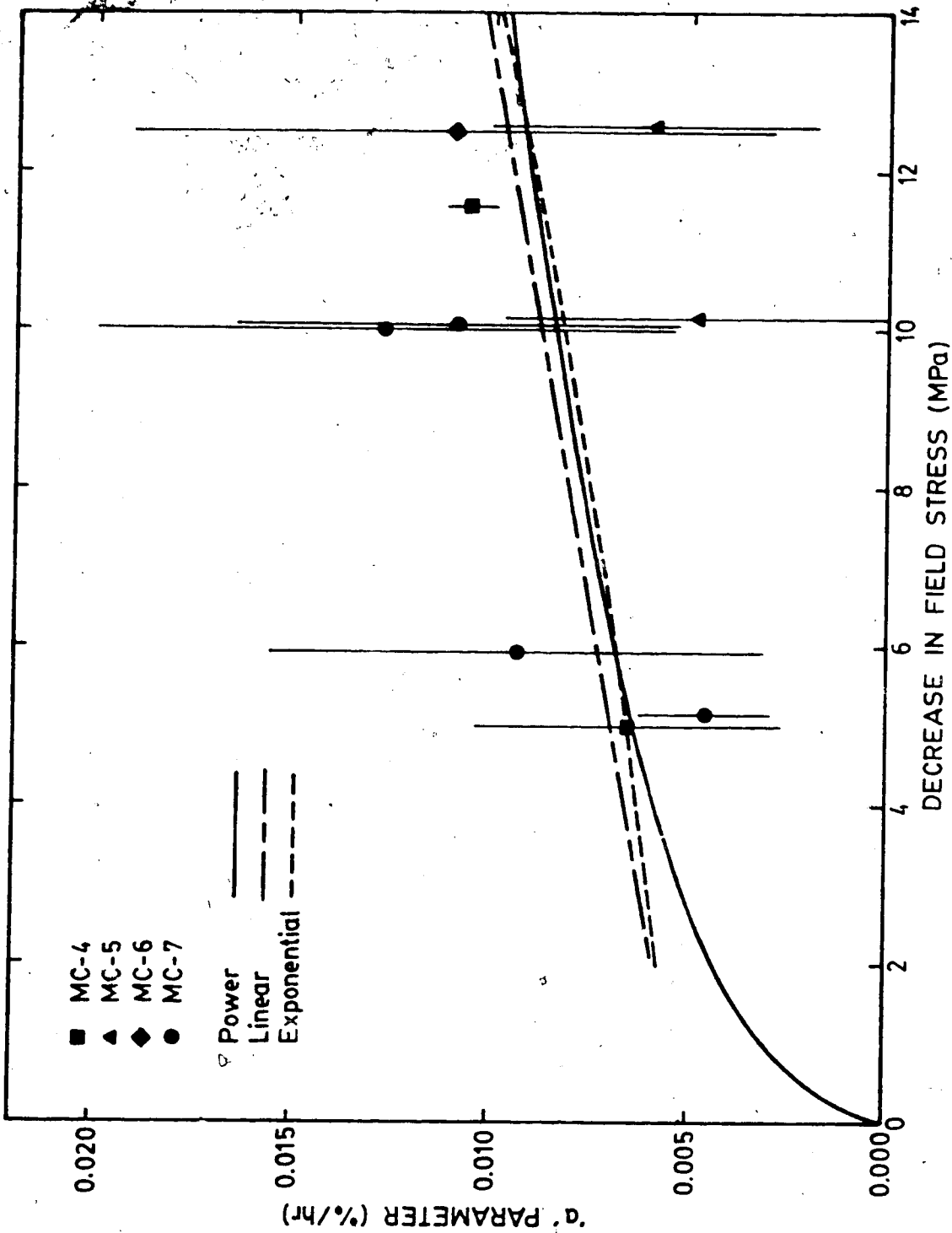


Figure 4.13 Variation in 'a' Parameter with Decreasing Stress

The resulting expression for the creep rate due to a decrease in stress is:

$$\epsilon'_{sr}(t) = C \Delta \sigma_d^s t^{-p} \quad \text{Eqn. 4.2}$$

where $C = 3.241 \times 10^{-5}$;

$\Delta \sigma_d$ = stress decrease in Mpa;

$s = 0.41$; and

$p = 1.05$.

4.2.4.3 Deviatoric Creep

The creep of the coal under deviatoric loading was investigated by da Fontoura (1980). He concluded that the hardening parameter 'm' was on average equal to 0.9 and independent of the stress level. The stress level was defined as the ratio of the current stress to the current strength, both referring to the same state of confinement (to determine the current strength a cohesion intercept of 2 MPa and an angle of internal friction of 50° were selected as representing average conditions). He also concluded that the 'a' parameter could best be represented as an exponential function of the stress level. The resultant expression for the deviatoric creep rate was:

$$\epsilon'_{d}(t) = A e^{\beta \sigma} t^{-q} \quad \text{Eqn. 4.3}$$

where $A = 1.506 \times 10^{-5}$;

$\beta = 1.9$;

σ = stress level; and

q = 0.9.

Only one single stage creep test of the intact specimen under deviatoric loading conditions (Test MC-7.05) was undertaken. The mean and range of the measured values of the radial strain rates both parallel and perpendicular to the major principal stress direction for this test are presented in Figure 4.14.

Two methods, each involving different assumptions were employed in the derivation of an expression for the deviatoric creep rate of Sample MC-7 at the stress level (0.321) of Test MC-7.05.

In the first method it was assumed that Equation 4.1 correctly described the hydrostatic creep rate component. The deviatoric component could therefore be calculated as the difference between the mean measured creep rate parallel to the major principal stress direction and the predicted hydrostatic creep rate. The deviatoric creep rate thus calculated is shown in Figure 4.15. Least squares linear regression analysis yielded the following expression for this curve:

$$\epsilon'_d(t) = 8.916 \times 10^{-3} t^{-0.91} \quad (\%/hr) \quad \text{Eqn. 4.4}$$

which is approximately 3.2 times greater than the expression proposed by da Fontoura.

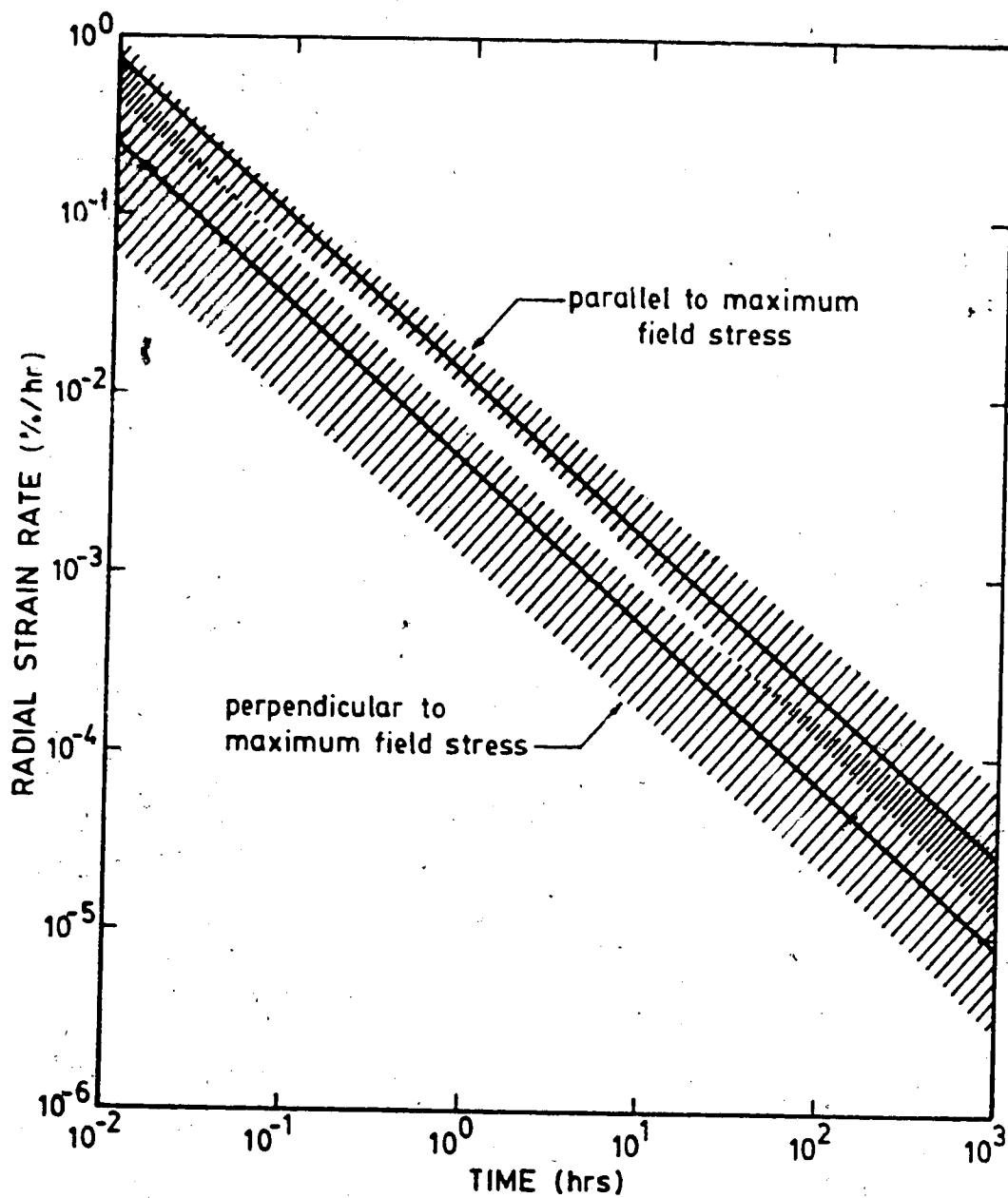


Figure 4.14 Mean and Range of Measured Creep Rates in Test MC-7.05

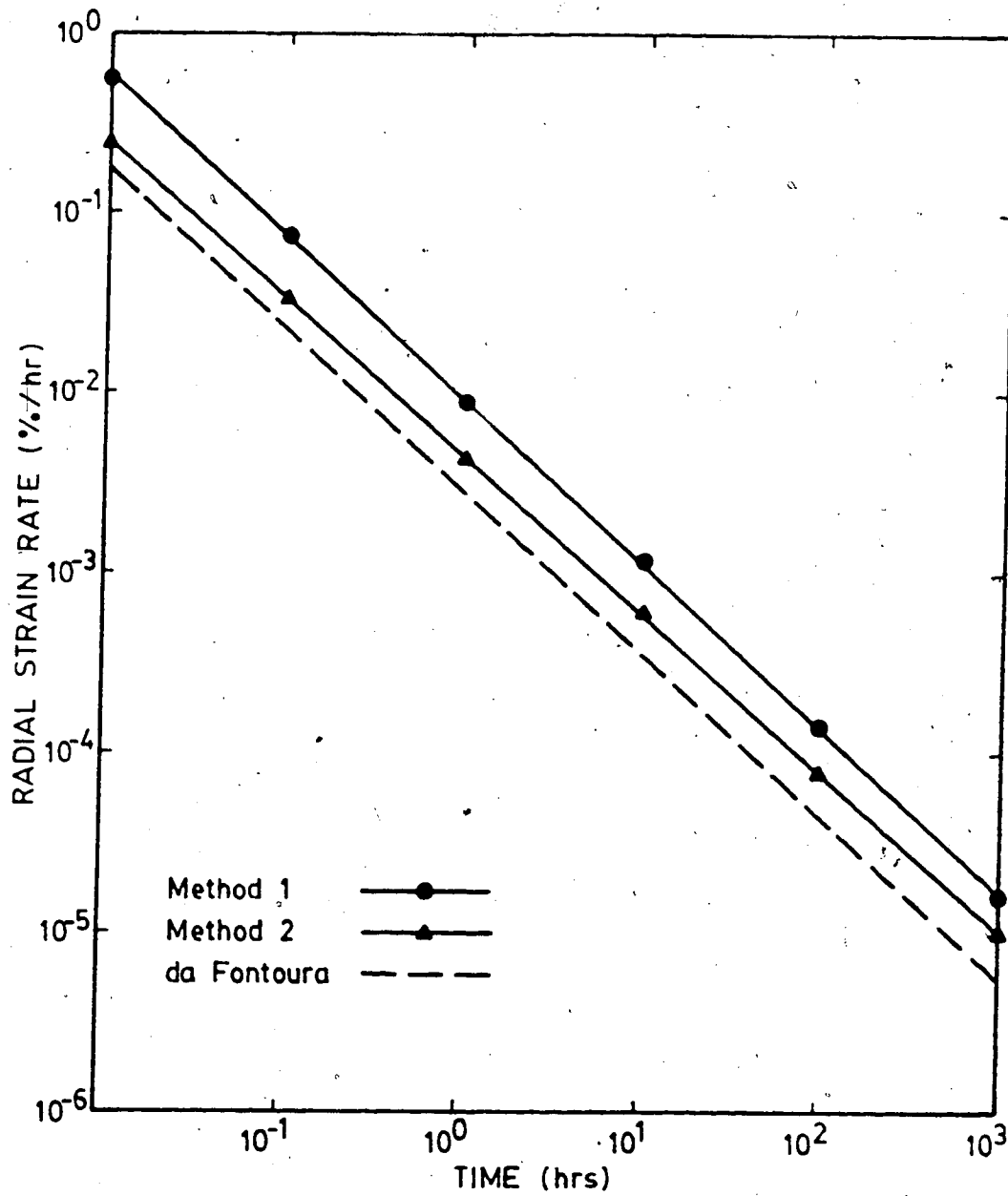


Figure 4.15 Deviatoric Creep Rates - Test MC-7.05

In the second method it was assumed that there was no volume change due to deviatoric creep. Therefore the deviatoric creep rate components parallel and perpendicular to the major principal stress direction would be equal but of opposite sign. The deviatoric component of the creep rate can then be calculated as one half the difference between the mean creep rates measured parallel and perpendicular to the major principal stress direction. No assumptions regarding the hydrostatic component are required. The resultant values of the deviatoric creep rate components are also shown in Figure 4.15. Least squares linear regression analysis yielded the following expression for this curve:

$$\epsilon'_d(t) = 4.372 \times 10^{-3} t^{-0.91} \quad (\%/hr) \quad \text{Eqn 4.5}$$

which is approximately 1.6 times greater than the expression proposed by da Fontoura.

No other testing of the intact specimen at different stress levels was undertaken. Therefore a general expression for a stress level dependent deviatoric creep rate could not be established for Sample MC-7.

No further refinement of the deviatoric creep rate expression was attempted and Equation 4.3 with the listed parameters was assumed applicable.

4.2.4.4 Multi-Stage Testing

The expressions describing the creep rate components developed in the preceding sections are not directly

applicable to multi-stage testing (i.e., tests where the load is applied incrementally with large time intervals between successive increments). In multi-stage tests the representative components are assumed to superpose in the following manner:

$$\epsilon'_h(t) = B\Delta\sigma_h^r (t + t_0)^{-n} + B\Delta\sigma_{h_1}^{-n} t \quad \text{Eqn 4.6}$$

$$\epsilon'_{sr}(t) = C\Delta\sigma_{sd}^s (t + t_0)^{-p} + C\Delta\sigma_{d_1}^s t^{-p} \quad \text{Eqn 4.7}$$

$$\epsilon'_d(t) = A e^{\beta\sigma t^{-q}} + A e^{\beta\Delta\sigma t^{-q}} \quad \text{Eqn 4.8}$$

where $\Delta\sigma_{h_1}$ = increment of hydrostatic stress applied at time t_0 ;
 $\Delta\sigma_{d_1}$ = decrement in stress achieved at time t_0 ;
 and
 $\Delta\sigma$ = increment in stress level applied at time t_0 .

Similar expressions are assumed applicable for successive stages.

Recent studies by Cruden (1983) suggest that a more appropriate form of the incremental creep rate is given by:

$$\epsilon'(t) = CS_1^{\frac{2n(m-1)}{(n-2)} - \frac{(n-2m)}{(n-2)}} t$$

$$\left[1 + \left(\frac{S_0}{S_1} \right)^n \frac{t_0}{t} \right]^{-2/(n-2)}$$

where C = factor independent of stress and time;

S_0 = initial uniaxial compressive stress;
 S_1 = higher uniaxial compressive stress;
 t_0 = duration of creep under S_0 ;
 t = time of creep under S_1 ; and
 n, m = material constants which determine the exponents of both the time and stress dependence of creep rate.

An investigation of the suitability of this expression for the results recorded during this test program was not undertaken, however it does warrant further investigation.

4.2.5 Verification of Time Dependent Relationships

As the expressions describing the three creep rate components were independently determined it was decided to verify their general applicability by comparing their predicted response with that measured during both single and multi-stage external loading tests under hydrostatic and non-hydrostatic loading conditions. The predictions of creep rate were made assuming stresses and stress changes corresponding to stress distributions in a linear elastic, isotropic medium with the properties previously determined. No verification of the stress relief creep rate was attempted.

The expression for the time-dependent response of the rock mass to the external (i.e., boundary) loading of the specimen containing a tunnel would be a combination of hydrostatic and deviatoric creep. The hydrostatic creep

component is compressional whereas the deviatoric component in the radial direction is extensional. If superposition is acceptable the form of the radial creep rate expression would be:

$$\epsilon'_r(t) = \epsilon'_h(t) - \epsilon'_d(t) \quad \text{Eqn. 4.9}$$

which when expanded yields:

$$\epsilon'_r(t) = B \Delta \sigma \frac{r^{-n}}{h} - A e^{-\beta \sigma} t^{-q} \quad \text{Eqn. 4.10}$$

Comparison of the radial strain rates predicted by Equation 4.10 using the previously determined parameters with those measured during external loading of the three specimens containing a 152 mm diameter tunnel are presented in Figures 4.16a to c. The shaded area in each figure represents the range of strain rates recorded (all extensional) by the ring of extensometers closest to the tunnel wall.

The measured radial strain rates are well predicted for Sample MC-5, however, they are significantly underestimated for Samples MC-6 and MC-7 (in Sample MC-6 even the sense of the strain rate is incorrectly predicted). In these two specimens the error is believed to lie predominantly in the deviatoric creep rate component. Earlier it had been demonstrated that the deviatoric strain rate determined by da Fontoura's relationship (Equation 4.3) significantly

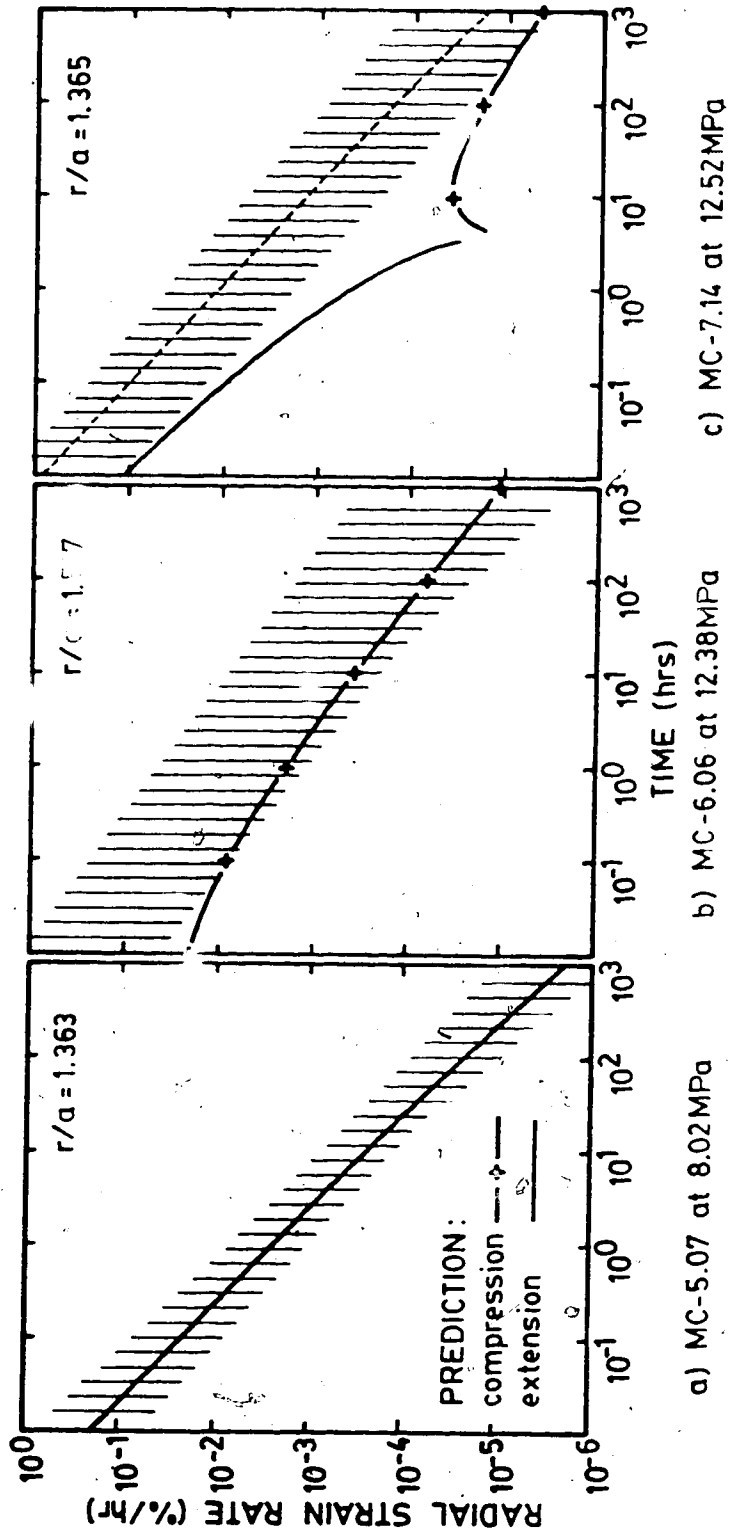


Figure 4.16 Comparison of Near Tunnel Predicted and Observed Radial Strain Rates

underestimated the rate observed in Sample MC-7 (by a factor of 3.2). Assuming the ratio of the actual deviatoric strain rate to that predicted by Equation 4.3 to be stress level independent one can arrive at a new prediction for the net radial strain rate for Sample MC-7 as shown by the dashed line in Figure 4.16c. This clearly demonstrates that the error lay in the deviatoric component. These results imply that the actual deviatoric rate in Sample MC-6 must be approximately five times that predicted by Equation 4.3.

Figures 4.17 and 4.18 present a comparison of predicted (solid line) and observed (shaded area) radial strain rates under multi-stage testing of the intact specimens under 'hydrostatic' stress conditions. Both figures show an initial slight overestimation of the rate with a continuing inclination to underestimation, particularly at times less than one hour, with successive increments. Overall, however, the hydrostatic creep rate is suitably represented.

Figures 4.19 and 4.20 present a comparison of the observed and predicted net creep rate under non-hydrostatic multi-stage testing conditions. Also shown on each figure is the predicted hydrostatic creep rate (dashed line). Parallel to the major principal stress direction (Figure 4.3a) there is reasonably good correlation between the predicted and observed. As had been the case under hydrostatic loading, there is an initial slight overestimation of the net rate followed by increasing underestimation particularly at times less than one hour.

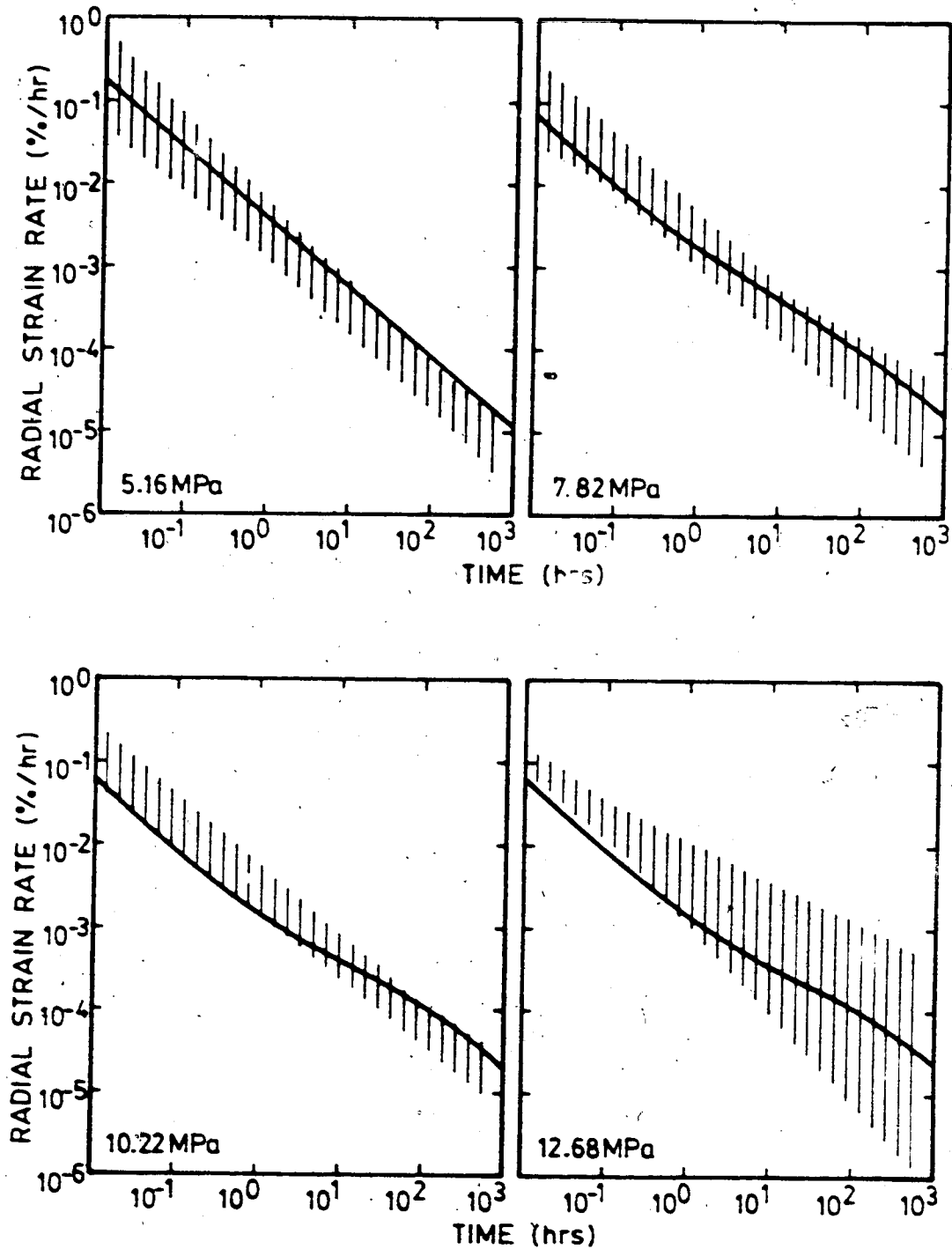


Figure 4.17 Comparison of Observed and Predicted Radial Strain Rates Under Multi-Stage Hydrostatic Loading - Sample MC-5

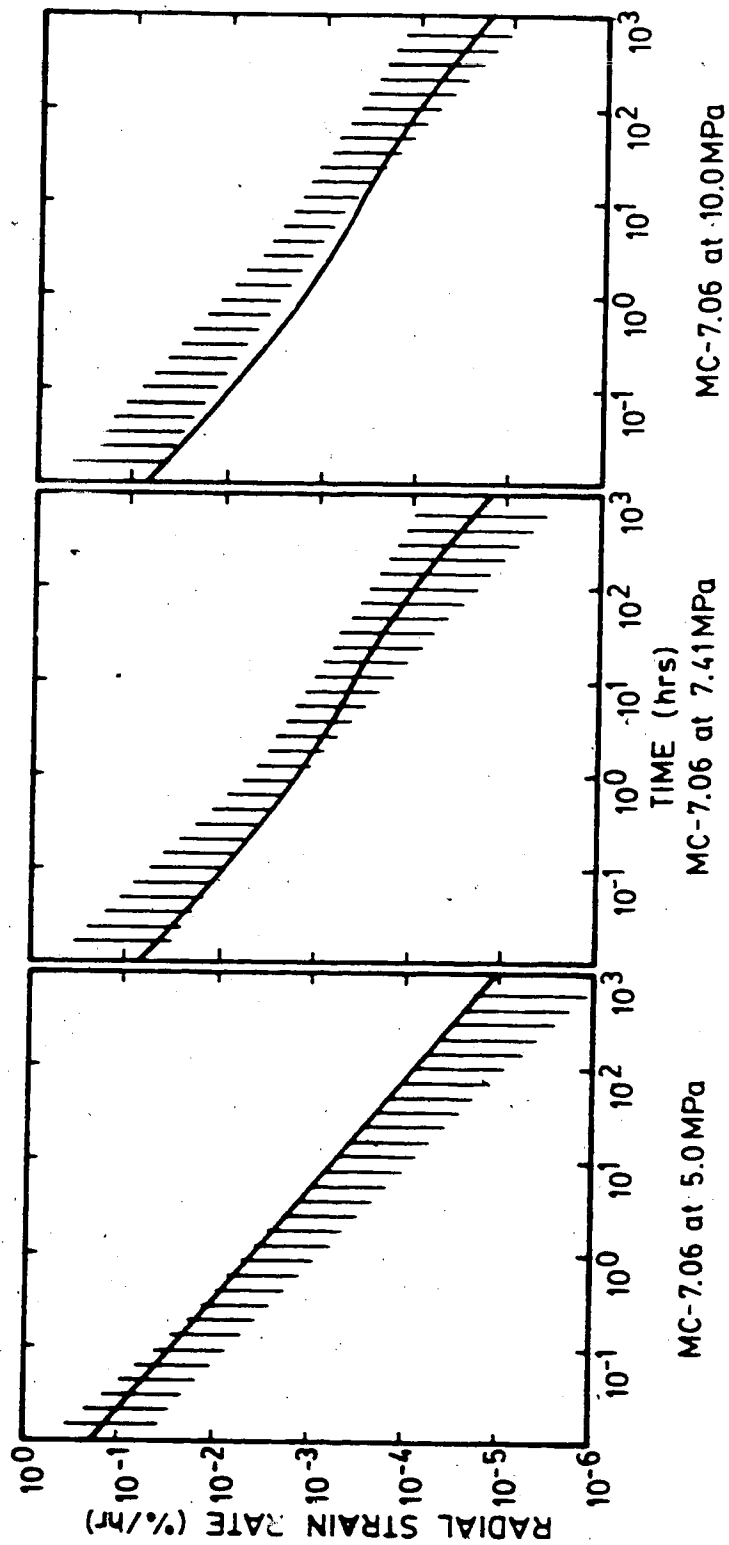


Figure 4.18 Comparison of Observed and Predicted Radial Strain Rates Under Multi-Stage Hydrostatic Loading - Sample MC-7

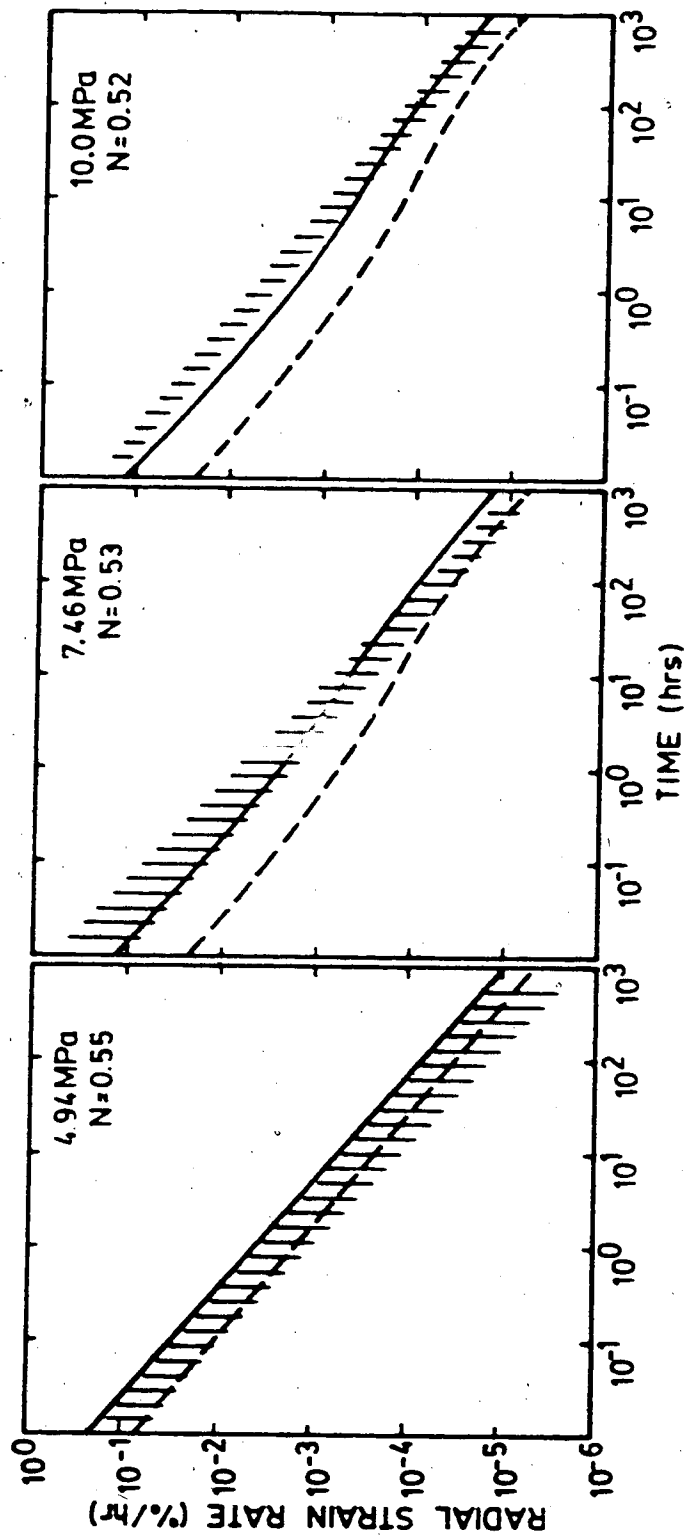


Figure 4.19 Comparison of Observed and Predicted Radial Strain Rates Parallel to the Maximum Field Stress - Sample MC-7

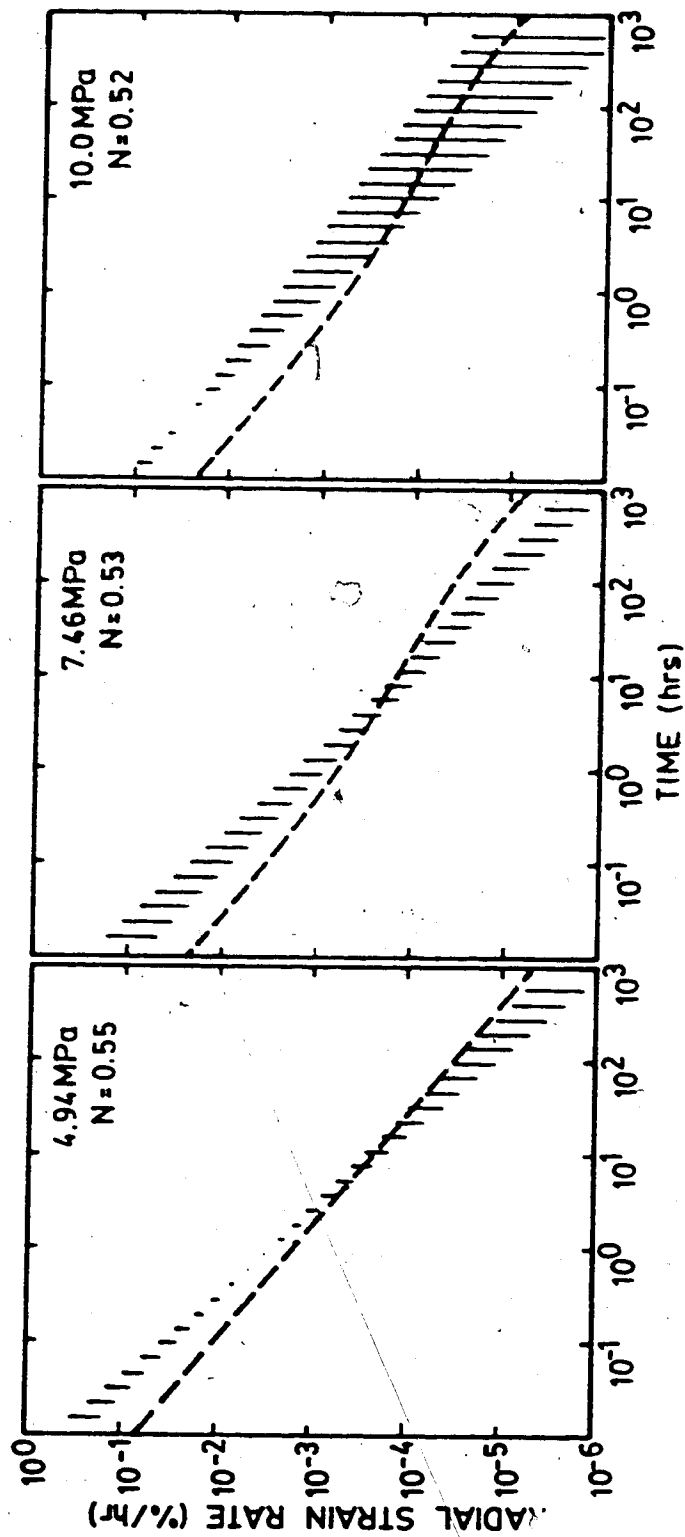


Figure 4.20 Comparison of Observed and Predicted Radial Strain Rates Perpendicular to the Maximum Field Stress - Sample MC-7

Perpendicular to the major principal stress direction (Figure 4.20), there is virtually no correlation between predicted and observed strain rates. All observed rates (shaded area) were compressional whereas the predicted (not shown) were extensional. The observed rate exceeded even the predicted hydrostatic rate. The predicted net rates were determined using the parameters suggested by da Fontoura (1980) for the deviatoric rate component. These had previously been shown to significantly underestimate the deviatoric rate in this sample. Use of the sample specific parameters, however, would have resulted in even poorer predictions in this orientation. No explanation for this behaviour can be given at this time.

The above results demonstrate that reasonably good approximations to material behavior can be achieved under single stage external loading conditions by superposition of the hydrostatic and deviatoric creep rate components. Under multi-stage loading conditions the superposition of hydrostatic creep rate terms as given by Equation 4.6 yields sufficiently accurate predictions of sample response. The deviatoric component of creep rate is not well represented by Equation 4.7 in multi-stage testing. As no alternate relationship is currently available, Equation 4.7 will continue to be employed but with due consideration of its doubtful validity.

Care must be employed in the general application of all the above relationships as sample to sample variations can

be considerable. There is an inherent risk involved in ascribing universal parameters to a highly heterogeneous material such as coal. However, it is important to point out that the proposed equations describe the time-dependent behaviour of the coal mass with all its joints and other discontinuities and hence, are of more practical value than results from small samples of 'intact' coal.

The accurate representation of material behavior under complex loading conditions was not the purpose of this research. It was to identify the parameters sufficiently accurately to provide a basis for the understanding of the time-dependent processes occurring near an advancing tunnel face. For this purpose the proposed expressions should be adequate.

5. RESULTS OF LABORATORY INVESTIGATION

5.1 Introduction

Current tunnelling technology is very much dependent on the analysis of deformations (closure, radial displacement) around the excavation. As explained in Chapter 2, these analyses are employed to establish the validity of the design and assess the stability of the excavation. While the magnitude of these deformations are important, particularly in reference to the serviceability of the opening, it is their evolution with time that is most beneficial to ascertain.

The stand-up time and rate of tunnel closure are dominated by the excavation method and sequence, the type of support and its installation procedure. The time-dependent tunnel wall convergence is initially dominated by the time-dependent stress redistribution processes resulting from the advance of the tunnel face. Far behind the tunnel face the time-dependent behaviour is controlled largely by the creep properties of the rock mass. These time-dependent deformation mechanisms must be understood to achieve accurate evaluation of instrument response.

In order to critically evaluate the current deformation monitoring practice, specifically the measure of tunnel convergence and the measure of radial displacement by borehole extensometers, a series of tests were performed on three laboratory specimens. Both external loading tests and

excavation simulation tests were conducted. The results of this extensive laboratory investigation follow.

5.2 Behaviour During External Loading Tests

The term external loading test refers to all tests in which the load was applied to the specimen containing a pre-drilled tunnel. Loading was either quick (continuous increase from zero field stress to desired level) or slow (discontinuous increase from zero field stress with variable number of creep stages). Details of this loading sequence are presented in Chapter 3. The tunnel convergence and radial strain were monitored during both load application and each creep stage. These represent the time-independent and time-dependent responses respectively. The results of the external loading tests are presented according to these divisions.

5.2.1 Time-Independent Behaviour

The material property distribution within a sample is very non-uniform, as demonstrated by the contour plots of the spatial distribution of Young's modulus presented in Chapter 4 (Figure 4.2). As a result of this spatial variation, the extensometer response recorded will be very much location dependent and wide variations in instrument response can be expected. Similar variations in the field must also be expected. The range of extensometer response under hydrostatic loading of the intact specimen is

presented in Figure 5.1 for Sample MC-7 (typical of the response recorded for all samples). In this and subsequent figures, the numbers in the lower right corner designate the location of the instrumentation along the tunnel axis. Compressive strains range from 0.6% ($\theta = 45^\circ$, Sta. 56) to 1.9% ($\theta = 90^\circ$, Sta. 56) at a stress level of 10 MPa. This is much in excess of the predicted elastic strain of 0.46% obtained using the value of Young's modulus and Poisson's ratio suggested in Chapter 4. The principal reason for this excess deformation results from the extreme non-linearity of the stress-strain relationship at low stresses (due to crack closure under load application or opening under stress relaxation) which is not accounted for in the simple linear elastic relationships employed. From this preliminary investigation of the extensometer response, it is evident that it will be strongly dependent on local material properties, stress level and orientation with respect to intersecting discontinuities. The detection of abnormal behaviour from strain magnitudes recorded by extensometers will be complicated by these influences.

Figure 5.2 presents the tunnel convergence and radial strains recorded during hydrostatic loading of Sample MC-5 containing a 120 mm diameter unlined tunnel (Test MC-5-04). Closure significantly in excess of the average is observed across the $0^\circ - 180^\circ$ diameter, although the radial strains do not indicate any abnormality in this orientation. They do however, indicate abnormal behaviour near the tunnel wall

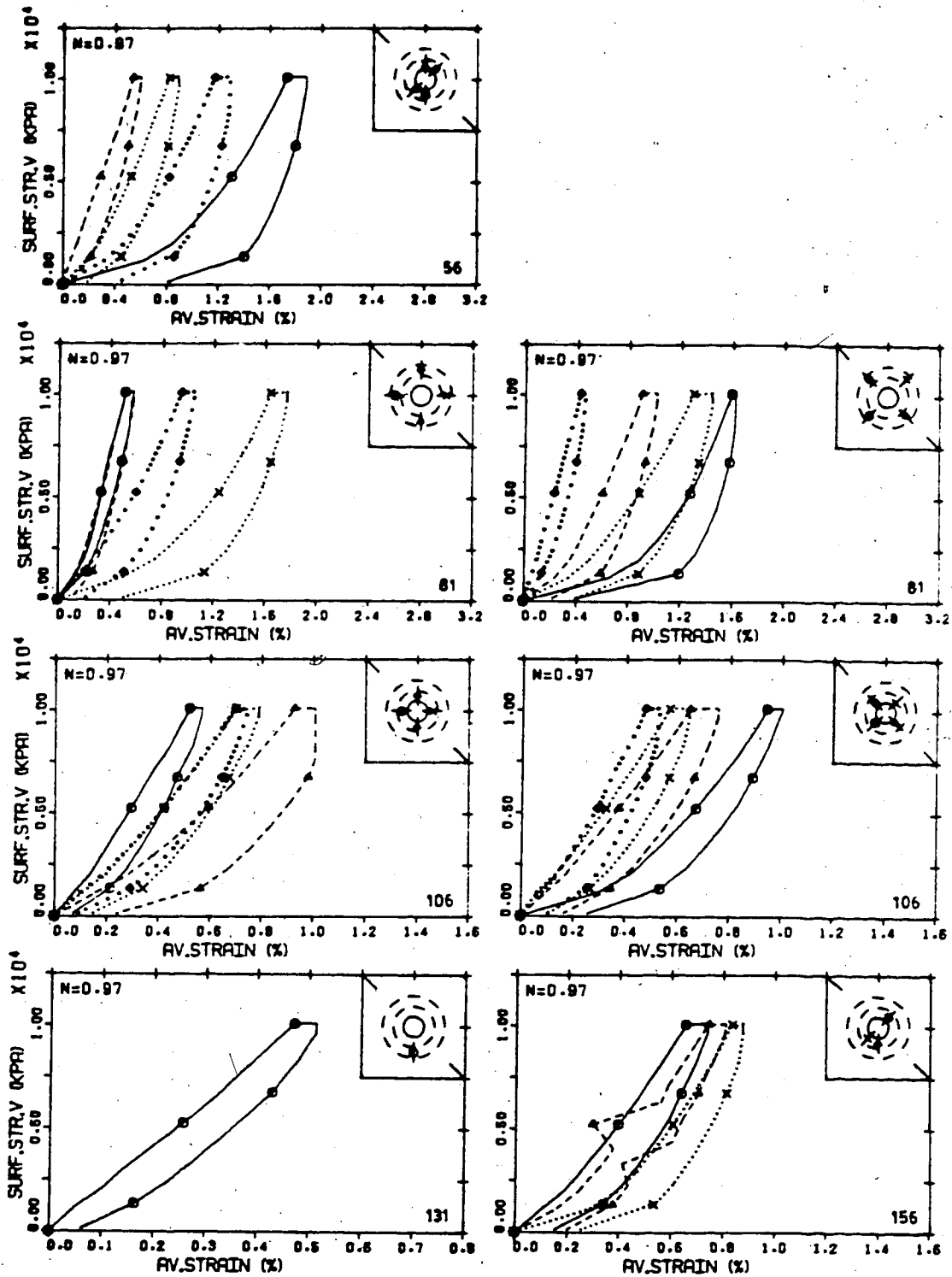


Figure 5.1 Extensometer Response : Test MC-7.02

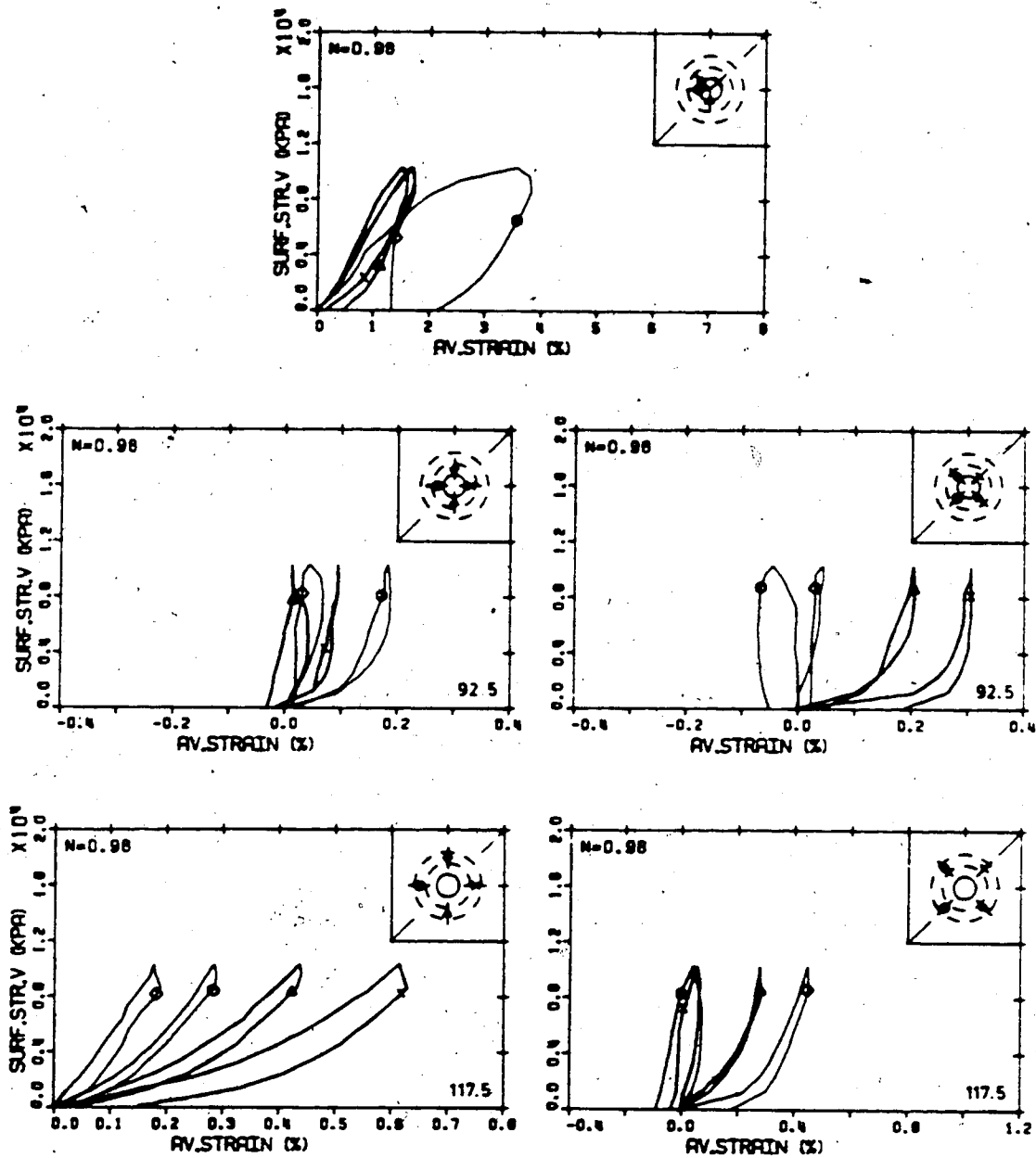


Figure 5.2 Tunnel Closure and Extensometer Response :
Test MC-5.04

(Sta. 92.5) approximately normal to the maximum closure (particularly at $\theta = 45^\circ$). A wider variation in closure response is noted during the next loading sequence (Test MC-5.05) as shown in Figure 5.3. Maximum closure is again across the $0^\circ - 180^\circ$ diameter but now a distinct minimum closure is observed across the $135^\circ - 315^\circ$ diameter. The closure is recoverable in the latter direction, but permanent closures of 2.5% to 4% are observed in the other orientations suggesting that yielding has occurred. These results are confirmed by the extensometer readings which indicate yielding near the tunnel wall (Sta. 92.5). Yielding processes appear concentrated in the $135^\circ - 270^\circ/315^\circ$ orientations. It is of particular interest to note that yielding is occurring in the direction of minimum tunnel convergence and almost normal to the maximum convergence. This contradicts the oft-held assumption of large dilation in the yield zone.

In the above analysis of the observed responses, it was not so much the magnitude of the response that allowed interpretation as the difference when compared to previous measurements at that location or to other instrument behaviour. Similar comparative procedures must also be employed in practice.

Figure 5.4 presents the tunnel convergence and radial strains measured during hydrostatic quick loading of the 108 mm diameter tunnel of Sample MC-7 (Test MC-7.11). Maximum closure was observed across the $135^\circ - 315^\circ$ diameter,

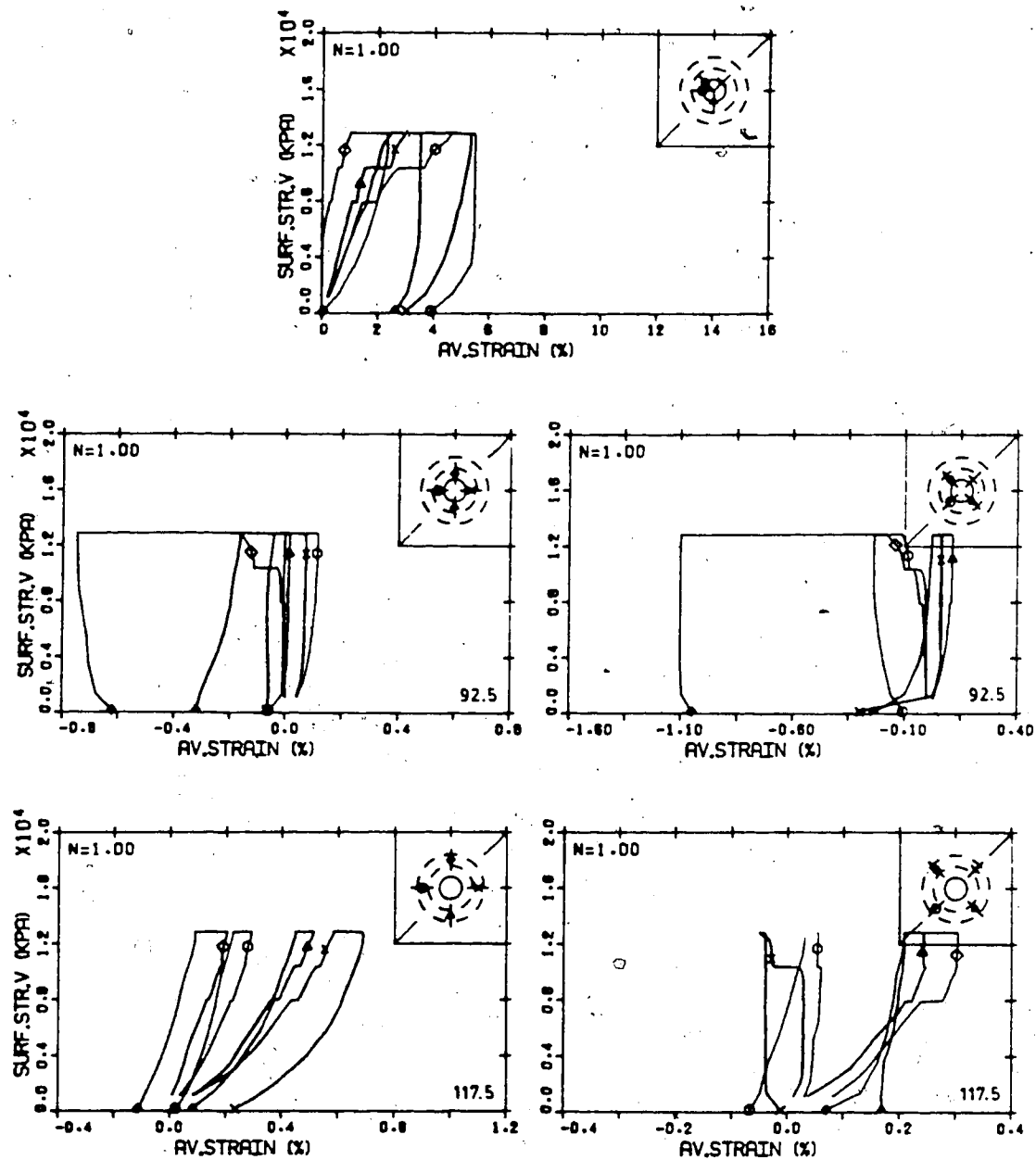


Figure 5.3 Tunnel Closure and Extensometer Response :
Test MC-5.05

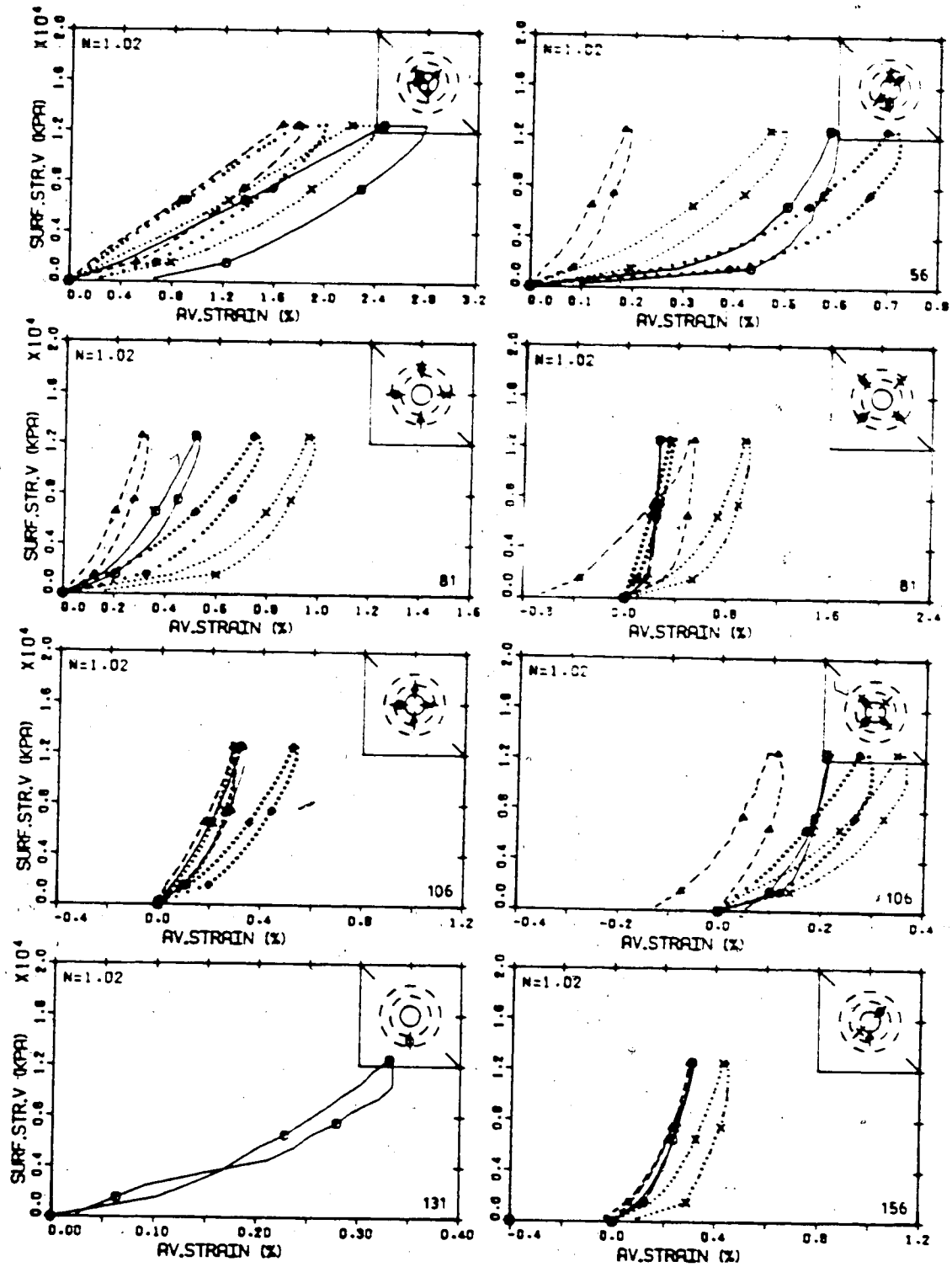


Figure 5.4 Tunnel Closure and Extensometer Response :
Test MC-7.11

however, the variation in closure was not as severe as that observed in Sample MC-5 under similar conditions (Figure 5.2). No abnormal extensometer responses were noted during loading, however, upon load removal, in the 135° orientation both near (Sta. 106) and far (Sta. 81) from the tunnel wall, permanent, extensional strains of up to 0.7% suggest that some slip along jointing occurred. In this case the orientation of maximum convergence corresponded to the zone of activity.

The results of the slow, hydrostatic loading of the 152 mm diameter tunnel of Sample MC-7 (Test MC-7.15) are presented in Figure 5.5. Closure is maximum in the 135° - 315° orientation and minimum in the 45° - 225° orientation. Abnormal straining, indicative of yielding processes, is again predominant in the 135° orientation with some expansion of the yield zone to the 90° orientation noted near the tunnel wall (Sta. 56, 106 and 156). Again the maximum convergence corresponded to the active zone as denoted by the extensometers.

Figure 5.6 presents the measurements recorded during non-hydrostatic ($N=0.5$) quick loading of the 152 mm diameter tunnel of Sample MC-7 (Test MC-7.16). The loading response of the convergence gauges corresponds to that expected in a homogeneous, elastic material with minimum closure normal to the principal stress direction (90° - 270° orientation) and maximum parallel to it (0° - 180°) orientation. Upon unloading, the closures in all but across the 0° - 180°

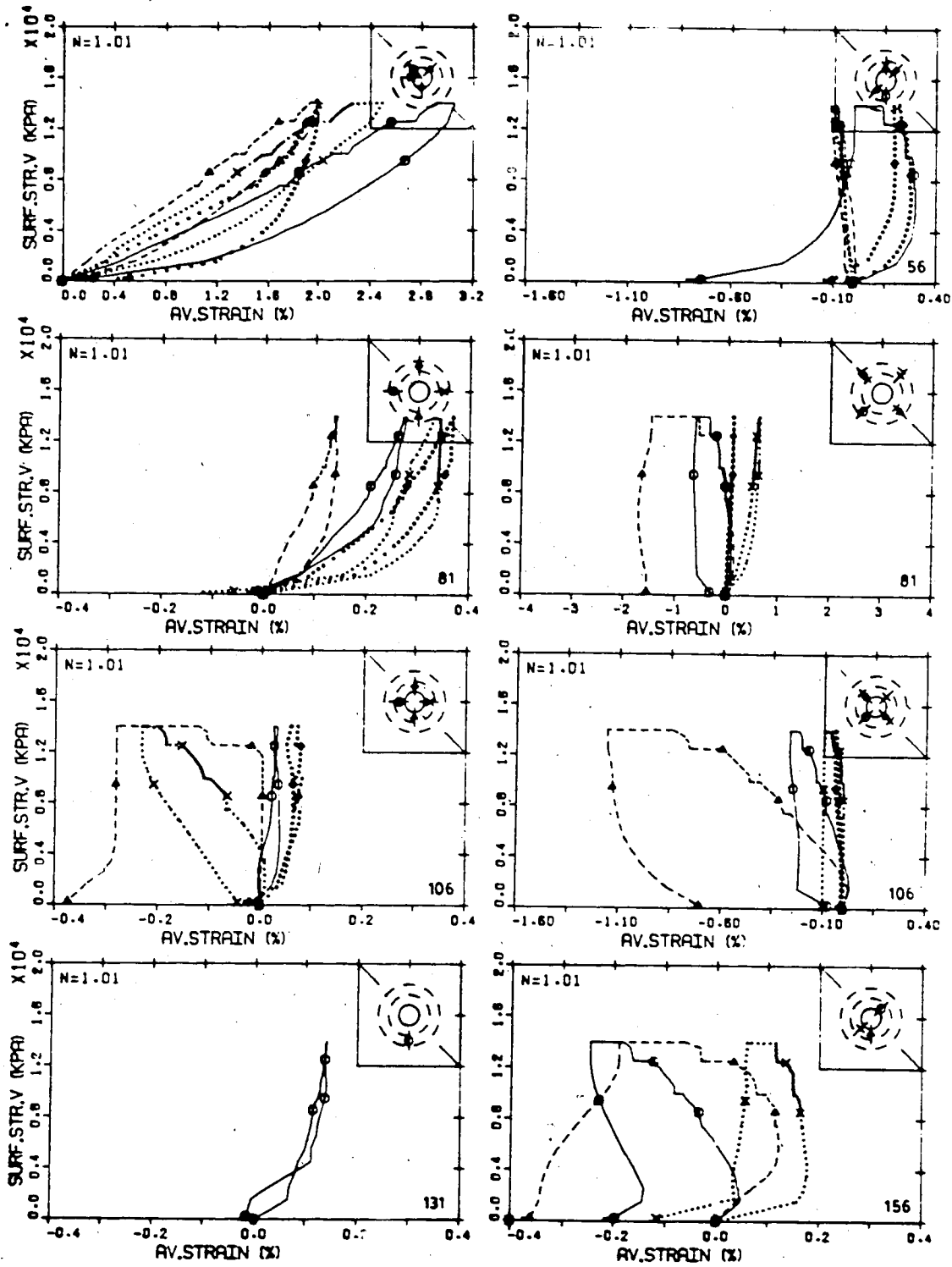


Figure 5.5 Tunnel Closure and Extensometer Response :
Test MC-7.15

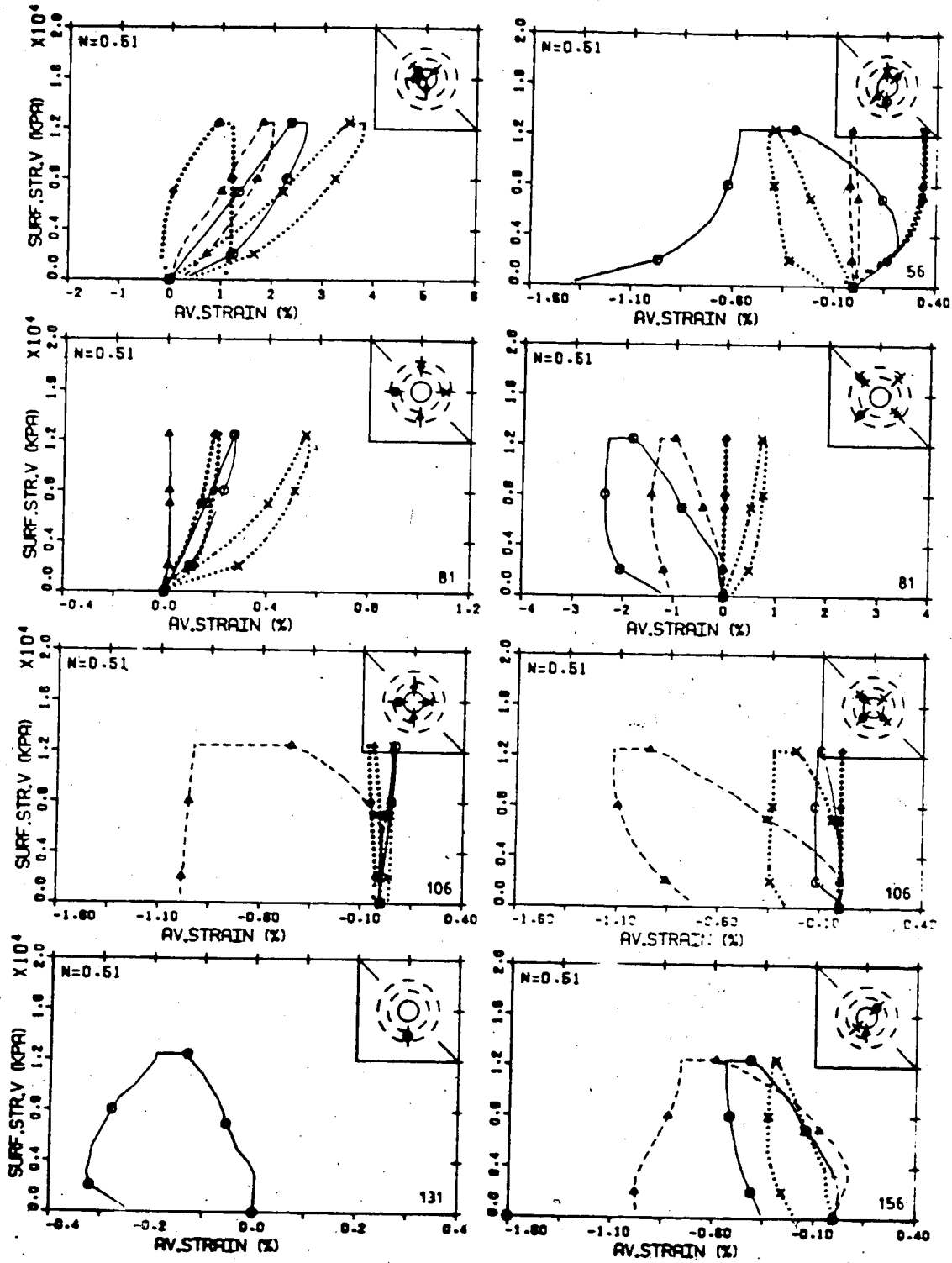


Figure 5.6 Tunnel Closure and Extensometer Response :
Test MC-7.16

diameter are essentially recoverable. The measured radial strains continued to indicate yielding in the 135° orientation with expansion through 90° to 45° (Sta. 81). An interesting observation with regard to the strains recorded in the 45° orientation is that strains on the order of 2% (extension) were recorded far from the tunnel wall (Sta. 81) while much less straining was observed near the wall (Sta. 56, 106 and 156). There is no reason to discard the reading at Sta. 81 as the instrument performed satisfactorily in earlier tests. Therefore, it must be concluded that both anchor points of the near tunnel extensometers are moving in unison as a result of deep seated deformation processes.

As a result of these investigations, it can be further concluded that while tunnel convergence may give an indication of yielding or other stress redistribution processes, it does not provide any information regarding the type or location of the process. Extensometers can provide that information, however, they must be properly located and of sufficient extent.

5.2.2 Time-Dependent Behaviour

The absolute magnitude of tunnel closure or radial strain cannot generally be determined in the field due to the impracticality of instrumentation ahead of the face in deep tunnels or the limited face access during advance. It has thus been found convenient to use the rate of deformation rather than the magnitude of deformation as an

indicator of tunnel performance (see Chapter 2). For this reason, interpretation of the results of this test program will be based on the time-dependent observations presented in double logarithmic plots of deformation rate versus time.

As shown in the previous section and discussed by Kaiser (1981d) and Kaiser and Morgenstern (1982), tunnel convergence reflects the overall behaviour of the underground opening but must be combined with extensometer measurements to delineate the yield or failure mechanisms, their locale and extent. The above observations led to the selection of the closure rate as an indicator of tunnel behaviour with the extensometer response employed to define the behaviour.

5.2.2.1 Critical Closure Rates

The time-dependent response of the rock mass depends, to a large extent, on the intensity of the applied load. At low stress levels, terminating (primary) creep will lead to a finite creep strain whereas at high stress levels, a transition from primary to tertiary creep with increasing creep rates leading to failure will be observed. It would therefore seem likely that there is a strain rate boundary separating the terminating from the accelerating creep range. This critical creep rate function, $CCR(t)$, is shown schematically in Figure 5.7a.

This behaviour is typical of that encountered in uniaxial compression tests. Under load P_1 , the observed creep rate function falls below the critical creep rate

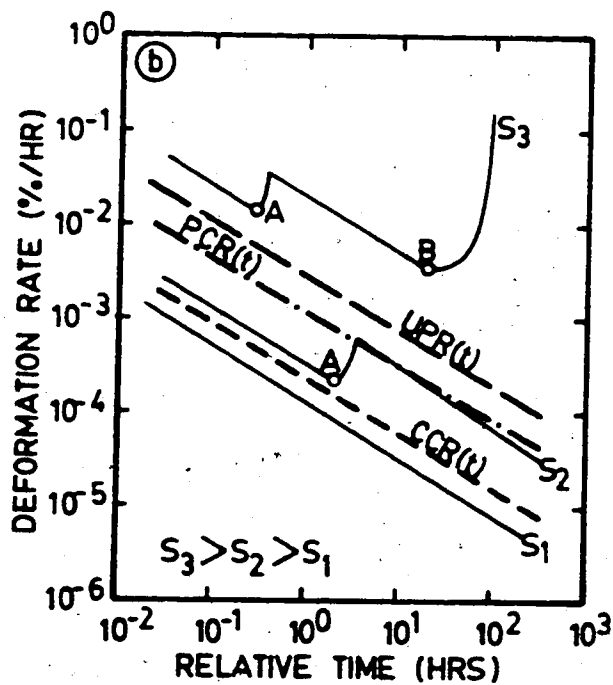
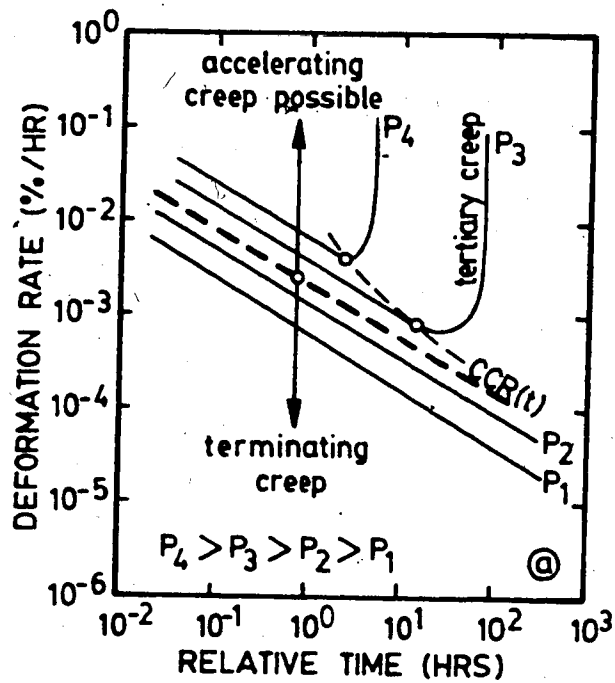


Figure 5.7 Schematic Representation of the Critical Rate Functions : a) uniaxial compression test; b) tunnel

function and creep terminates. Under P_2 , the observed creep rate function is greater in magnitude than under P_1 , but still less than the $CCR(t)$ and the creep terminates. Under loads P_3 and P_4 , the strength of the material is exceeded. The observed rates are greater in magnitude than the $CCR(t)$ and accelerating creep resulting in failure occurs.

In tunnelling situations, initiation of yielding will not necessarily lead to collapse but to a change in the rate of deformation due to the change in the rock mass structure and hence, its deformation properties. The type of response expected in tunnelling situations is shown schematically in Figure 5.7b. Under a field stress S_1 , only primary creep and no yielding occurs (below $CCR(t)$). Under field stress S_2 , some yielding occurs as noted by the increase in deformation rate at point A. Stress is redistributed around the opening and a higher terminating creep rate curve is reached. This creep rate is called the post-yield creep rate, $PCR(t)$. It is the rate that is reached after propagation has terminated. Besides other factors, it will depend on the extent and shape of the yield zone generated under field stress S_2 . Under an even higher field stress S_3 , yielding may occur first at point A and again at point B. At this point the structure may collapse and become unstable if the degree of freedom is sufficiently high to create a collapse mechanism. Under S_3 , the creep rate function is such that no stable equilibrium is possible. The rate function at which this unstable failure propagation occurs is called the

unstable propagation rate function, $UPR(t)$. The $UPR(t)$ can only be reached in near surface openings or in cohesionless materials where unstable propagation is possible.

Figure 5.8 summarizes the observed closure rates observed in Test MC-4.2 [Guenot (1979)]. According to the rate function definitions given previously, two closure rate functions have been sketched. A linear $CCR(t)$ was chosen to follow the upper limit of the non-yielding creep curves (shaded region). The $PCR(t)$ was assumed to be parallel to the $CCR(t)$ and was drawn touching the highest rates measured during the test at 14 MPa when stable yield zone propagation was observed. The $UPR(t)$ could not be accurately located as no tests leading to collapse were executed.

For simplicity and comparison with other test results, it was decided to consider rates at $t = 1, 5$ and 20 hours rather than the entire creep rate function. The applicable values obtained from Figure 5.8 are:

$$\left. \begin{array}{ll} t=1 \text{ hr} & CCR(1)=30 ; PCR(1)=80-100 \\ t=5 \text{ hrs} & CCR(5)=9 ; PCR(5)=25-30 \\ t=20 \text{ hrs} & CCR(20)=3 ; PCR(20)=8-10 \end{array} \right\} \times 10^{-3} \%/\text{hr}$$

The two creep rate functions defined in this manner allow characterization of the tunnel behaviour.

The direct application of the closure rate functions, determined from external loading tests, in the evaluation of tunnel behaviour is questionable as the condition of external loading does not correspond with reality. However, if the processes are independent of the loading sequence,

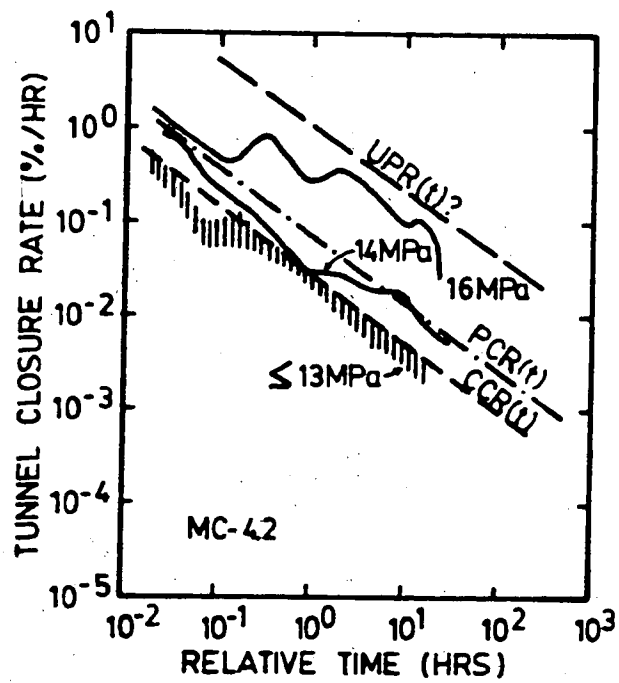


Figure 5.8 Typical Tunnel Closure Rates During Test MC-4.2

then they are applicable. In order to determine the loading history dependence, the range of closure rate curves for tests with a stress ratio, N , of unity (shaded areas) were compared with the the mean compressional strain rates of the intact coal sample in Figure 5.9.

Comparing pre- and post-excavation test results from Sample MC-5, it can be seen that the tunnel closure rates are consistently one order of magnitude (or more) greater than the mean compressional strain rate. Hence the component of pre-excavation creep in tests performed on Sample MC-5 is negligible and the measured rates correspond closely to the rates that would be measured in a test correctly modelling reality.

Because of the higher creep potentials of Samples MC-6 and particularly MC-7, under compression, a significant portion of the tunnel closure rate may be due to the compression of the coal block in external loading tests. Comparison of closure rates measured during external loading and an excavation simulation test on Sample MC-7 (Figure 5.10) however, indicates that there is little, if any difference and that the closure rate functions as defined may be applied.

The evaluation of tunnel behaviour by closure rate measurements during excavation simulation and when the tunnel diameter was less than 108 mm was not possible. In these situations, tunnel behaviour was evaluated by radial creep strain rate functions defined in a manner analogous to

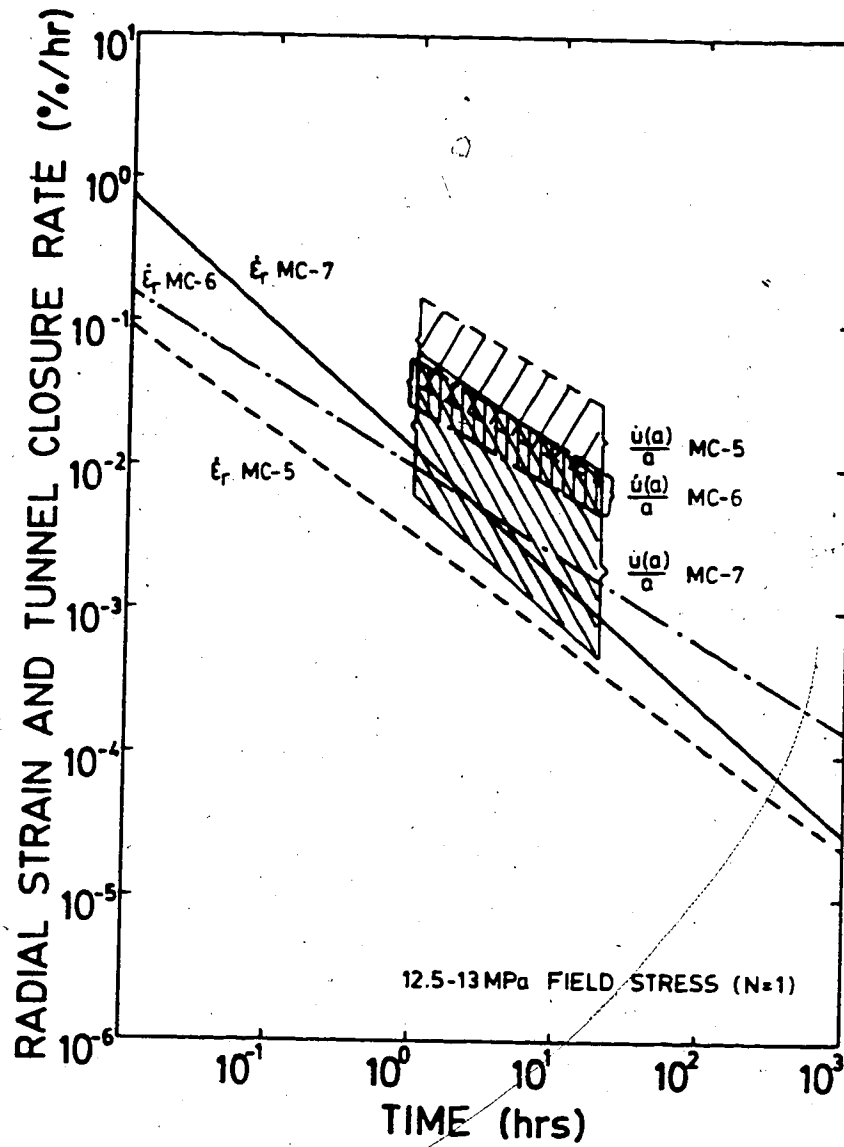


Figure 5.9 Compressional Strain Rates for Intact Samples and Ranges of Tunnel Closure Rates for Samples MC-5 to MC-7

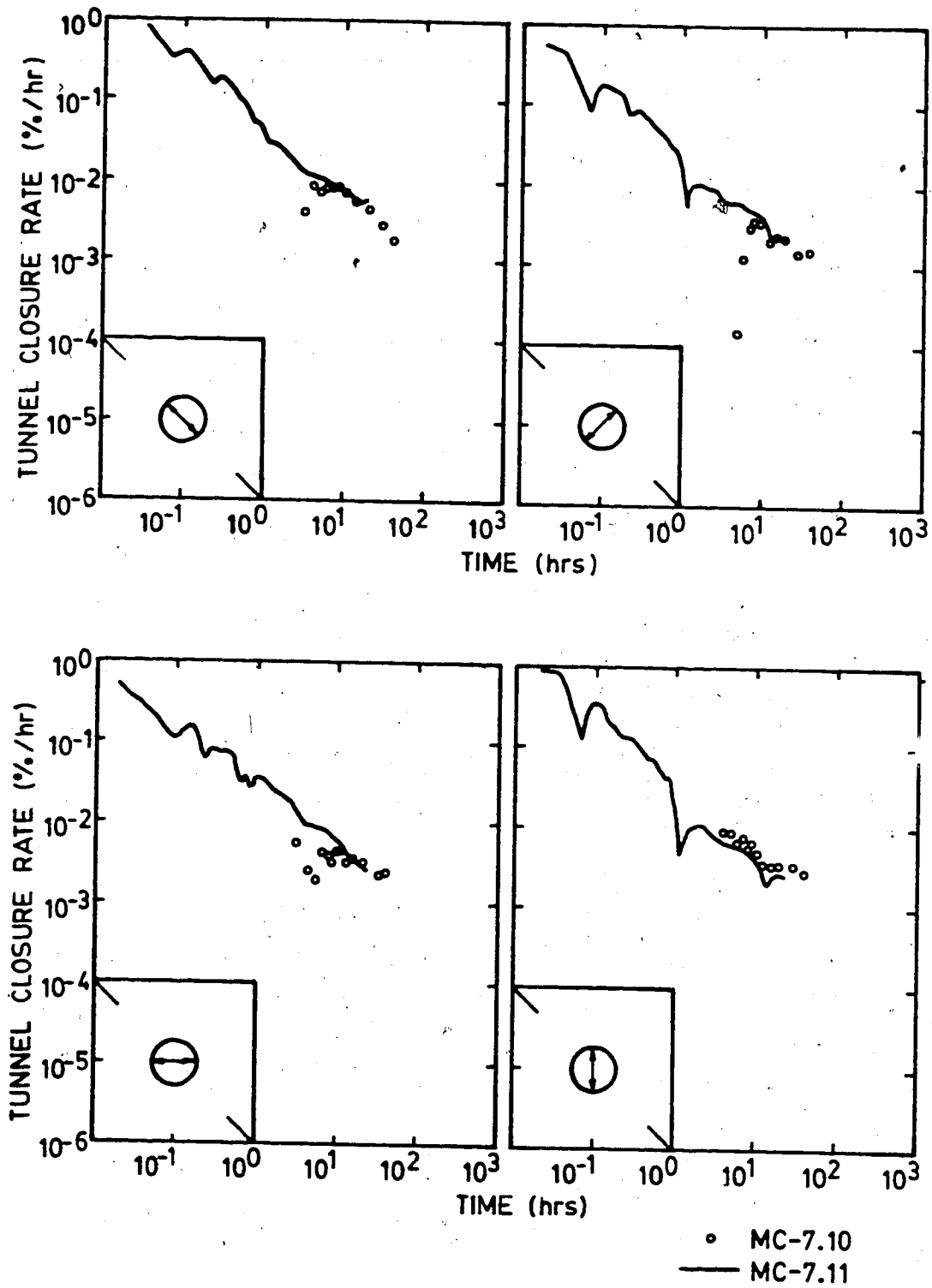


Figure 5.10 Comparison of Observed Tunnel Closure Rates under Excavation (Test MC-7.10) and External Loading (Test MC-7.11) Conditions

those presented for closure. In order to avoid confusion with the closure rate functions new labels have been assigned to the strain rate functions as follows:

CSR(t) corresponding to the CCR(t);

PSR(t) corresponding to the PCR(t); and

USR(t) corresponding to the UPR(t).

While the compressional creep component could be neglected in evaluating the tunnel closure rates, it cannot be disregarded in the evaluation of radial creep strain rates. The creep strain increment observed in the test may be dominated by the sample compression depending on the magnitudes of the elastic (i.e., Young's) and bulk moduli [Kaiser and Morgenstern (1982), Eqn. 10].

In an isotropic elastic medium under conditions of plane strain and equal lateral field stresses ($N=1$), the time-independent closure resulting from the excavation of a tunnel is given by:

$$u(a)/a = p_o/2G \quad \text{Eqn. 5.1}$$

where $u(a)$ = tunnel wall displacement;

a = tunnel radius;

p_o = field stress; and

G = shear modulus.

and the time-independent radial strain by:

$$\epsilon(r) = -p_o a^2 / 2Gr^2 \quad \text{Eqn. 5.2}$$

where r = distance from tunnel centre to the point of interest.

The ratio of tunnel closure to radial strain for the elastic case is then given by:

$$\frac{[u(a)/a]}{r} = -(r/a)^2 \quad \text{Eqn. 5.3}$$

Assuming that the same relationship holds for the time-dependent behaviour under simulated field conditions, the appropriate values for the radial creep rate functions are $-(r/a)^2$ times the closure rate functions. For external loading tests the required values of the strain rate functions may be obtained from the following relationships:

$$\begin{aligned} \text{CSR}(t) &= -(a/r)^2 \times \text{CCR}(t) + \text{COMP}(t) \\ \text{PSR}(t) &= -(a/r)^2 \times \text{PCR}(t) + \text{COMP}(t) \\ \text{USR}(t) &= -(a/r)^2 \times \text{UPR}(t) + \text{COMP}(t) \end{aligned} \quad \text{Eqn. 5.4}$$

where $\text{COMP}(t)$ = the compressional strain rate at time (t) calculated assuming an elastic stress distribution.

5.2.2.2 Evaluation of Test Results

Tables 5.1 and 5.2 summarize the stress levels at which the $\text{CCR}(20)$ or $\text{CSR}(20)$ and $\text{PCR}(20)$ or $\text{PSR}(20)$ were reached for the mean (in brackets), the maximum and the minimum tunnel closure or radial strain rate. These stress levels were determined from the plots of stress versus log closure rate presented in Appendix B. In the same tables are listed

Table 5.1 Predicted Stress Level for CCR(20) and PCR(20) and Observed Stress Level where Propagation Clearly Observed from Extensometers - Samples MC-5 and MC-6

TEST NO. MC-	PREDICTED STRESS LEVEL		Observed Max. Radial Creep Strain Increment (Extensometer)	Predicted Mode	Observed Mode	Agreement ?
	CCR(20) () Mean	PCR(20) () Mean				
5.05	<7.5-(8.2)-11.0	9.5-(10.5)-12.2	13-<0.92 10-<0.22 8-<0.12	13-P 10-1P 8-1	13-P 10-1 8-17	Yes Yes ?
5.07	11.5-(12)-12.7	--	13-<0.42 10-<0.12	13-1	13-1P 10-17	Yes ?
5.09	<6.7->13.5	13.0->13.5	13-<1.92 11-<0.22 7-<0.12	13-P 11-1P 7-17	13-P 11-1 7-17	Yes Yes Yes
5.11	<11.0-(11.5)->13.5	13.0-(>13.5)->13.5	13-<2.82 11-<0.52	13-P 11-1	13-P 11-1	Yes Yes
5.13	<11.0->11.0	>11.0 after unloading	13-No creep 11-<1.52 9-<0.72	13-P 11-1P 9-1	13-P 11-P 9-1	Yes Yes Yes
6.02	<<12.6	<12.6	13-<3.82*	13-P	13-P*	Yes ?
6.03	<12.5	>12.5	13-<0.12	13-1	13-17	Yes
6.04	12.2-(12.7)-13.0	14.4-(14.8)-15.2	15-<0.22 13-<0.12	15-1P 13-17	15-1 13-17	Yes Yes
6.05	<12.5	>12.5	13-<0.12 (comp.)**	13-1	13-<1**	No?
6.050	<12.5	<12.5-(>12.5)->12.5	13-<0.82	13-P	13-P	Yes
6.06	<12.5-(<12.5)->12.5	>12.5	13-<0.42	13-1	13-1P	Yes
6.08	8.2-(10)-11.2	13.5-(14)-15.0	15-<0.82 13-<0.22 10-<0.12	15-P 13-1P 10-1	15-P 13-1P 10-1	Yes Yes Yes
6.09	10-(12)-12.7	15.2-(>15)->15	15-<0.62 13-<0.22 10-<0.12	15-1P 13-1 10-17	15-P 13-1 10-17	Yes Yes Yes
6.10	<12.0->12.0	<12-12.0	12-<0.62	12-1P	12-P	Yes
6.11	10-14	13->15	15-<0.92 12-<0.32 10-<0.12	15-P 12-1P 10-17	15-P 13-1P 10-1	Yes Yes Yes

[MPa]

[MPa]

[inner ring strain recorded during entire creep stage]
[MPa - %]

[MPa - Mode]

[MPa - Mode]

* only observed in last measurement; prior to this, the maximum creep strain increment was 0.12% indicating initiation rather than propagation

** nearest strain measurement at 36 mm from tunnel wall; near tunnel strain not observed, hence, yielding may not be detected by instruments.

Table 5.2 Predicted Stress Level for CCR(20) and PCR(20) and Observed Stress Level Where Propagation Clearly Observed from Extensometers - Sample MC-7

N	Test No	Predicted Stress Level [MPa]		Observed Maximum Radial strain Increment	Predicted Mode	Observed Mode	Agreement
		CCR(20) (mean)	PCR(20) PSR(20) (mean)				
1.01	7.08	<12.5	<12.5	12.5-<0.02%	12.5-1P		No*
1.01	7.10pw	<12.5		12.5-<0.01%	12.5-1P		No*
1.01	7.10	<12.5		12.5-<0.10%	12.5-1	12.5-1	Yes
1.01	7.11	<12.5		12.5-<0.05%	12.5-1	12.5-1	Yes
1.02	7.12	11.5-(13.1)-13.8	14.2	7.5-<0.02% 10.0-<0.02% 12.5-<0.08% 14.3-<0.25%	12.5-1 12.5-1 14.3-P	12.5-1 12.5-1 14.3-1P	Yes Yes
1.01	7.13pw			12.5-<0.20%		12.5-1	No**
1.02	7.13	12.5		12.5-<0.30%	12.5-1	12.5-1P	Yes
1.02	7.14			12.5-<0.80%		12.5-P	No**
1.01	7.15	13.5-(13.8)-14.0		7.5-<0.06% 10.0-<0.08% 12.5-<0.35% 14.0-<1.00%	14.0-1	12.5-1P 14.0-P	No** No**
0.52	7.16	<12.5		12.5-<0.50%	12.5-1	12.5-1P	Yes
0.51	7.17	12.5		7.5-<0.11% 10.0-<0.17% 12.5-<0.35%	12.5-1	7.5-1 10.0-1 12.5-1P	No** No** Yes?

pw = pre-widening

* = instruments not sufficiently close to tunnel wall

** = rates exceeded at times other than 20 hrs, therefore agreement with prediction achieved

the observed maximum radial creep strain increments occurring during the corresponding creep stage indicated by the stress level. The mode of behaviour was predicted by comparisons of the actual closure or radial strain rate with the proposed rate functions at a time of 20 hours. The observed mode of behaviour was determined from the creep strain increment in the following manner. If the creep strain increment was less than 0.2%/20 hrs but obviously larger than at lower stress levels "initiation" (I) was assumed; if it was about 0.2 to 0.4%/20 hrs "initiation-propagation transition" (IP) was assigned; and if it was greater than 0.6%/20 hrs "propagation yielding" (P) was assigned. This latter limit was selected arbitrarily, however, a creep strain of 0.6%/20 hrs will clearly lead to accumulated strains in excess of the failure strain of coal and hence does reflect propagating yielding. In the final column it is shown whether prediction and observation agree.

Excellent agreement between prediction and observation were achieved for Samples MC-5 and MC-6. Good agreement was achieved for Sample MC-7 (Table 5.2) Apparent conflicts between predicted and observed behaviour for Sample MC-7 can be resolved by comparison of the full closure rate functions with the double log plots of closure rate versus time or consideration of test limitations as follows:

Tests Mc-7.08 and MC-7.10 pre-widening - Because of future test requirements no instrumentation was sufficiently close to

the tunnel wall to detect any yielding;

Tests MC-7.13 pre-widening and MC-7.14 - While the limits of the appropriate functions are not exceeded at a time of 20 hours, an examination of the complete curves shown in Figure 5.11 show jumps indicative of yielding in the closure rate curves at earlier times. Two possible explanations for the failure of the proposed CCR in indicating the onset of yielding are:

1. The values for the critical rate functions are too high for this specimen. Reduction of the functions by approximately 30% would yield more accurate predictions; and
2. The behaviour mode is different than those previously described. Early high rates indicative of local slip or local yield are rapidly dissipated by stress redistribution without global yielding (i.e., the overall structure of the rock mass is not significantly altered). The longer term behaviour is that of a non-yielding tunnel even though the local strain magnitudes indicate that yielding has occurred.

Test MC-7.15 - Examination of the complete curves show closure rates in excess of those defined by the CCR curve and approaching the PCR curve at a field stress of 12.5 MPa (Figure 5.12a). Figure 5.12b shows that at a stress of 14 MPa the closure rate was again in excess of the CCR curve and then exceeded the PCR curve at a time of 20 hours (this late surge in closure rate had been previously ascribed to

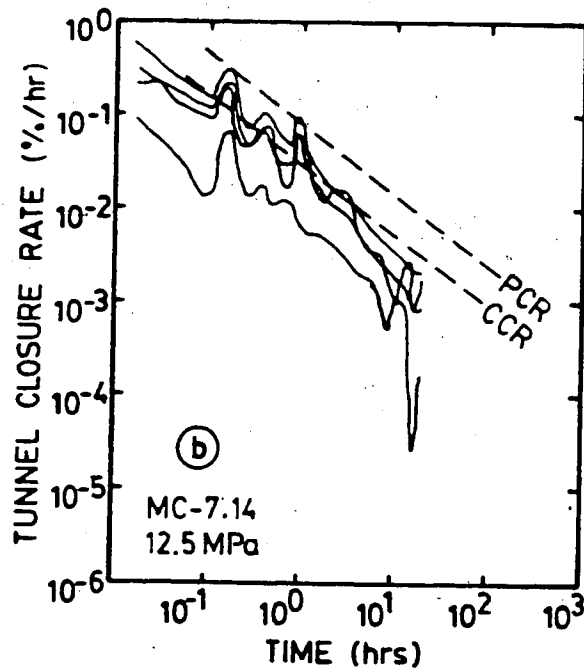
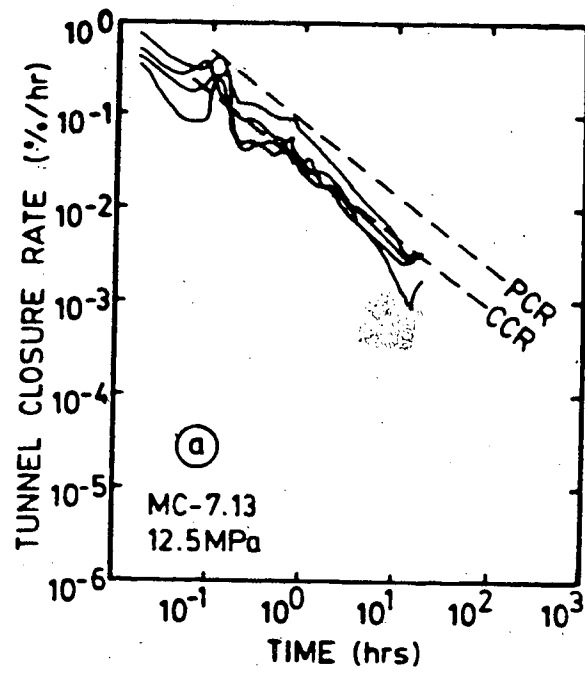


Figure 5.11 Observed Tunnel Closure Rates : a) Test MC-7.13 pre-widening; b) Test MC-7.14

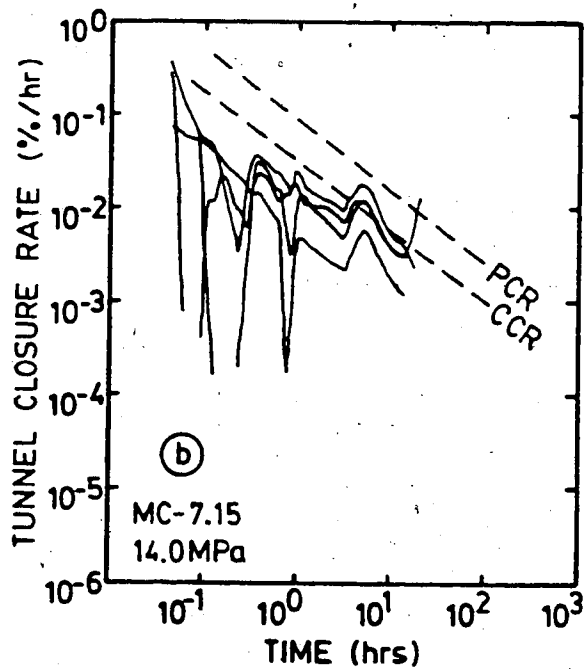
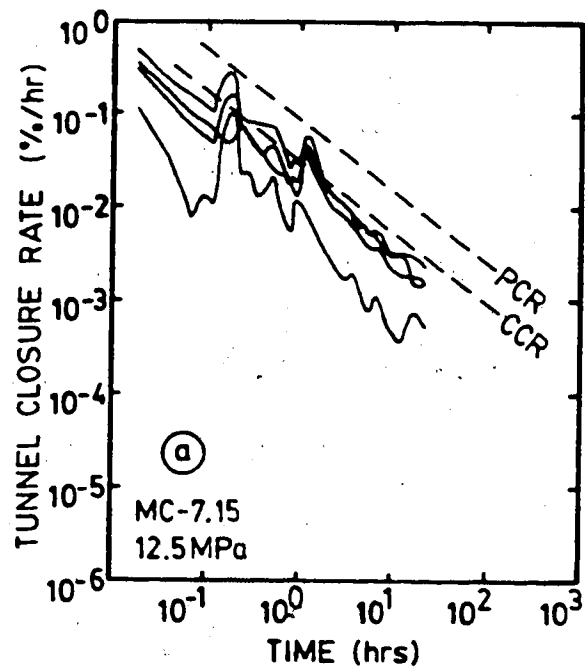


Figure 5.12 Observed Tunnel Closure Rates - Test MC-7.15

instrument fluctuation). Hence, agreement with the observed was achieved; and

Test MC-7.17 - Examination of the complete curves (Figures 5.13 a to c) shows that while the prescribed limits were not exceeded at a time of 20 hours, they had been at an earlier time (at principal field stresses of 10 and 12.5 MPa). At a maximum field stress of 7.5 MPa, the CCR curve was not exceeded, however a marked increase in closure rate between 1 and 2 hours indicated that some yielding had occurred. Again, complete curves show agreement between predicted and observed behaviour even though at the specified time of 20 hours, agreement had not been observed.

It may therefore be concluded that the mode of behaviour could be predicted with reasonable accuracy for all external loading tests. The closure rate trend or change in closure rate seem to provide an excellent indication of the proximity and extent of stress redistribution processes (even though neither the failure mechanism nor its location can be determined) and hence is a good measure to evaluate the short and long-term stability of an underground opening.

The derivation of displacement rate criteria for tunnel evaluation and their subsequent verification in model tests resulted in some important observations in the use of displacement rate criteria. These are as follows:

1. The agreement achieved between predicted and observed behaviour in the three specimens indicate that the concept of critical rate functions should be suitable

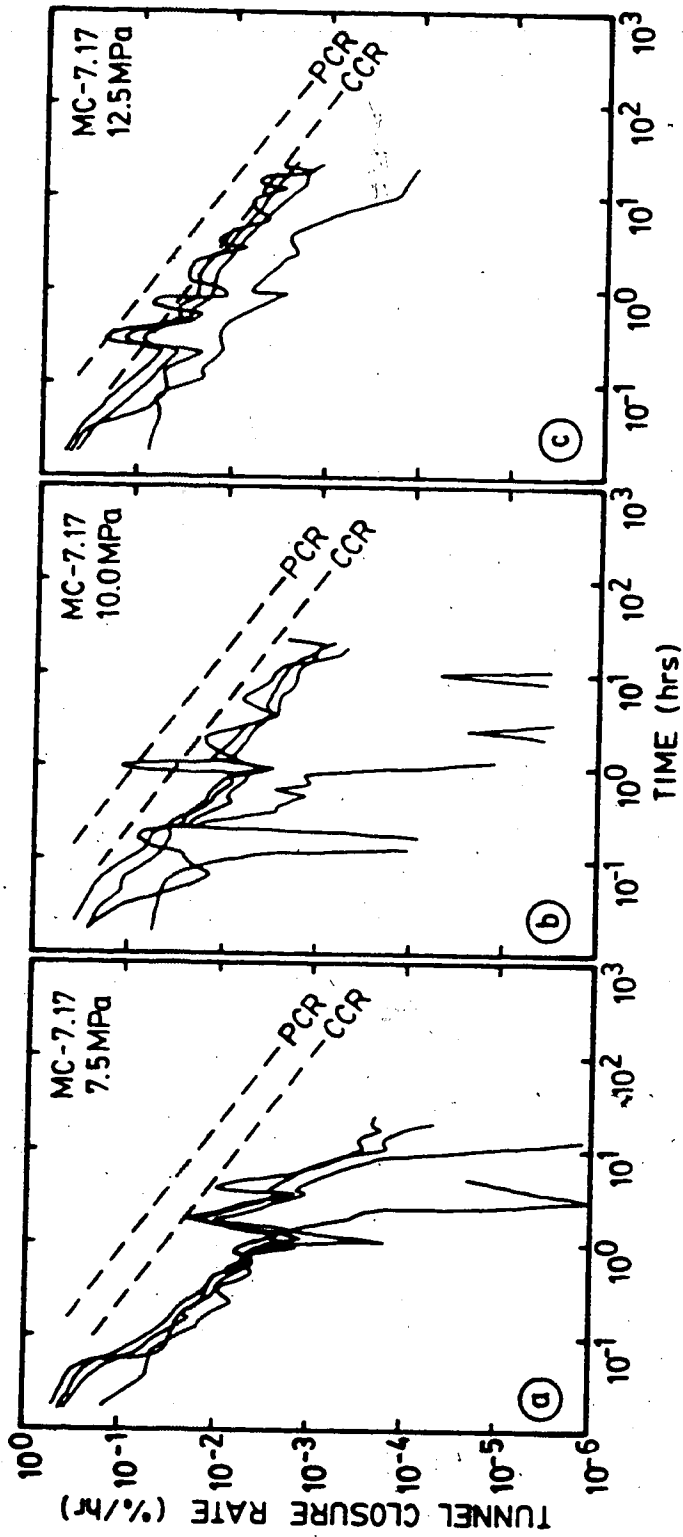


Figure 5.13 Observed Tunnel Closure Rates - Test MC-7.17

- for stability evaluation practice;
2. It is necessary to consider the complete (or at least a significant portion of the) closure or strain rate curve and not just the rates at specific times. As shown in Figures 5.11 to 5.13 the observed rate may be less than the critical rates at the 'test' times but may have exceeded the limits at intermediate times. This in turn raises two further points:
 - (i) Tunnel closure or radial strain measurement should be started as soon as possible after excavation and should be taken as often as possible to avoid masking of intermediate behaviour. In addition, reliable determination of tunnel advance effects are only possible if the early part of the rock response is known; and
 - (ii) The tendency towards linearization (i.e. best fit) of the closure or strain rate versus time relationship in a double log plot should be discouraged. Apparent fluctuations in rate, that may be attributed to instrument error, may be indicative of real processes and have considerable bearing on the tunnel behaviour;
 3. Multi-directional tunnel closure or radial strain measurements are required to detect behaviour indicative of yielding. Too few readings may result in misinterpretation. Figures 5.11 to 5.13 show that often only one of the four diameters is experiencing closure

rates in excess of the prescribed limits. If measurement had not been made in this critical orientation the prediction of adverse behaviour could not have been made. This also supports the argument for local yielding; and

4. Rates in excess of the prescribed closure or strain rate functions are not the exclusive indicator of behaviour mode. Anomalies in the double log plots of closure rate versus time as shown in Figure 5.13a at a time of 2 hours are an indication of yielding or softening as well. It is the deviation from the normal trend that should be considered rather than a strict adherence to specific critical values.

In practice, the problem of determining the site specific closure or radial strain rate functions for a specific rock type remain to be solved. However, by continuous monitoring of rates in stable, intermediate and unstable sections of an opening, one should be able to determine appropriate values. These can then be related to construction procedure and support capacity. This latter process requires the separation of the effects due to face advance from the time-dependent rock deformation.

5.3 Behaviour During Excavation Simulation Tests

A total of five tests on two specimens, Samples MC-6 and MC-7, were performed to evaluate the behaviour of the tunnel during its advance. The processes involved could only

be determined from extensometer measurements as the recording of tunnel convergence during excavation was not possible. These extensometer measurements will to some extent be influenced during the excavation process by the proximity of the sample boundaries (perpendicular to the tunnel axis) that are one or less tunnel diameter from the measuring points. The effect of these boundaries in the direction of the tunnel axis should not dominate the behaviour because of the close simulation of the real condition by maintaining plane strain conditions in the plane perpendicular to the tunnel axis.

5.3.1 Behaviour Near the Tunnel Face

Panet and Guenot (1982) have analyzed the convergence behind the tunnel face and identified an apparently unique relationship between convergence related to tunnel advance and radius of the plastic zone. This relationship cannot be directly applied to the test results because of the lack of convergence measurements during excavation. Hence, it was necessary to determine a relationship between convergence and radial strain. This is simple for a tunnel in a linear elastic material but complicated for tunnels in yielding rock.

As a first approximation the test results were compared with the prediction for advance in a linear elastic material. The effect of time-dependent deformations are treated independently of the tunnel advance effect and are

assumed to superpose directly.

For a circular tunnel in a linear elastic medium under uniform field stresses ($N=1$) the radial strains are given by Equation 5.2 and the displacements by:

$$u(r) = (p_0/2G) (a^2/r) \quad \text{Eqn. 5.5}$$

The ratio of radial strain to tunnel wall displacement, $u(a)$, is then:

$$\frac{e(r)}{u(a)} = -a/r^2 \quad \text{Eqn. 5.6}$$

According to Panet and Guenot (1982) the tunnel wall displacement rate $u'(x)$ for the elastic case is:

$$u'(x) = -2u(\infty)[(ka)/(ka+x)]^2/ka \quad \text{Eqn. 5.7}$$

where $k = 0.84$ (found by curve fitting);

x = distance from tunnel face in the direction of the tunnel axis; and

$u(\infty)$ = ultimate elastic tunnel wall convergence (i.e., the difference between the convergence recorded when the face is at the measuring station and when the face is at an infinite distance from the station).

Employing the relationship defined by Equation 5.6 results in the following expression for the radial strain rate as a

function of the distance from the tunnel face:

$$\epsilon'_r(x) = 2a^3 u(\infty) [(ka)/(ka+x)]^3 / kr^2 \quad \text{Eqn. 5.8}$$

For the condition of tunnel widening it is necessary to consider only the differential tunnel wall displacement, $\Delta u(\infty)$ (i.e., the difference in convergence, $u(\infty)$, for the two tunnel sizes), due to incremental stress change to predict the rates. Equation 5.8 can be rewritten to yield an expression for the radial strain rate as a function of time by use of the Chain Rule:

$$\epsilon'_r(t) = (d\epsilon'_r / dx)(dx/dt) \quad \text{Eqn. 5.9}$$

where $d\epsilon'_r / dx = \epsilon'_r(x)$ as given by Equation 5.8; and $dx/dt =$ rate of tunnel advance, d' .

Expanding Equation 5.9 and substituting $d't$ for x yields:

$$\epsilon'_r(t) = 2a^3 u(\infty) d' [k/(ka+d't)]^3 / kr^2 \quad \text{Eqn. 5.10}$$

A similar expression for the tunnel closure rate as a function of time can be derived as:

$$u'(t) = -2u(\infty) d' [(ka)/(ka+d't)]^3 / ka \quad \text{Eqn. 5.11}$$

The rates predicted by Equations 5.10 and 5.11 are applicable only during active advance of the tunnel. If

excavation or widening is interrupted or completed, the effect of advance is lost and only rates due to the time-dependent properties of the rock mass are measured.

In order to verify the validity of Equation 5.10 comparisons of predicted response were made with the observed response in four excavation simulation tests, MC-6.02, MC-7.08, MC-7.10 and MC-7.13. Test MC-6.05 was not similarly investigated due to the number of interruptions during excavation. Rather than just comparing the observed rate which included all time effects with the predicted rate due to face advance, it was decided to compare it with the predicted total response (obtained by incorporating those expressions developed in Chapter 4 for the time-dependent response of the rock mass).

Rigorous simulation of the actual response to excavation or widening was considered too refined for the purpose of this investigation, however, it was felt that reasonable approximations to the behaviour could be made by application of some simplifying assumptions:

1. The material is homogeneous and isotropic with respect to both its time-independent and time-dependent properties.
2. The time-independent response is linearly elastic;
3. The time-dependent response is as specified in Chapter 4;
4. The stress change due to the creation or widening of the tunnel at a given station along the tunnel axis occurs

immediately upon the arrival of the tunnel face.

Comparison of this assumed stress response with observed stress changes during widening (Figure 5.14) as recorded by Korpach (1983) shows that this assumption is reasonable for preliminary analysis. Alternatively, a progressive change in stress such as proposed by Sakurai (1978) may be employed; and

5. Direct superposition of the various components of time-dependent deformation is acceptable.

Predictions of the radial strain rate were made, at a given station along the tunnel axis for the instruments nearest to and furthest from the tunnel wall (inner ring of extensometers only) in order to bound the expected behaviour. The predicted response was determined by superposition of the following:

1. Extensional strain rate due to face advance;
2. Extensional strain rate due to stress relaxation;
3. Extensional strain rate due to the deviatoric stress conditions created by the excavation and;
4. Compressive strain rate due to the hydrostatic compression of the test specimen.

The respective components along with the net rates after superposition are shown in Figure 5.15 for Test MC-7.08 at Station 81, $r/a=4.64$ (extension negative).

Figures 5.16 and 5.17 show the predicted (heavy solid line) and observed radial strain rates during and following excavation of a 120 mm diameter tunnel in Sample MC-6. While

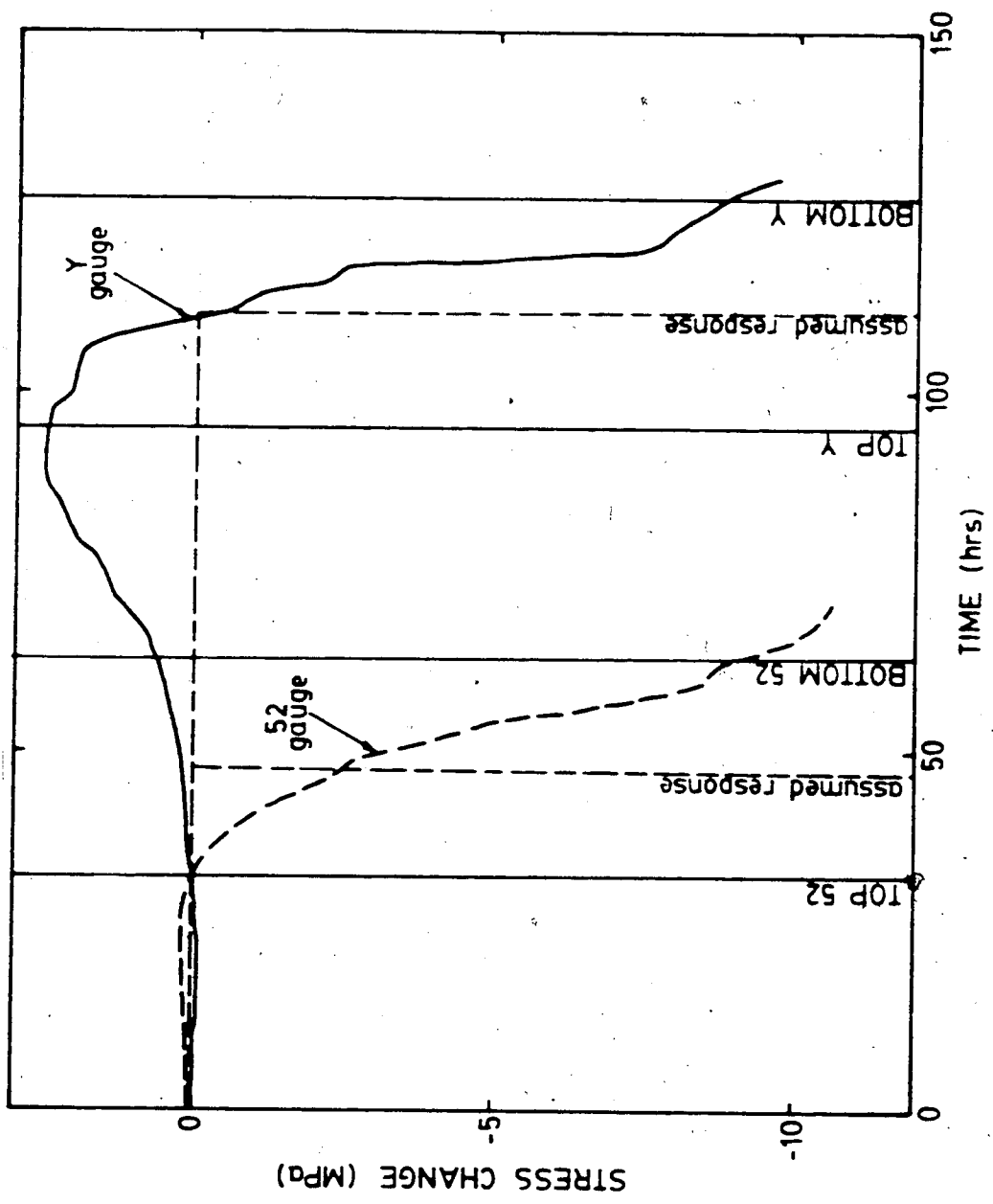


Figure 5.14 Observed Stress Changes in Tunnel Widening

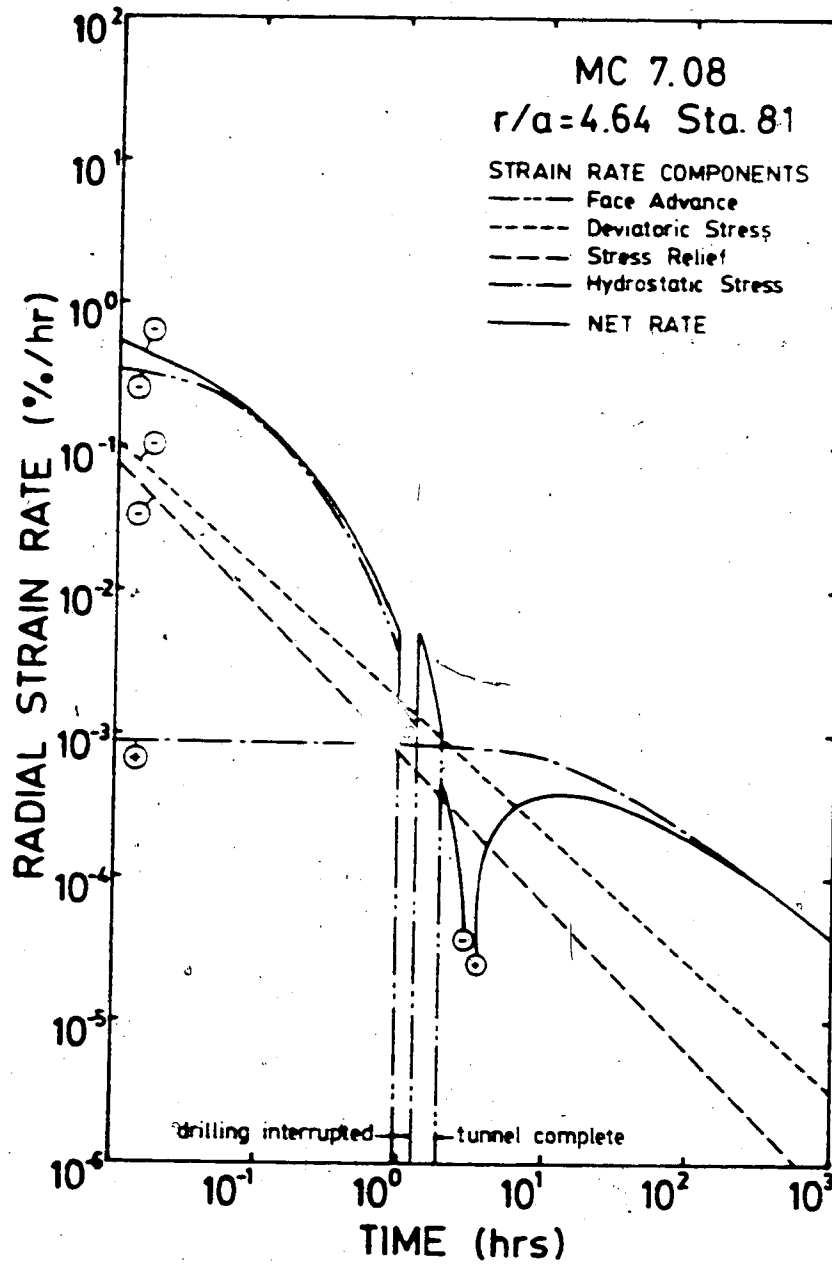


Figure 5.15 Predicted Radial Strain Rate Components - Tunnel Excavation (Test MC-7.08)

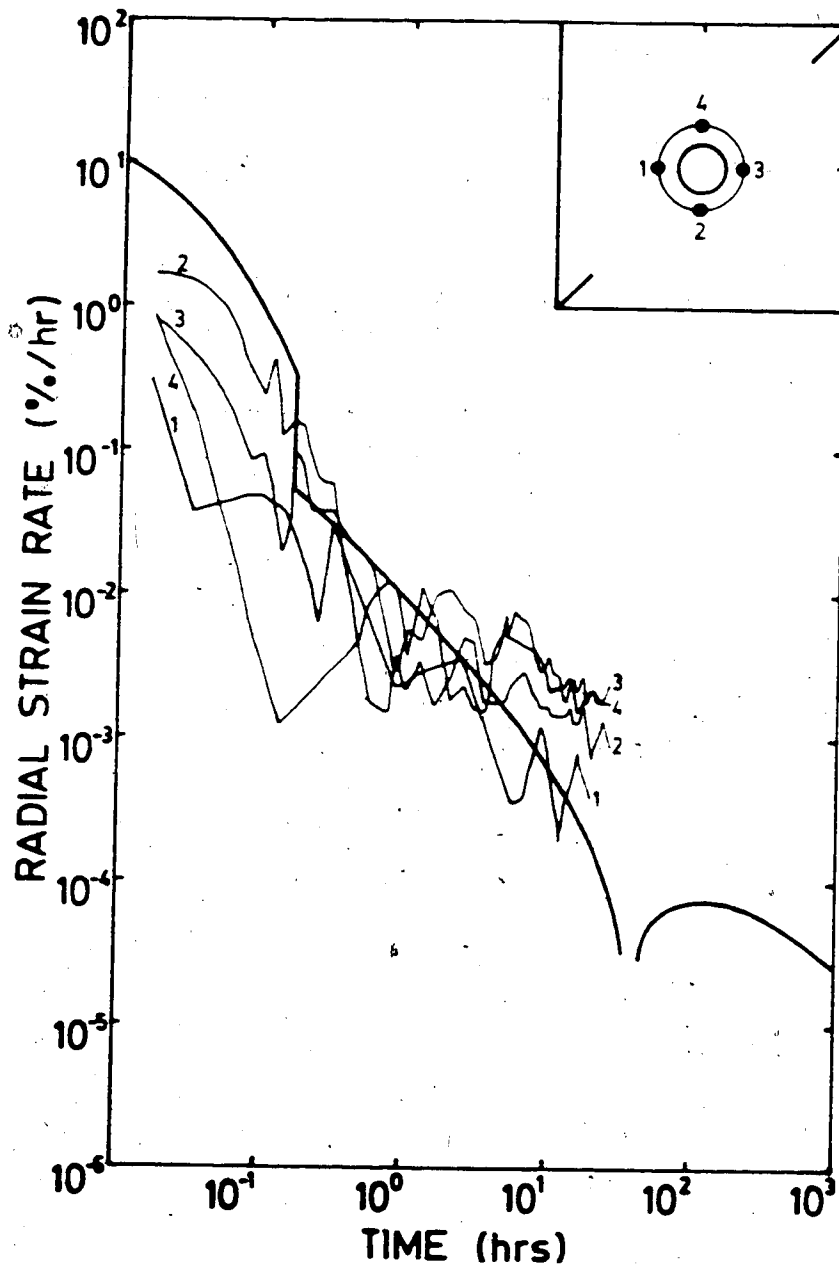


Figure 5.16 Comparison of Observed and Predicted Radial Strain Rates - Test MC-6.02, Parallel to Principal Stress Directions

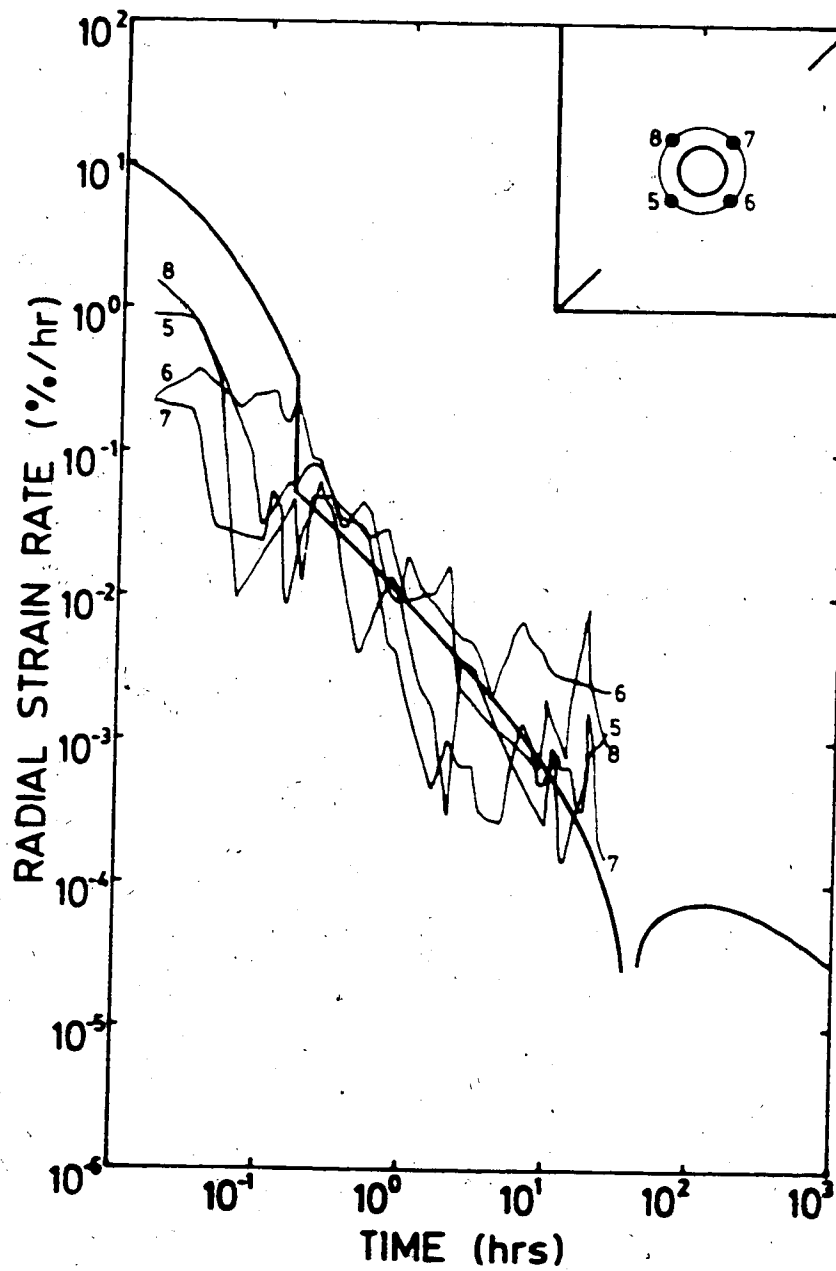


Figure 5.17 Comparison to Observed and Predicted Radial Strain Rates - Test MC-6.02, 45° to Principal Stress Direction

the post-excavation behavior is reasonably well predicted the strain rates during excavation are significantly overestimated. The poor agreement between predicted and observed radial strain rates is most probably a result of the boundary conditions of the model. Negligible shear stresses at the sample boundary result in little load transfer during advance to and slightly beyond the measuring station. Strains and therefore strain rates are below those expected in an infinite medium. As the tunnel face approaches the other boundary which again has negligible shear stresses the load increases more rapidly than would be the case in reality and strains and strain rates exceed those predicted. These effects would be most pronounced during initial excavation. Behaviour such as this was observed during both excavation and widening operations.

Figures 5.18 and 5.19 show the predicted (shaded area) and observed radial strain rates during and following excavation of the 42 mm diameter tunnel in Sample MC-7. The general trend of the radial strain rate is reasonably well predicted after a time of 0.2 hours. Prior to this the rates are overestimated as before. The face advance effect is clearly dominating the observed strain rates during excavation as demonstrated by the rapid increase in strain rate when drilling recommences following an interruption. Better correlation with the predicted value may have been achieved with instrumentation closer to the opening.

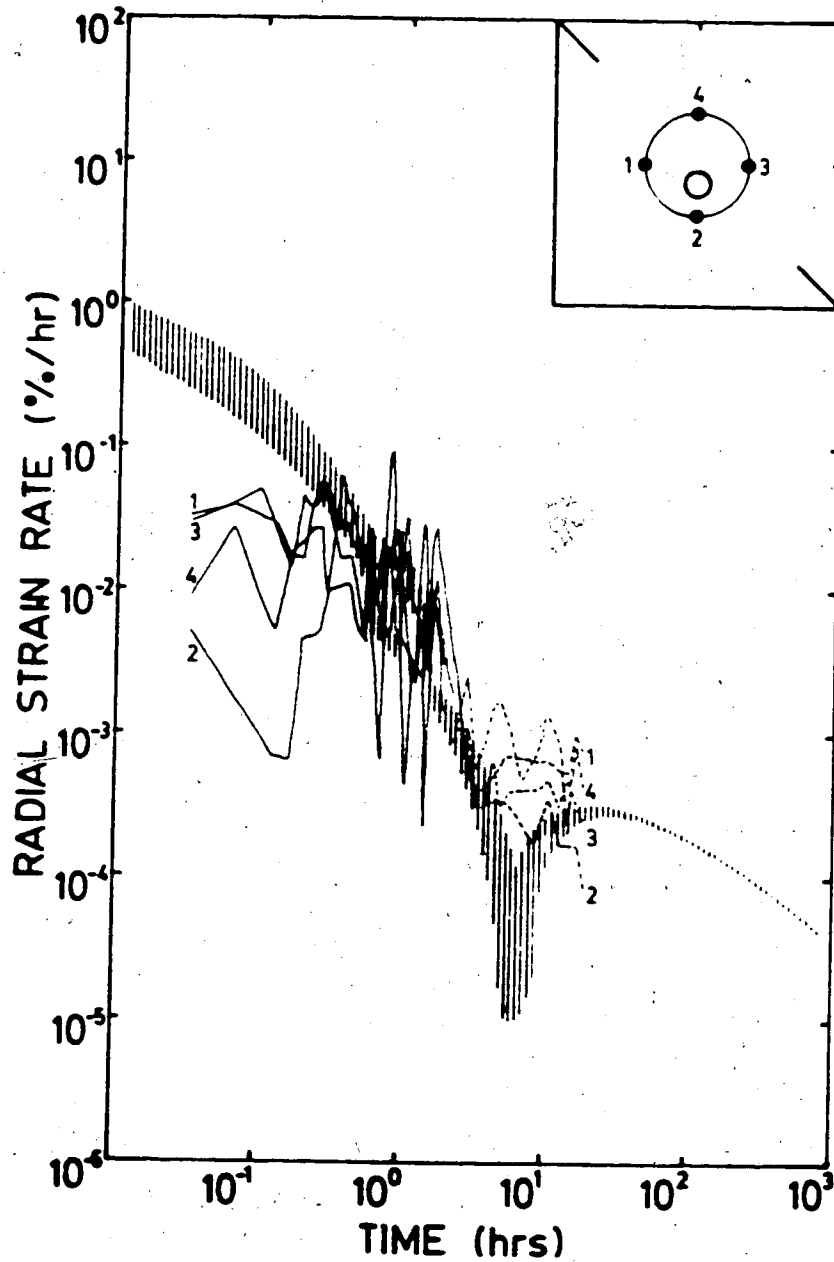


Figure 5.18 Comparison of Observed and Predicted Radial Strain Rates - Test MC-7.08, Parallel to Principal Stress Directions

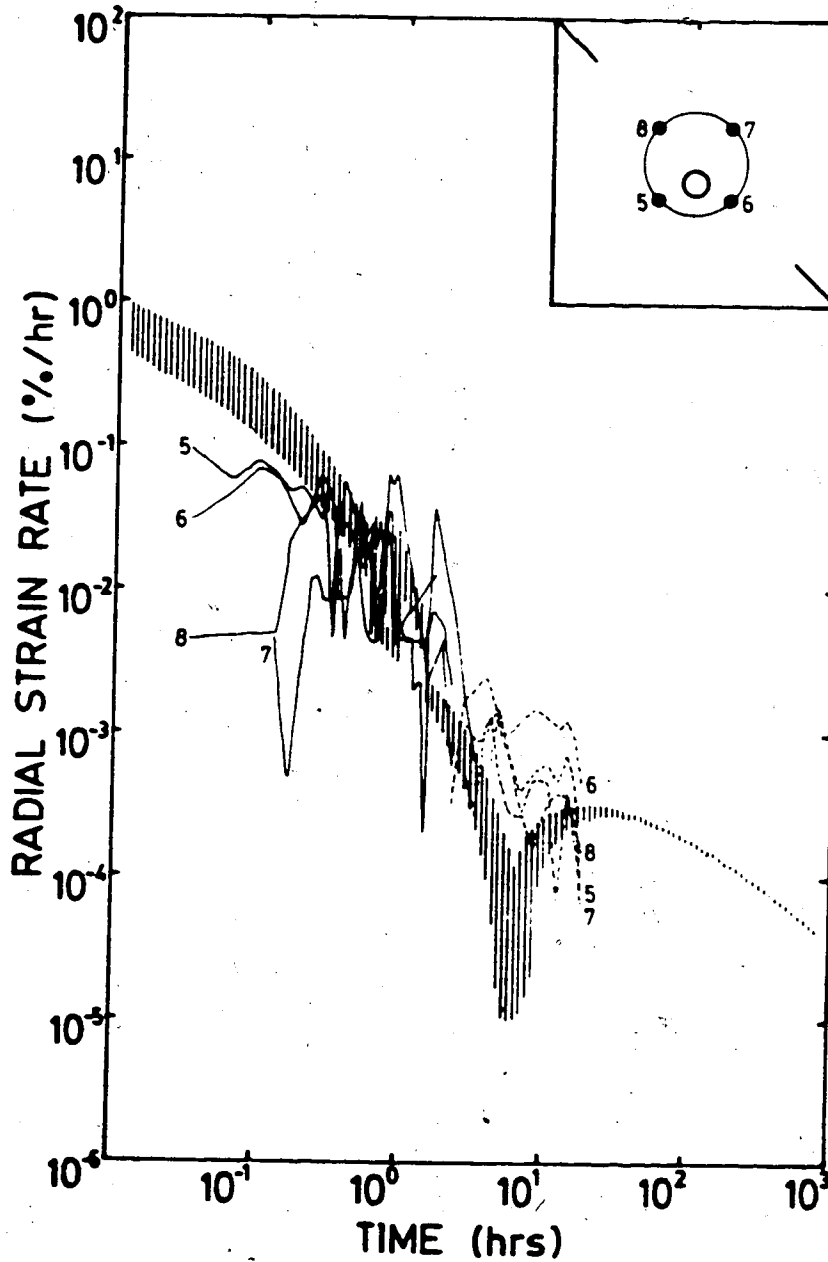


Figure 5.19 Comparison of Observed and Predicted Radial Strain Rates - Test MC-7.08, 45° to Principal Stress Directions

Figures 5.20 to 5.23 present the predicted (shaded area or heavy line) and observed radial strain rates during and following the two tunnel widenings performed on Sample MC-7 (Tests MC-7.10 and MC-7.13). Excellent agreement between prediction and observation was achieved. The divergence of the predicted and observed responses with increasing time can be related to the inaccuracy of the instruments at low strains and the deviation, at that instrument location, from the mean time-dependent parameters employed. Once again the dominance of the face advance effect is evident.

In both widenings extensometer #6 ($\theta=135^\circ$) exhibits strain rates considerably in excess of the others and of that predicted. This excess rate resulted from the initiation of yielding or softening during excavation which occurred during the tests at this location (see Figures 10.23 and 10.29) This yielding would have caused an upward shift (due to dilation and radial yield zone expansion) on the extensional strain rate curves resulting in the observed behavior. In the vicinity of the yielding zone the stress distribution is no longer elastic, as was assumed. The drop in radial stress will be greater than predicted and the stress level is definitely greater than predicted (equal to 1 if yielding occurred). Both these effects will result in an increase in the extensional strain rate. This increase may, in some cases, be sufficient to mask the face advance effect. A trend in that direction is evidenced by the response of extensometer #6 during the second widening

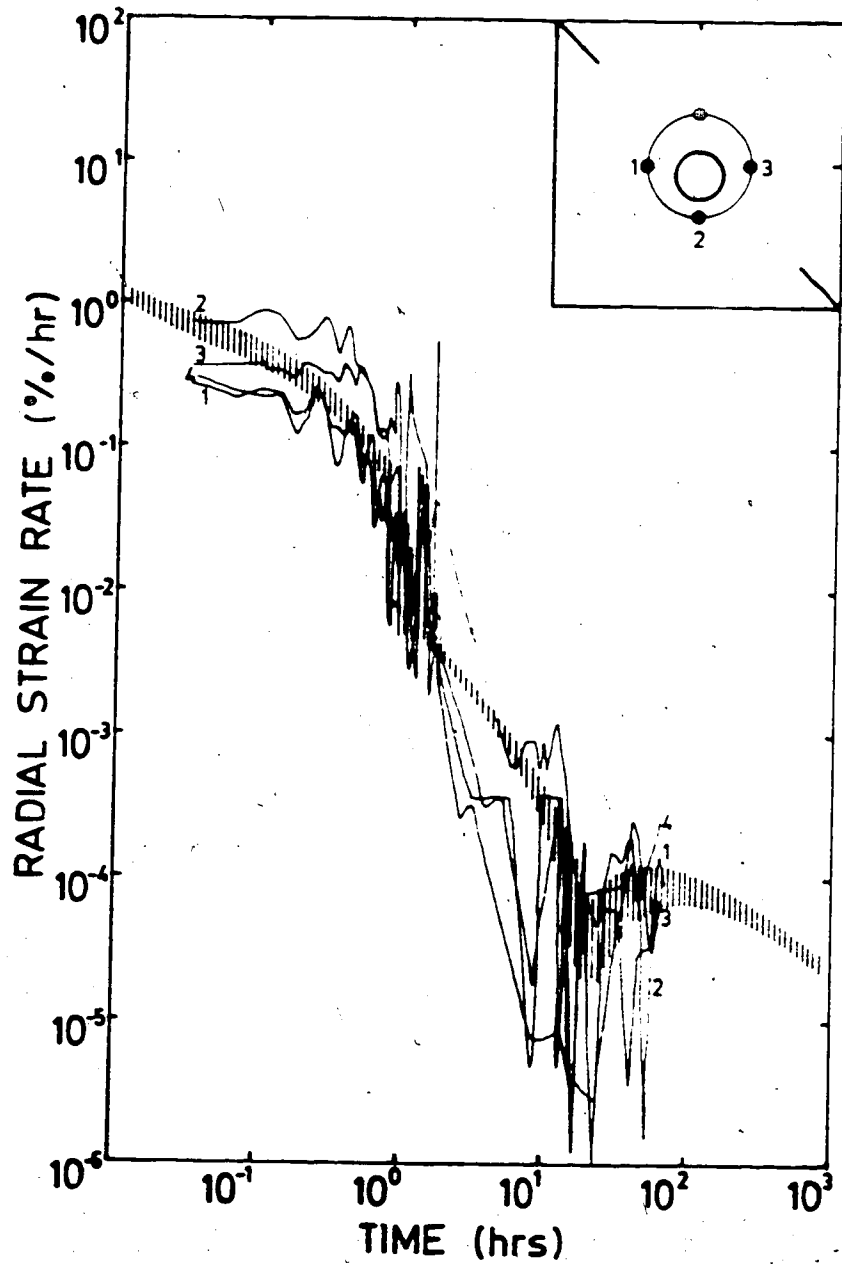


Figure 5.20 Comparison of Observed and Predicted Radial Strain Rates - Test MC-7.10, Parallel to Principal Stress Directions

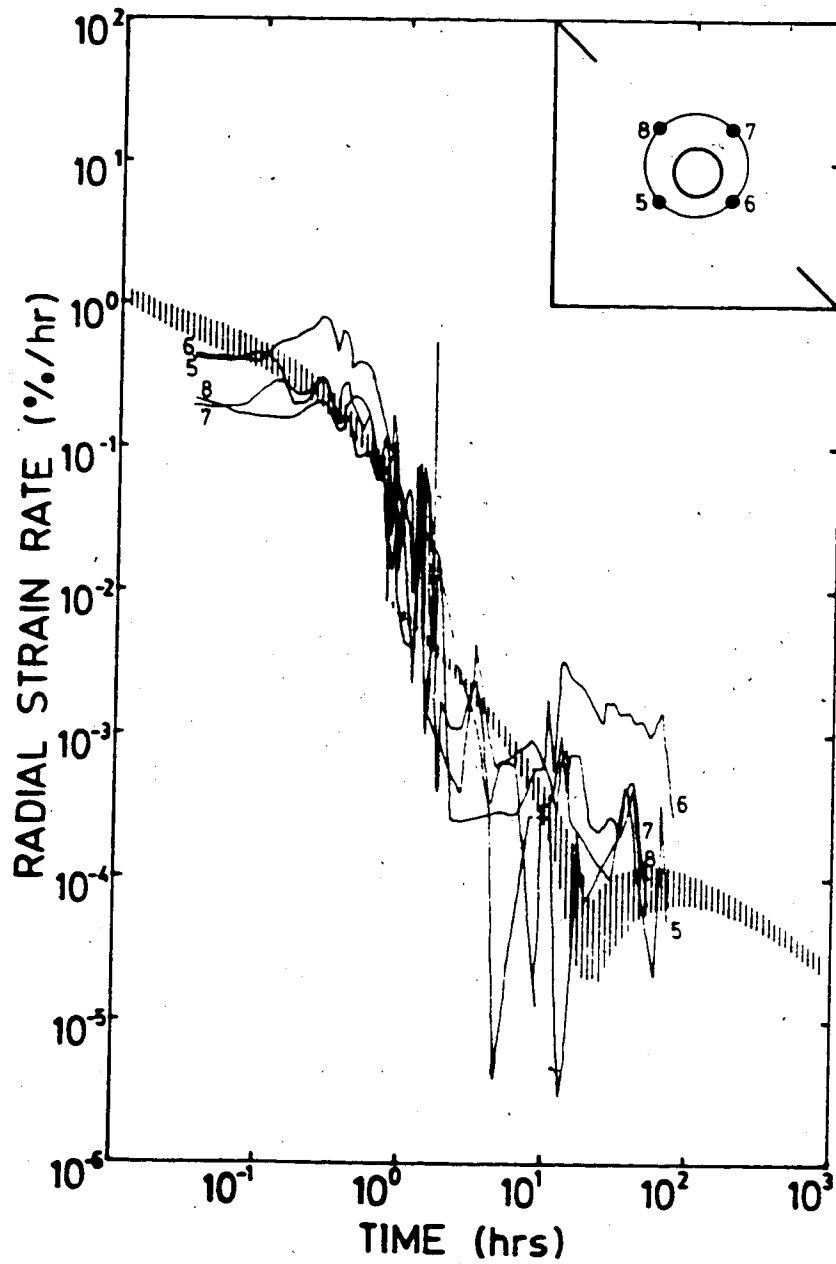


Figure 5.21 Comparison of Observed and Predicted Radial Strain Rates - Test MC-7.10, 45° to Principal Stress Directions

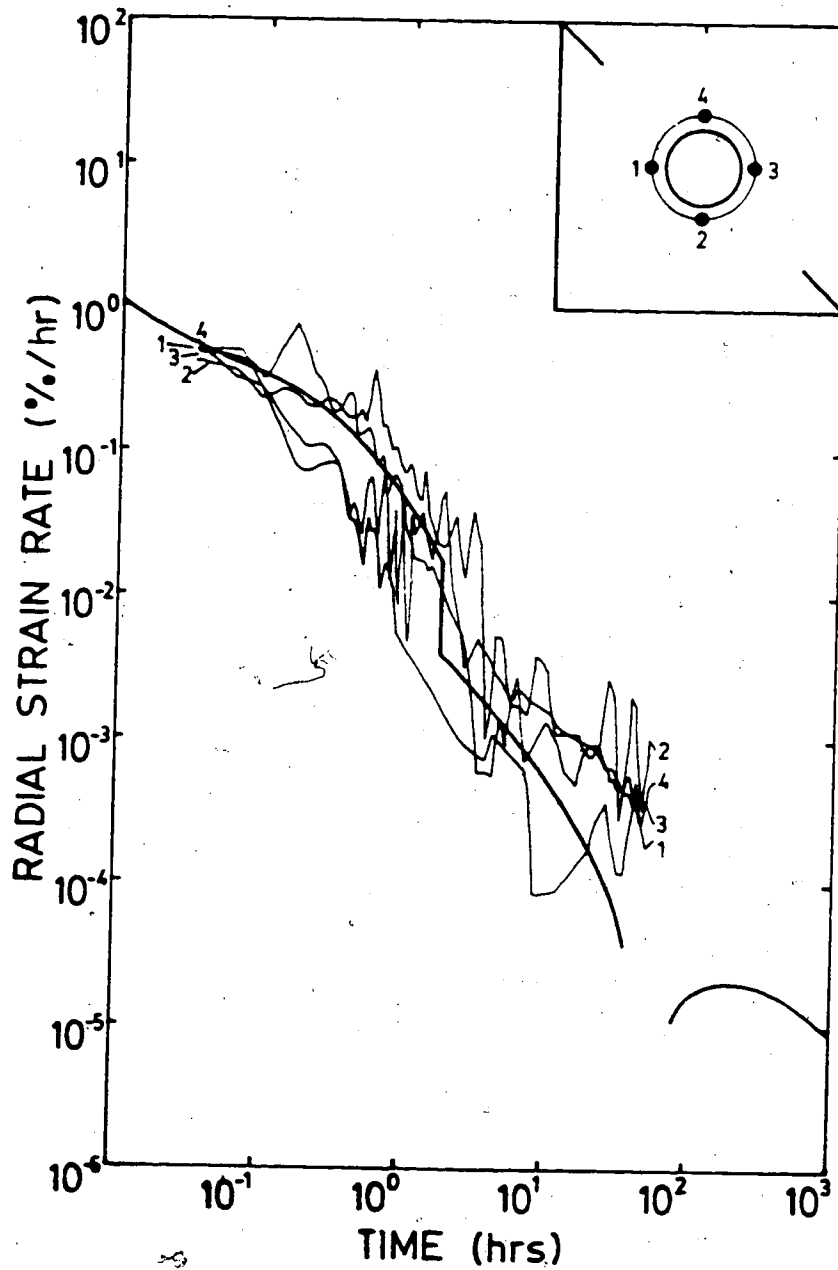


Figure 5.22 Comparison of Observed and Predicted Radial Strain Rates - Test MC-7.13, Parallel to Principal Stress Directions

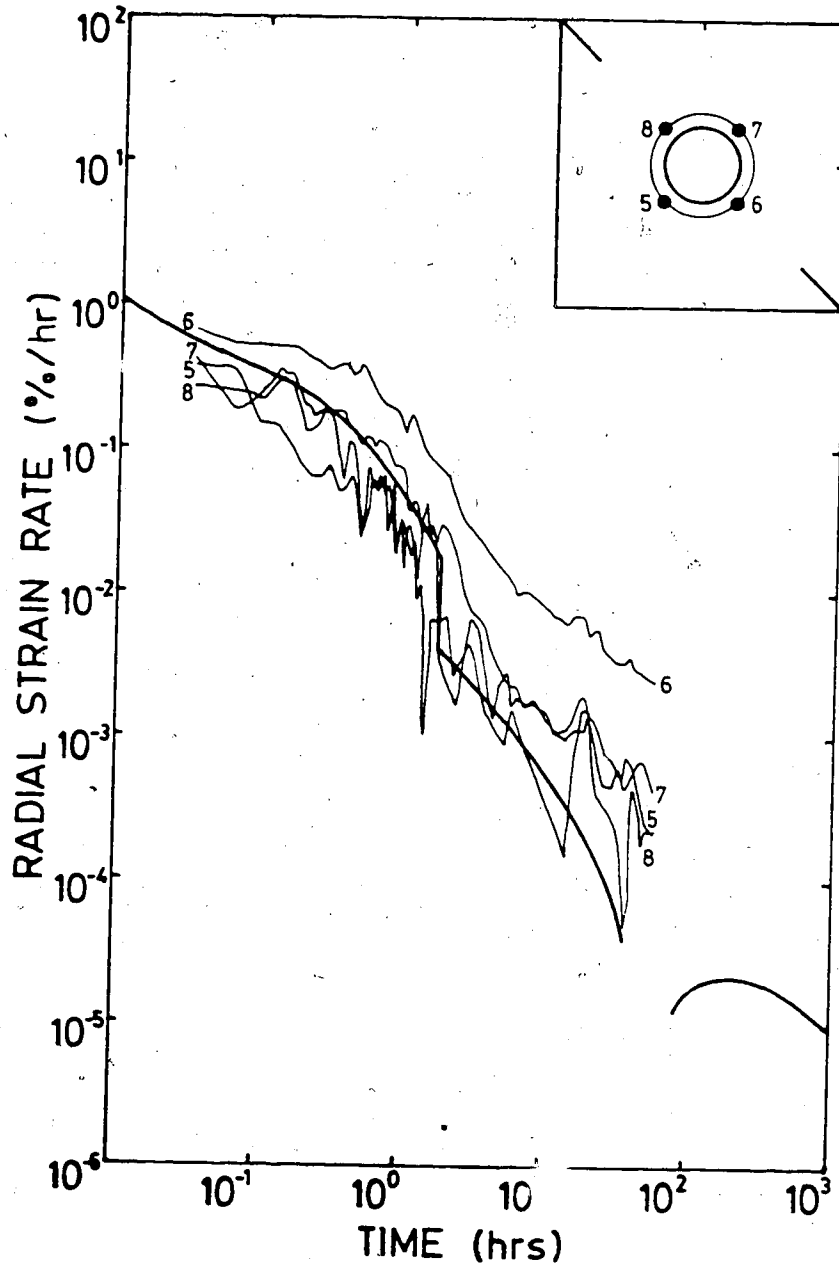


Figure 5.23 Comparison of Observed and Predicted Radial Strain Rates - Test MC-7.13, 45° to Principal Stress Directions

(Figure 5.23).

According to Panet and Guenet (1982) the convergence rate depends on the extent of the plastic or yield zone and the ultimate tunnel convergence. As it has clearly been demonstrated that the face advance generally dominates the strain rate for a sufficient time after advance, it should be possible to use these measured rates to determine the extent of the yield zone.

The tunnel convergence rate, as a function of the distance from the tunnel face, x , is given by Panet and Guenet (1982) as

$$u'(x) = (-2R^2 u(\infty) / k) [(k - kR/x)]^2 \quad \text{Eqn. 5.12}$$

where R = radius of the plastic (yield) zone;

k = 0.84 as before; and

$u(\infty)$ = ultimate tunnel wall displacement.

According to Kaiser (1980) the ultimate tunnel wall displacement in an elastic, brittle plastic material is given by

$$u(\infty) = \frac{\lambda}{e} [(1/a)] [2(R/a)^{1+a} + a - 1] p_0 a / 2G \quad \text{Eqn. 5.13}$$

where λ = $[1/(m+1)] [m-1 + (\sigma_c / p_0)]$;

a = dilation coefficient;

m = $\tan^2(45^\circ + \phi/2)$;

ϕ = angle of internal friction; and

σ_c = unconfined compressive strength.

Rewriting Equation 5.12 in terms of time, t , and substituting $d't$ for x yields:

$$u'(t) = [-2R^2 d' u(\infty) / k] [k / (kR + d't)]^3 \quad \text{Eqn. 5.14}$$

where d' = rate of tunnel advance.

The ratio of radial strain in the elastic zone to the displacement of the tunnel wall is given by:

$$\frac{\epsilon_r^e}{u(a)} = -[(R/r)^2 (1+a)] / a [2(R/a)^{1+a} + a - 1] \quad \text{Eqn. 5.15}$$

and the ratio of radial strain in the plastic zone to the displacement of the tunnel wall by:

$$\frac{\epsilon_r^{e+p}}{u(a)} = \{ -(1+a) / 2 - a [(R/r)^{1+a} - 1] \} / \{ a [2(R/a)^{1+a} + a - 1] \} \quad \text{Eqn. 5.16}$$

The above relationships allow determination of the radial strain rate due to face advance in a yielding medium as:
in the elastic zone:

$$\epsilon_r'(t) = [2R^4 (1+a) d' u(\infty) / k r^2 a] [k / (kR + d't)]^3 / [2(R/a)^{1+a} - 1] \quad \text{Eqn. 5.17}$$

in the plastic or yield zone:

$$\epsilon'_r(t) = \left\{ \left[\frac{(1+a)}{2} \right] + a \left[\left(\frac{R}{r} \right)^{1+a} - 1 \right] \right\} \left[\frac{2R^2 d'u(\infty)}{ka} \right] \left[\frac{k}{(kR+d't)} \right]^2 \left[\frac{2(R/a)^{1+a}}{1+a-1} \right] \quad \text{Eqn. 5.18}$$

Assuming that the plastic flow causes no change in volume (i.e., $\alpha=1.0$) Equations 5.17 and 5.18 can be reduced to:

$$\epsilon'_r(t) = \left[\frac{2R^2 ad'u(\infty)}{kr^2} \right] \left[\frac{k}{(kR+d't)} \right]^2 \quad \text{Eqn. 5.19}$$

and

$$\epsilon'_r(t) = \left[\frac{R^2 ad'u(\infty)}{kr^2} \right] \left[\frac{k}{(kR+d't)} \right]^2 \quad \text{Eqn. 5.20}$$

respectively.

As mentioned previously, yielding was noted in the 135° orientation during widening of the tunnels of Sample MC-7. In an attempt to determine the extent of this yield zone, Equation 5.19 was employed to predict the relationship between strain rate and time for different extents of the yield zone. The actual behaviour cannot be modelled as Equation 5.19 assumes axisymmetric behaviour; hence, only an equivalent, annular, yield zone radius is reported. The results of this investigation are presented in Figures 5.24 to 5.27 for the two extensometers located in this orientation. While these two instruments were located in the

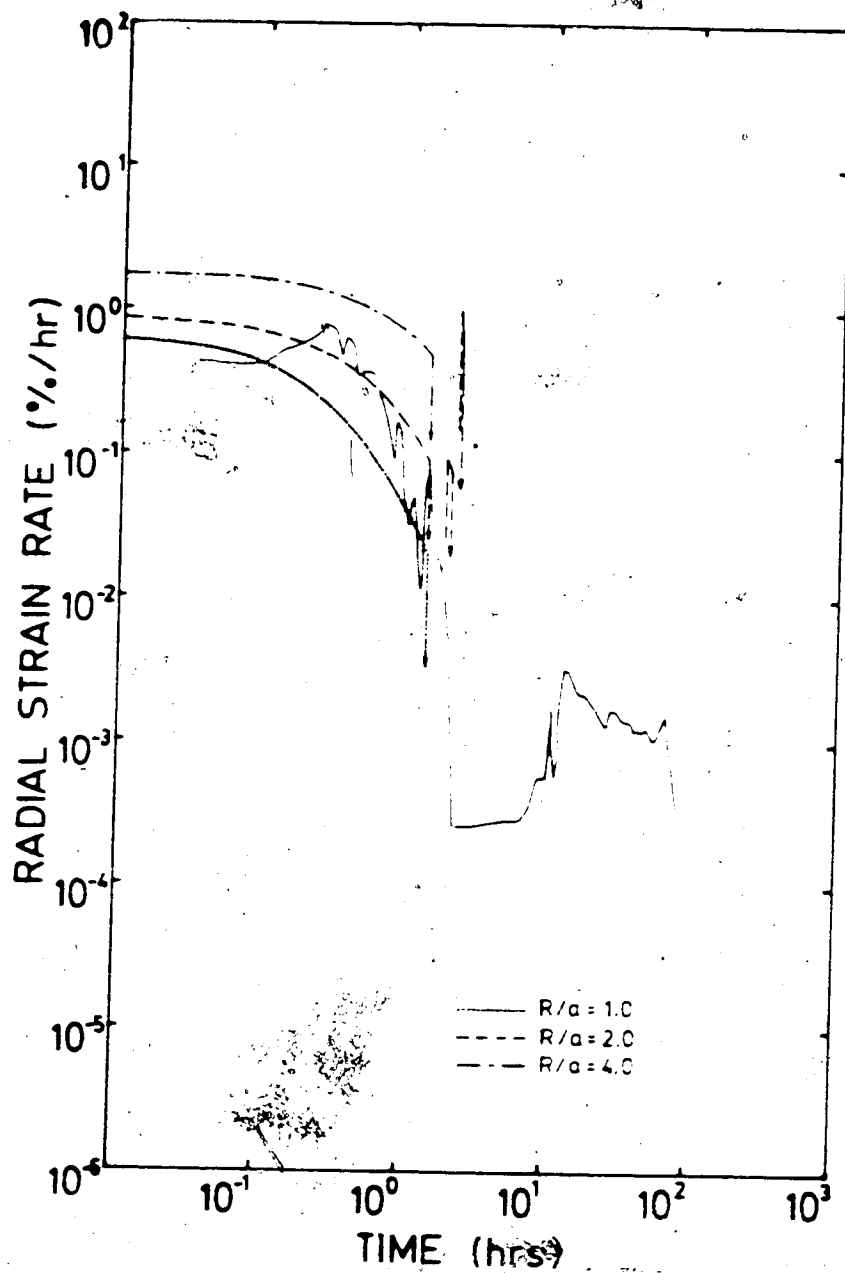


Figure 5.24 Comparison of Radial Strain Rates: Observed and Predicted Face Advance - Test MC-7.10 ($r/a=1.77, \theta=135^\circ$)

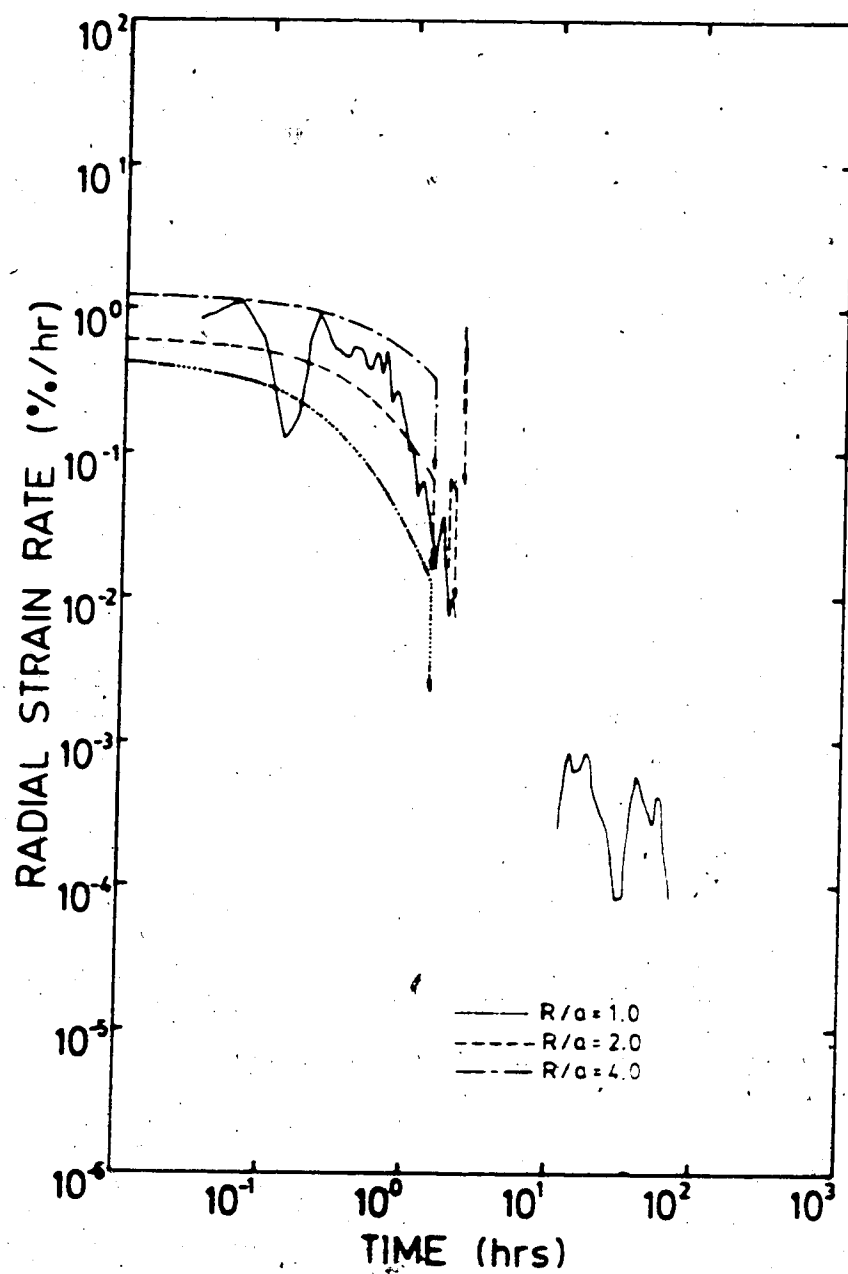


Figure 5.25 Comparison of Radial Strain Rates: Observed and Predicted Face Advance - Test MC-7.10 ($r/a=2.12, \theta=135^\circ$)

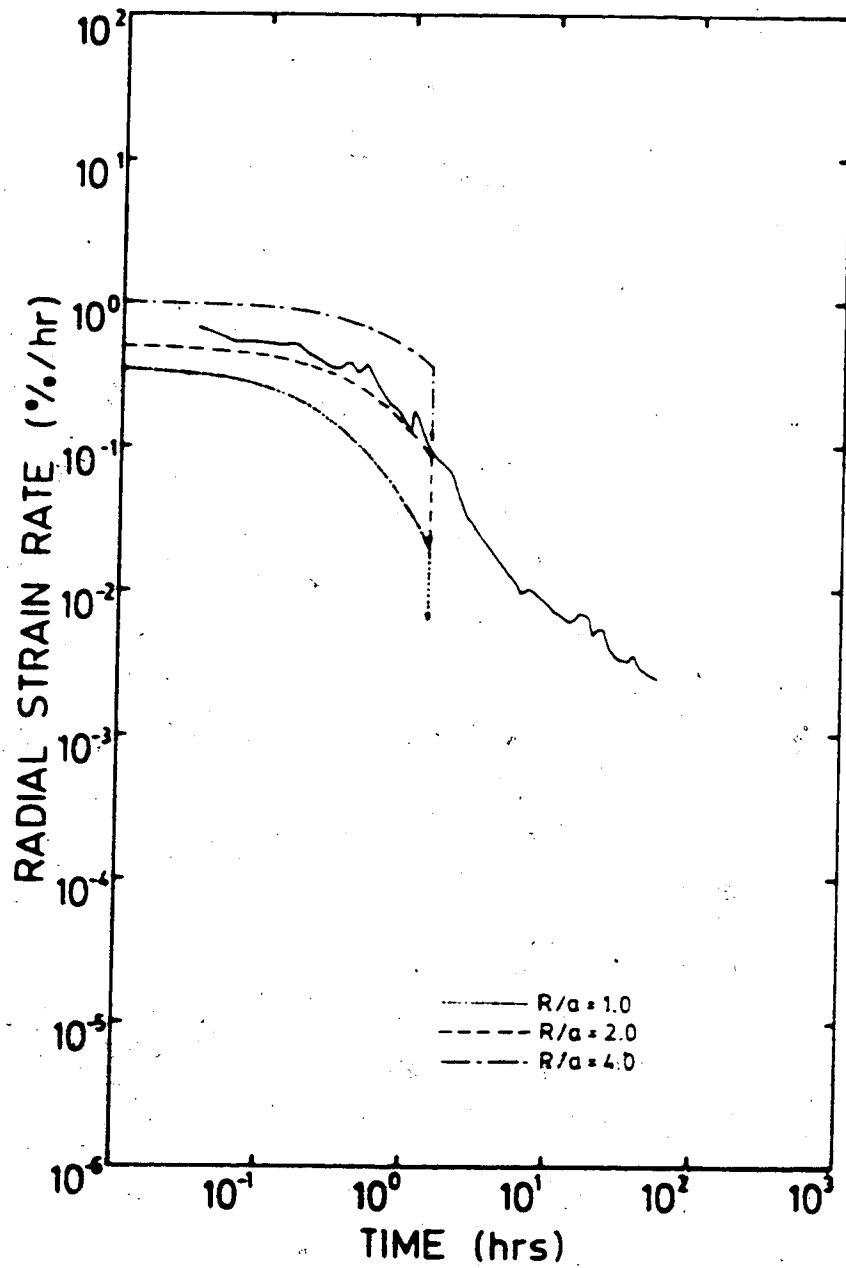


Figure 5.26 Comparison of Radial Strain Rates: Observed and Predicted Face Advance - Test MC-7.13 ($r/a=1.36, \theta=135^\circ$)

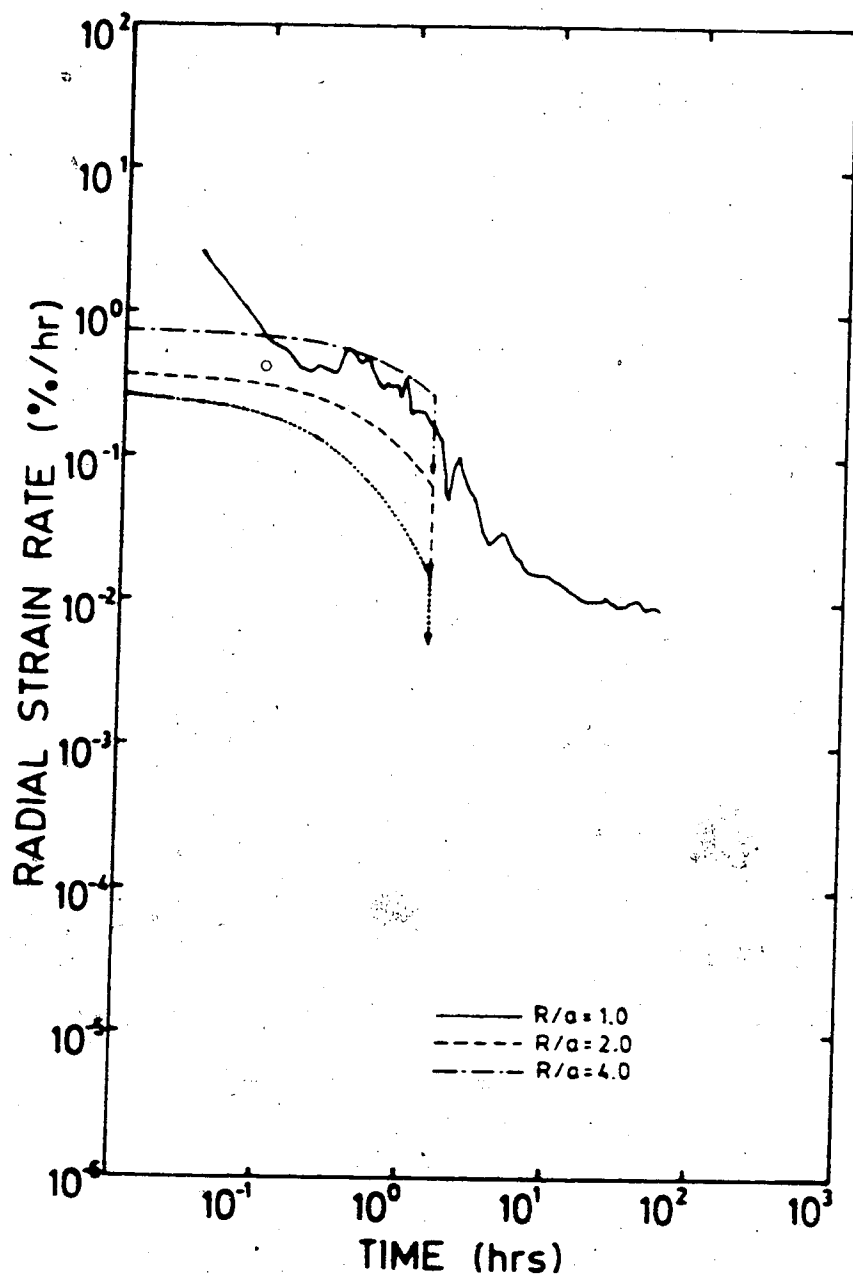


Figure 5.27 Comparison of Radial Strain Rates: Observed and Predicted Face Advance - Test MC-7.13 ($r/a=1.61, \theta=135^\circ$)

yield zone Equation 5.19 was still employed due to the uncertainty in the value of the dilation coefficient and the fact that the yield zone was localized (i.e., not annular) and therefore more rigorous analysis would not be justified.

The results suggest that an equivalent radial yield zone would extend some 1 to 2 tunnel radii from the tunnel wall. The extensometer closest to the tunnel wall (Figures 5.24 and 5.26) predicts a smaller extent of the yield zone, however, this is probably due to the fact that there is less dilation occurring in this region as compared to the active yield front. In any event, the results of this study show that it should be possible to determine the probable extent of the yield zone around an advancing tunnel by means of displacement rate measurements. Limitations to be considered in the analysis are the certainty of the values selected for the variables in the equations and the axisymmetric nature of the solution.

Several conclusions based on the above results may be drawn:

1. Reliable prediction of material behaviour can be achieved by relatively simple models in the absence of yielding or softening;
2. In the absence of yielding, immediately after the tunnel face advances past a given point, the radial strain rate is dominated by the continued advance, for a period of time that depends on the material properties and the rate of advance;

3. The face advance effect may not be as dominant in the presence of a propagating yield zone but, as will be seen later, will dominate for a longer period of time;
4. Significant deviation from anticipated behavior is indicative of yielding or softening processes; and
5. A first approximation of the extent of the yield zone can be achieved by analysis of the strain or closure rates due to face advance.

In order to more fully understand the significance of the face advance effect the behavior under field conditions for this rock type has been investigated by means of the previously described relationships. The radial strain rate was determined at a distance of $1/2$ tunnel radii from the tunnel wall ($r/a=1.5$); the tunnel was assumed to be 5 m in diameter and the field stress to be 12.5 MPa (corresponding to a depth of 500-600 m). It was further assumed that the material behaved in a linear elastic manner, the tunnel excavation process was not interrupted nor terminated before 1000 hours and there was no scale effect on the material properties.

The radial strain rates experienced in the rock mass upon excavation of a tunnel at three rates, 0.1, 1.0 and 10 m/hr, were predicted and are presented in Figure 5.28. Both the total strain rate and the rate excluding the effect of face advance are plotted. The dominance of the face advance effect over a significant time interval (and hence, tunnel length) is evident. These results show that the

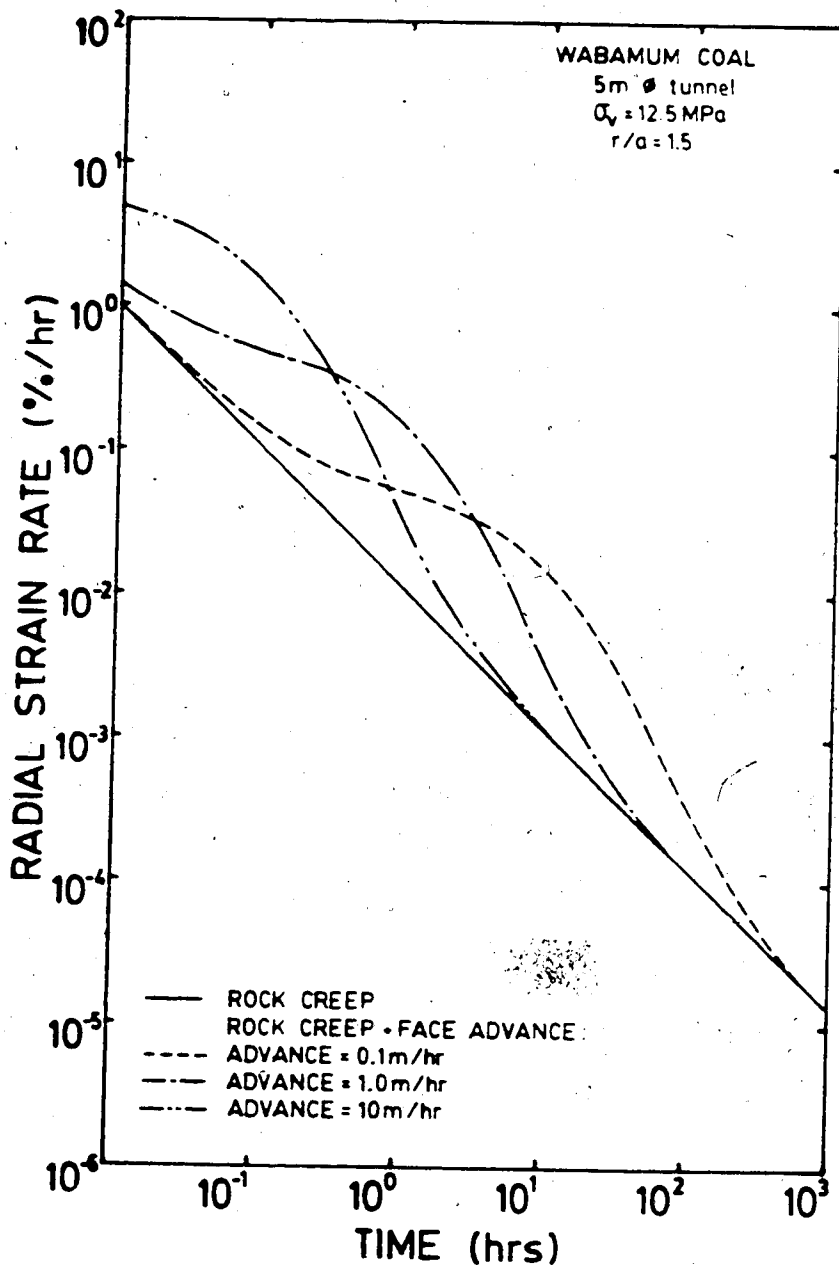


Figure 5.28 Comparison of Predicted Radial Strain Rates Assuming Various Tunnel Advance Rates in Wabamun Coal

effect of face advance on the measured strain rate cannot be neglected in this material until the face is further than 10 tunnel diameters from the point of measurement. Displacement rate measurements made to evaluate tunnel performance or rock mass properties (for extrapolation) will therefore require adjustment prior to comparison with prescribed limits until the face is far advanced. In addition the use of the slope of the strain rate decay curve in estimating the long term displacement will result in significant underestimates of closure if taken prior to the dissipation of the face effect.

Figure 5.29 presents the accumulated strain versus log time plots resulting from the excavations described above. From this figure it is apparent that the radial strain actually measured in the field will be very much dependent on the rate of tunnel advance as well as the time elapsed prior to instrument installation. If the instrument was installed 1 hour after the face advanced (Pt. A) 59 % of the total time-dependent rock mass response would be recorded regardless of the rate of advance. The amount of strain recorded due to the face advance would be very much dependent on the rate of advance with only 3 % of the total at an advance rate of 10 m/hr, 45.9 % at 1.0 m/hr and 91.1 % at 0.1 m/hr. If, however, the instrument was installed 5 hours after the face advanced (Pt. B) the time-dependent rock mass response measured would be only 46.1 % of the total and the face effect strain would be 0.2 % of the total

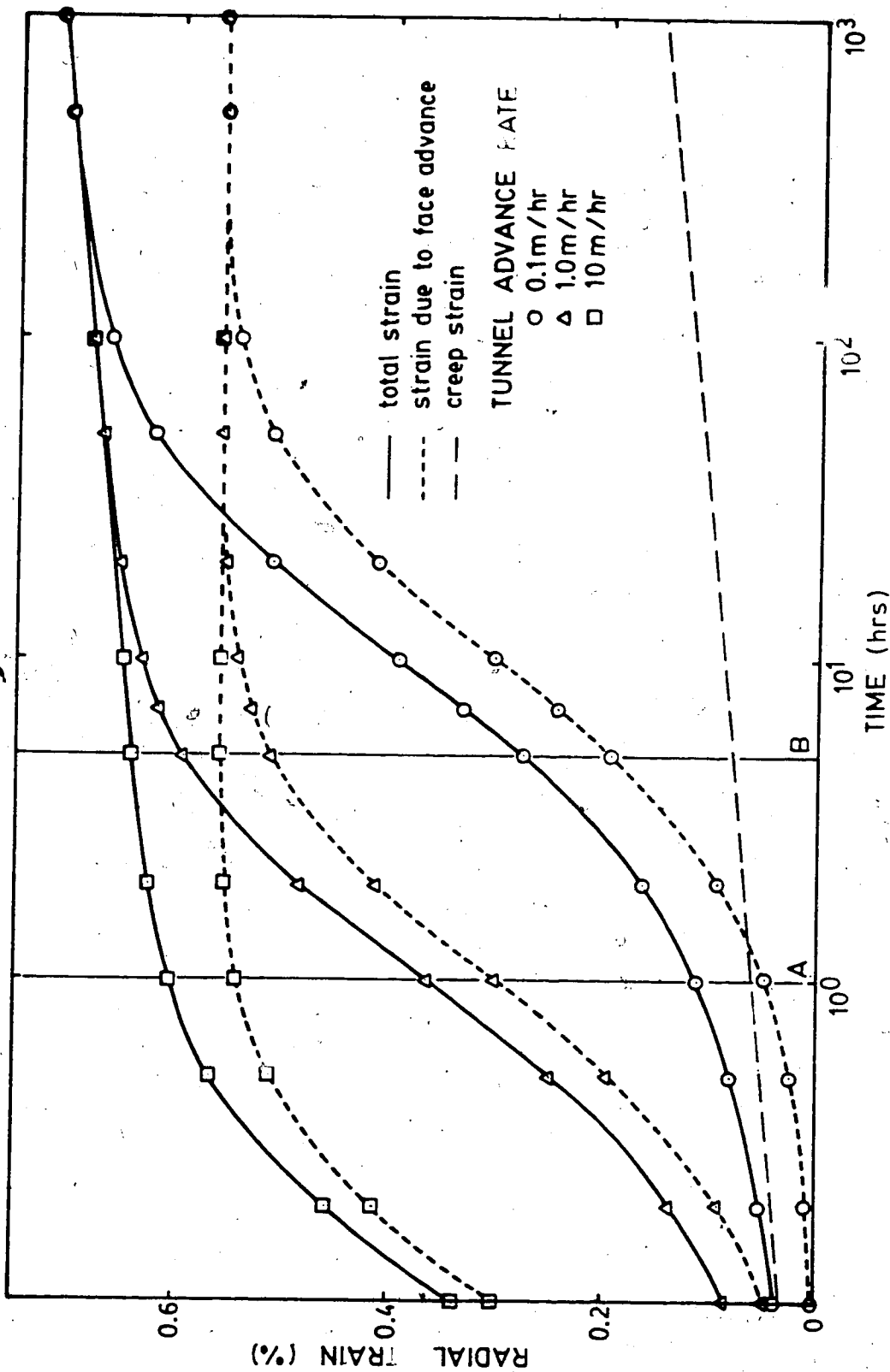


Figure 5.29 Comparison of Predicted Radial Strains Assuming Various Tunnel Advance Rates in Wabamun Coal

at an advance rate of 10 m/hr, 8.8 % at 1.0 m/hr and 65.2 % at 0.1 m/hr. These results demonstrate the combined effect of instrument installation time and rate of tunnel advance on radial strain measurements and hence, instrumentation design.

If the purpose of the instrumentation is to provide information regarding the possible extent of yielding and the development of radial strain around the opening then it should be installed very soon after face advance and be of sufficient range to accommodate large strains. If, however, the purpose is to determine the long-term strain to give an idea of ultimate lining load then more accuracy is required and late installation is acceptable. This generally implies a shortened range and therefore the instrument should possibly not be installed until the face advance effect has dissipated.

The degree to which the face advance effect influences the instrumentation design and analysis depends very much on the material through which the tunnel is excavated. As the face advance effect is directly proportional to the ultimate tunnel closure (excluding creep closure), the greater this closure the greater the influence of the face advance on measured strain or closure rates. Large values of the ultimate tunnel convergence may be a result of soft rock (low deformatio modulus) or the creation of a yield zone. The influence of the yield zone on the face advance effect for the situation previously described is presented in

Figure 5.30 for the tunnel closure rate and Figure 5.31 for the radial strain rate. An increase in the radius of the plastic zone causes an increase in both the magnitude of the deformation rate and an extension of the time period over which it is of influence. This is clearly seen in Figure 5.32. In the elastic case ($R=a$) convergence to the ultimate is achieved within approximately 2 tunnel diameters. For increased extents of the plastic zone, the total closure increases as well as the distance from the face where it reaches its ultimate value.

The significance of the face advance effect on the measured radial strain or tunnel closure rate has been clearly demonstrated and the expressions for its determination verified in the model tests. As these tests were of limited time and extent, extrapolations to field behaviour were made to provide additional insight. The results of this study have demonstrated that the influence of the face advance effect is very much dependent on the material through which the excavation is made and the rate of advance. Instrumentation for tunnel monitoring requires an appreciation of this effect for its reliable design.

5.3.2 Development of Radial Strains Near the Tunnel Face

The layout of the instrumentation provided an excellent opportunity to investigate the near face behavior during the initial excavation and subsequent widenings of the tunnel. The tunnel excavation and widening of Sample MC-6 were

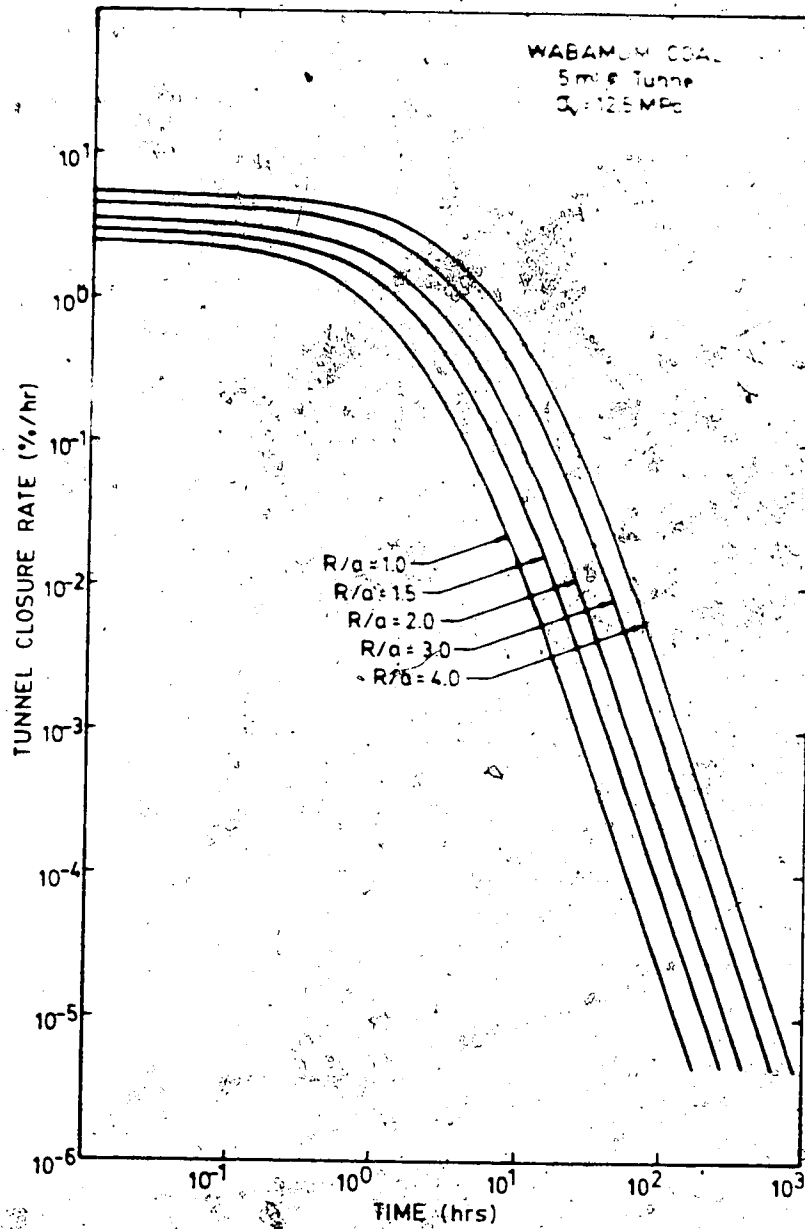


Figure 5.30 Variation in Tunnel Closure Rate with Radius of Yield Zone

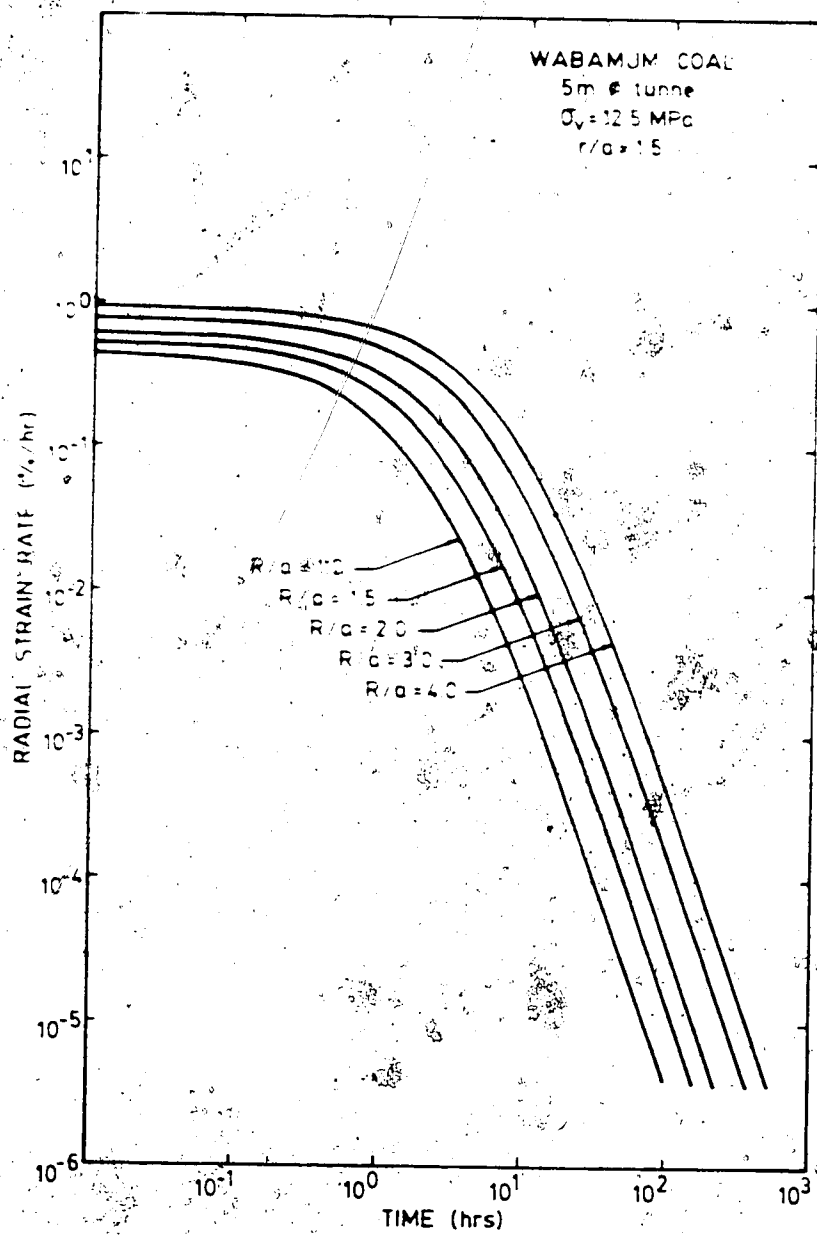


Figure 5.31 Variation of Radial Strain Rate with Radius of Yield Zone

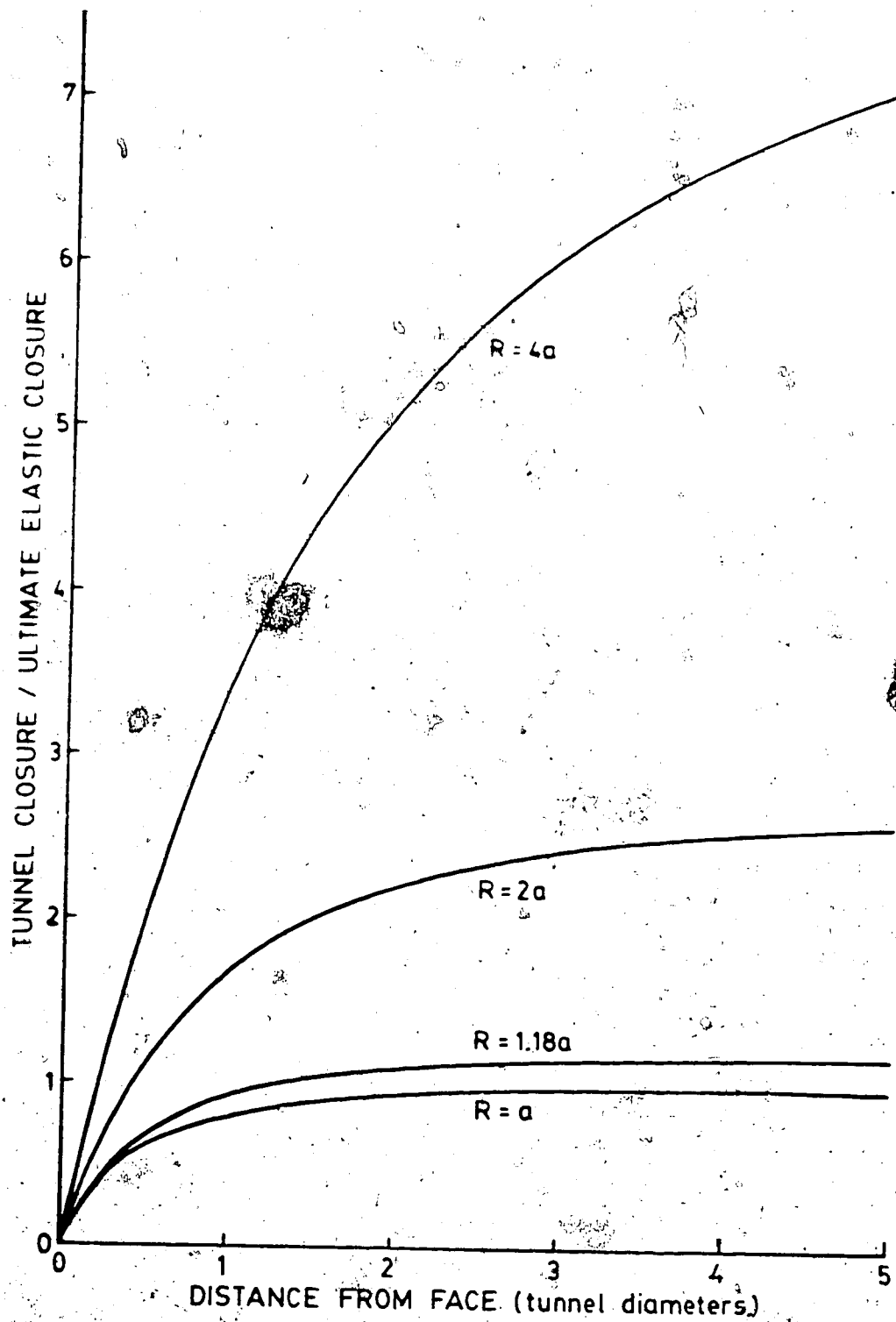


Figure 5.32 Predicted Tunnel Convergence as a Function of the Distance from the Tunnel Face and the Extent of the Yield Zone

performed in a relatively rapid manner whereas those undertaken on Sample MC-7 were performed at a slow rate, allowing more refined analysis of extensometer response.

Sample MC-6

Figures 5.33 and 5.34 show the development of radial strain around the initial excavation of Sample MC-6. Little straining was noted until the tunnel was within 2 diameters of the instrument level. Typically the instruments underwent a rapid increase in extensional strain as the tunnel advanced. Once the excavation extended beyond the instrument level, the slope of the radial strain versus time curves approached zero indicating little creep response (over a short time period). Instrument response was generally uniform with the exception of those located near the tunnel wall at $\theta=90^\circ$, 135° and 270° which exhibited approximately twice the average strain. This suggested that stress redistribution processes were occurring in these orientations.

Widening of the above tunnel to a diameter of 152 mm was done in a step-wise manner due to several interruptions in the drilling operation. The instrument response (Figures 5.35 and 5.36) generally followed the form of the tunnel advance curve with rapid increases in extensional strain during excavation. Upon interruption the straining abruptly levelled off into a creep strain response. The advance of the tunnel face was tracked by the extensometer response. There was a wider variation in response as

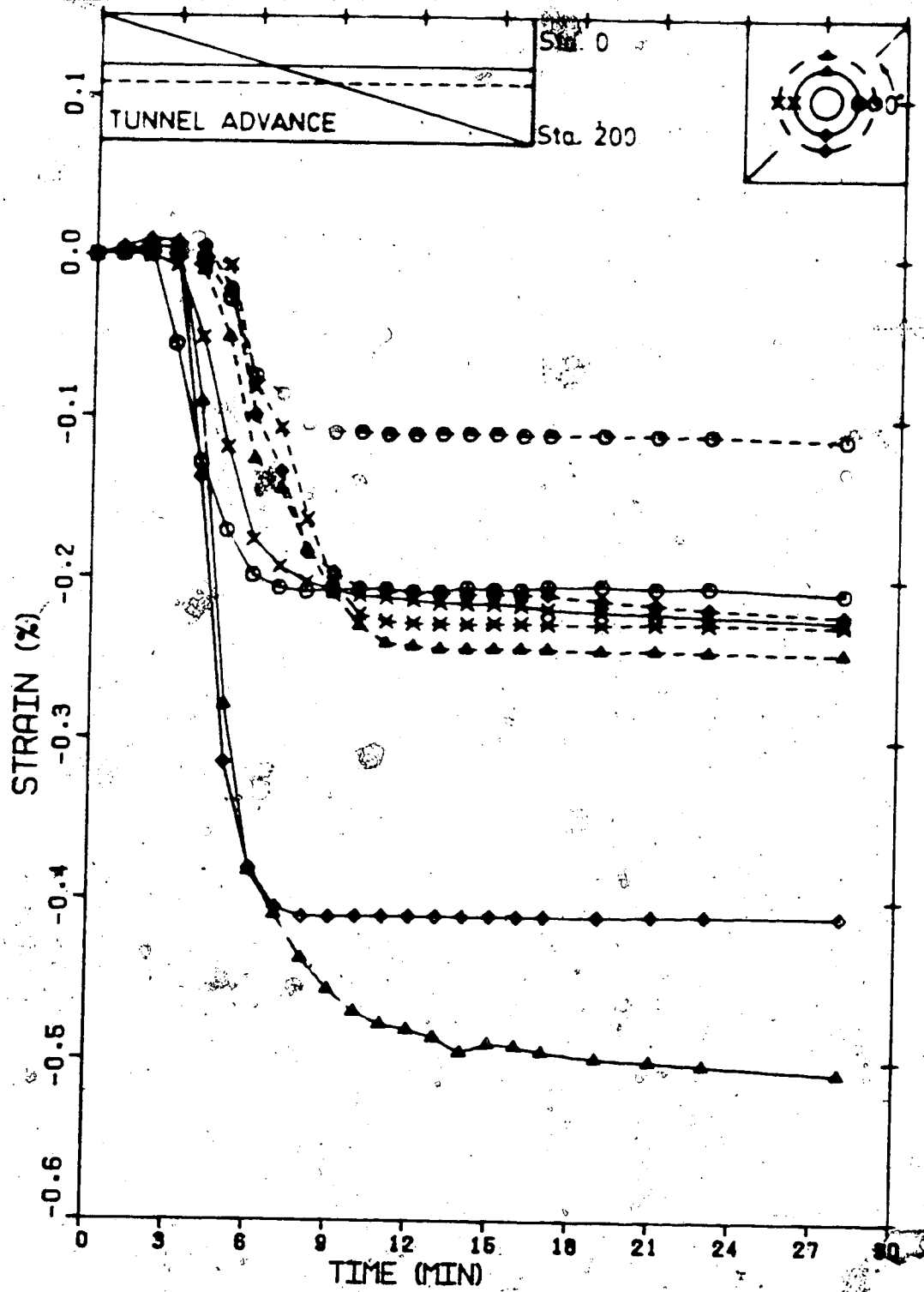


Figure 5.33 Development of Radial Strain - 108mm Tunnel Excavation, Sample MC-6 (parallel to the principal stress directions)

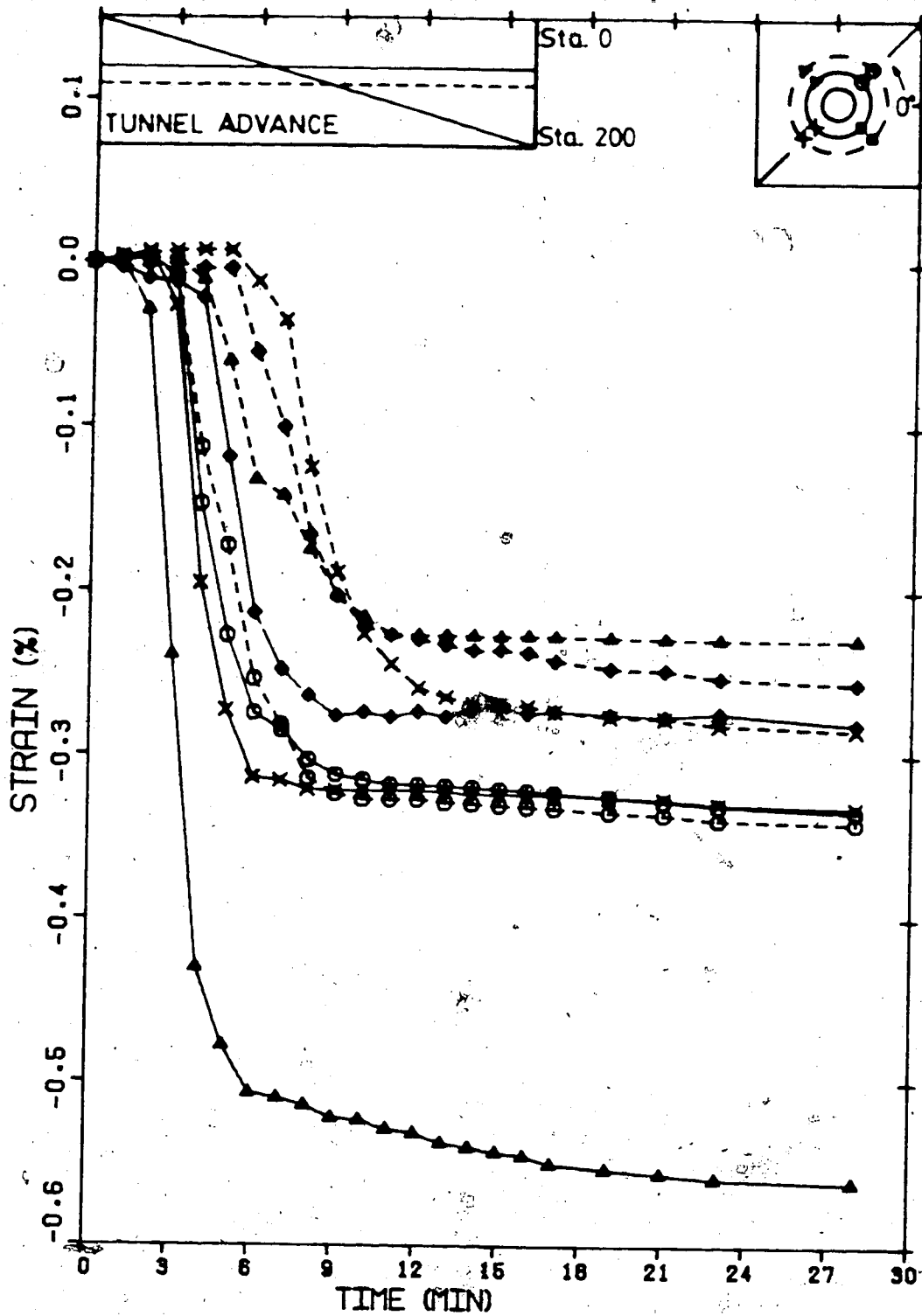


Figure 5.34 Development of Radial Strain - 108mm Tunnel Excavation, Sample MC-6 (45° to the principal stress directions)

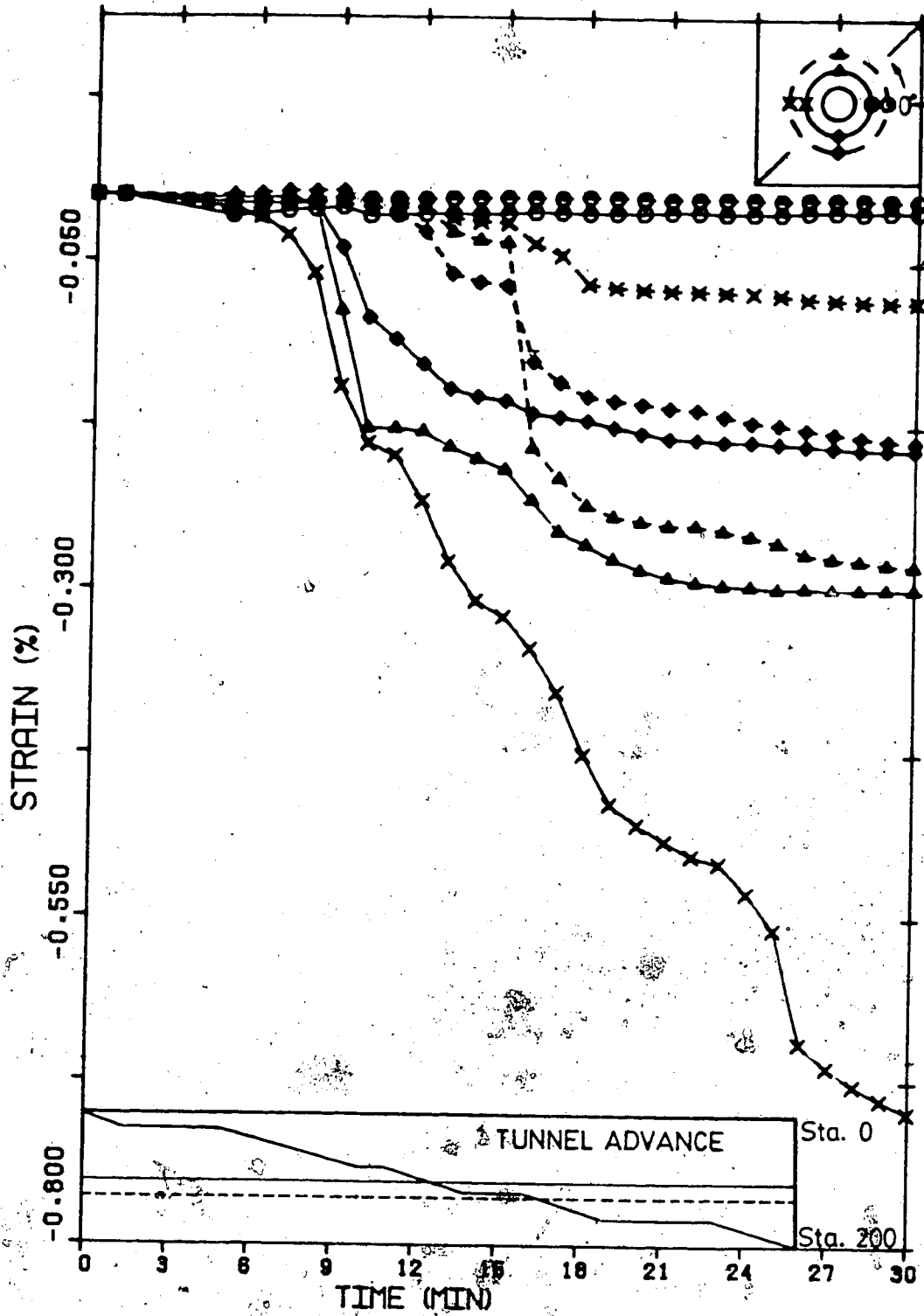


Figure 5.35 Development of Radial Strain - Widening 152mm, Sample MC-6 (parallel to the principal stress directions)

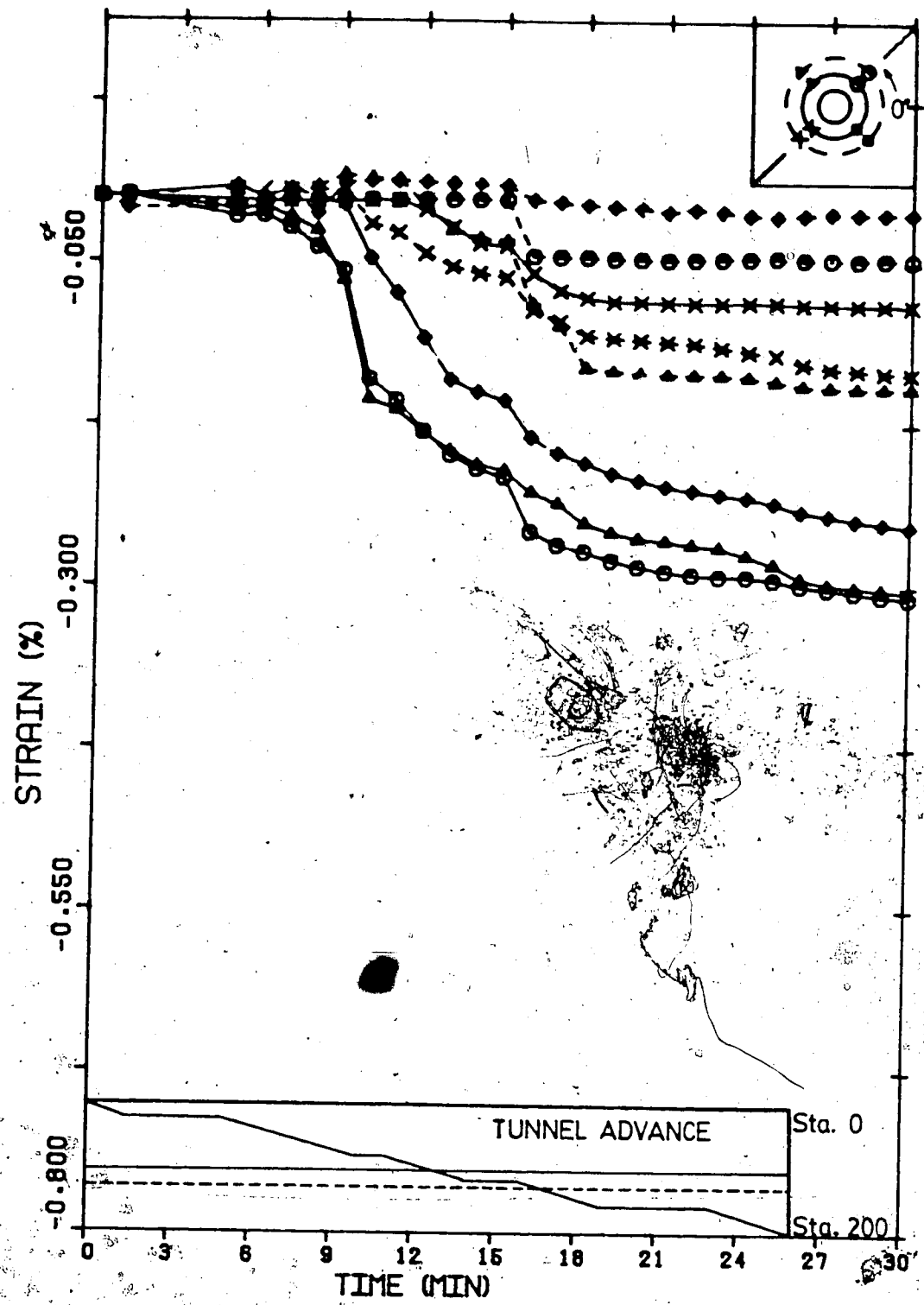


Figure 5.36 Development of Radial Strain - Widening to 152mm, Sample MC-6 (45° to the principal stress directions)

compared to that noted during the original excavation, suggesting that significant alteration of the sample had occurred. Strains were maximum in similar, though more extensive, areas as during the initial excavation (45° - 180° and 270° - 315°) indicating that stress redistribution was continuing.

Sample MC-7

Figures 5.37 to 5.39 present the radial strain response recorded during excavation and widening of the tunnel for those extensometers nearest to and furthest from the tunnel wall. These instruments were always oriented in a true radial direction during all three tests. The complete record of measured radial strains for all extensometers during advance are presented in Appendix D. The time at which the tunnel face arrives at the level of each instrument is denoted by a vertical line, the type corresponding to the appropriate radial strain versus time curve (also indicated by arrows). The near face behavior is also summarized in Table 5.3.

In all tests, but particularly Tests MC-7.08 and MC-7.10, there was some increase in compressional radial strain prior to the expected extensional straining. This was caused by both an increase in radial stress ahead of the face (see Figure 5.14) and the time-dependent sample compression.

Neglecting the compressional effect of face advance, the instruments near the tunnel wall ($r/a < 4.54$) detected the

Table 5.3 Near Face Radial Strain Behavior

Test No	Location	r/a	Face Advance Noted	Face Advance Complete	Max'm Radial Strain at	ϵ_a/ϵ_t (%)
7.08	Sta. 56 n	3.45	-1.20	1.54	-0.24	52.4
	Sta. 56 e	6.40	-0.32	1.57	1.10	17.4
	Sta. 81 n	4.64	-1.20	2.37	0.26	27.6
	Sta. 81 e	7.64	-0.54	2.68	0	5.1
	Sta. 106 n	3.48	N/A	N/A	N/A	0
	Sta. 106 e	6.48	-0.54	2.71	1.19	28.2
	Sta. 131 n	4.62	-0.32	1.20	-0.25	13.7
	Sta. 156 n	3.50	-1.32	1.94	-1.19	88.4
	n	<4.64	-1.01+/-0.46	1.76+/-0.51		36.4+/-34.9
	e	>6.40	-0.47+/-0.13	2.32+/-0.65		16.9+/-11.6
	Sta. 56 to 156				0.16+/-0.82	29.1+/-28.9
	Sta. 56 to 131				0.38+/-0.62	20.6+/-17.5
7.10	Sta. 56 n	1.69	-0.43	1.85	0.13	18.9
	Sta. 56 e	2.14	-0.51	0.93	0.12	21.6
	Sta. 81 n	2.15	-0.46	1.10	-0.12	25.7
	Sta. 81 e	2.62	-0.42	1.23	-0.07	38.7
	Sta. 106 n	1.70	-0.46	0.93	-0.22	27.3
	Sta. 106 e	2.17	-0.77	0.78	-0.22	50.0
	Sta. 131 n	2.14	-0.69	0.46	-0.55	52.3
	Sta. 156 n	1.71	-0.72	0.96	-0.42	61.2
	n	<1.71	-0.54+/-0.16	1.25+/-0.52		35.8+/-22.4
	e	>2.14	-0.57+/-0.15	0.90+/-0.30		37.7+/-13.9
	Sta. 56 to 156				-0.17+/-0.24	37.1+/-18.5
	Sta. 56 to 131				-0.33+/-0.23	36.8+/-14.3
7.13	Sta. 56 n	1.36	-0.63	0.47	-0.22	43.8
	Sta. 56 e	1.36	-0.74	0.76	-0.49	66.1
	Sta. 81 n	1.69	-0.48	0.44	-0.30	64.0
	Sta. 81 e	1.70	-0.71	0.44	-0.47	59.4
	Sta. 106 n	1.36	-0.30	0.92	-0.13	31.0
	Sta. 106 e	1.38	-0.87	0.16	-0.30	74.5
	Sta. 131 n	1.68	-0.56	0.48	-0.46	61.4
	Sta. 156 n	1.37	-0.81	0.68	-0.31	42.5
	n	1.37	-0.67+/-0.23	0.60+/-0.29		51.7+/-18.2
	e	1.69	-0.58+/-0.12	0.47+/-0.02		61.5+/-2.3
	Sta. 56 to 156				-0.34+/-0.13	48.5+/-13.8
	Sta. 56 to 131				-0.34+/-0.14	66.8+/-7.8
					55.4+/-14.7	
					57.2+/-15.0	

n = instruments near initial heading
e = instruments towards which tunnel expanded
 ϵ_a/ϵ_t = ratio of strain ahead of the face to total strain

NOTE: all values, unless otherwise specified, are given in terms of tunnel radii (a).

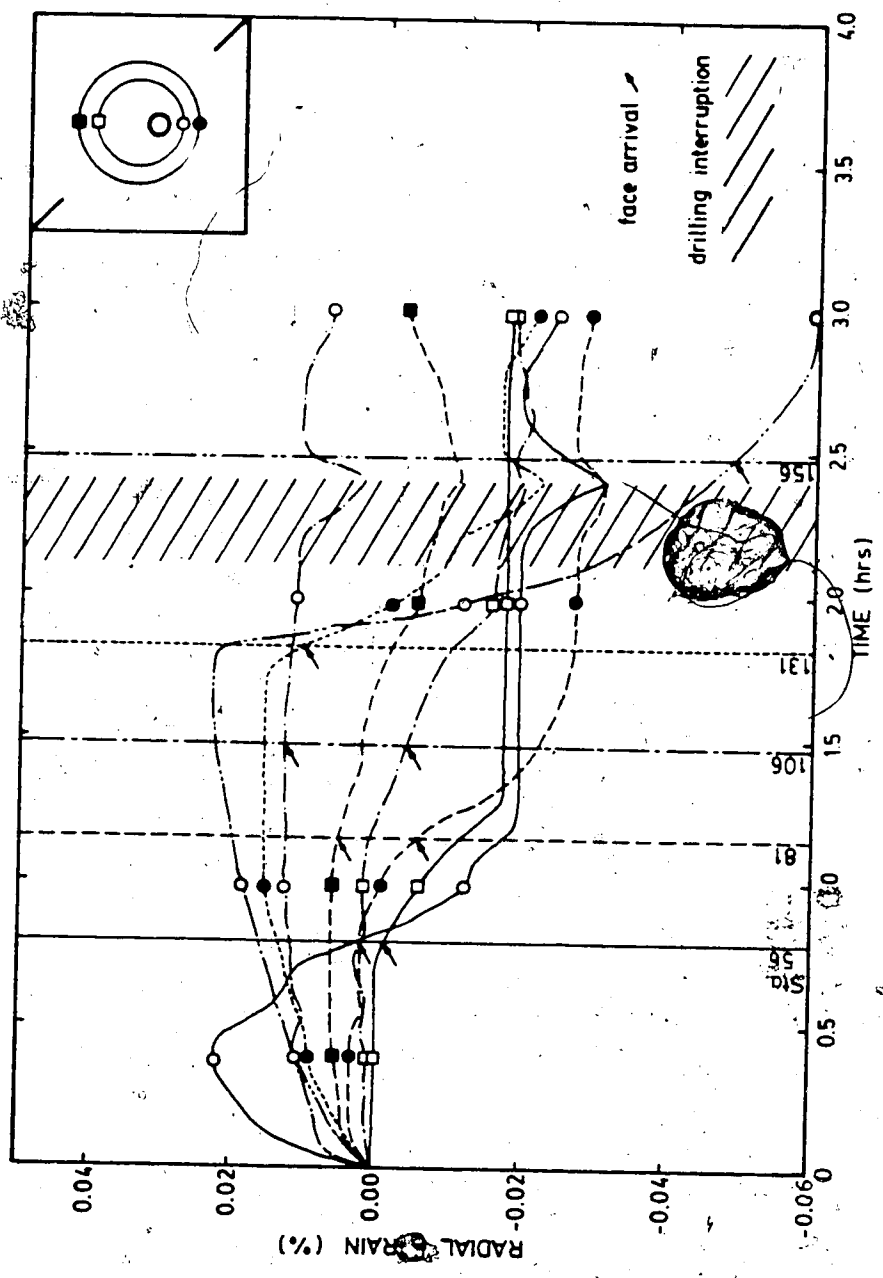


Figure 5.37 Development of Radial Strain - 42mm Tunnel Excavation, Sample MC-7

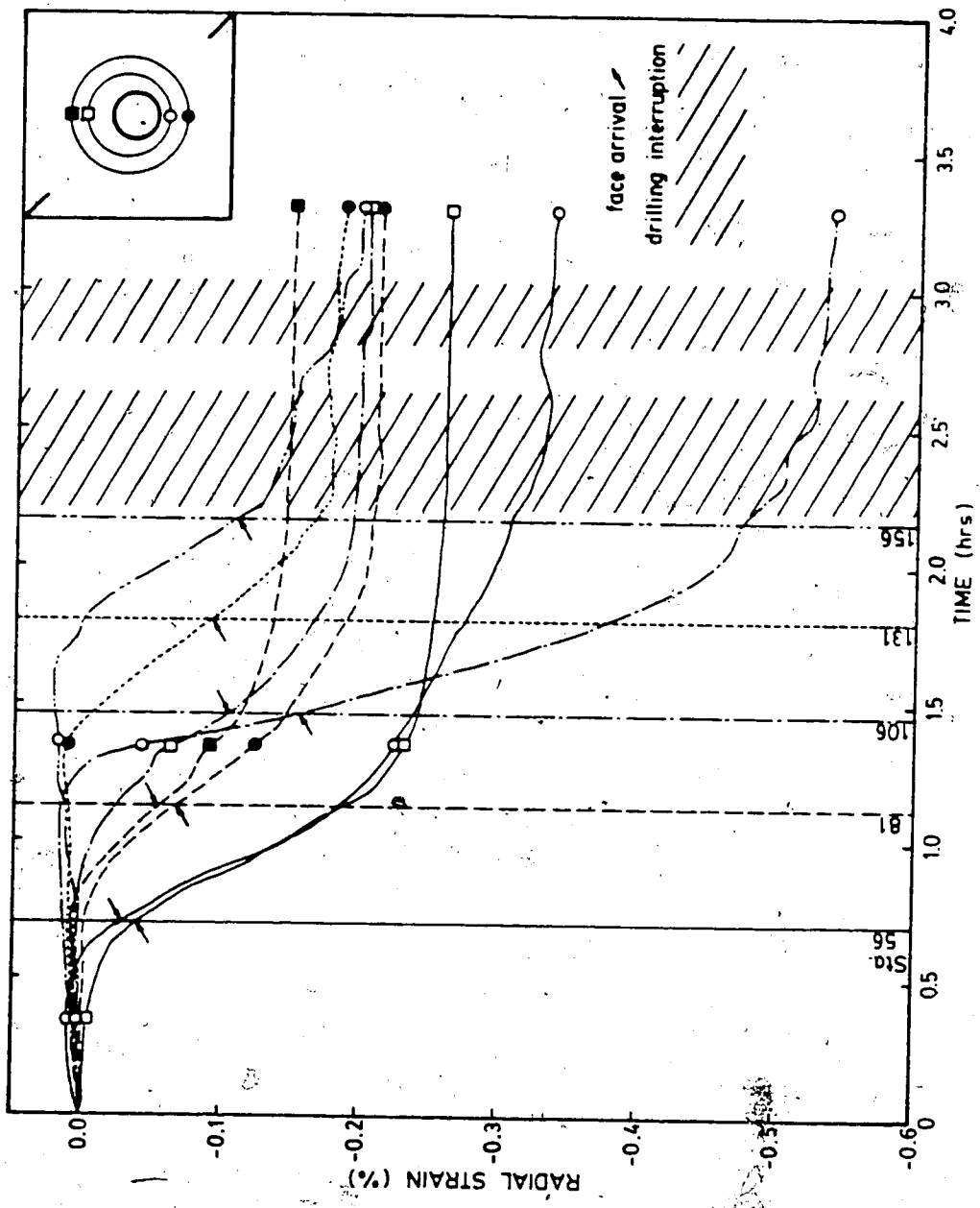


Figure 5.38 Development of Radial Strain - Widening to 108mm, Sample MC-7

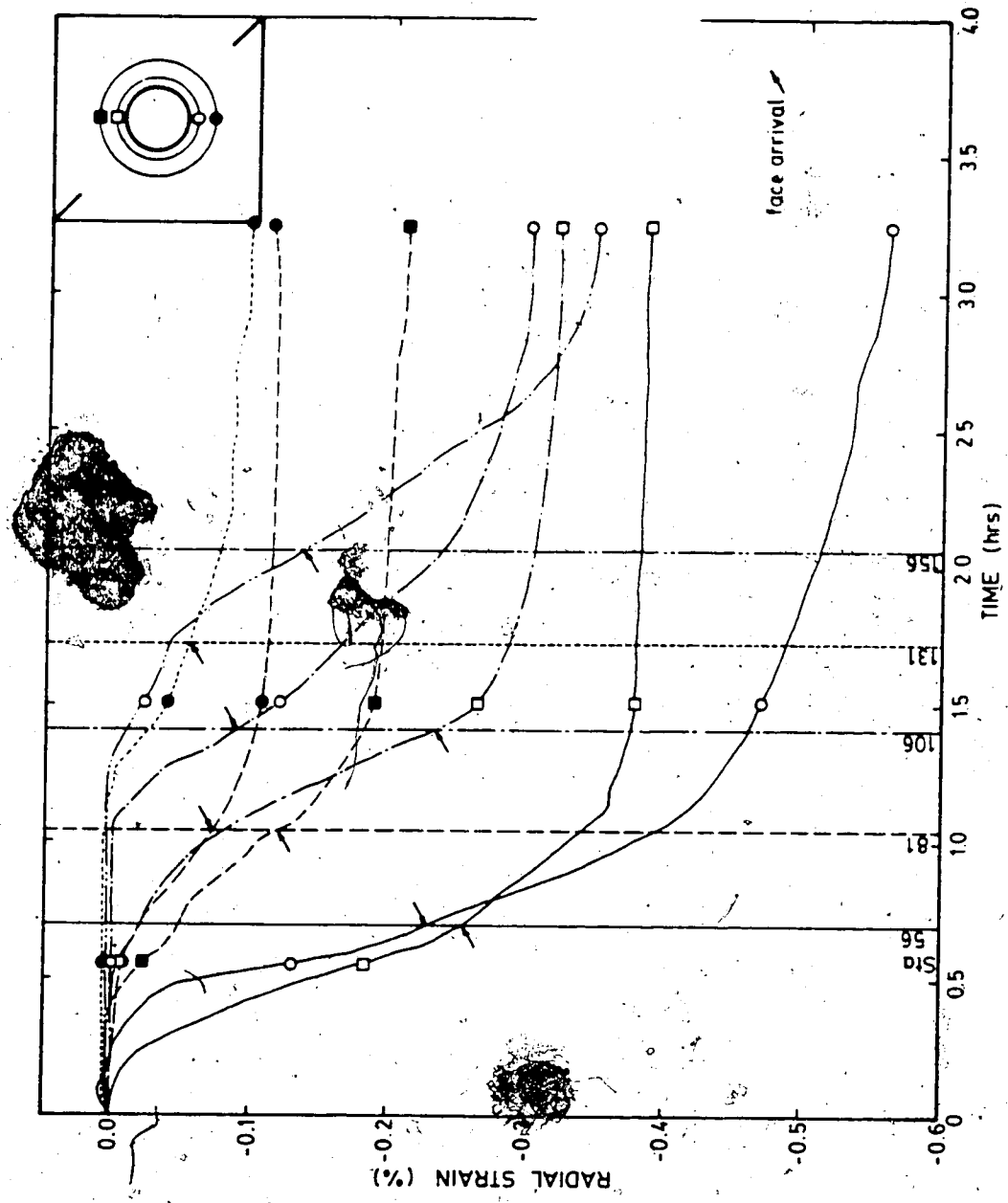


Figure 5.39 Development of Radial Strain - Widening to 152mm, Sample MC-7

presence of the initial tunnel advance approximately 1 tunnel radius in advance while those further away ($r/a \geq 6.4$) detected it only 0.5 tunnel radii in advance on average. A similar lag in response behind the advancing face was also noted; displacement levelled off at 1.76 radii for near instruments and at 2.32 tunnel radii for far instruments. This is indicative of the 3-D nature of the near face behavior.

During widening, extensometers at lower r/a ratios (< 2.62) reacted when the face was approximately 0.5 to 0.67 radii from the measuring section. All instrument response levelled off between 0.45 and 1.25 tunnel radii behind the face.

The distance over which the displacements occur due to face advance during the initial excavation is approximately 2.8 tunnel radii for all instruments. During widenings this distance is between 1.59 and 1.18 radii.

An increasing proportion of the total strain occurred ahead of the tunnel face during subsequent widenings. Approximately 20.6% (standard deviation $s=17.5\%$) of the total strain occurred ahead of the face during the initial excavation, 33.5% ($s=13.6\%$) during the first widening and 57.2% ($s=15.0\%$) during the second and final widening (note: readings at Sta. 156 neglected because of proximity to sample boundary). The relative increase in the ratio of strain ahead of the face during widening also was found to depend on the location of the extensometers. Those located

in the region towards which the excavation was expanded (denoted by 'e' in Table 5.3) showed increasing percentages of straining ahead of the face as compared to those near the initial heading (denoted by 'n' in Table 5.3). This resulted, most probably, from propagation of the yield zone in the direction of tunnel expansion. Appropriate values corresponding to the percentages of strain ahead of the face relative to the total strain for the three tests are:

n	36.4±34.9%	37.1±18.5%	48.5±13.8%
e	16.9±11.6%	36.8±14.8%	66.8±7.8%

There was also a shift of the maximum strain rate from approximately 0.16 radii behind the face during initial excavation to 0.17 radii ahead of the face during first widening and then to 0.34 radii ahead during final widening. A probable explanation of the above monitored processes and their significance with regard to deformation monitoring follow.

During the initial excavation, the stress originally carried by the now excavated material is transferred around the excavation and to some extent to the rock at the advancing face. This increase in stress ahead of the face causes the initial increase in compressive radial stress and strain as previously mentioned. These increased stresses can lead to deformation and possible failure of the tunnel face resulting in the onset of extensional straining ahead of the

face. During tunnel widening, there is only a weakened (by initial excavation) unexcavated rock core (hollow cylinder) left to resist the additional stresses. Overstressing near the tunnel wall is increased. This results in the increased straining ahead of the tunnel face. This process as well as yielding of the tunnel walls ahead of the face has effectively advanced the tunnel ahead of its present location.

The significance of the above findings to the instrumentation designer are as follows:

1. In order to maximize the amount of information on the deformation field around the excavation, where multiple heading advance is employed, the instrumentation should be installed from the pilot headings. With each successive expansion of the excavation the magnitude of the post-excavation deformation will decrease;
2. Particular attention should be paid to deformations in the direction of cavity expansion. Yielding initiated around the original heading will tend to propagate in the direction of expansion as the magnitude of the stress change in the other direction will be much lower; and
3. Interruptions in the tunnel advance provide an opportunity to determine tunnel stability by displacement rate criterion or to determine the time-dependent rock mass response.

6. CONCLUSIONS AND RECOMMENDATIONS

6.1 Introduction

A rational design of underground excavations in rock should employ the concept of the convergence-confinement method where the ground-support interaction is considered as presented in Figure 6.1. The convergence curve (ground reaction curve) depends on the rock mass properties. It is linear in a linear elastic material, curved if yielding occurs and may tend upwards if gravitational forces dominate in weak loosening rock. Equilibrium can be reached at any point along this curve if the appropriate pressure is applied at the corresponding displacement (intersection of confinement (support) and convergence curves). Where the rock mass properties are time-dependent the convergence curve is a function of time, rotating about its origin ($u = 0, p = p_0$) with time as shown in Figure 6.1. Equilibrium is therefore not assured at the intersection of the convergence and confinement curves at a given time (Pt. A). Additional creep deformation can shift the equilibrium position to Pt. B on the confinement curve for infinite time. This result in overstressing or failure of the support system. Similarly a shift of the convergence curve may occur if the field stress increases due to nearby mining operations. This may lead to a further increase in support load (Pt. C). For design it is therefore necessary to determine the ground convergence curve from the rock mass

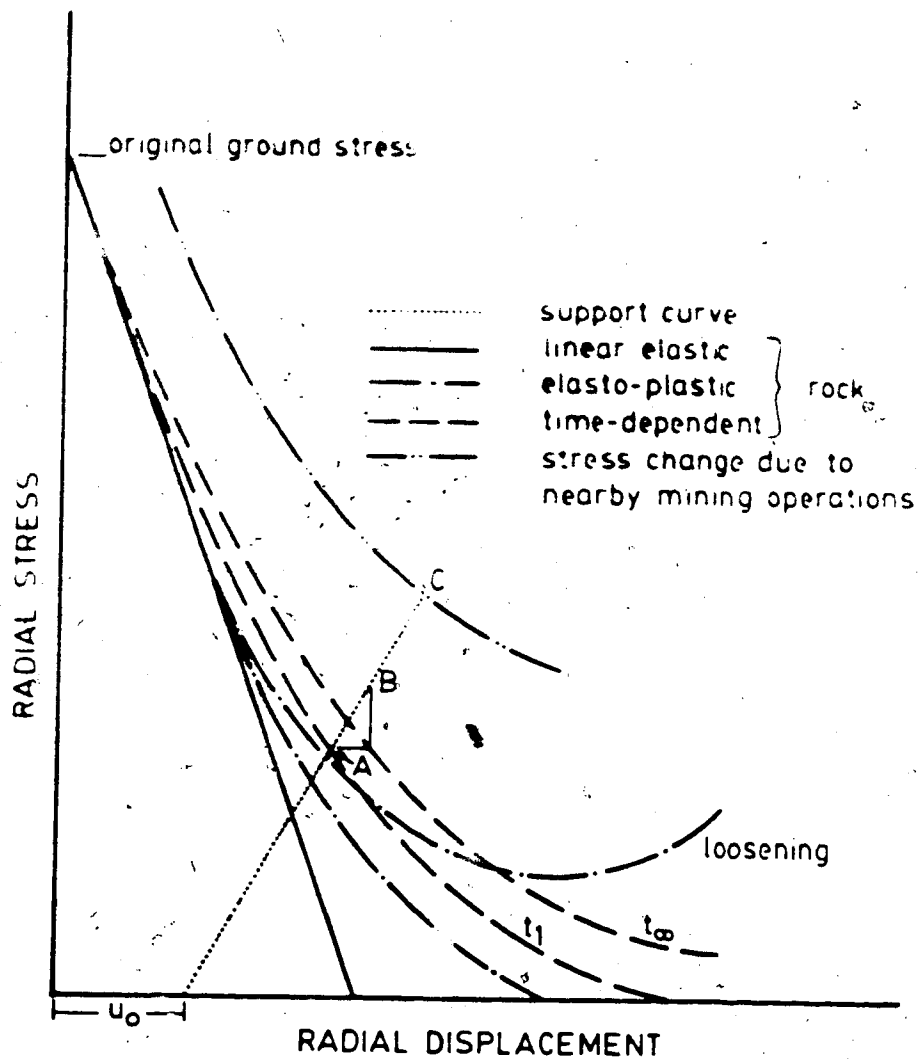


Figure 6.1 Confinement-Convergence Curve

properties and the established mode of opening behavior in order to calculate the shape of the confinement curve for the selected support system and support activation time.

The ground convergence curve can be determined analytically by methods such as those presented by Brown *et al.* (1983) if the rock behavior is time-independent. For rock masses with time-dependent responses, the determination of the ground convergence curve becomes much more difficult. In this situation two approaches to the problem are possible; an analytical or an observational approach.

The analytical approach entails employment of visco-elastic or visco-plastic material models. These, however, have difficulty in incorporating geologic complexities and different modes of failure. In addition, the required parameters can seldom be determined in a rational manner because they do not represent actual rock properties. Hence, this approach is generally unsuccessful in accurately representing the ground response. The method proposed by Ladanyi (1974) can, however, be used for parametric studies.

In the observational approach, the designer resigns himself to the fact that the ground response is analytically incalculable and that the design must be derived from in-situ experience. This experience is gained from the analysis of performance records of openings constructed under similar conditions or preferably during pilot excavations.

Deformation or displacements serve as the best indicator of opening performance because stress and stress changes are difficult to measure reliably. The displacements and especially displacement rates constitute the most easily obtained and most reliable measurement and, hence, are selected as performance indicators during most tunnelling operations.

Because of the importance of the deformation monitoring program to the design of underground excavations in rock, a review of its application and limitations was in order. This, essentially, constituted the thrust of the research reported herein.

6.2 Conclusions from Model Tests

The design verification and stability assessment aspects of deformation monitoring in typical underground excavations are performed in different manners. The stability of the excavation is generally made on the basis of convergence measurements recorded at regular intervals along the tunnel axis while design verification is performed at selected sites representative of typical conditions by more intensive instrumentation arrays, particularly borehole extensometers. Both generally employ displacement rate criteria in their application, however, design verification also relies on displacement magnitudes (for serviceability requirements) and often includes support stress measurements.

The response of the selected instrumentation depends on the material property distribution and its stress level dependence. In a heterogeneous, discontinuous rock mass the variation in instrument response will be significant. The application of a universal displacement criterion in such situations is not practical. Judgements must be based on the change in response at a given location or on the difference when compared to other instruments under similar conditions. Similar conclusions were also drawn by Guenot *et al.* (1984).

Convergence measurements were found to be insensitive to the deformation field around the excavation. The non-axisymmetric nature of the yield process was not always readily identifiable from the convergence records. In addition the magnitudes of the observed closures did not allow for the identification of the deformation process or its location and extent. Extensometers, however, were able to provide the required information concerning the displacement field.

The magnitude of the deformation observed at any station along the tunnel axis will depend on the time of instrument installation and the stage of the excavation process. In order to maximize the deformation information, instrumentation should be installed ahead of the advancing face. This is often impossible or impractical in deep excavations. In these instances, installation at the face will provide sufficient information for analysis. In multi-stage excavation, instrumentation should be placed

during the heading excavation as the magnitude of the deformations decrease with each successive stage (unless instability arises).

The intended use of the instrumentation, to a large extent, dictates the measurement range and time of installation. If the objective is the determination of the development of radial strain around the opening in order to ascertain the location and extent of yielding or the verification of design assumptions then the instruments should preferably be installed ahead of the face or as soon as possible after face advance and be of sufficient range to accommodate large strains. If, however, the purpose is the prediction of ultimate lining loads from extrapolated creep strain curves then later installation of reduced range (more accurate) instrumentation is permissible. In fact, it may be appropriate in these circumstances to allow dissipation of face advance effects prior to installation.

The distance (in tunnel diameters) over which the displacements are influenced by the advancing face depends on the type of excavation as well. The distance is maximum during the initial excavation and becomes progressively less in subsequent widenings. In such circumstances, instruments designed to detect the yield zone must be installed during the initial heading excavation or at the face during widening. Instrumentation for long term displacement measurements may be installed soon after final widening.

In order that the maximum amount of information be obtained from the instrumentation frequent readings are required. This is becoming more practical with the advent of rugged, remote data acquisition systems and computer data processing. Continuous records of displacement can yield information on the intermittent, localized behaviour which may be of assistance in understanding the overall tunnel behaviour. Frequent readings near the tunnel face are essential if determination of the face advance effect is required.

During external loading tests, it was observed that critical deformation rates, indicative of a behaviour mode, existed for the small tunnels in the coal. These critical rates, which were employed as tunnel behavior evaluation criteria, were applicable to the time-dependent rock mass deformation rate (i.e., creep rate). The existence of such critical rates should be tested by field measurements.

The deformation rate measured during tunneling operations is a function of the rate of tunnel advance and the time-dependent rock mass properties. Time-dependent measurements made to evaluate tunnel performance or rock mass properties therefore require adjustment prior to comparison with prescribed limits until the face is far advanced. In order to apply the critical rate functions previously described, it is necessary to separate the observed rate into that due to the face advance and that due to creep including time-dependent yield processes. This was

achieved by extension of an expression relating tunnel closure to face advance proposed by Panet and Guenot (1982). Relationships for both the tunnel closure and radial strain rates due to the advance of the tunnel as functions of time and advance rate were derived and subsequently verified in the model tests. Substitution of reasonable values for the parameters in these expressions demonstrated that the face advance may dominate the observed deformation rate for a considerable distance behind the tunnel face (approximately 10 tunnel diameters for this coal). Where the slope of the strain rate decay curve is used in estimating the long term displacement, elimination of the face advance effect must be achieved in order to prevent significant underestimates of tunnel closure.

Closure rates in excess of the closure rate functions, while indicating a behavior mode, did not indicate where the process was occurring. Measurements of radial strains were found to be necessary in combination with closure rates to delineate the location and extent of the yielding or softening zone. Furthermore it was found necessary to measure the tunnel closure rate or radial strain rate in many directions and continuously, beginning as soon after the tunnel advance as possible, to ensure correct interpretation of the mode of abnormal behavior.

6.3 Recommendations

Deformation monitoring of underground excavations in weak rock can be adequately achieved by the use of convergence measurements and borehole extensometers. These two means complement each other and should be incorporated as such in the monitoring scheme. This research has shown that the onset on incipient instability can be predicted by comparison of tunnel convergence rates with appropriate critical rate functions but that the location and extent of the instability requires the use of borehole extensometers. A recommended procedure for the suitable application of such a deformation monitoring scheme follows:

1. Establish critical closure rate functions. These may be obtained from performance records of tunnels of similar geometry, constructed in similar geologic settings or from test sections or pilot headings of the same tunnel;
2. Take convergence readings as soon as possible after tunnel advance. Frequent readings should be taken until the mode of behavior is well established.

Multi-directional closure measurements should be made with a 4-point convergence array as a minimum;

3. Separate the time-dependent closure from the face advance effect by application of the derived expressions and compare with the appropriate functions to determine behavior mode; and
4. If yielding is indicated or anticipated, install multi-point borehole extensometers around the excavation

or locally, if the probable location of yielding is known, to delineate the location and extent of the overstressed rock so that remedial measures may be taken.

The above procedures are very much dependent on quick data assembly and processing as well as flexible contract arrangements that allow for instrumentation based on rational design criteria rather than predetermined criteria. However, instruments may be placed for other reasons as mentioned in the introductory chapters.

This proposed deformation monitoring program was derived from a series of model tests conducted on coal samples under controlled laboratory conditions. To verify their suitability for other materials would require additional laboratory investigations. However, it would be much more beneficial to explore their validity in field scale operations and possibly some parametric studies performed with sophisticated numerical material models.

An additional requirement identified in this research is the need for the development of instrumentation capable of continuously recording the radial displacement or strain ahead of the face in deep excavations. Only with these fully defined deformation records will verification of design assumptions be established.

7. REFERENCES

- Amberg, R. 1983. Design and Construction of Furka Base Tunnel. *Rock Mechanics* Vol. 16, No.4, pp.215-231,
- Bieniawski, Z.T., 1967. Mechanism of brittle fracture of rock. *CSIR Report*, MEG 580, Pretoria, 226pp.,
- Blake, W., 1982. Microseismic monitoring for underground stability. *Proc. First International Conference on Stability in Underground Mining*. Vancouver, pp. 272-294.,
- Brown, E.T., J.W. Bray, B. Ladanyi and E. Hoek, 1983. Ground response curves for rock tunnels. *Journal of Geotechnical Engineering, ASCE*, Vol. 109, No. 1, pp.15-39.,
- Cording, E.J., Hendron, A.J., Hansmire, W.H., et al, 1975. Methods of geotechnical observation and instrumentation in tunneling. *Report for National Sciences Foundation*. 2 Volumes, 566 pp.,
- Cruden, D.M., 1970. A theory of brittle creep in rock under uniaxial compression. *Journal of Geophysical Research*, 75, pp.3431-3442.,
- Cruden, D.M., 1971a. Single-increment creep experiments on rock under uniaxial compression. *International Journal of Rock Mechanics and Mining Sciences & Geomechanics Abstracts*, Vol. 8, No. 2, pp.127-142.,
- Cruden, D.M., 1971b. The recovery of Pennant sandstone from uniaxial compressive load. *Canadian Journal of Earth Sciences*, Vol. 8, No. 5, pp.518-522.,
- Cruden, D.M., 1983. Creep in brittle rock after an increment of uniaxial load. *Canadian Geotechnical Journal*, (in

press).

- da Fontoura, S. and Morgenstern, N. R., 1981. Stress - strain time relationship for a jointed coal. *Proc. International Symposium on Weak Rock*, Tokyo, Vol. 1, pp. 105-110.
- da Fontoura, S., 1980. Time-dependent response of rock masses during tunneling. *Ph.D. thesis, Department of Civil Engineering, University of Alberta*, 314p.
- Dahl, H.D., 1978. The state-of-the-art in underground coal mine design. *Proc. First International Symposium on Stability in Coal Mining*. Vancouver, pp. 125-134.
- Dunnicliff, J., Hampton, D., and Selig, E., 1981. Tunnel instrumentation; why and how? *Proc. Fourth Rapid Excavation and Tunneling Conference*. San Francisco, Vol. 2, pp. 1455-1472.
- Franklin, J.A., 1977. The monitoring of structures in rock. *International Journal of Rock Mechanics and Mining Sciences & Geomechanics Abstracts*, Vol.14, pp. 163-192.
- Goodman, R.E., and Dubois, J., 1972. Duplication of dilatancy in analysis of jointed rocks. *Journal of the Soil Mechanics and Foundation Division, ASCE*, Vol. 98. No. SM4, pp. 399-422.
- Guenot, A., P.K. Kaiser and N.R. Morgenstern, 1984. Deformation of small tunnels - Part IV. Behaviour during failure. *International Journal of Rock Mechanics and Mining Sciences & Geomechanics Abstracts*, in press.
- Guenot, A., 1979. Investigation of Tunnel Stability by Model Tests. *M.Sc. thesis, Department of Civil Engineering, University of Alberta*, 217 p.
- Hams, A.H., 1978. Research to improve structural stability and percentage of coal extracted in Australian coal mines. *Proc. First International Symposium on Stability in Coal Mining*, Vancouver, pp. 148-157.
- Hargraves, A.J., and Martin, C.H., 1977. Current methods of

development support in deeper collieries in Australia. *Proc. Sixth International Strata Control Conference, Banff.*,

- Hawk, D.J. and Ko, H.Y., 1980. Constitutive relations of coal and coal measure rocks - Vol. II. A study of the orthotropy of coal and other rock materials. *U.S. Bureau of Mines Open File Report, 54(2)-83, 129pp.*,
- Heuer, R.E., and Hendron, A.J., 1971. Geomechanical model study of the behavior of underground openings in rock subjected to static loads. *U.S. Corps of Engineers Report N-69-1, Report 2, Contract No. DACA39-67-C-0009. 370pp.*,
- Hoek, E. and Brown, E.T., 1980. *Underground Excavation in Rock*. Institution of Mining and Metallurgy, London, 527 pp.,
- John, M., 1977. Adjustment of programs of measurements based on the results of current evaluation. *International Symposium on Field Measurements in Rock Mechanics, Vol. 2, pp. 639-656.*,
- Kaiser, P.K. and N.R. Morgenstern, 1981a. Time-dependent deformation of small tunnels - I. Experimental facilities. *International Journal of Rock Mechanics and Mining Sciences & Geomechanics Abstracts, Vol. 18, pp. 129-140.*,
- Kaiser, P.K. and N.R. Morgenstern, 1982. Time-independent and time-dependent deformation of small tunnels - III. Pre-failure behaviour. *International Journal of Rock Mechanics and Mining Sciences & Geomechanics Abstracts, Vol. 19, pp. 307-324.*,
- Kaiser, P.K., and C. Mackay, 1982. Development of rock mass and liner stresses during sinking of a shaft in clay shale. *1st International Conference on "Stability in Underground Mining", Vancouver, Ch. 36, pp. 790-809.*,
- Kaiser, P.K., 1979. Time-Dependent Behaviour of Tunnels in Jointed Rock Masses. *Ph.D. thesis, Department of Civil Engineering, University of Alberta, 395pp.*,

- Kaiser, P.K., 1980. Effect of stress history on the deformation behaviour of underground openings. *13th Canadian Rock Mechanics Symposium, CIM Special Volume 22*, pp.133-140.,
- Kaiser, P.K., 1981d. Monitoring for the evaluation of the stability of underground openings. *1st Annual Conference on Ground Control In Mining, West Virginia*, pp. 90-97.,
- Ko, H.Y. and Gerstle, K.H., 1976. Elastic properties of two coals. *International Journal of Rock Mechanics and Mining Sciences & Geomechanics Abstracts*, Vol. 13, pp.81-90.,
- Korpach, D., 1983. Stresses and Displacements near the Tunnel Face. *M.Sc. thesis, Department of Civil Engineering, University of Alberta*, 248pp. ,
- Kuesel, T.R., 1983. On hard rock and hard progress. *Underground Space*, Vol. 7, No. 3, pp. 156-160.,
- Ladanyi, B., 1974. Use of the long-term strength concept in the determination of ground pressure on tunnel linings. *3rd Congress of the International Society of Rock Mechanics, Denver*, Vol. IIB, pp. 1150-1156.,
- Lama, R.D. and Vutukuri, V.S., 1978. *Handbook on mechanical properties of rocks. Vol. 2, Testing Techniques and Results*. Trans Tech Publications, Clausthal, 481pp.,
- Lane, K.S., 1977. Instrumental tunnel tests: a key to progress and cost saving. *Underground Space, Vol.1, No.3*, pp.247-259.,
- Lemcoe, M.M., Pratt, H., and Grams, W., 1980. State-of-the-art review of rock mechanics techniques for measurement of stress, displacement and strain. *Subsurface Space, Rockstore'80, Stockholm*, Vol. 2, pp.927-942.,
- Lo, K.Y., and Lukajic, B., 1984. Predicted and measured stresses and displacements around the Darlington Intake Tunnel. *Canadian Geotechnical Journal*, Vol. 21, No. 1, pp. 147-165.,

- Londe, P., 1977. Field Measurements in tunnels. *Proc. International Symposium on Field Measurements in Rock Mechanics*. Zurich, Vol. 2, pp. 619-638.,
- Lu, P.H., 1982. Rock mechanics instrumentation and monitoring for ground control around longwall panels. *State-of-the-Art of Ground Control in Longwall Mining and Mining Subsidence*, Y.P. Chugh and M. Karmis, ed., pp. 15-166.,
- McVey, J.R., and Howie, W.L., 1981. New Closure rate instrument for retreat mining operation. *Mining Engineering*, Vol. 33 No. 12, pp. 1699-1700.,
- Morgans, W.T.A., and Terry, N.B., 1958. Measurements of the static and dynamic elastic moduli of coal. *Fuel*, London, 37, pp. 201-209.,
- Muir Wood, A.M., 1979. Ground behavior and support for mining and tunneling. *Tunnels and Tunneling*, Vol. 11, No.4/5, pp. 43-48/47-51.,
- Noonan, D.K.J., 1972. Fractured rock subjected to direct shear. *M.Sc thesis, Department of Civil Engineering, University of Alberta*, 108pp.,
- Obert, L. and Duvall, W.I., 1967. *Rock Mechanics and the Design of Structures In Rock*. John Wiley and Sons, New York, 650 pp.,
- Panet, M. and A. Guenot, 1982. Analysis of convergence behind the face of a tunnel. *Tunnelling'82, The Institution of Mining and Metallurgy*, pp. 197-204.,
- Pearson, G.R., 1959. Coal reserves for strip mining, Wabamun Lake District, Alberta. *Research Council of Alberta, Geology Division, Preliminary Report 59-1*, 37 pp.,
- Pothini, B.R., and von Schonfeldt, H., 1978. Roof fall prediction at Island Creek Coal Company. *Proc. First International Symposium on Stability in Coal Mining*, Vancouver, pp. 214-227.,
- Sargent, D.W.J., 1981. A Process Simulation Test on a Small

- tunnel support considering progress of tunnel face. *International Journal for Numerical and Analytical Methods In Geomechanics*, Vol. 2, pp. 159-175.,
- Sargent, D.W.J., 1981. A Process Simulation Test on a Small Unlined Tunnel in Jointed Coal. *M.Sc. thesis, Department of Civil Engineering, University of Alberta*, 179 p.,
- Schuyer, J., Dijkstra, H., and van Kreveler D.W., 1954. Chemical structure and properties of coal VII elastic properties. *Fuel*, London, 33, pp. 409-418.,
- Schwartz, C.W., and Kolluru, S., 1981. Laboratory investigation of creep of jointed rock material. *22nd U.S. Symposium on Rock Mechanics*, Boston, pp. 283-289.,
- Serata, S., Iwasaki, Y., and Mochida, Y., 1976. New in situ instrumentation technique for tunneling and mining design: field examples. *Proc. Second Rapid Excavation and Tunneling Conference*, Las Vegas, pp. 722-741.,
- Standfield, E. and Lang, W.A., 1944. Coals of Alberta, their occurrence, analysis and utilization. *Research Council of Alberta*, Report No. 35, 174 pp.,
- Tocher, R.J. and Ko, H.Y., 1980. Constitutive relations of coal and coal measure rocks. Vol. 3. Drying, shrinkage and creep behavior of coal. *U.S. Bureau of Mines Open File Report*, 54(3)-83, 111pp.,
- Whittaker, B.N., 1974. An appraisal of strata control practice. *Mining Engineer*, Vol. 134, No.166, pp. 9-24.,
- Wieselmann, E.A., 1968. Closure measurements an important tool in mine design at the Cane Creek potash mine. *Tenth U.S. Symposium on Rock Mechanics*, Austin, pp. 741-758.,

8. APPENDIX A - DETERMINATION OF TIME-DEPENDENT PROPERTIES

Linear Elastic, Isotropic Parameters

The Young's modulus, E , and Poisson's ratio, ν , required for the linear elastic, isotropic representation of material response were determined by one of the following methods depending upon the sample loading history.

Method 1

In this method, developed by Guenot (1979), the response of an extensometer during the application of an increment of stress before and after tunnel excavation is compared. It assumes that, during subsequent reloadings of the sample, the elastic parameters are loading history independent, the rate of loading is similar for both situations and that linear elastic solutions and superposition are applicable.

The radial strain increment ($\Delta \epsilon_r$) due to a change in the major principal field stress ($\Delta \sigma_v$) in the intact specimen under plane strain conditions is given by:

$$\Delta \epsilon_r = \Delta \sigma_v (1+\nu) [(1-2\nu)(1+N) + (1-N)\cos 2\theta] / 2E \quad 8.1$$

where N = ratio of minor to major principal field stress
and

θ = angle with respect to σ_v .

Equation 8.1 can be rewritten to yield an expression for Young's modulus as:

$$E = \frac{\Delta\sigma}{\nu} (1+\nu) \left[\frac{(1-2\nu)(1+N) + (1-N)\cos 2\theta}{r} \right] / 2\Delta\epsilon_r \quad 8.2.$$

Both $\Delta\sigma$ and $\Delta\epsilon$ are measured during testing and can be incorporated into a single variable 'm' which represents the slope of the tangent to the stress strain curve at a given stress:

$$m = \frac{\Delta\sigma}{\nu} / \frac{\Delta\epsilon}{r} \quad 8.3$$

Equation 8.2 can then be rewritten as:

$$E = 0.5 m (1+\nu) \left[\frac{(1-2\nu)(1+N) + (1-N)\cos 2\theta}{r} \right] \quad 8.4$$

Under conditions of equal lateral field stress ($N=1$), Equation 8.4 can be rewritten as:

$$E = m(1+\nu)(1-2\nu) \quad 8.5$$

The radial strain increment due to a change in the major principal field stress in a specimen containing a tunnel of radius 'a' under plane strain and equal lateral stress ($N=1$) conditions is given by:

$$\Delta\epsilon_r = \frac{\Delta\sigma}{\nu} \left[\frac{(1-\nu)(1-a^2/r^2) - \nu(1+\nu)(1+a^2/r^2)}{E} \right] \quad 8.6$$

where r = distance from tunnel centre to point of measurement.

Equation 8.6 can be simplified and rewritten to yield an

expression for Young's modulus as:

$$E = m(1+\nu)(1-2\nu-a^2/r^2) \quad 8.7$$

Substituting m_1 for m in Equation 8.5 and m_2 in Equation 8.7 and then equating the two expressions yields an expression for Poisson's ratio as:

$$\nu = [m_2(1-a^2/r^2-m_1)]/2(m_2-m_1) \quad 8.8$$

The value thus obtained can be substituted in either Equation 8.5 or 8.7 to yield the value of Young's modulus.

Method 2

In this method comparison of the response of an extensometer under different loading conditions (N values) on the intact specimen are compared. Conducting two tests at different stress ratios, N_1 and N_2 , and employing Equation 8.4 results in the following expression for Poisson's ratio:

$$\nu = 0.5 - \frac{[m_2(1-N_2)-m_1(1-N_1)]\cos 2\theta}{2[m_1(1+N_1)-m_2(1+N_2)]} \quad 8.9$$

This value may then be substituted into Equation 8.4 to determine Young's modulus.

Linear Elastic, Transverse Isotropic Parameters

For a linear elastic, transverse isotropic body, whose plane of isotropy is the r - θ plane the relationship between stress and strain is:

$$\begin{pmatrix} \epsilon_r \\ \epsilon_\theta \\ \epsilon_z \\ \gamma_{r\theta} \\ \gamma_{rz} \\ \gamma_{zr} \end{pmatrix} = \begin{bmatrix} 1/E_r & -\nu_{r\theta}/E_r & -\nu_{zr}/E_z & 0 & 0 & 0 \\ -\nu_{r\theta}/E_r & 1/E_r & -\nu_{zr}/E_z & 0 & 0 & 0 \\ -\nu_{zr}/E_r & -\nu_{zr}/E_r & 1/E_z & 0 & 0 & 0 \\ 0 & 0 & 0 & 1/2G_{zr} & 0 & 0 \\ 0 & 0 & 0 & 0 & 1/2G_{zr} & 0 \\ 0 & 0 & 0 & 0 & 0 & 1+\nu_{r\theta}/E_r \end{bmatrix} \begin{pmatrix} \sigma_r \\ \sigma_\theta \\ \sigma_z \\ \tau_{r\theta} \\ \tau_{rz} \\ \tau_{zr} \end{pmatrix} \quad 8.10.$$

where ϵ denotes the normal strains, γ the shear strains, σ the normal stresses and τ the shear stresses. The 5 constants required for material description are:

- E_r = the Young's modulus in the plane of isotropy (r - θ plane);
- E_z = the Young's modulus normal to the plane of isotropy (z direction);
- G_{zr} = the shear modulus relating shear stresses to shear strains out of the plane of isotropy; and
- $\nu_{r\theta}, \nu_{zr}$ = the Poisson's ratio relating straining in the direction of the second subscript to the strain in the direction of the first.

Poisson's ratio and Young's modulus in and normal to the plane of isotropy are related by the following expression:

$$\frac{\nu}{zr} / E = \frac{\nu}{rz} / E \quad 8.11.$$

Considering normal stresses and strains only and substituting $K\sigma_r$ for σ_θ the following expressions are derived:

$$\epsilon_r = [\sigma_r (1 - K\nu) - \nu \sigma_z] / E \quad 8.12.$$

$$\epsilon_\theta = [\sigma_r (K - \nu) - \nu \sigma_z] / E \quad 8.13.$$

$$\epsilon_z = [\sigma_z - \nu \sigma_r (1 + K)] / E \quad 8.14$$

where: $K = [(1+N) - (1-N)\cos 2\theta] / [(1+N) + (1-N)\cos 2\theta]$.

Under plain strain conditions ($\epsilon_z = 0$) Equation 8.14 can be rewritten to yield an expression for ν_{zr} as:

$$\nu_{zr} = \sigma_z / [\sigma_r (1 + K)] \quad 8.15.$$

Under conditions of hydrostatic compression ($\sigma_r = \sigma_\theta = \sigma_z = \sigma$) Equation 8.15 can be rewritten to yield an expression for E once ν_{zr} is known as:

$$E = \sigma (1 - 2\nu_{zr}) / \epsilon_z \quad 8.16.$$

Equation 8.12 can then be rewritten as:

$$\epsilon_r = \left[\frac{\sigma_r (1 - \nu_{r\theta})}{E} \right] - \frac{\nu_{rz} \sigma_z}{E}$$

8.17.

$$\text{or } E = \left[\frac{\sigma_r (1 - K \nu_{r\theta})}{\epsilon_r + (\nu_{rz} \sigma_z / E)} \right]$$

As σ_r , σ_z , ϵ_r , $\nu_{r\theta}$ and E are all known, conducting two tests at different stress ratios (N) will result in two equivalent expressions for E . This then allows for the determination of $\nu_{r\theta}$ by inputting the values of the measured variables in the following expression:

$$E = \frac{\frac{\sigma_{r_1} (1 - K_1 \nu_{r\theta})}{\epsilon_{r_1} + \frac{\nu_{rz_1} \sigma_{z_1}}{E}}}{\epsilon_{r_1} + \frac{\nu_{rz_1} \sigma_{z_1}}{E}} = \frac{\frac{\sigma_{r_2} (1 - K_2 \nu_{r\theta})}{\epsilon_{r_2} + \frac{\nu_{rz_2} \sigma_{z_2}}{E}}}{\epsilon_{r_2} + \frac{\nu_{rz_2} \sigma_{z_2}}{E}} \quad 8.18.$$

Once $\nu_{r\theta}$ is known, substitution of its value in Equation 8.17 yields the value of E . Substitution of the values for $\nu_{r\theta}$, E and E into Equation 8.11 yields the value of ν_{rz} .

Similar expressions for the relationships and constants can also be derived in cartesian coordinates.

**9. APPENDIX B - RADIAL STRAIN AND TUNNEL CLOSURE RATES
MEASURED DURING CREEP TESTS PERFORMED ON THREE SAMPLES**

The mean and range of the radial strain rates measured by extensometers at times of 1 (empty symbol), 5 (half full) and 20 hours (full symbols) after load application are presented in Figure 9.1 for Sample MC-5, Figure 9.7 for Sample MC-6 and Figures 9.12 to 9.14 for Sample MC-7. Also shown on these figures are the boundary strain rates defined as the ratio of sample loading boundary displacement to sample width per unit time. The remaining figures present the measured tunnel convergence (closure) rates; Figures 9.2 to 9.6 for Sample MC-5, Figures 9.8 to 9.11 for MC-6 and Figures 9.15 to 9.19 for Sample MC-7. Also shown on these figures are the two behavior evaluation functions, CCR and PCR (range denoted by shaded area), at a time of 20 hours after load application. The region denoted by the arrow between the CCR and PCR denotes the range of closure rates where behaviour is determined by the trend of closure rate versus time curves (in a double log plot). If the closure rate function converges to the CCR, yielding has terminated and a new stable equilibrium will be reached. If the rates are approaching the PCR range then yielding will tend to propagate. A stable equilibrium may still be reached but the accumulated closure may be unacceptable.

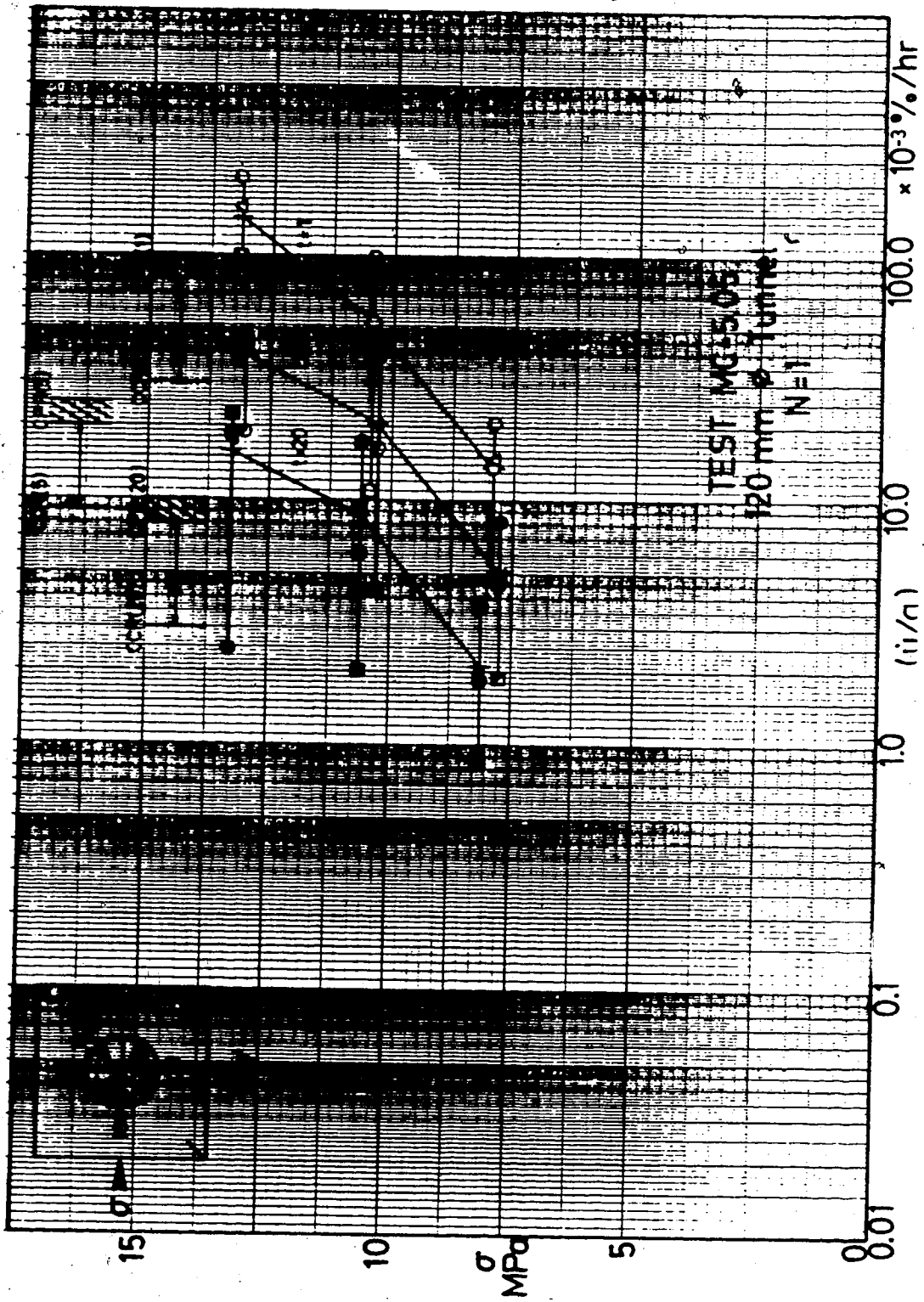


Figure 9.2 Closure Rates: MC-5.05

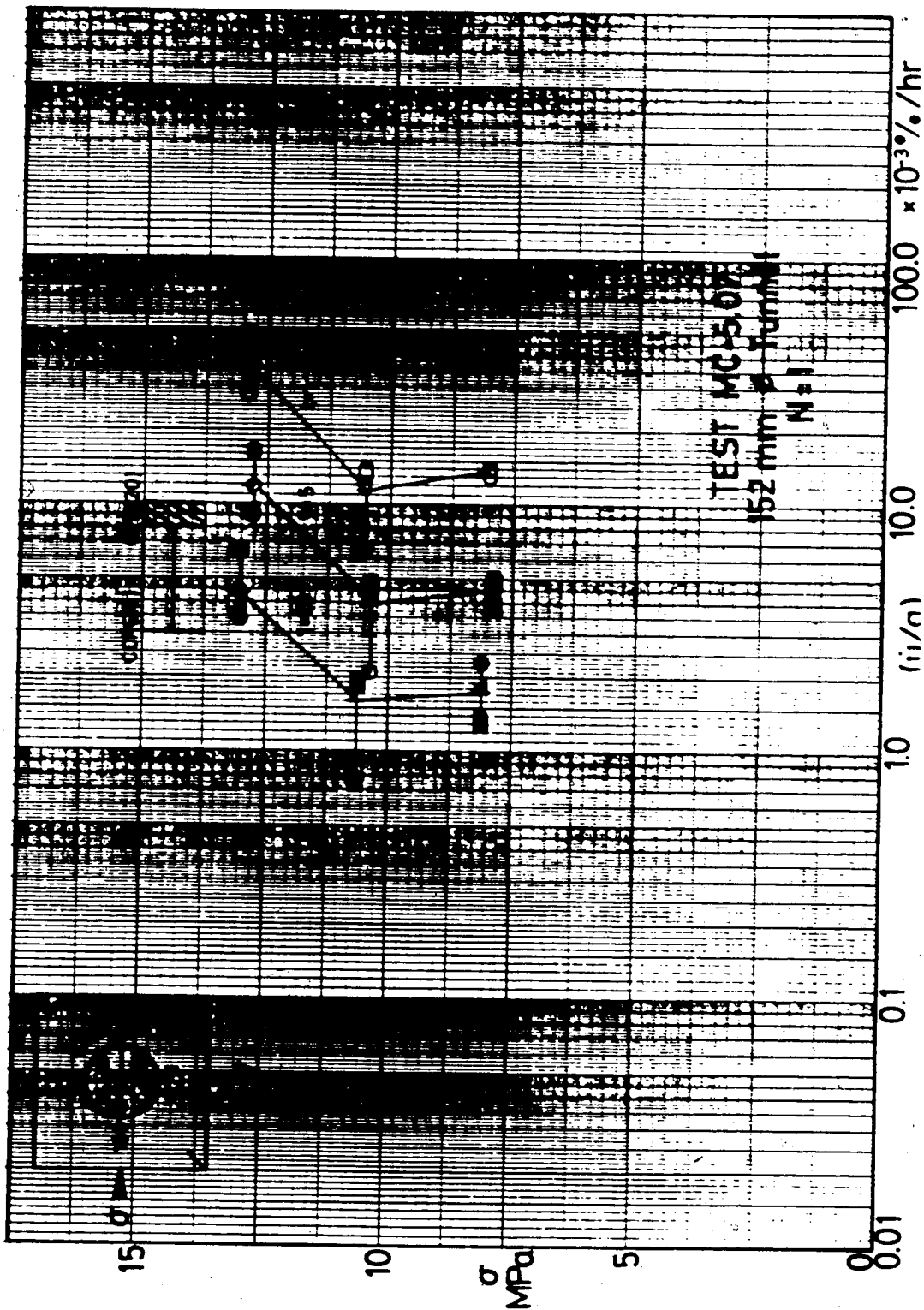


Figure 9.3 Closure Rates: MC-5.07

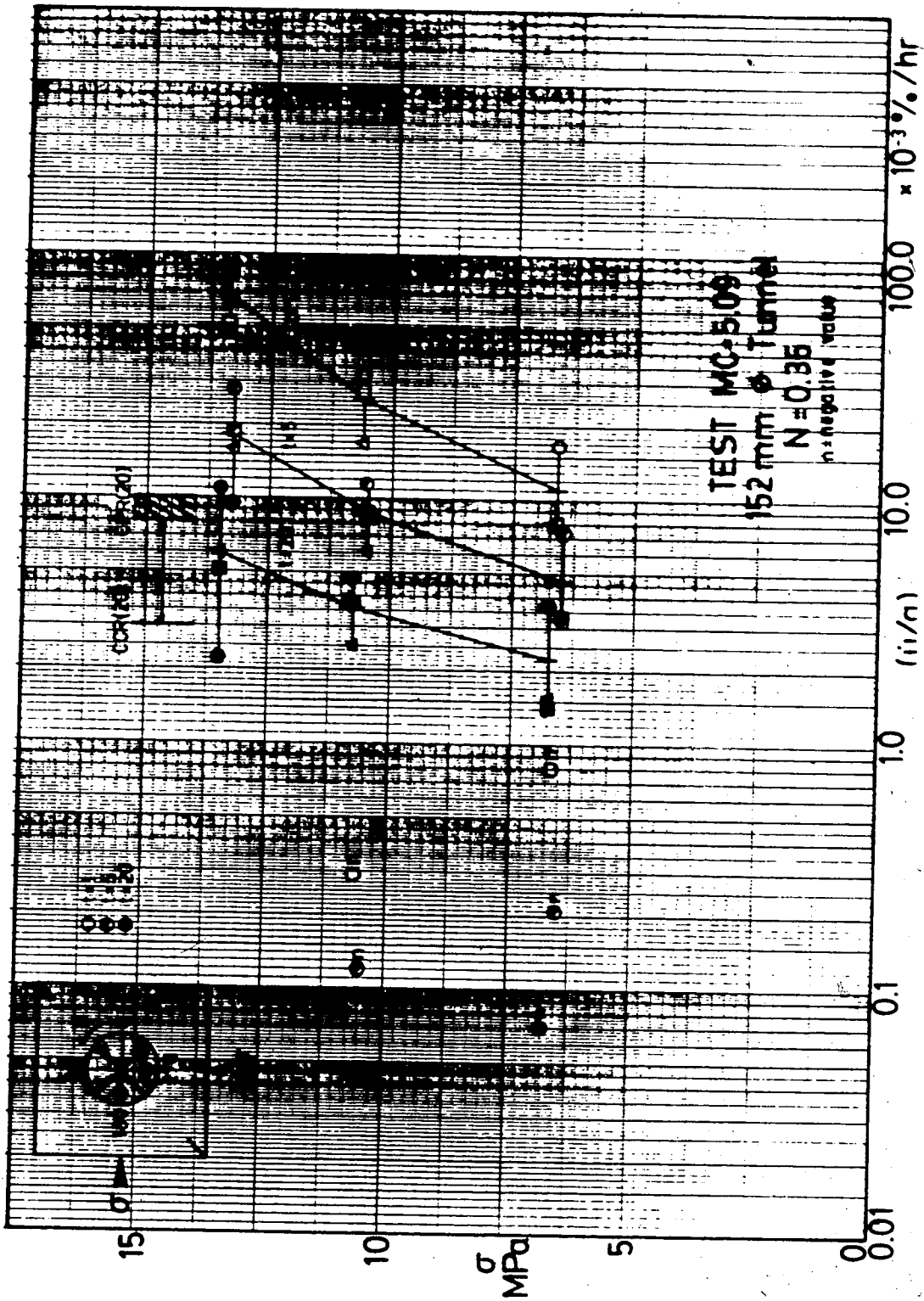


Figure 9.4 Closure Rates: MC-5.09

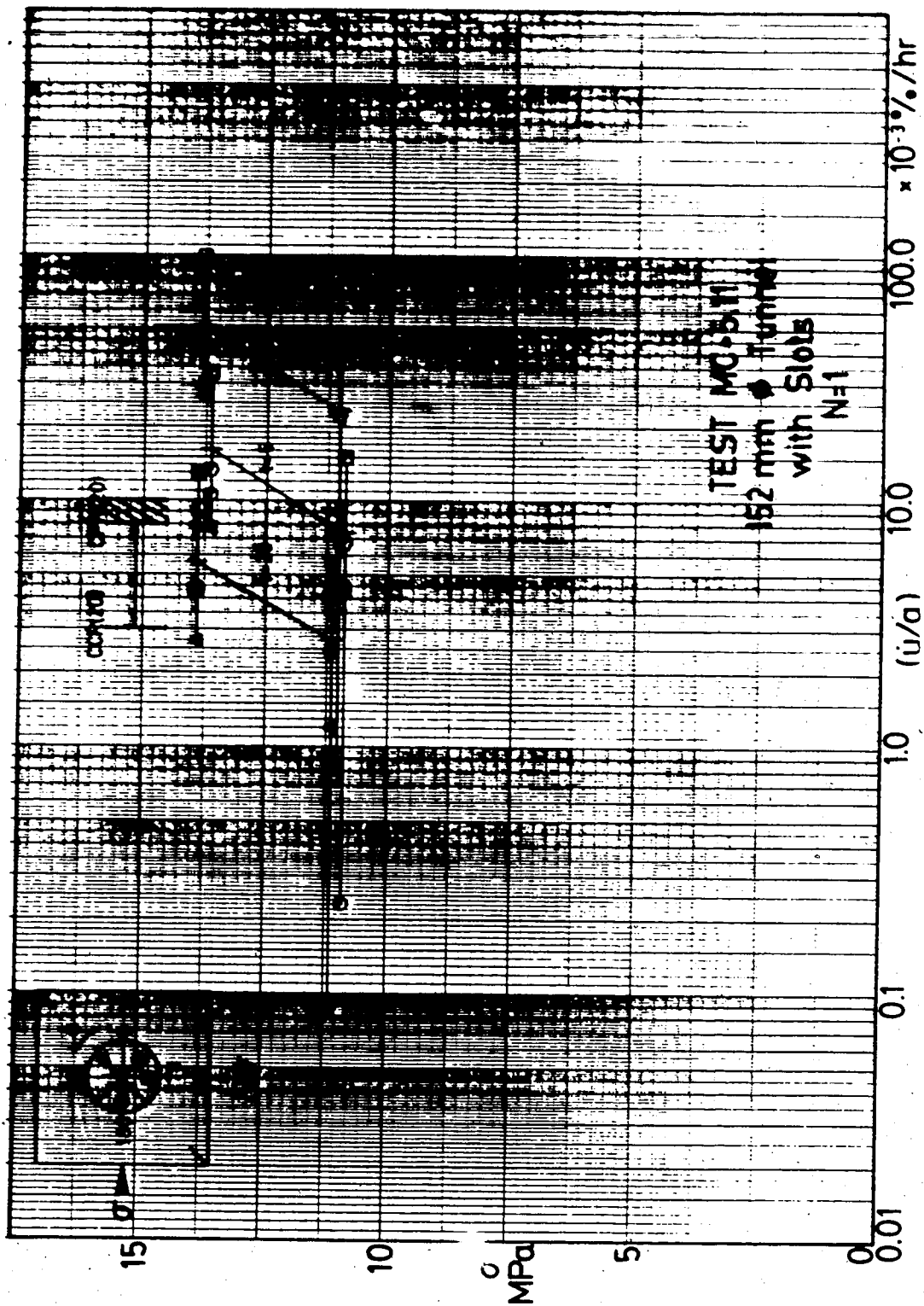


Figure 9.5 Closure Rates: MC-5.11

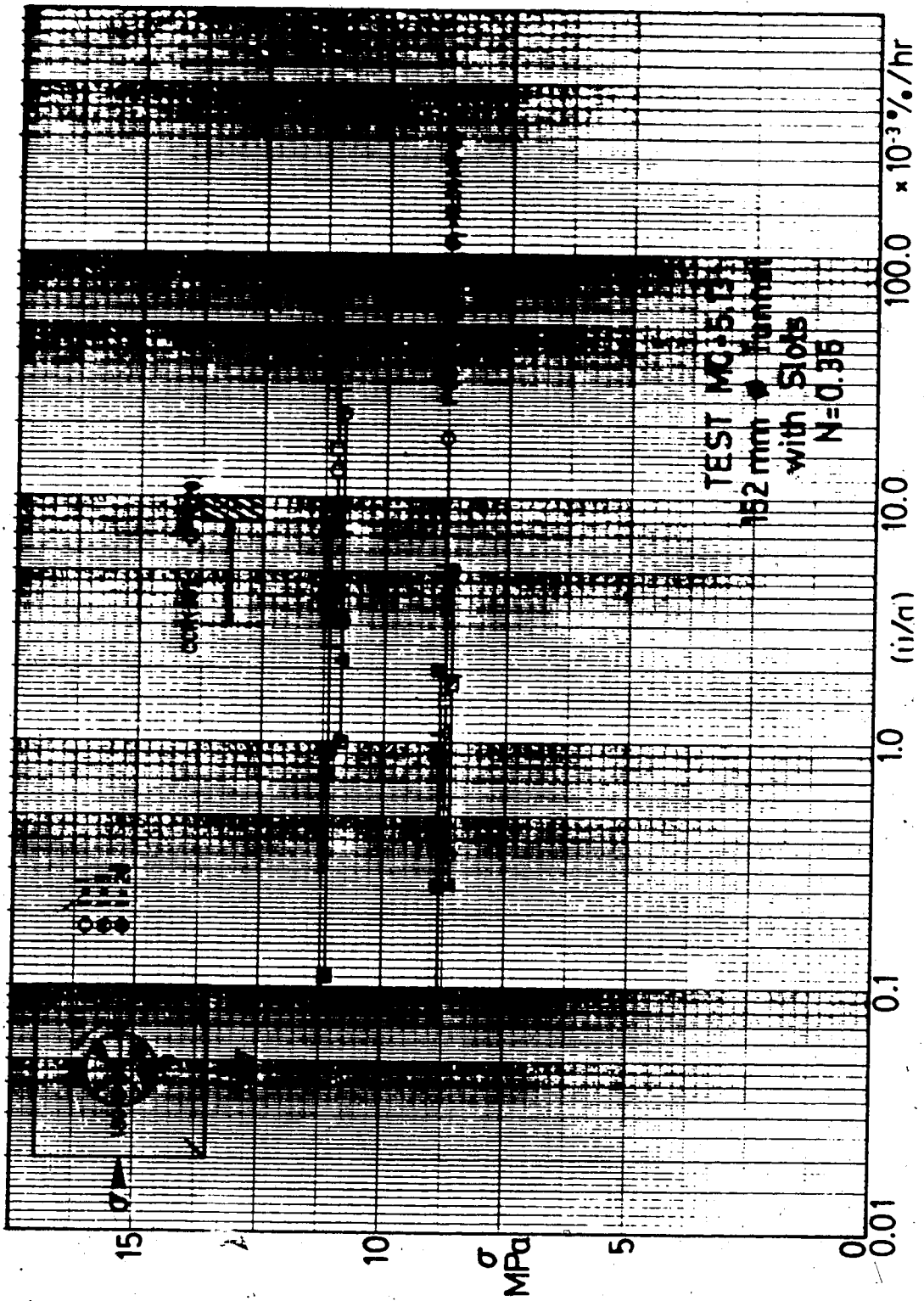


Figure 9.6 Closure Rates: MC-5.13

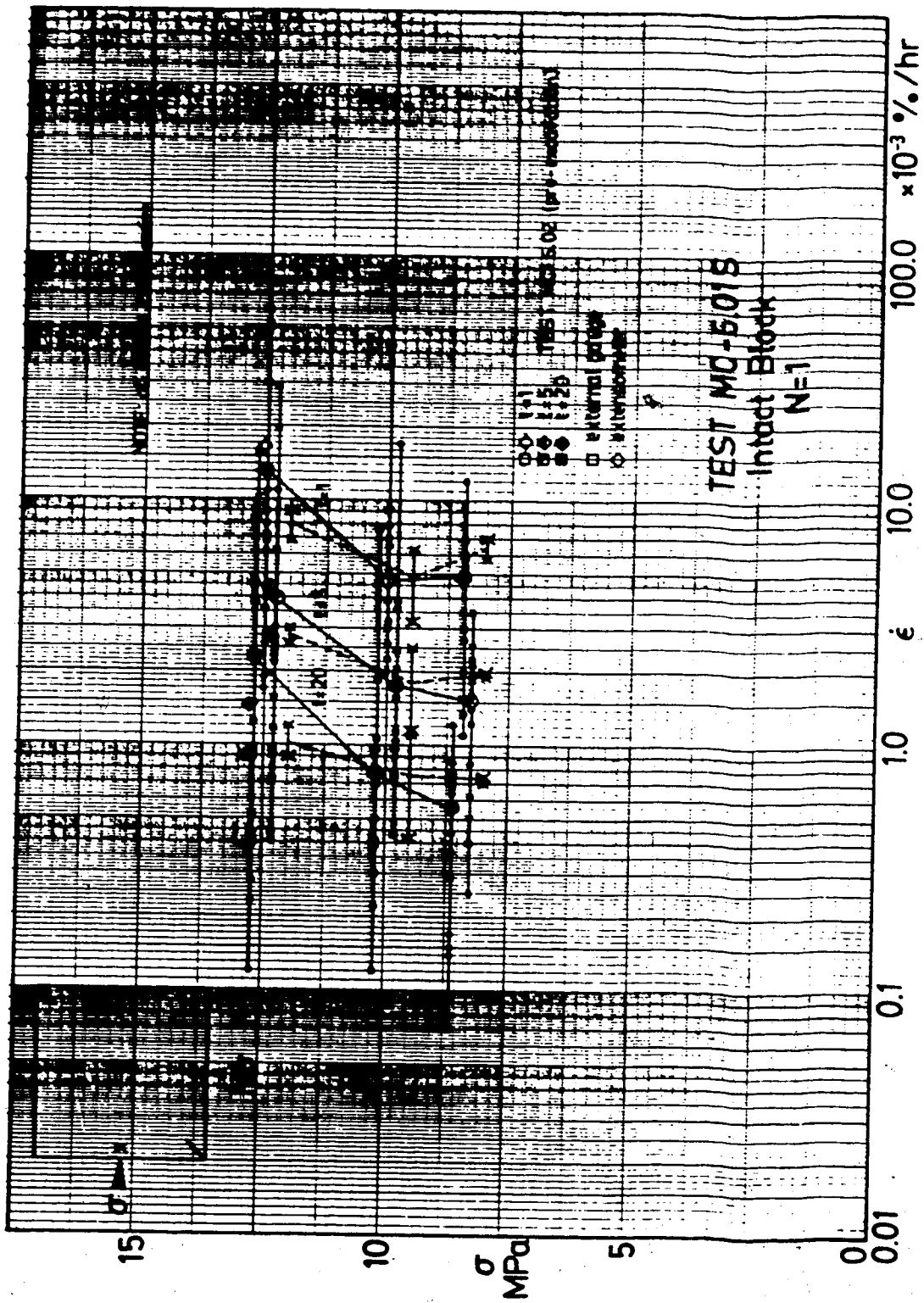


Figure 9.7 Strain Rates: MC6.01S and 6.02

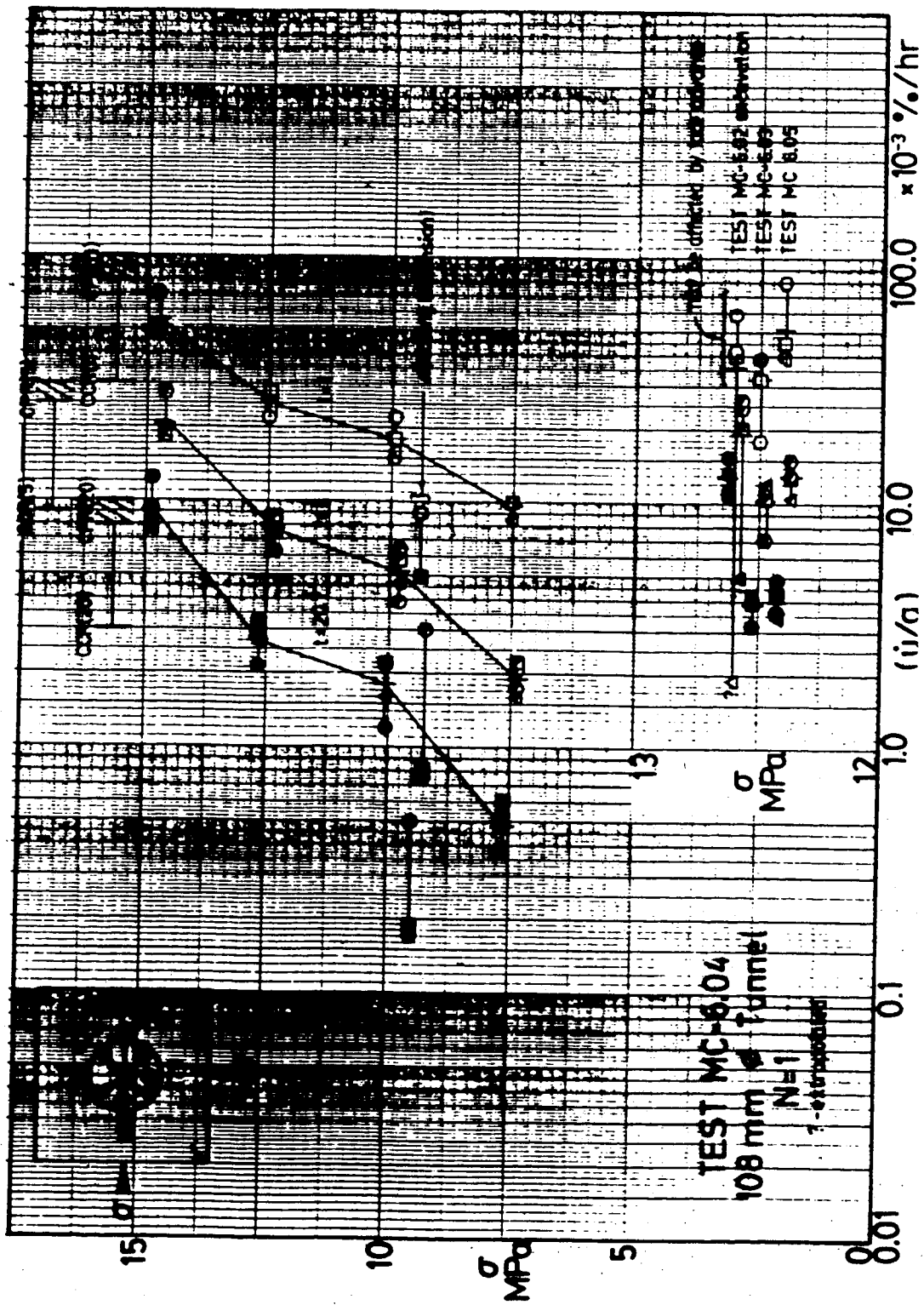


Figure 9.8 Closure Rates: MC-6.02, 6.03, 6.04 and 6.05 (108mm tunnel)

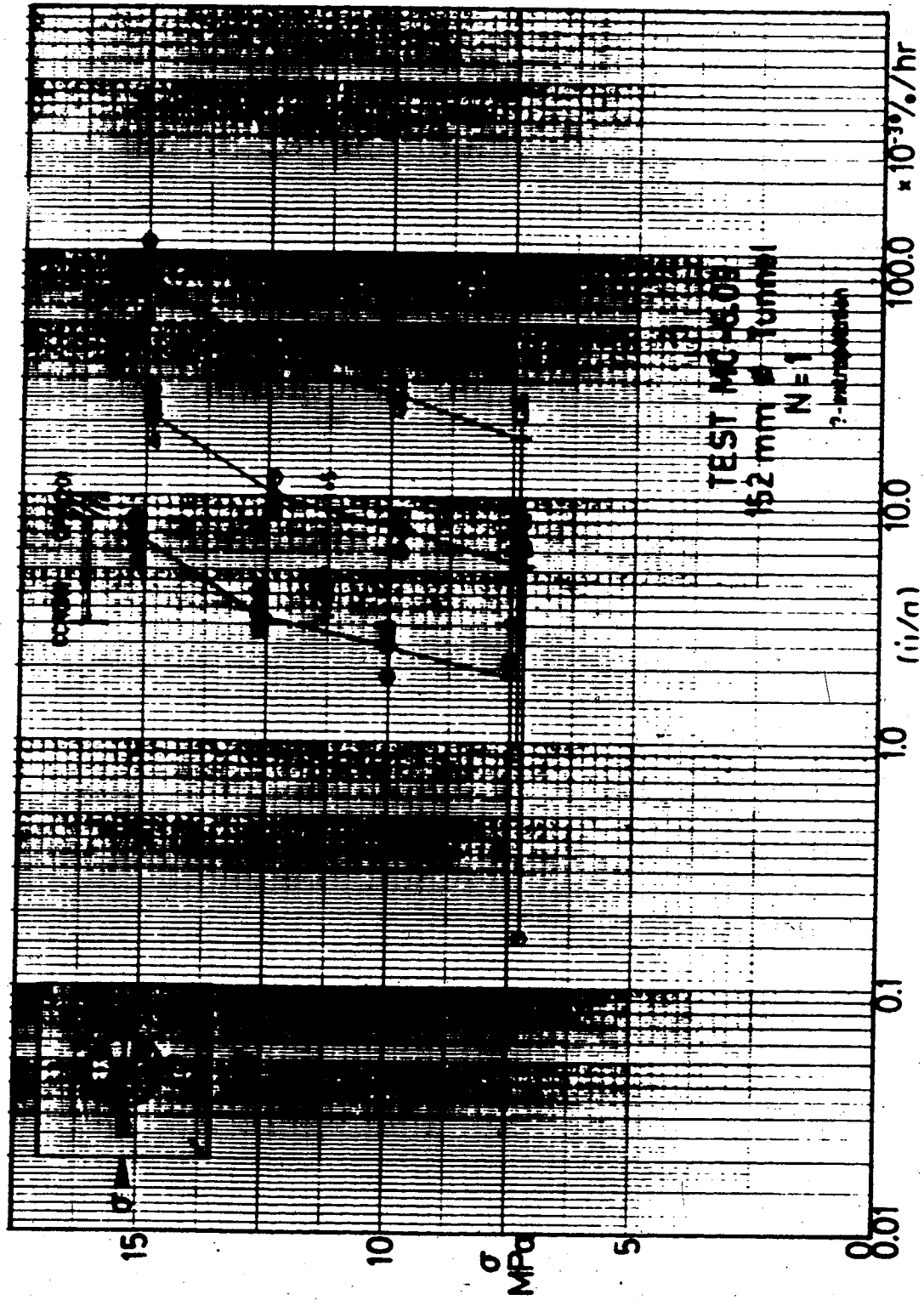


Figure 9.10 Closure Rates: MC-6.09

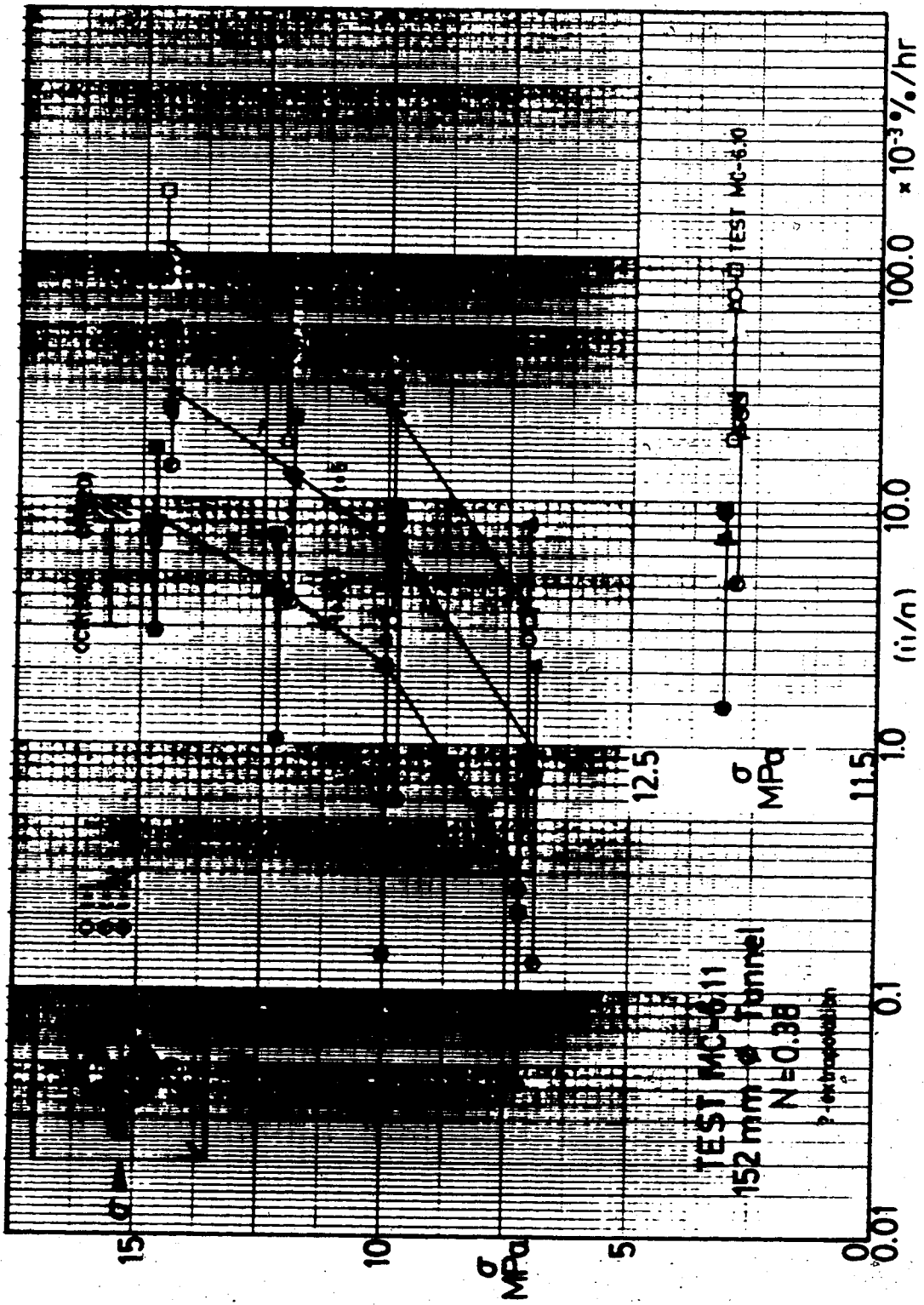


Figure 9.11 Closure Rates: MC-6.10 and 6.11

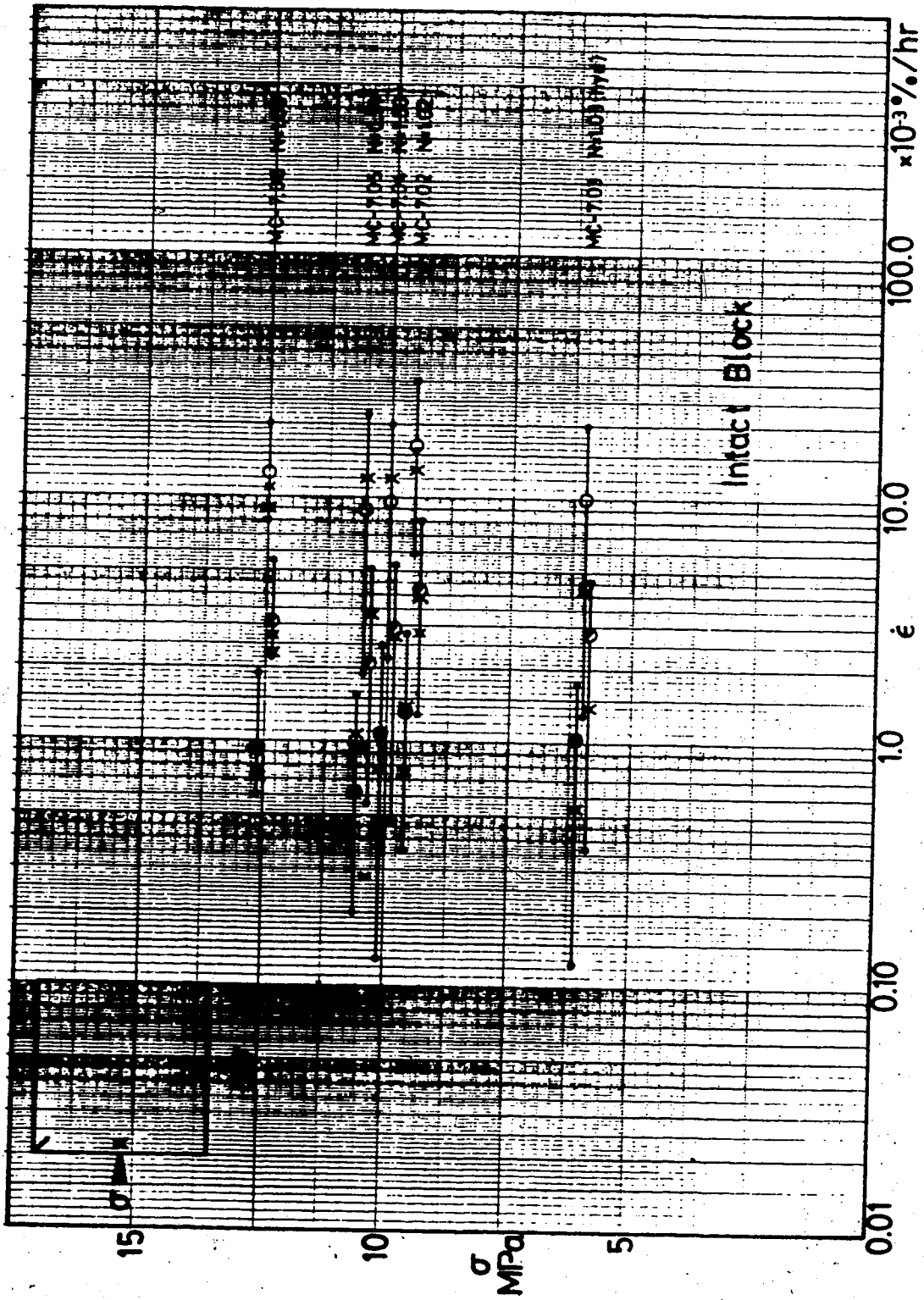


Figure 9.12 Strain Rates: MC-7.02, 7.03, 7.04, 7.05 and 7.08

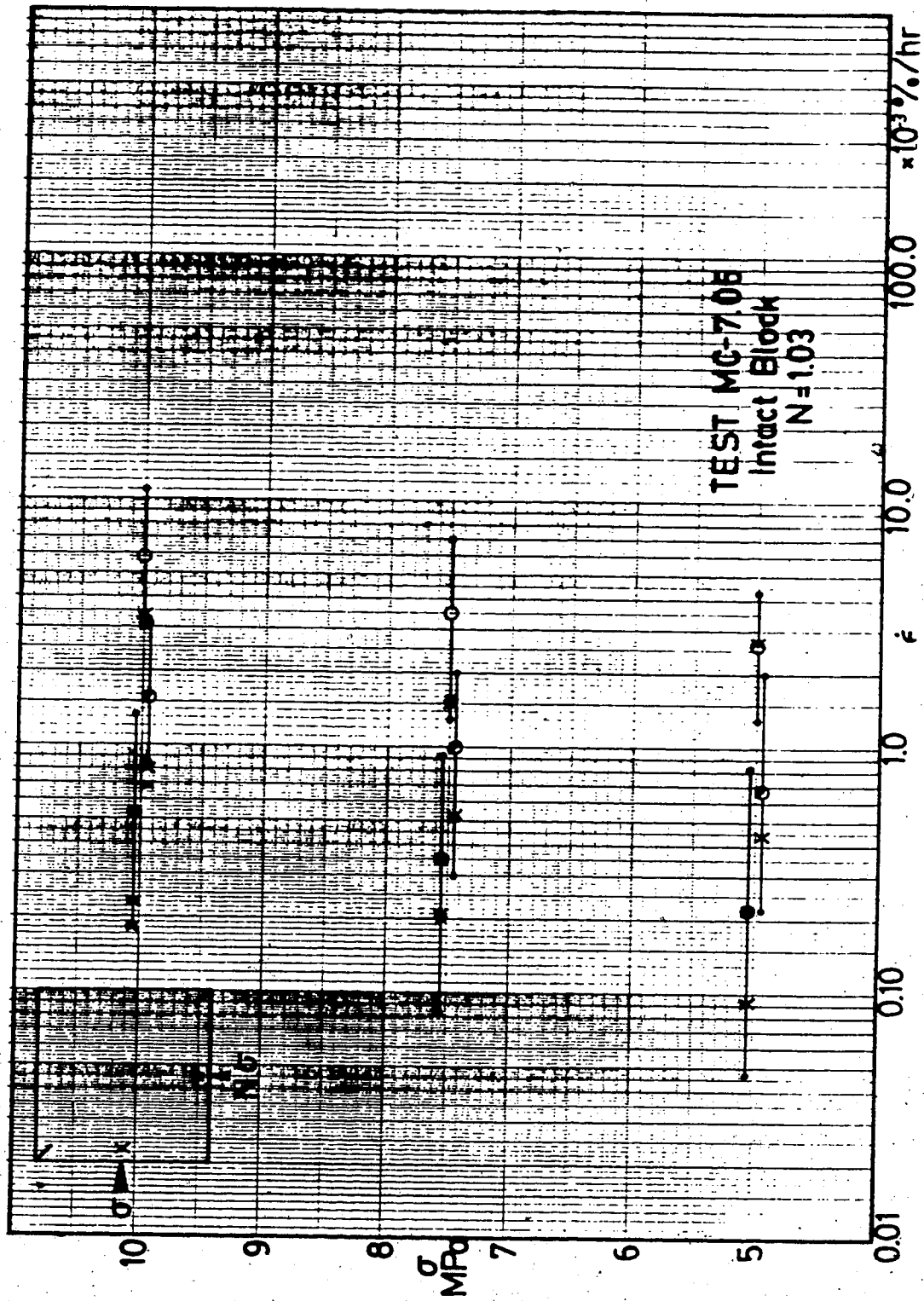


Figure 9.13 Strain Rates: MC-7.06

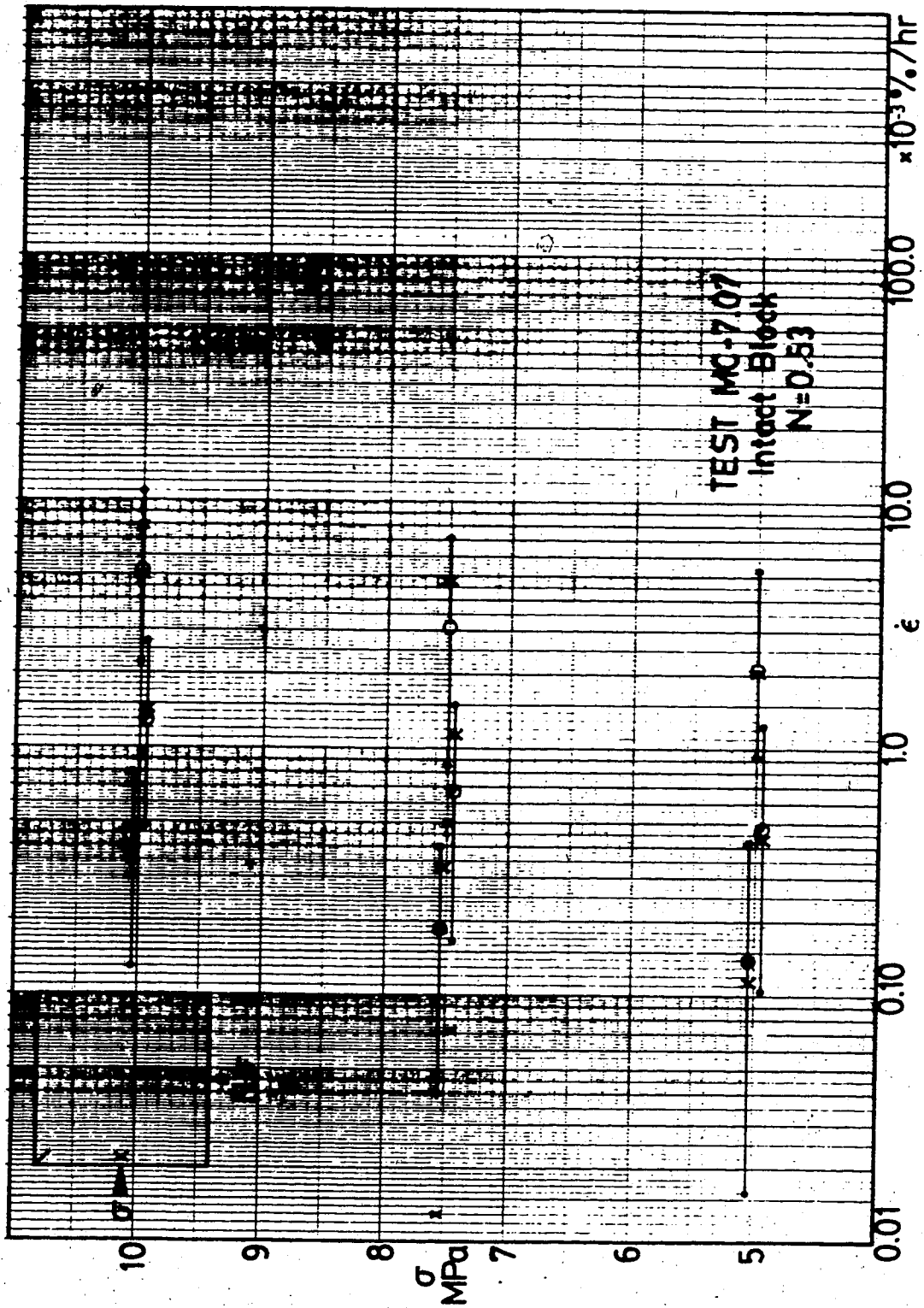


Figure 9.14 Strain Rates: MC-7.07

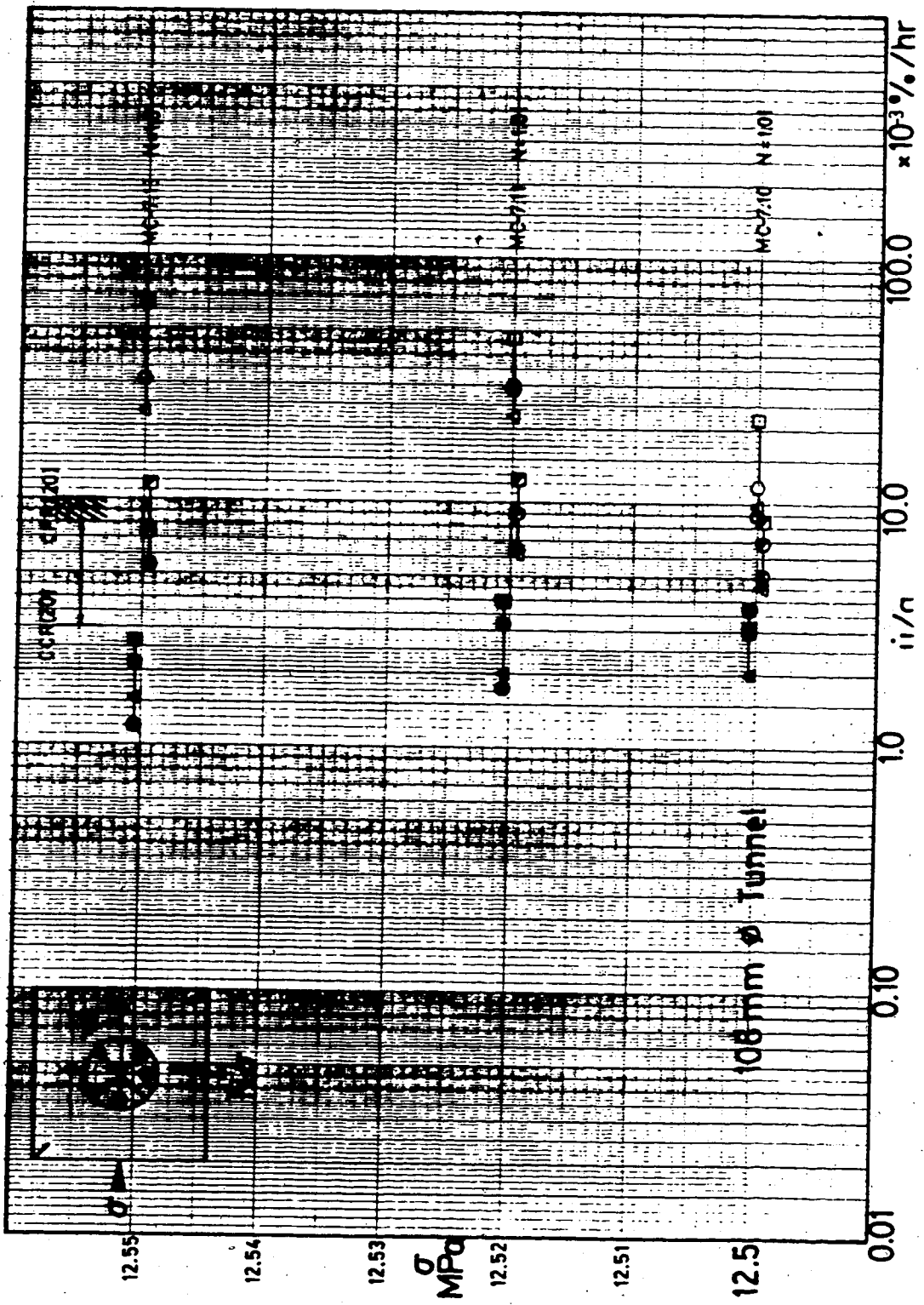


Figure 9.15 Closure Rates: MC-7.10, 7.11 and 7.13

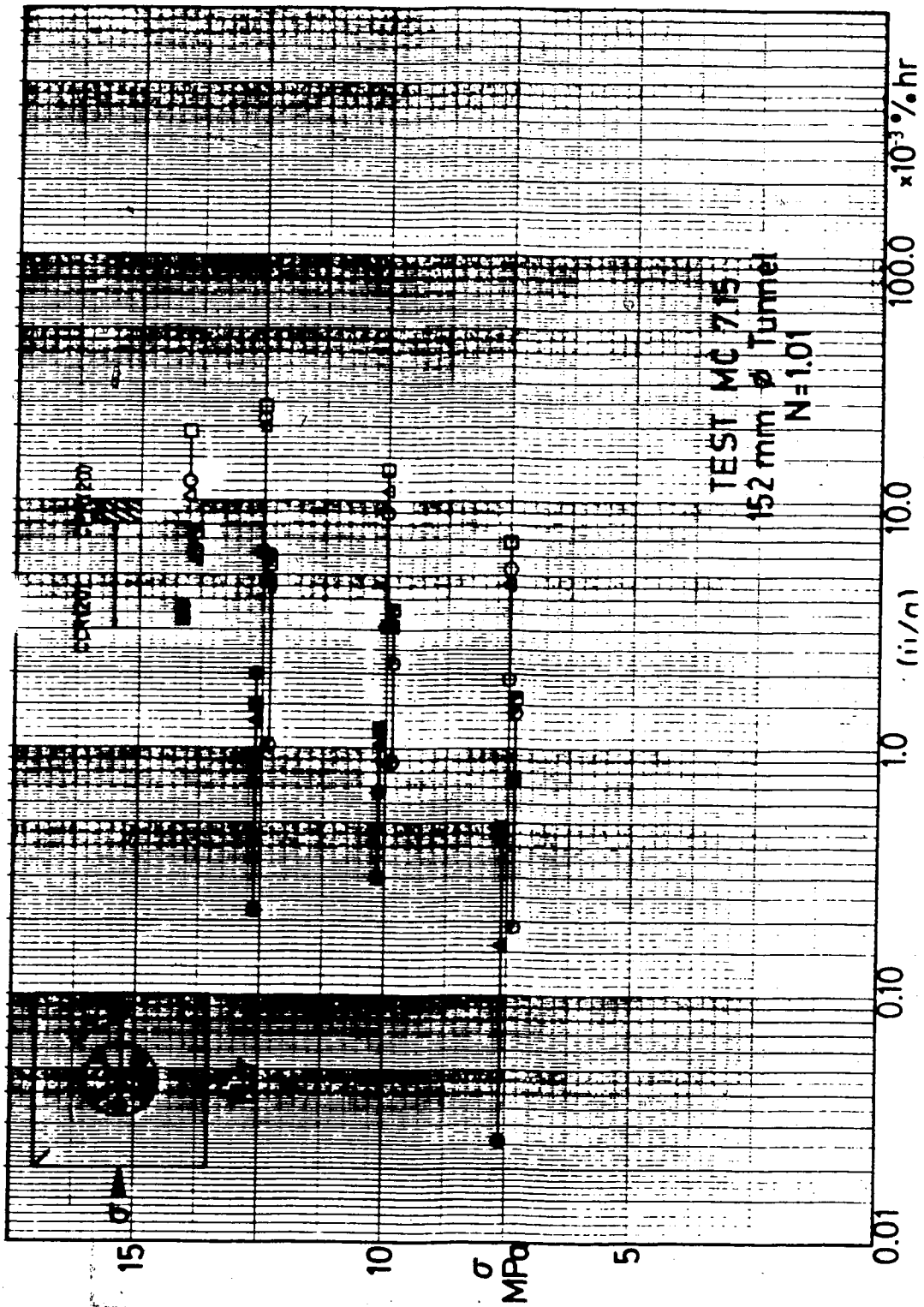


Figure 9.17 Closure Rates: MC-7.15

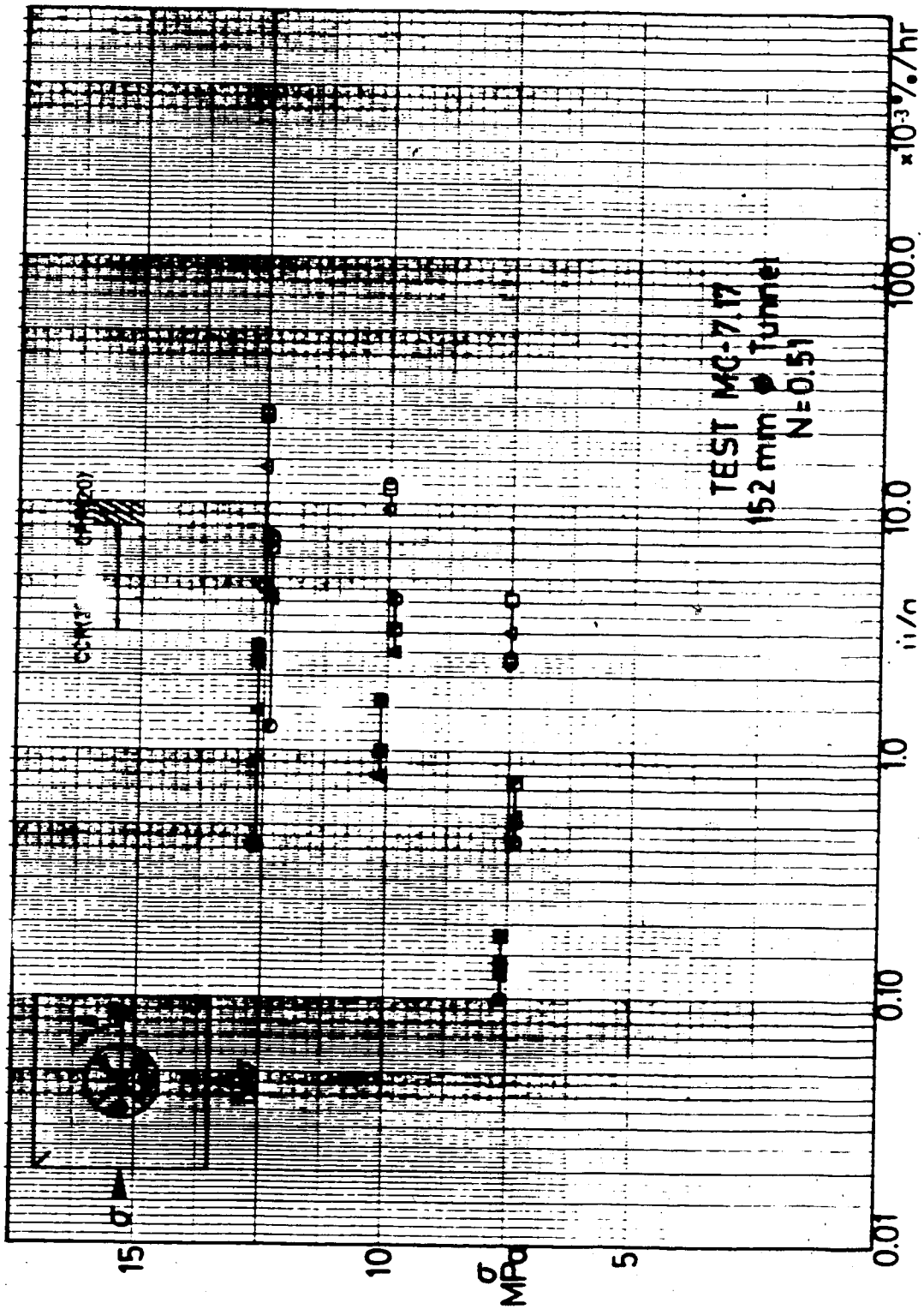


Figure 9.18 Closure Rates: MC-7.17

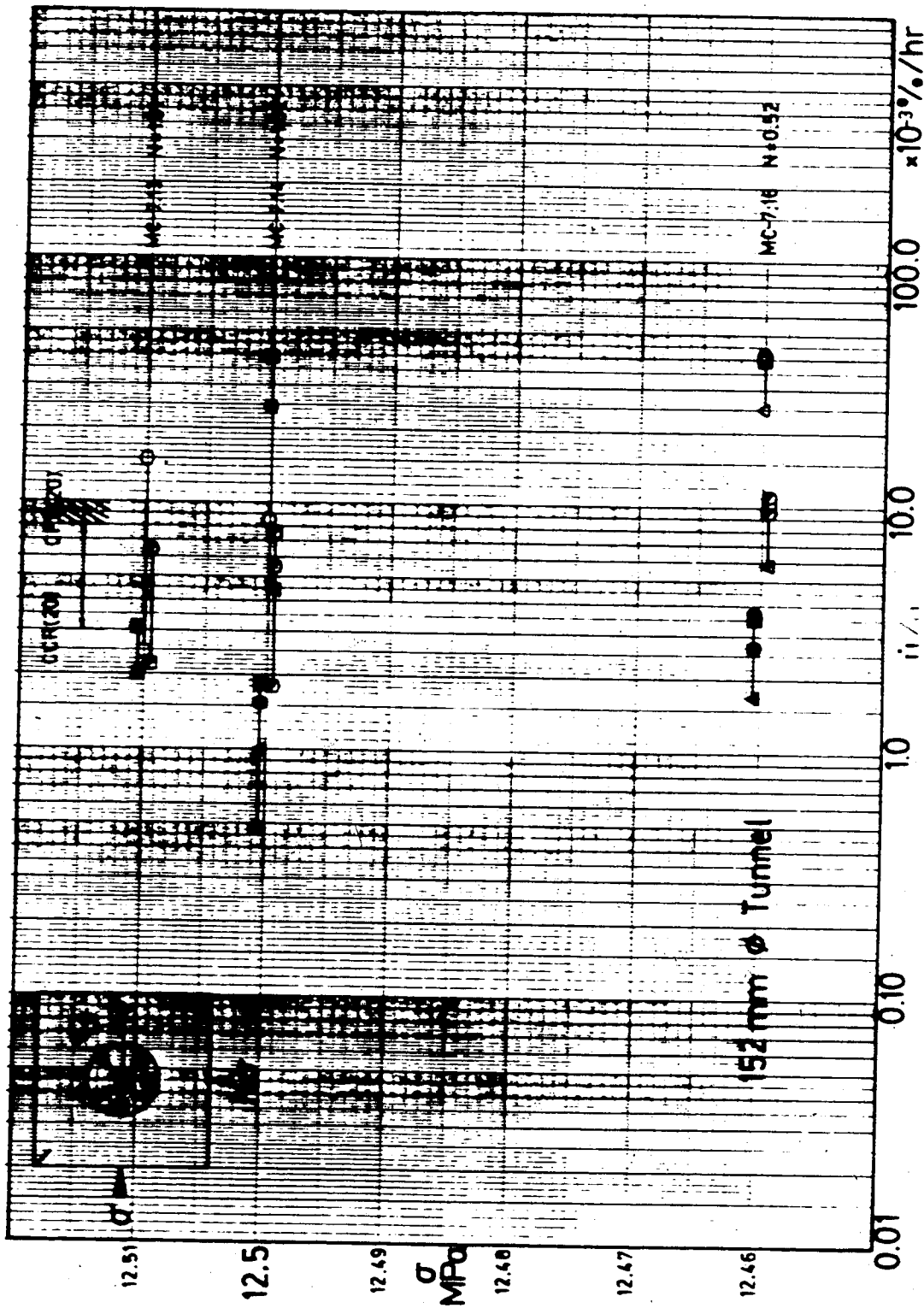


Figure 9.19 Closure Rates: MC-7.13, 7.14 and 7.16

10. APPENDIX C - TUNNEL CLOSURE AND RADIAL CREEP STRAIN
INCREMENT PATTERNS OBSERVED DURING TESTING OF THE THREE
SAMPLES

The time-dependent tunnel closure (across 4 diameters) and radial strain observed during a single creep stage (extensional strains and outward movement of the tunnel wall shown negative) are presented in Figures 10.1 to 10.6 for Sample MC-5, Figures 10.7 to 10.22 for Sample MC-6 and Figures 10.23 to 10.39 for Sample MC-7. The contours of radial strain were generated by a computer program that neglects the tunnel boundary and hence, do not accurately reflect strains near the tunnel wall. They do however adequately represent strain contours in the vicinity of the extensometers. Only those stages where significant creep strains were recorded are presented. These figures assist in the determination of zones of active overstraining and possible overstressing.

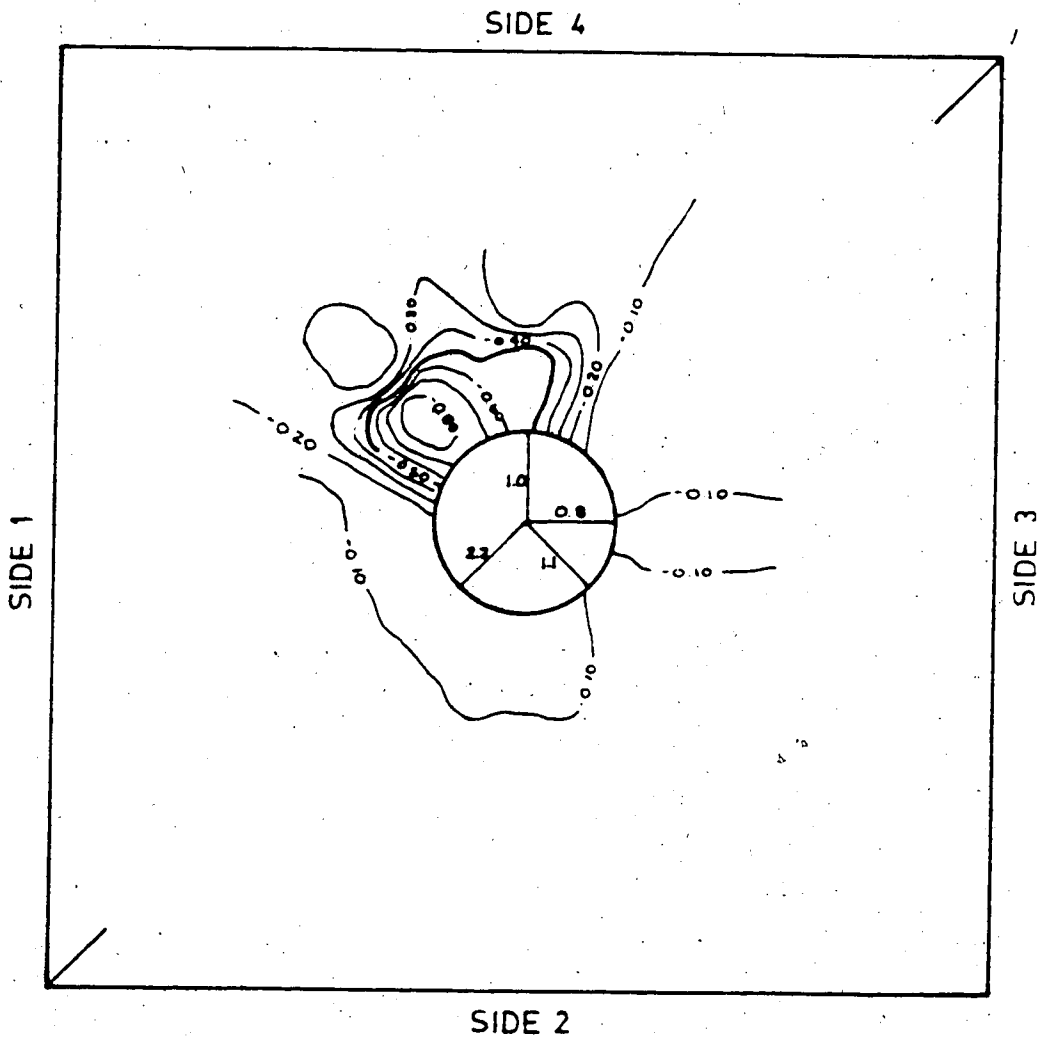


Figure 10.1 Creep Closure and Contours of Creep Strain - MC-5.05 at 12.8 MPa

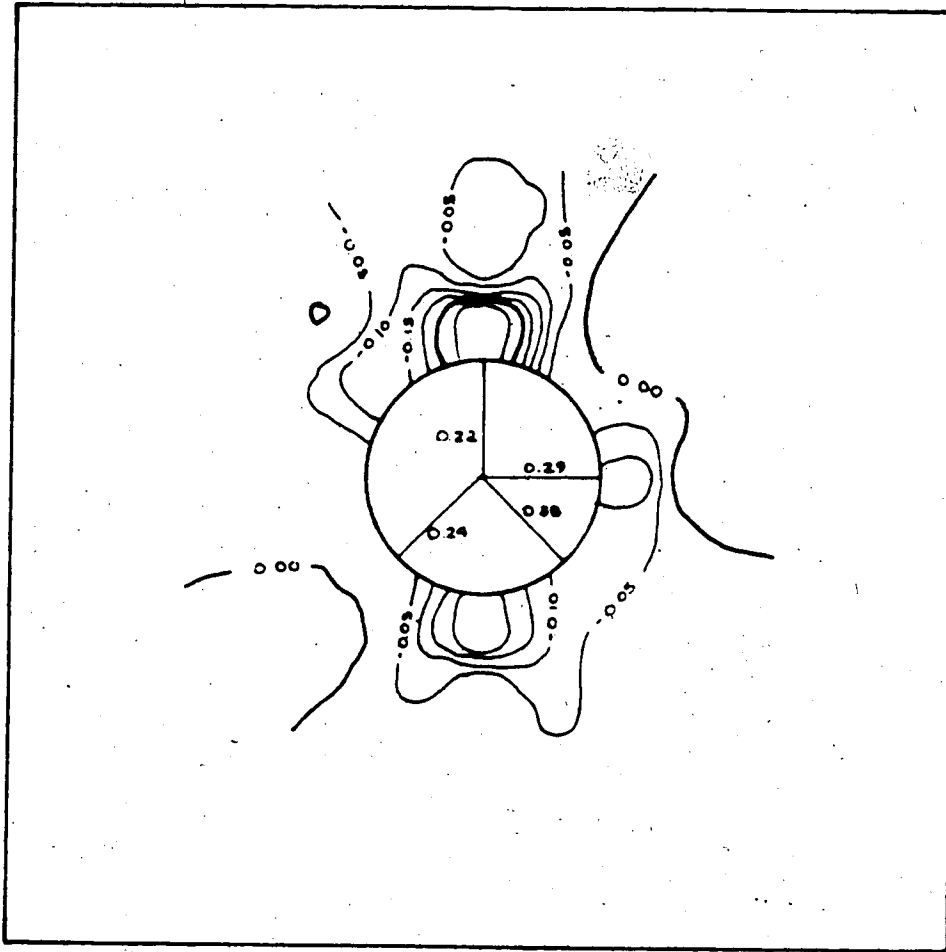


Figure 10.2 Creep Closure and Contours of Creep Strain -
MC-5.07 at 12.9 MPa

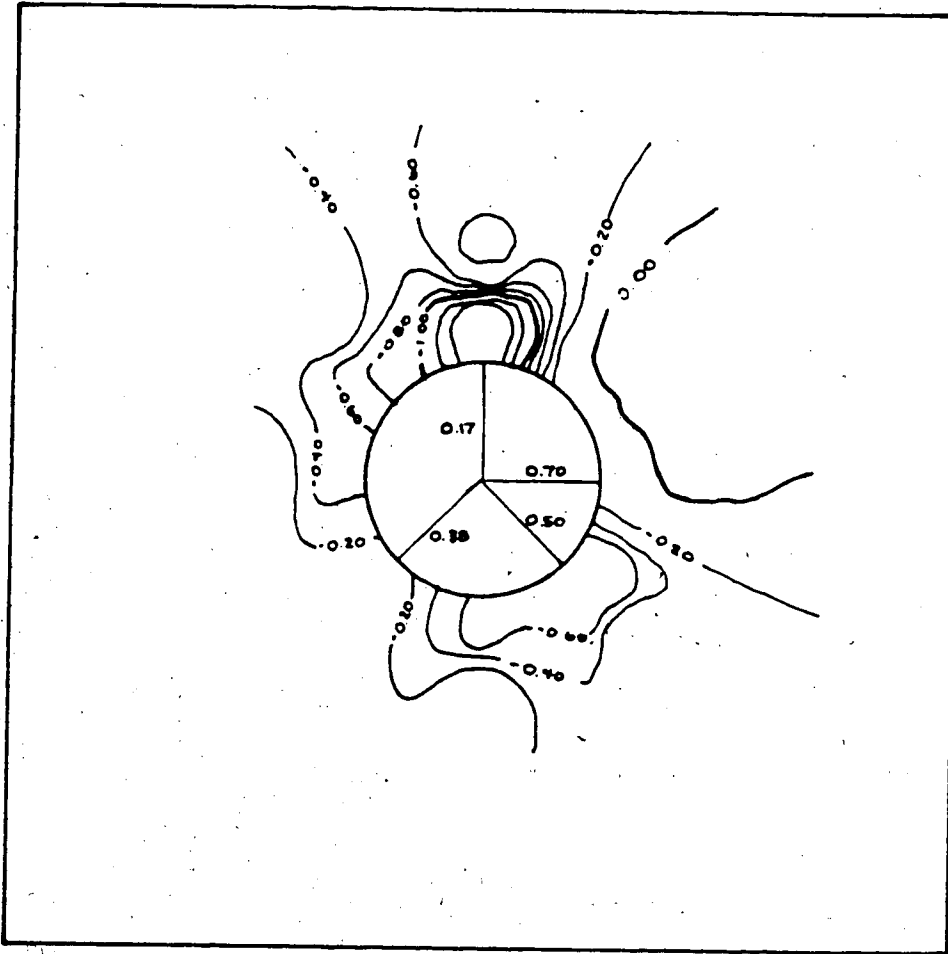


Figure 10.3 Creep Closure and Contours of Creep Strain -
MC-5.09 at 13.4 MPa

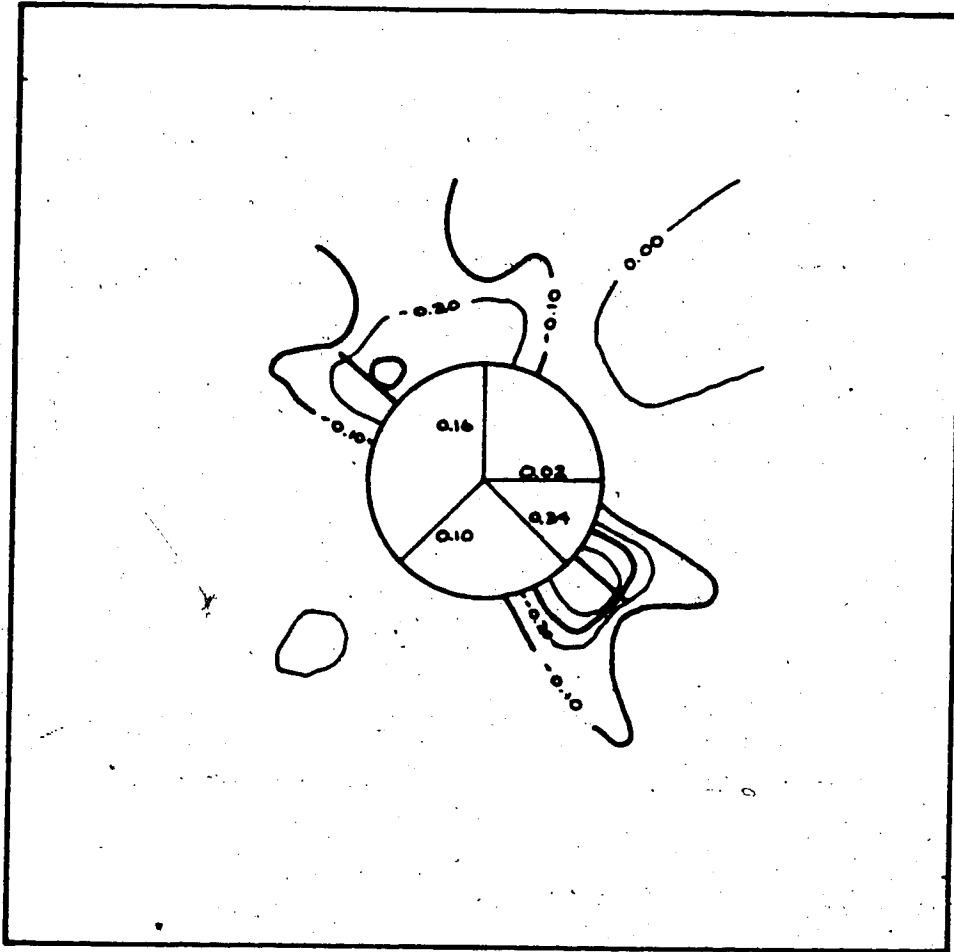


Figure 10.4 Creep Closure and Contours of Creep Strain - MC-5.11 at 11.1 MPa

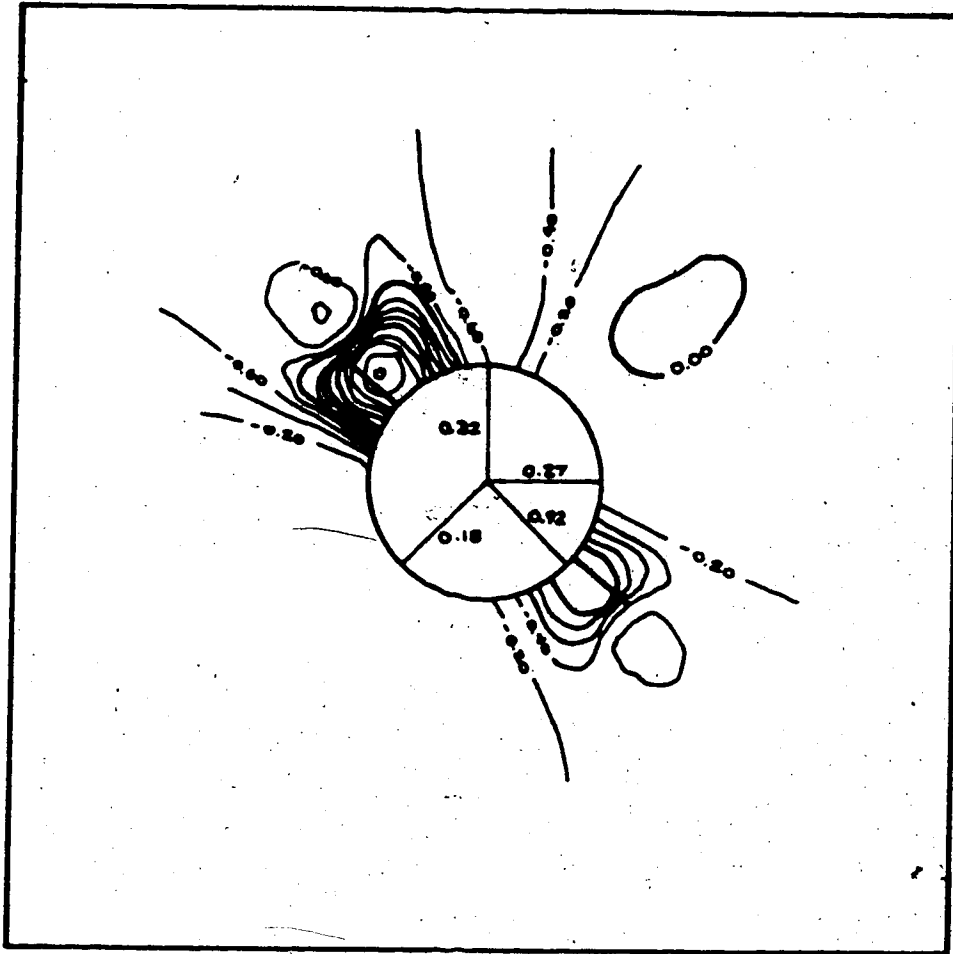


Figure 10.5 Creep Closure and Contours of Creep Strain -
MC-5.11 at 13.8 MPa

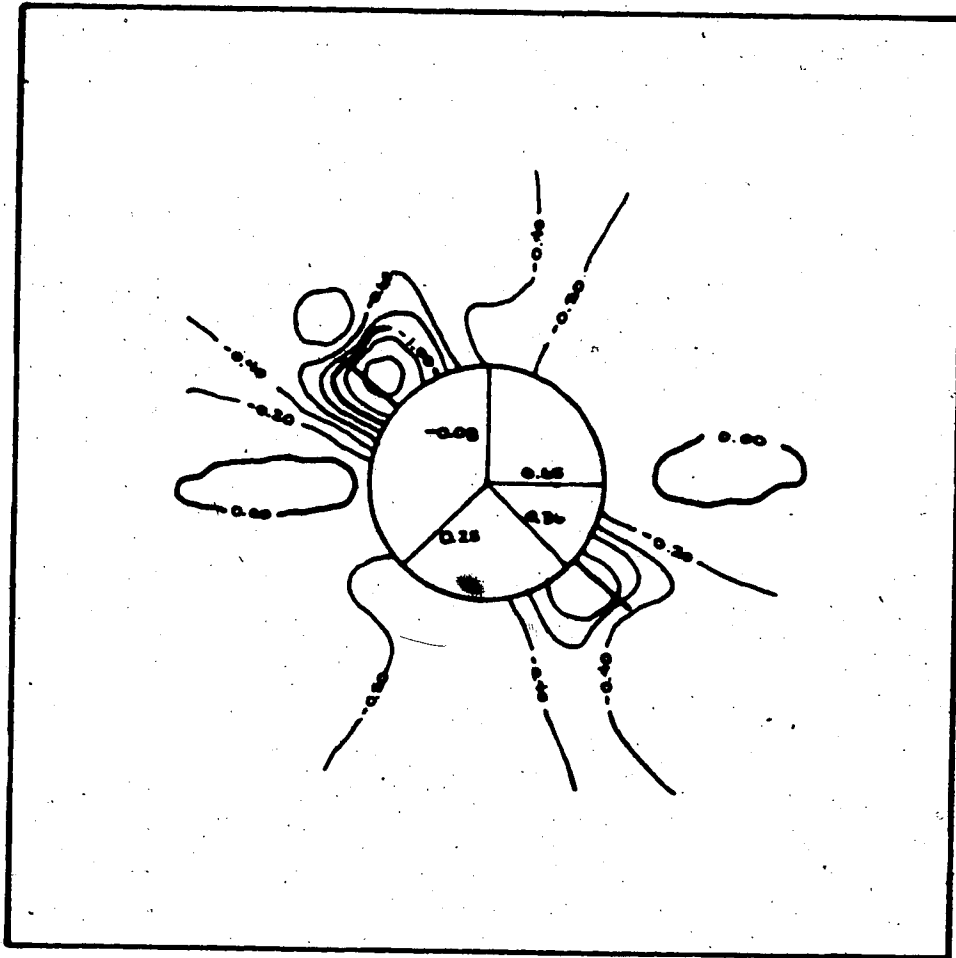


Figure 10.6 Creep Closure and Contours of Creep Strain -
MC-5.13 at 11.0 MPa

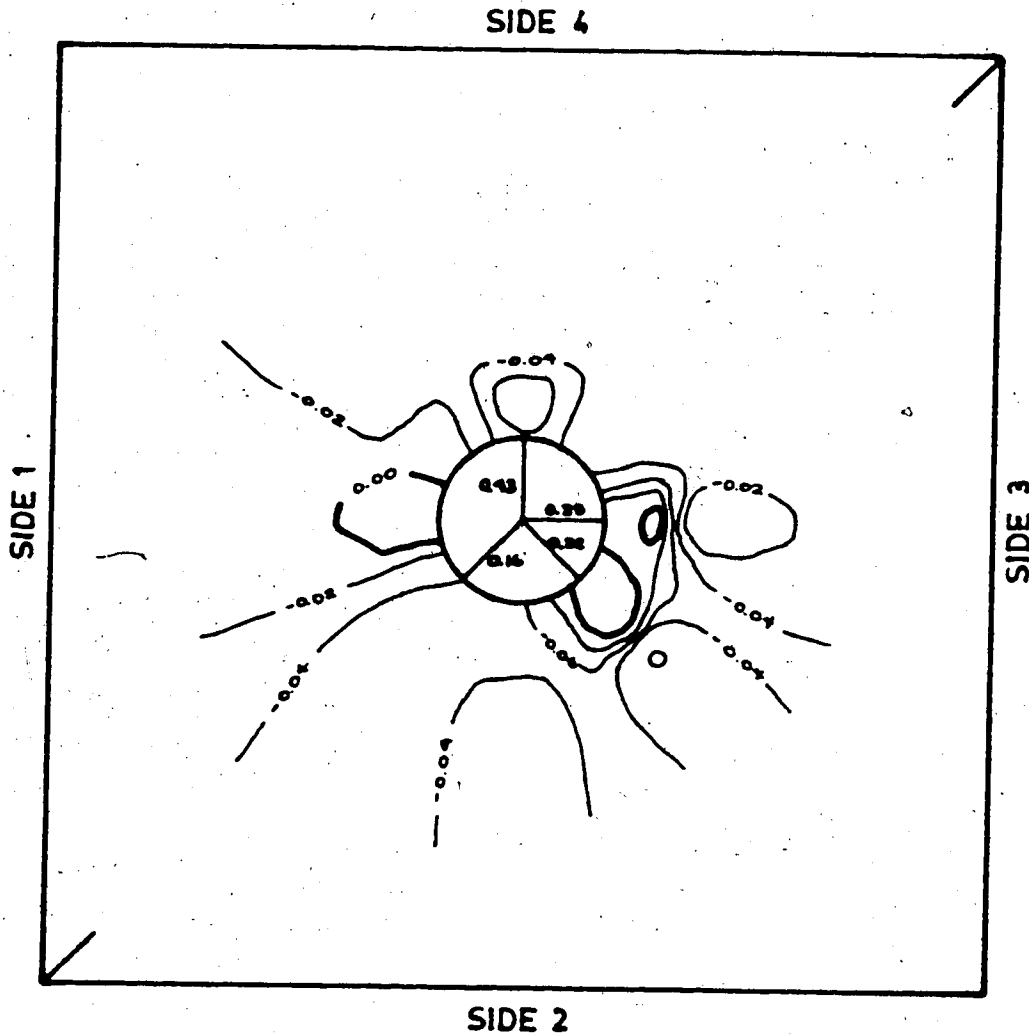


Figure 10.7 Creep Closure and Contours of Creep Strain -
MC-6.02 at 12.6 MPa (t=28.8)

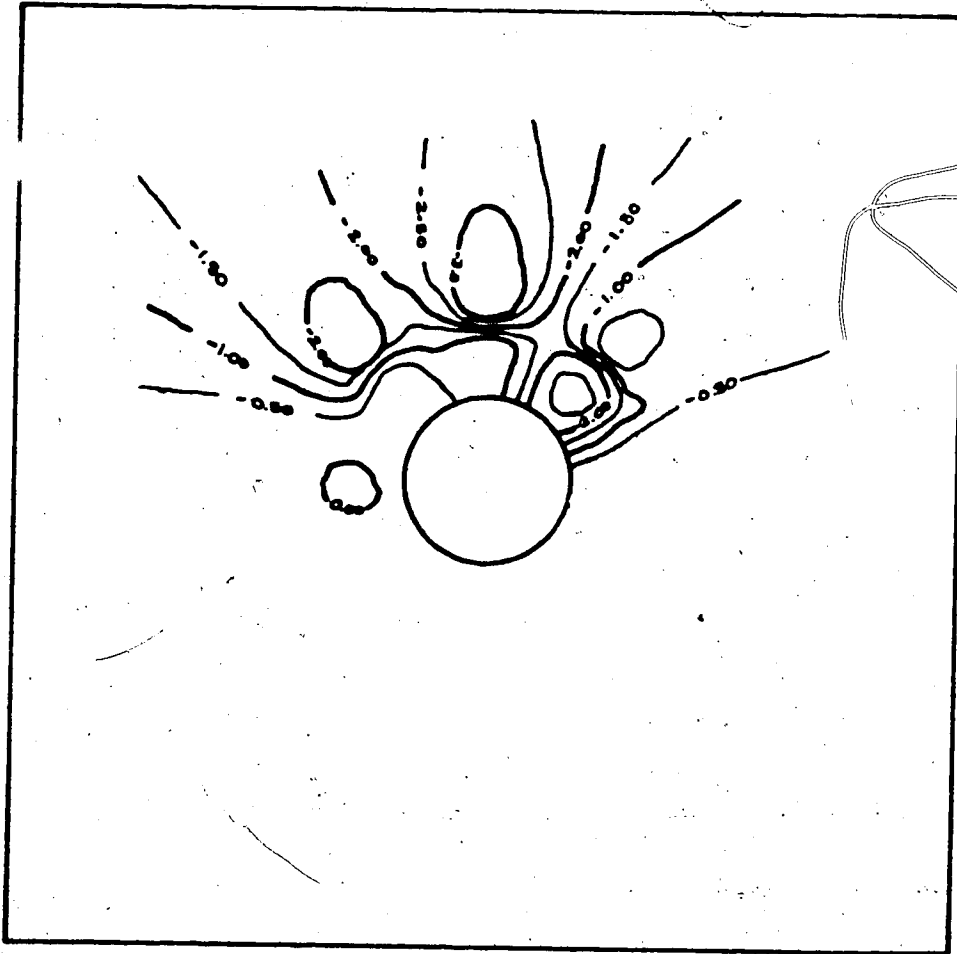


Figure 10.8 Creep Closure and Contours of Creep Strain -
MC-6.02 at 12.6 MPa ($t=29.9$)

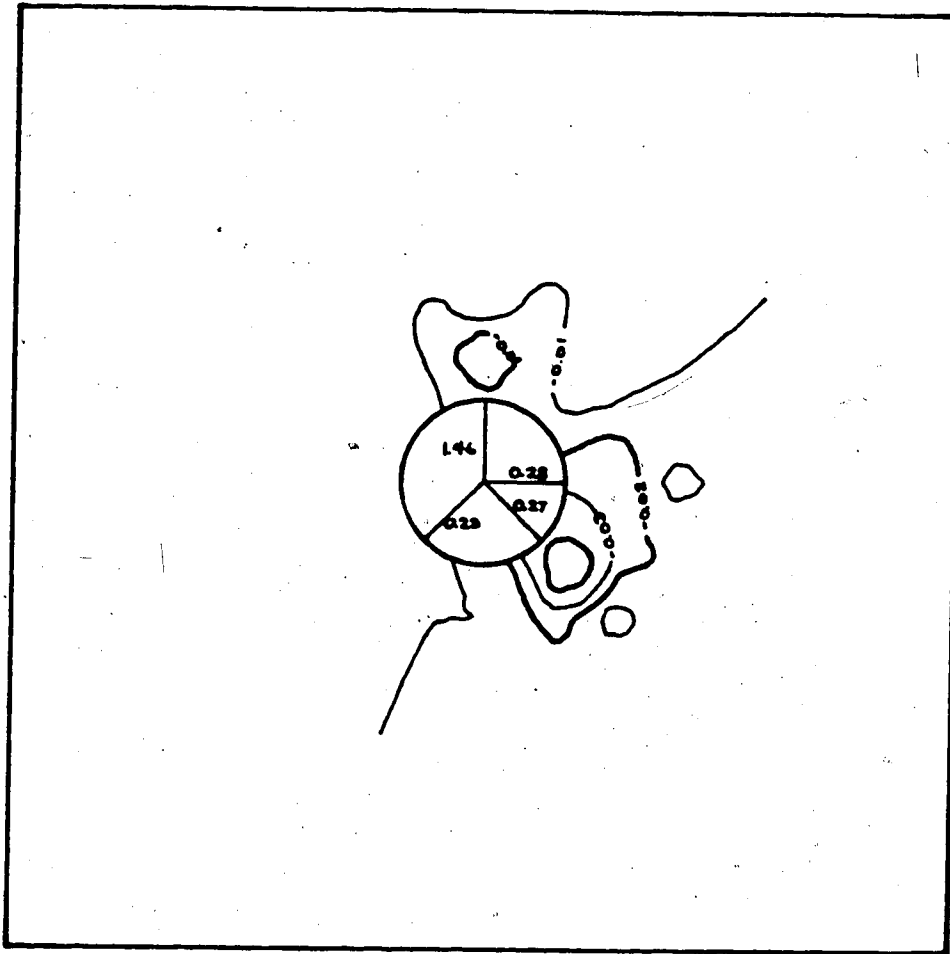


Figure 10.9 Creep Closure and Contours of Creep Strain -
MC-6.03 at 12.4 MPa

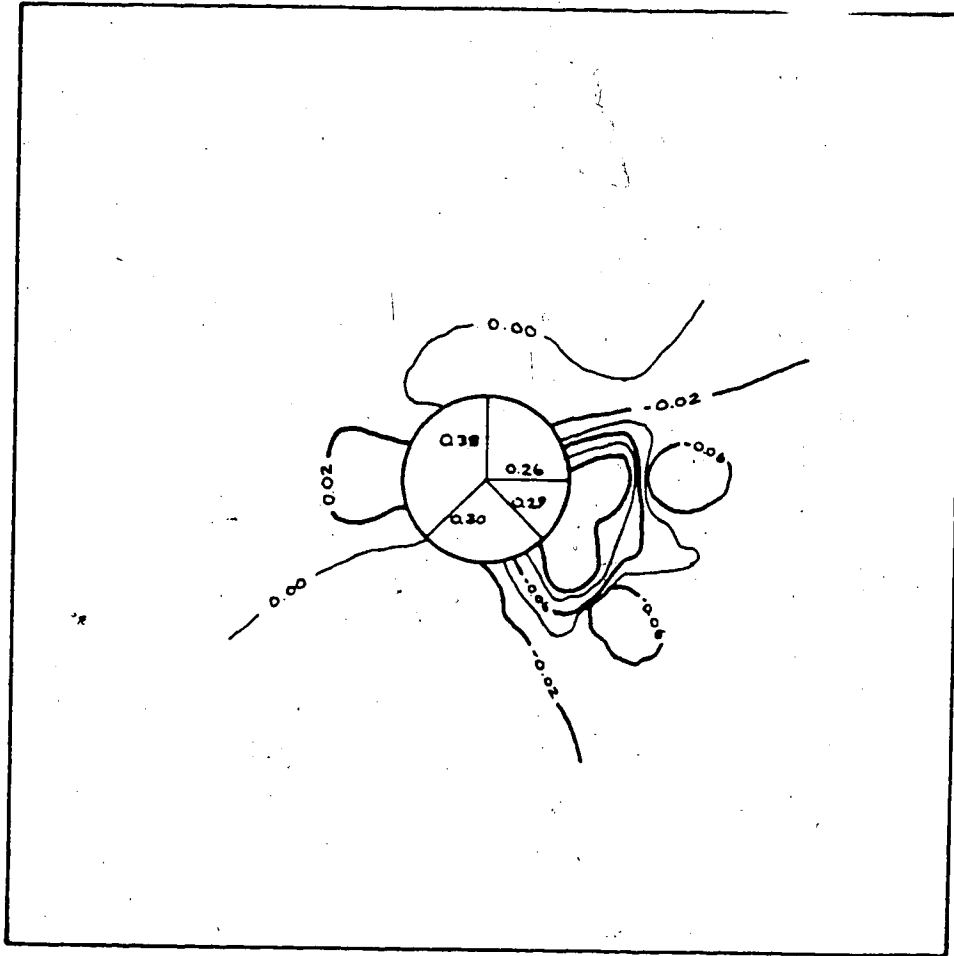


Figure 10.10 Creep Closure and Contours of Creep Strain -
MC-6.04 at 14.9 MPa

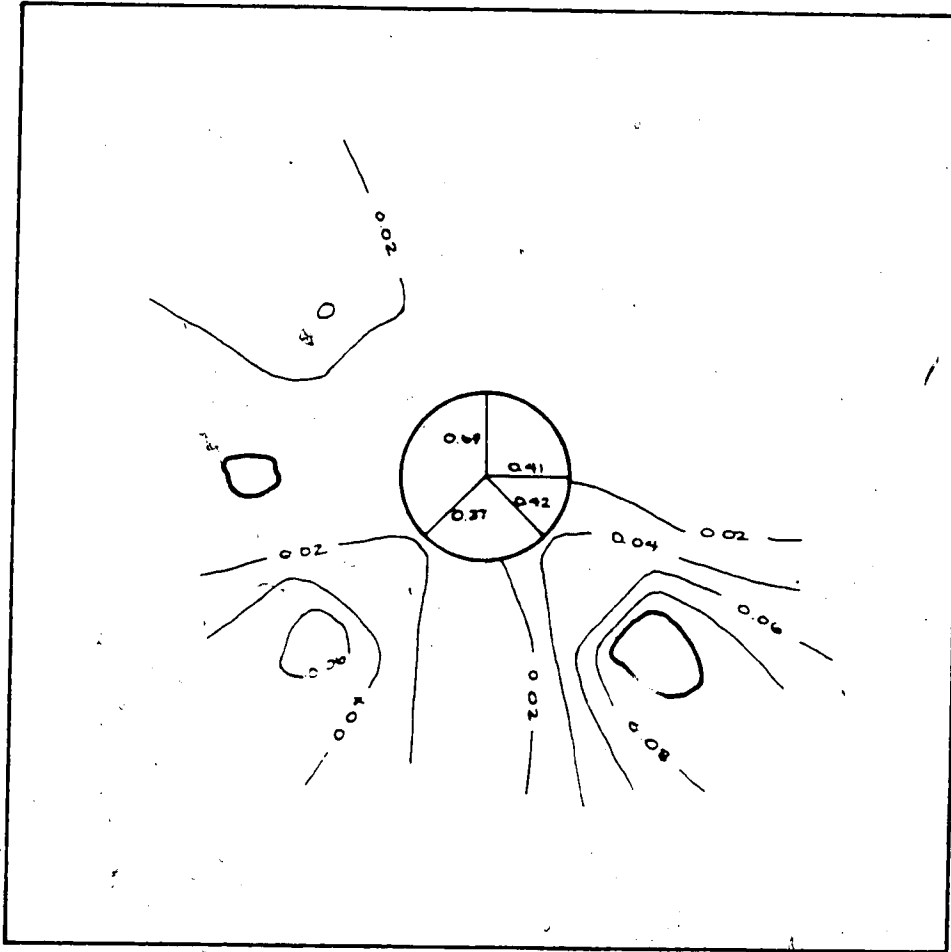


Figure 10.11 Creep Closure and Contours of Creep Strain -
MC-6.05 (108mm) at 12.4 MPa

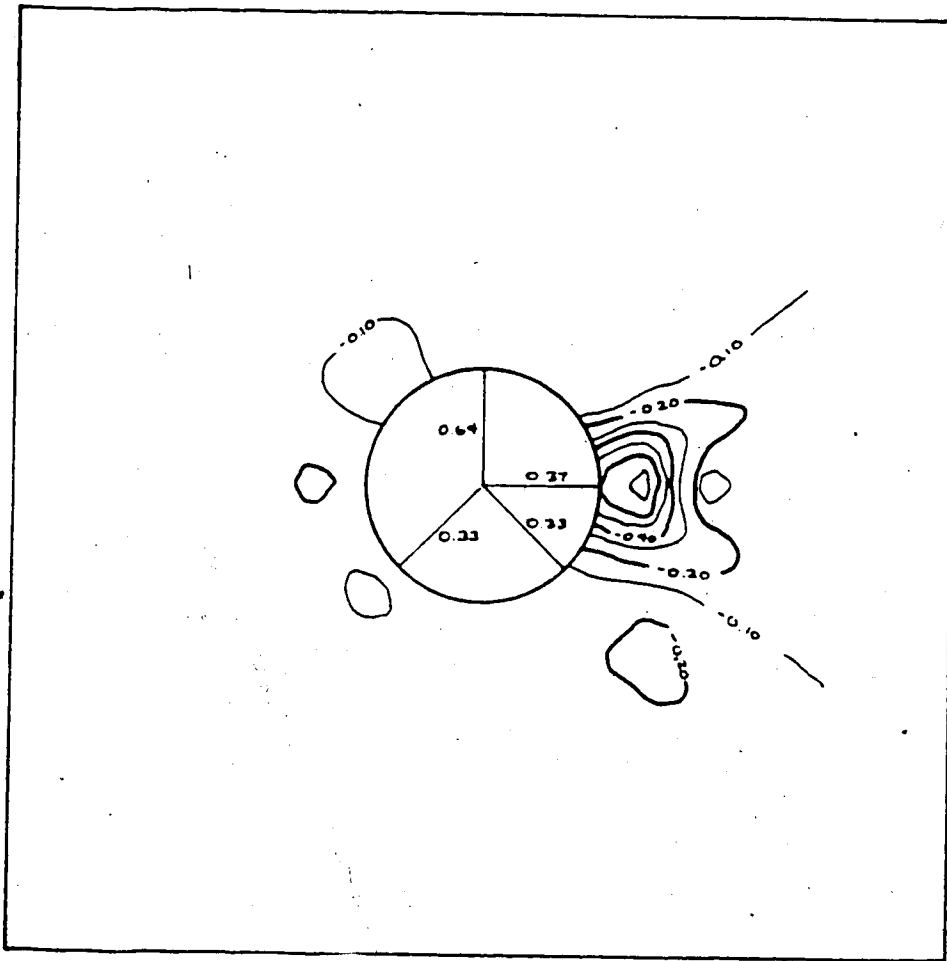


Figure 10.12 Creep Closure and Contours of Creep Strain -
MC-6.05 (152mm) at 12.4 MPa

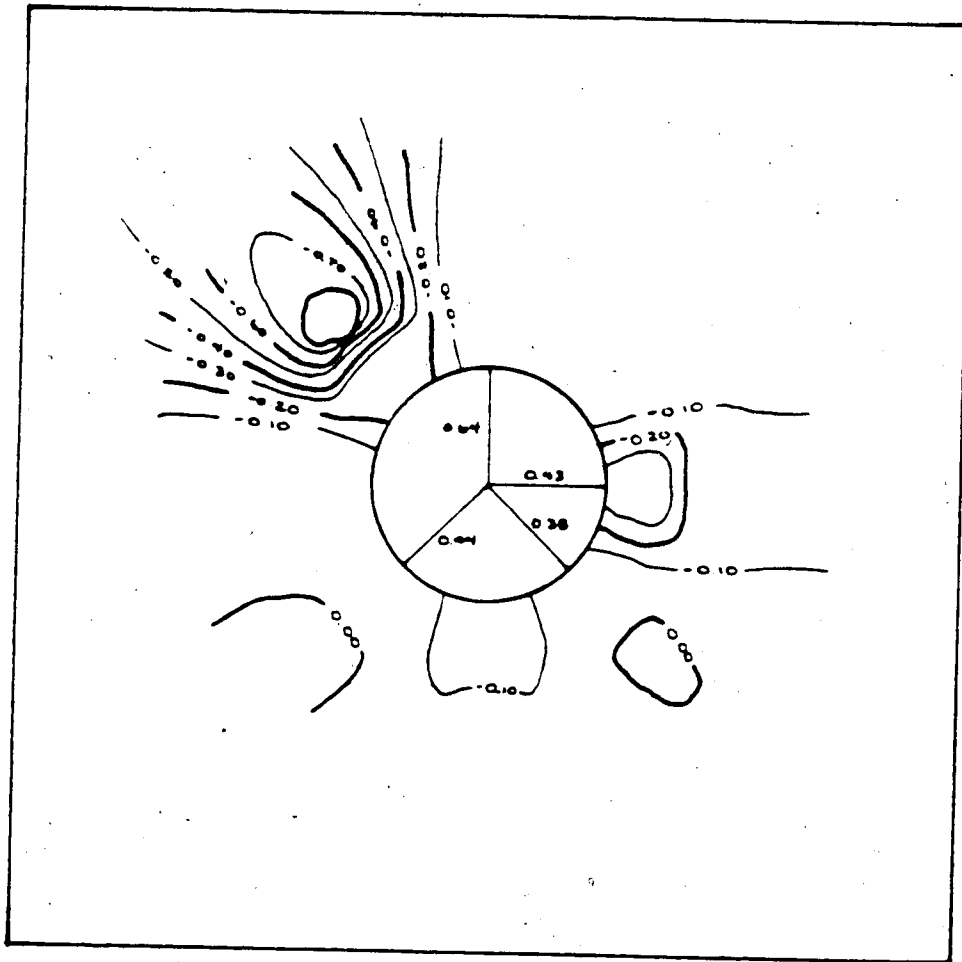


Figure 10.13 Creep Closure and Contours of Creep Strain -
MC-6.06 at 12.4 MPa

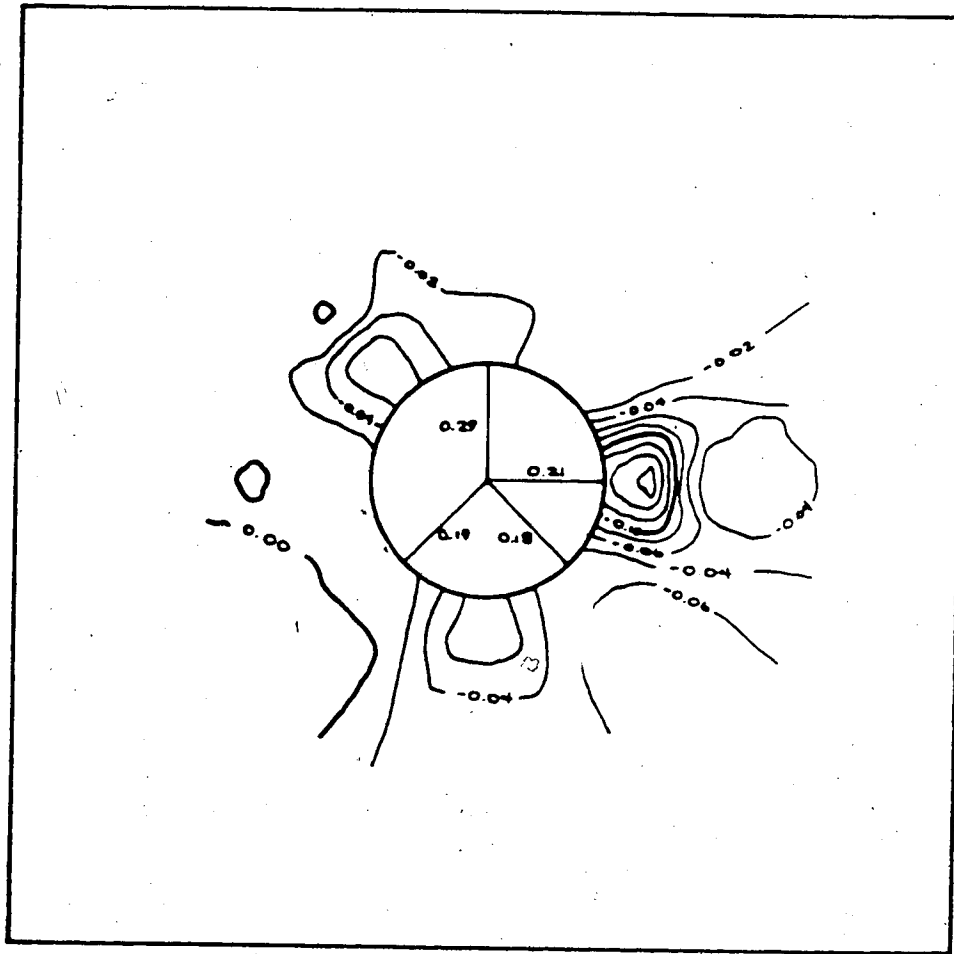


Figure 10.14 Creep Closure and Contours of Creep Strain -
MC-6.07 at 12.4 MPa

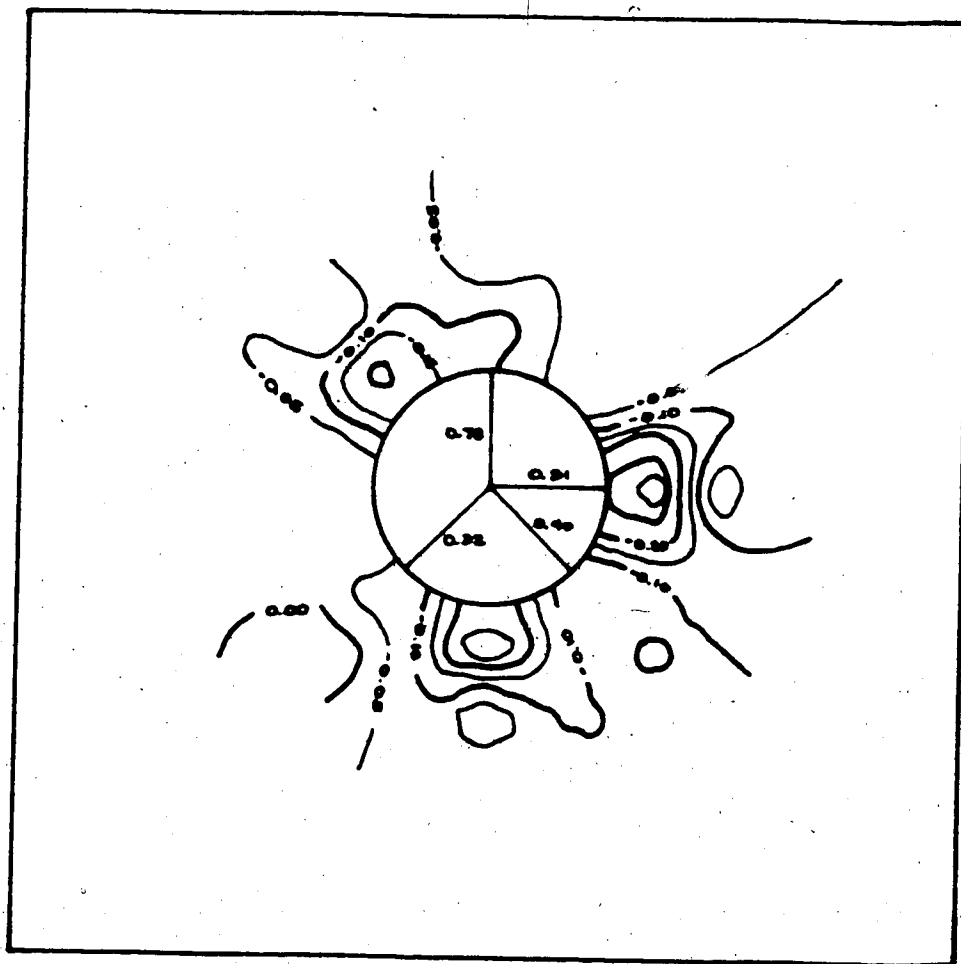


Figure 10.15 Creep Closure and Contours of Creep Strain -
MC-6.07 at 14.8 MPa

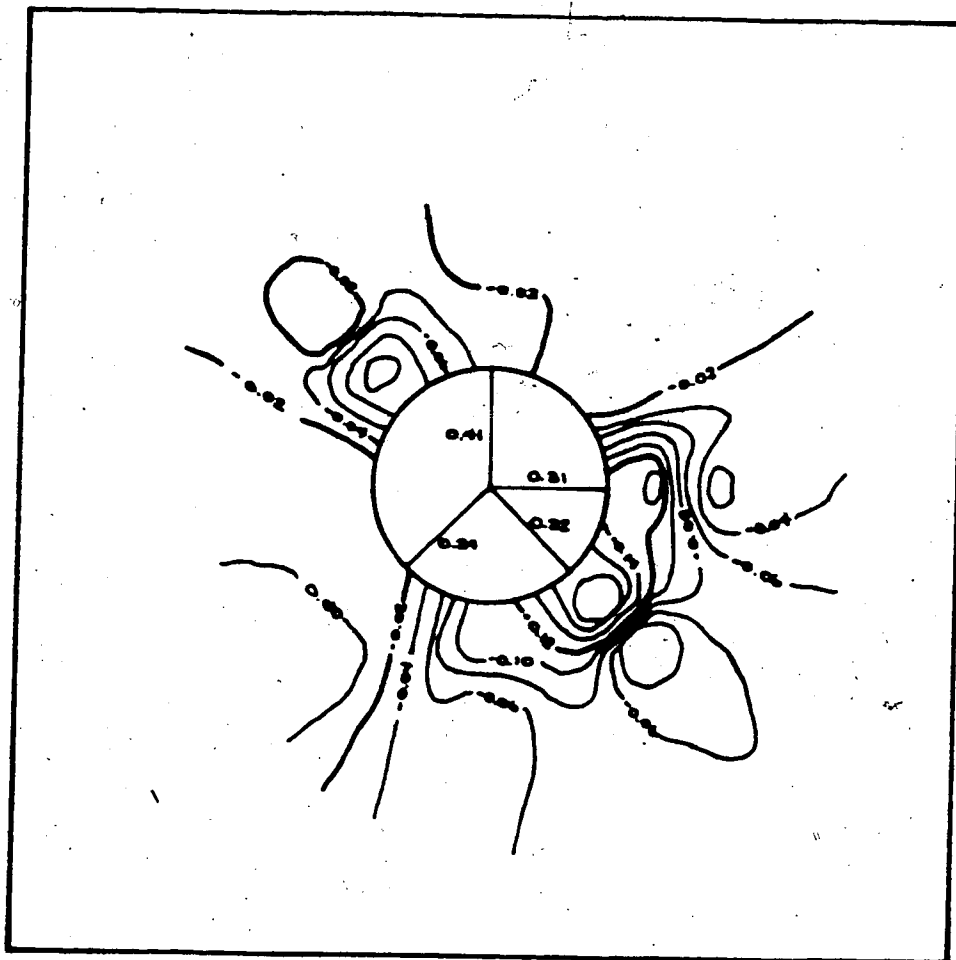


Figure 10.16 Creep Closure and Contours of Creep Strain -
MC-6.08 at 12.5 MPa

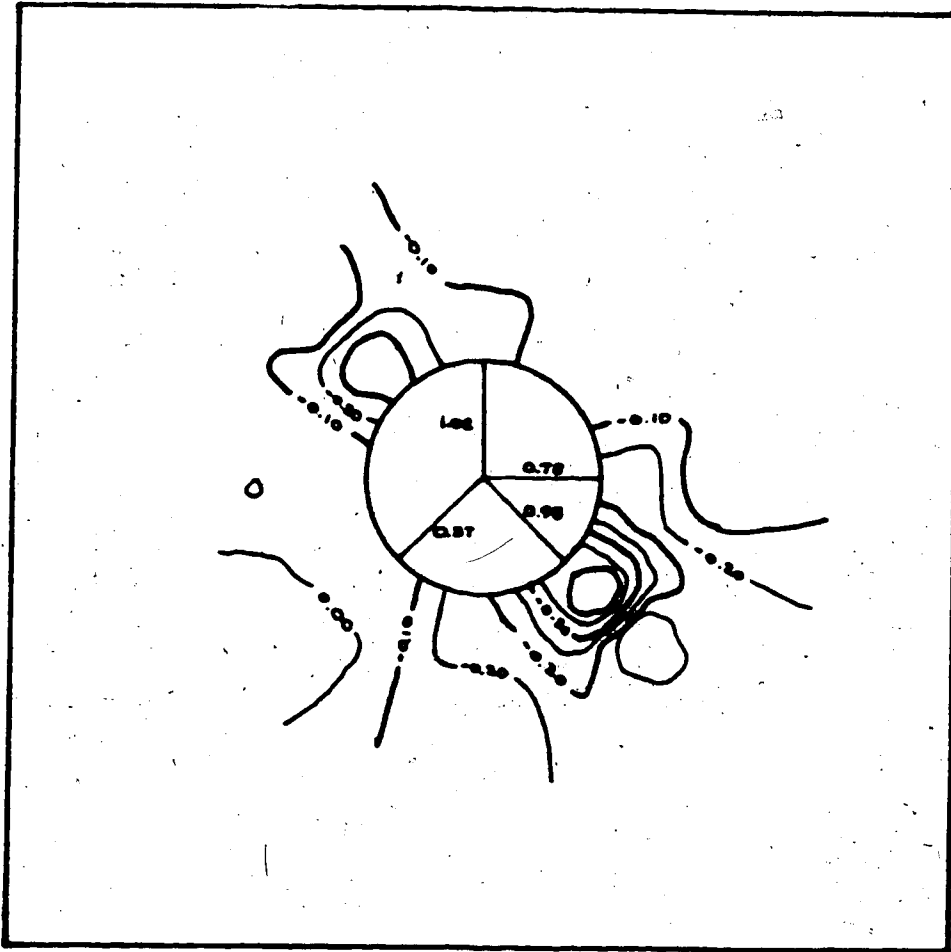


Figure 10.17 Creep Closure and Contours of Creep Strain -
MC-6.08 at 15.0 MPa

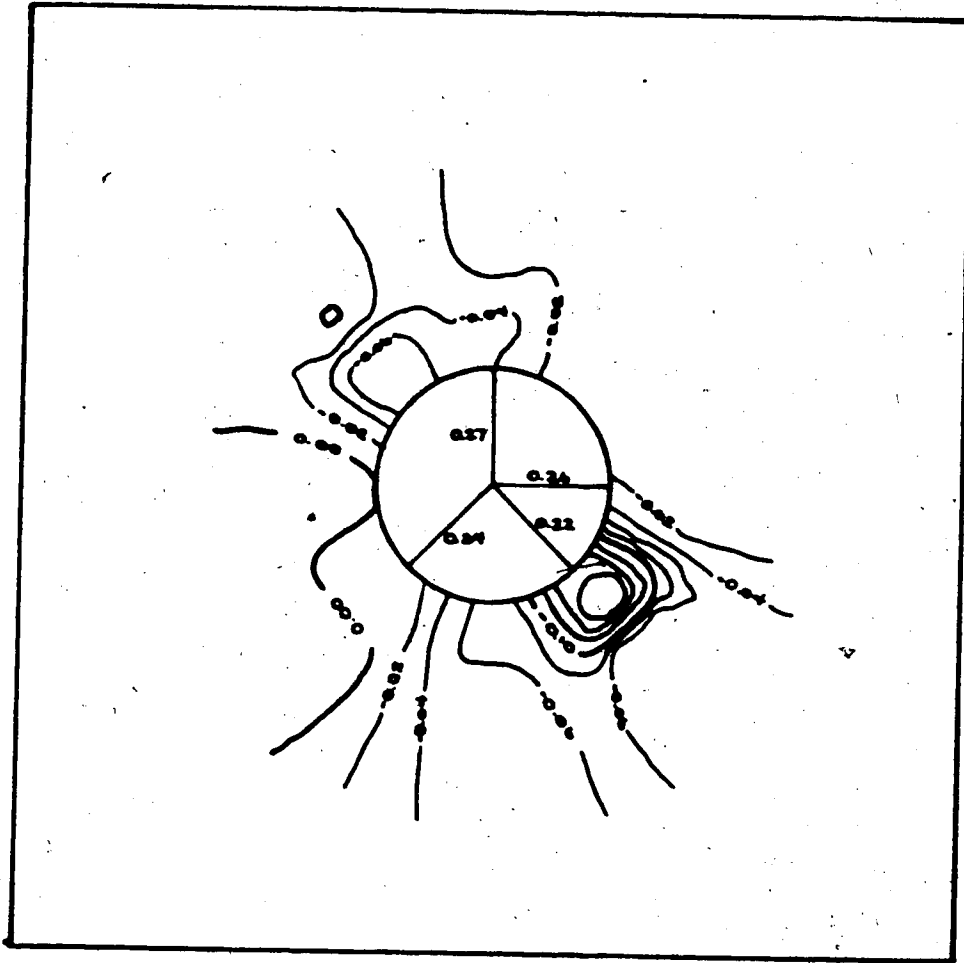


Figure 10.18 Creep Closure and Contours of Creep Strain -
MC-6.09 at 12.4 MPa

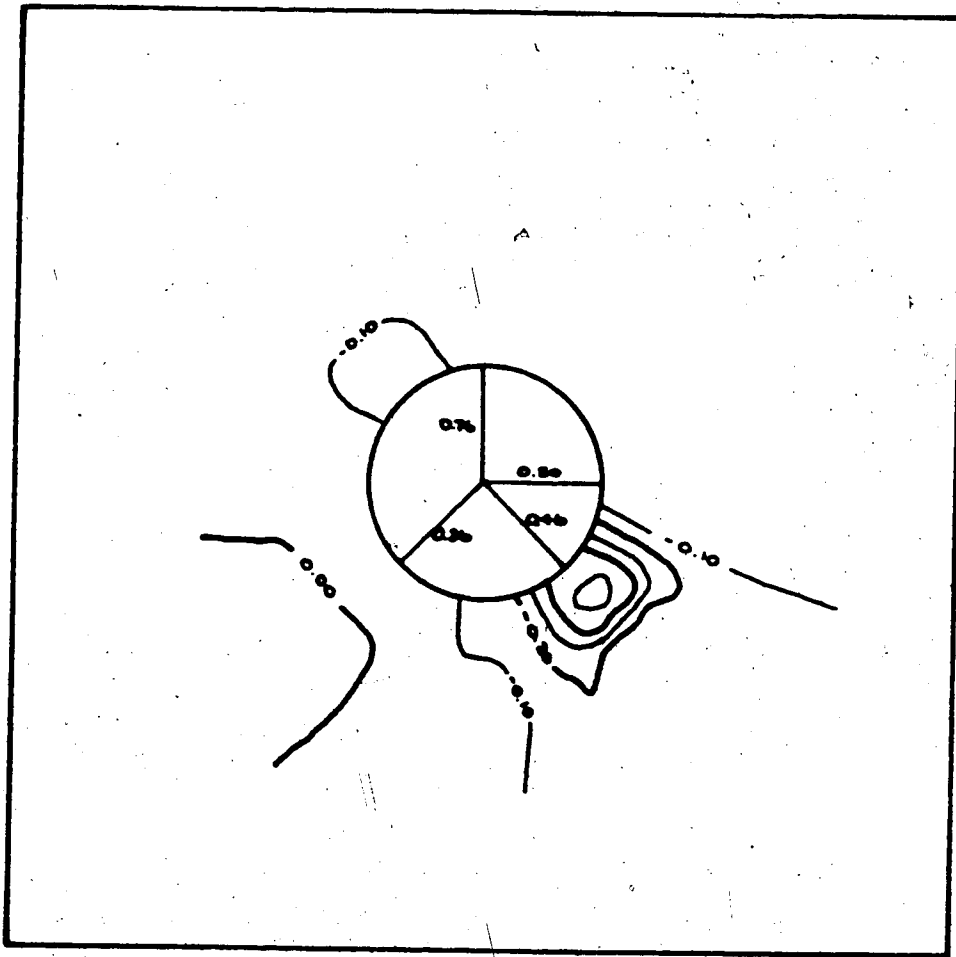


Figure 10.19 Creep Closure and Contours of Creep Strain -
MC-6.09 at 15.0 MPa

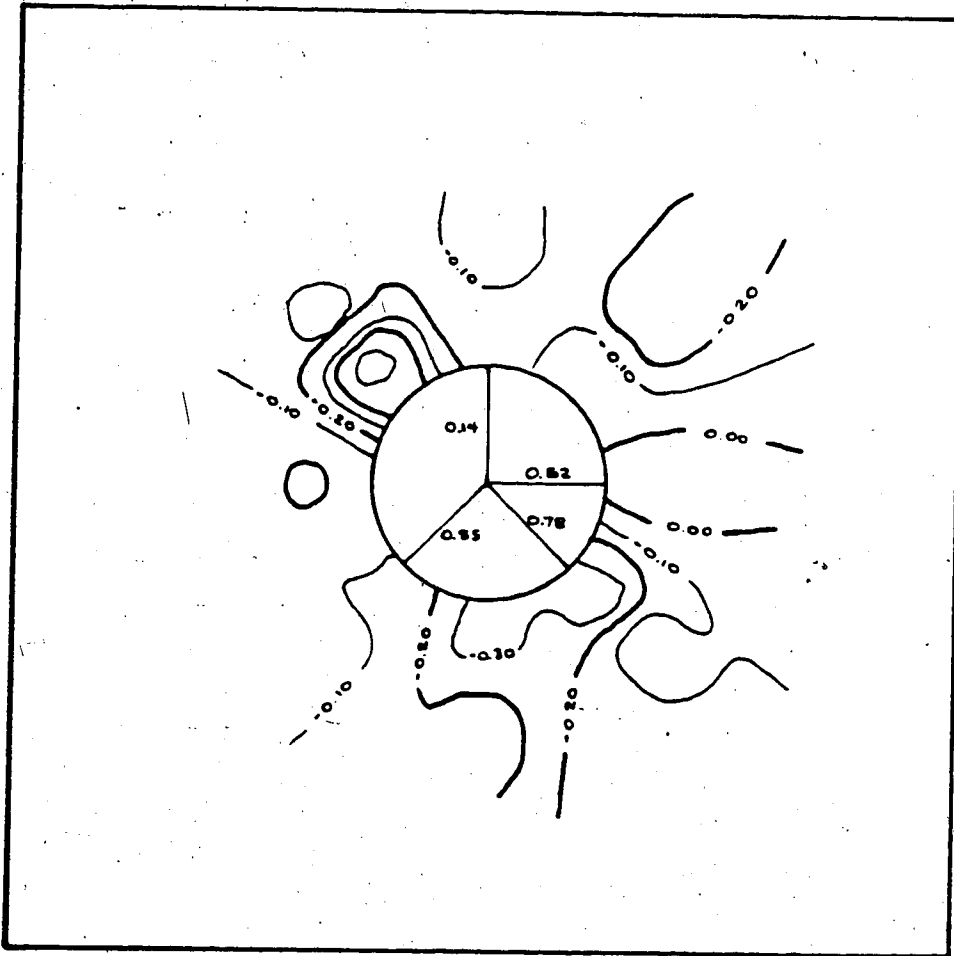


Figure 10.20 Creep Closure and Contours of Creep Strain -
MC-6.10 at 12.1 MPa

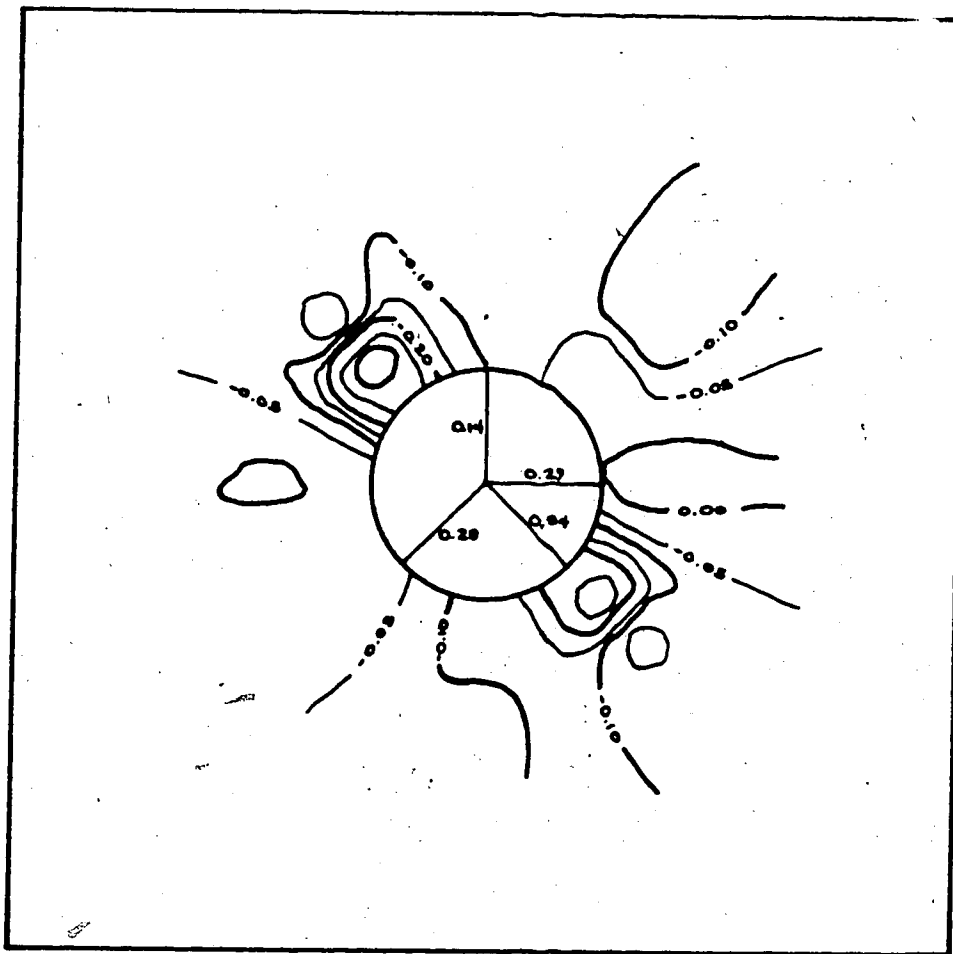


Figure 10.21 Creep Closure and Contours of Creep Strain -
MC-6.11 at 12.1 MPa

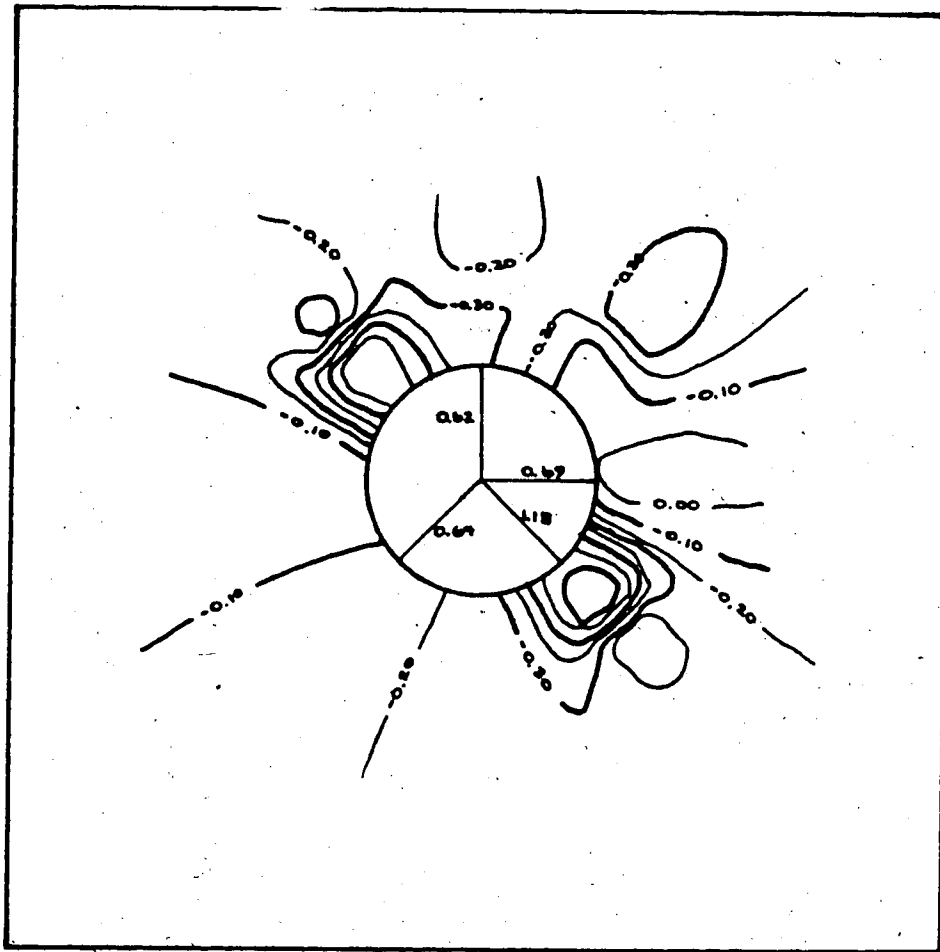


Figure 10.22 Creep Closure and Contours of Cr Strain -
MC-6.11 at 14.5 MPa

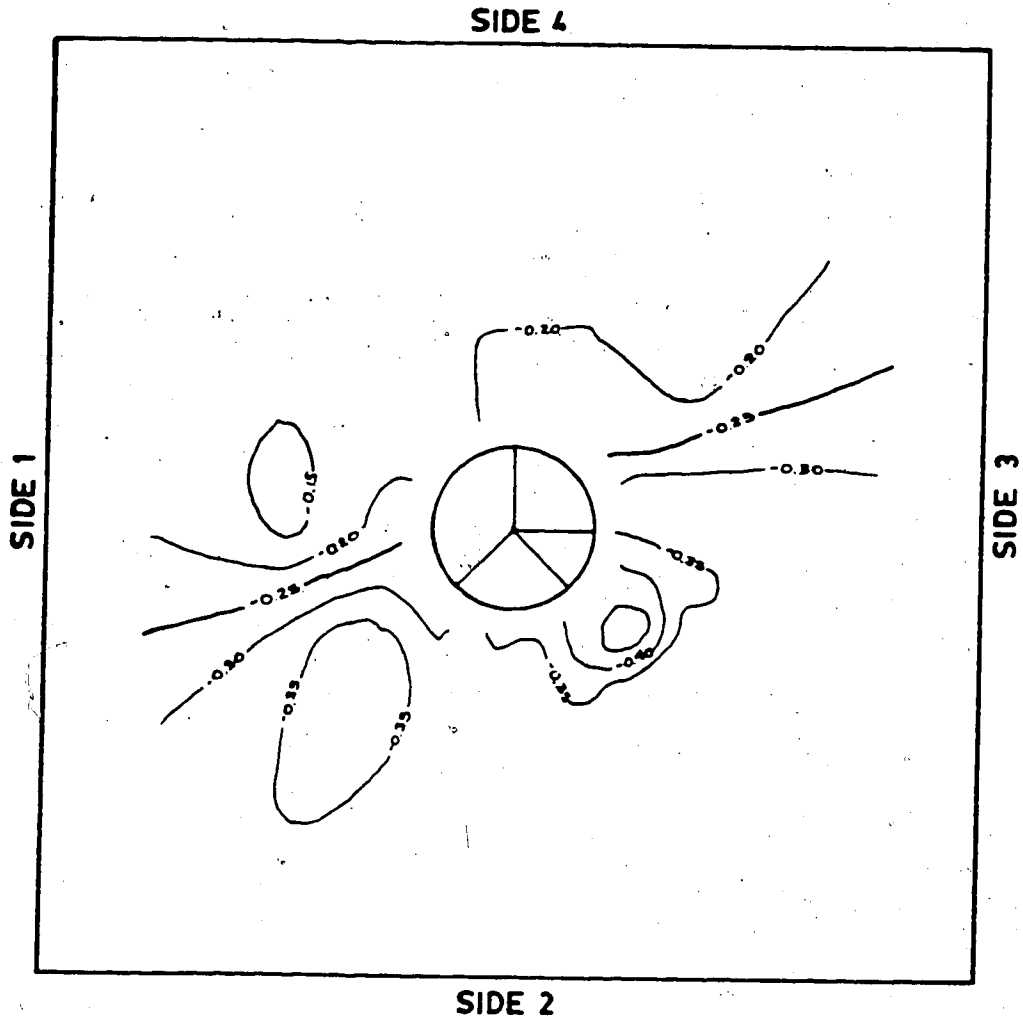


Figure 10.23 Creep Closure and Contours of Creep Strain -
MC-7.10 at 12.5 MPa ($t=31.5$)

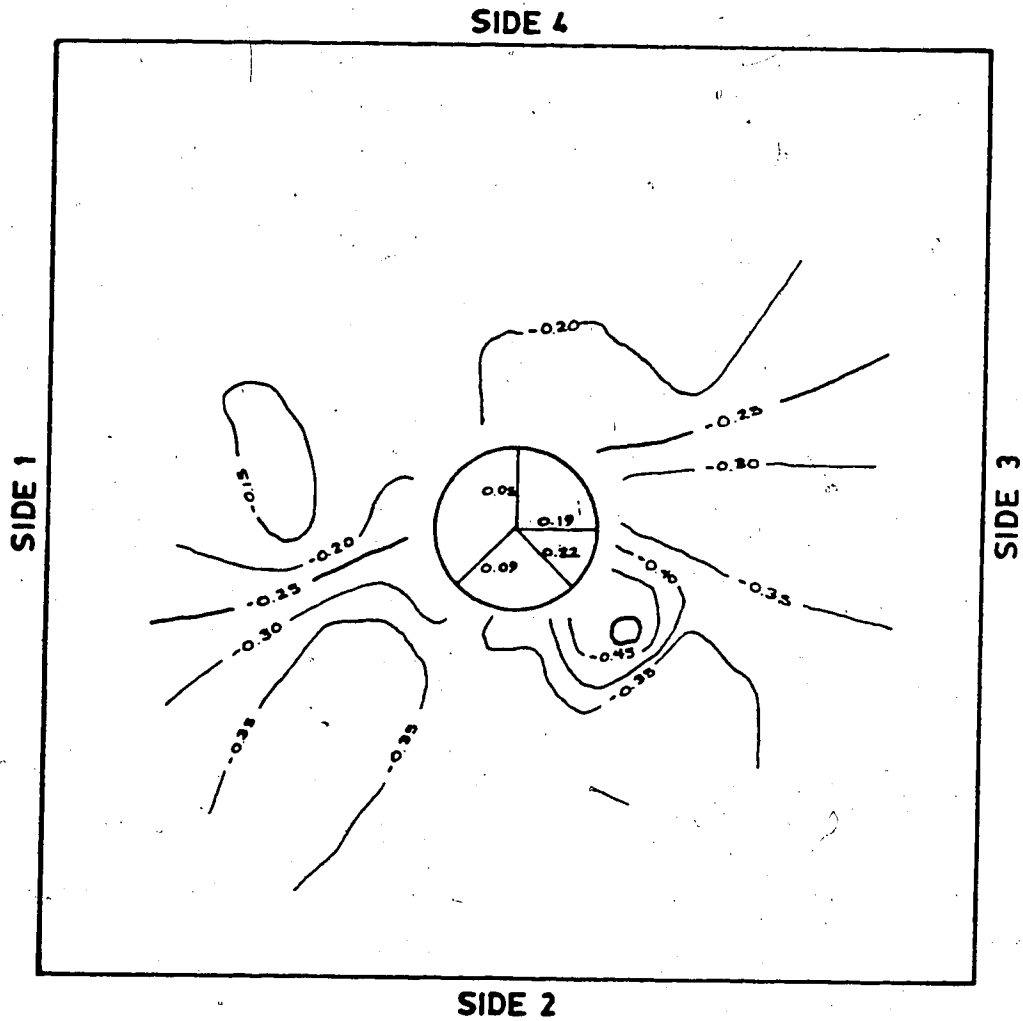


Figure 10.24 Creep Closure and Contours of Creep Strain -
MC-7.10 at 12.5 MPa (t=91.5)

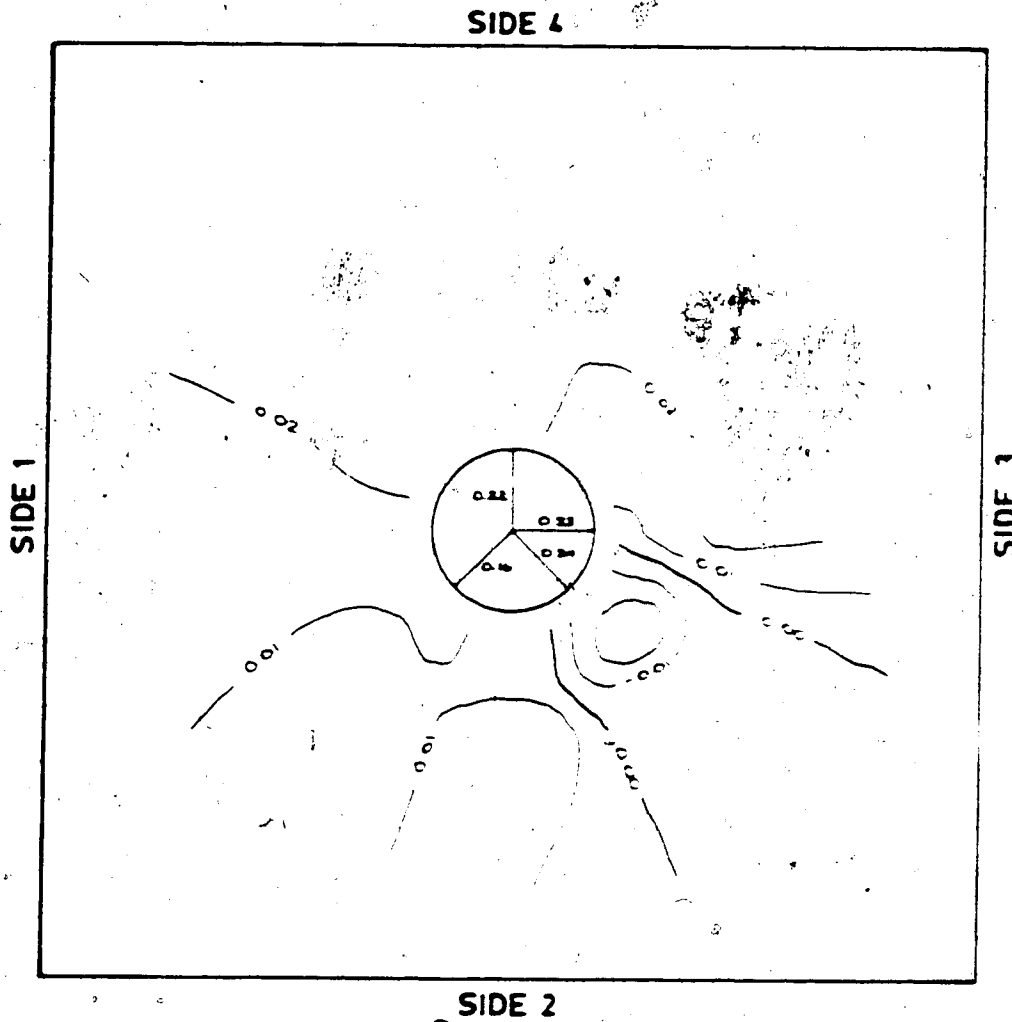


Figure 10.25 Creep Closure and Contours of Creep Strain - MC-7.11 at 12.5 MPa

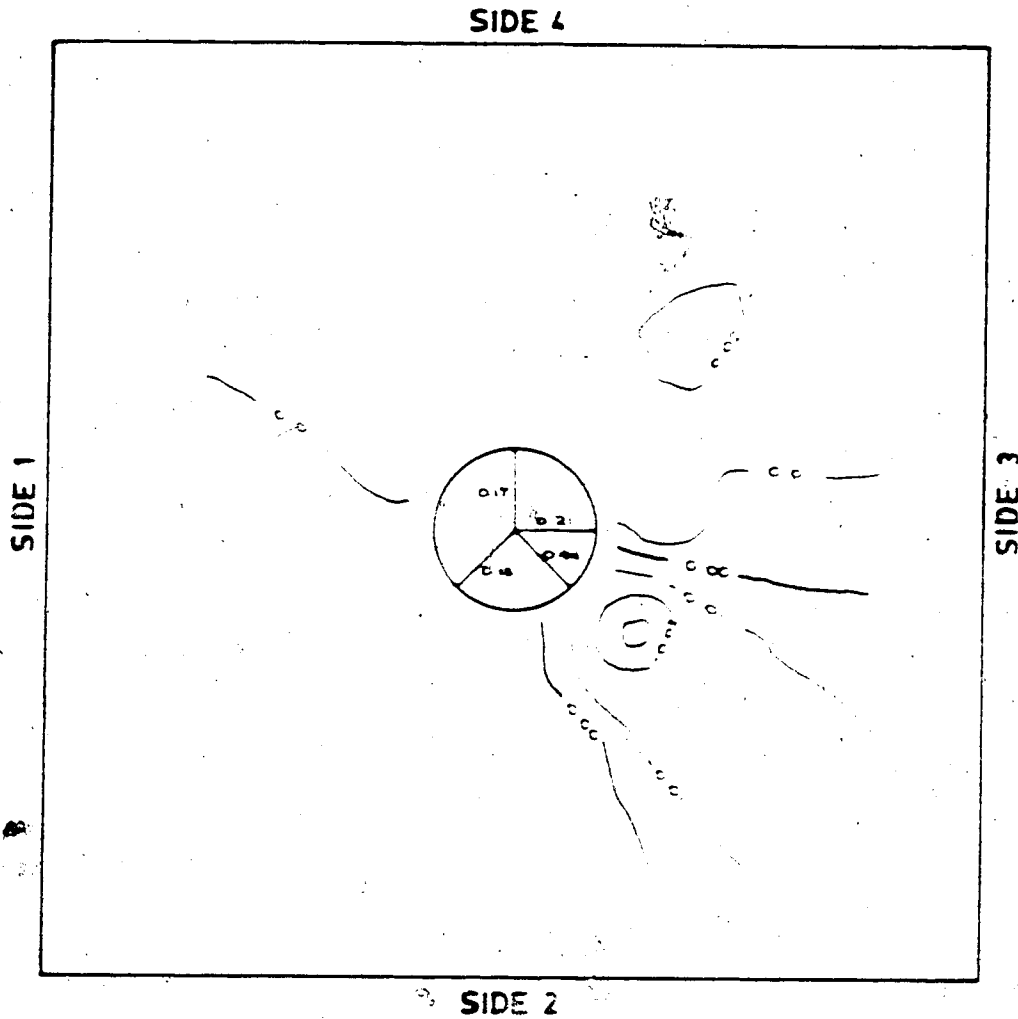


Figure 10.2 Creep Closure and Contours of Creep Strain
MC-7.12 at 12.5 MPa

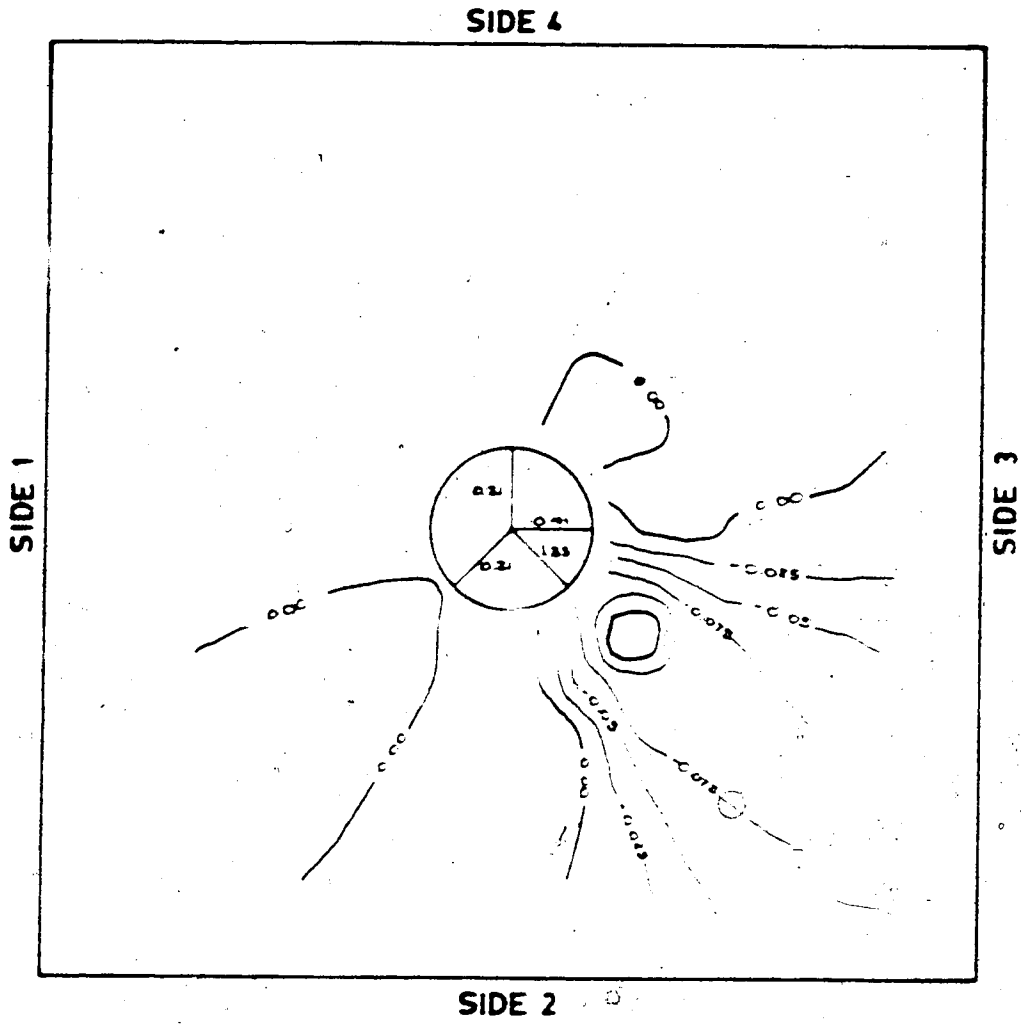


Figure 10.27 Creep Closure and Contours of Creep Strain - MC-7.12 at 14.3 MPa

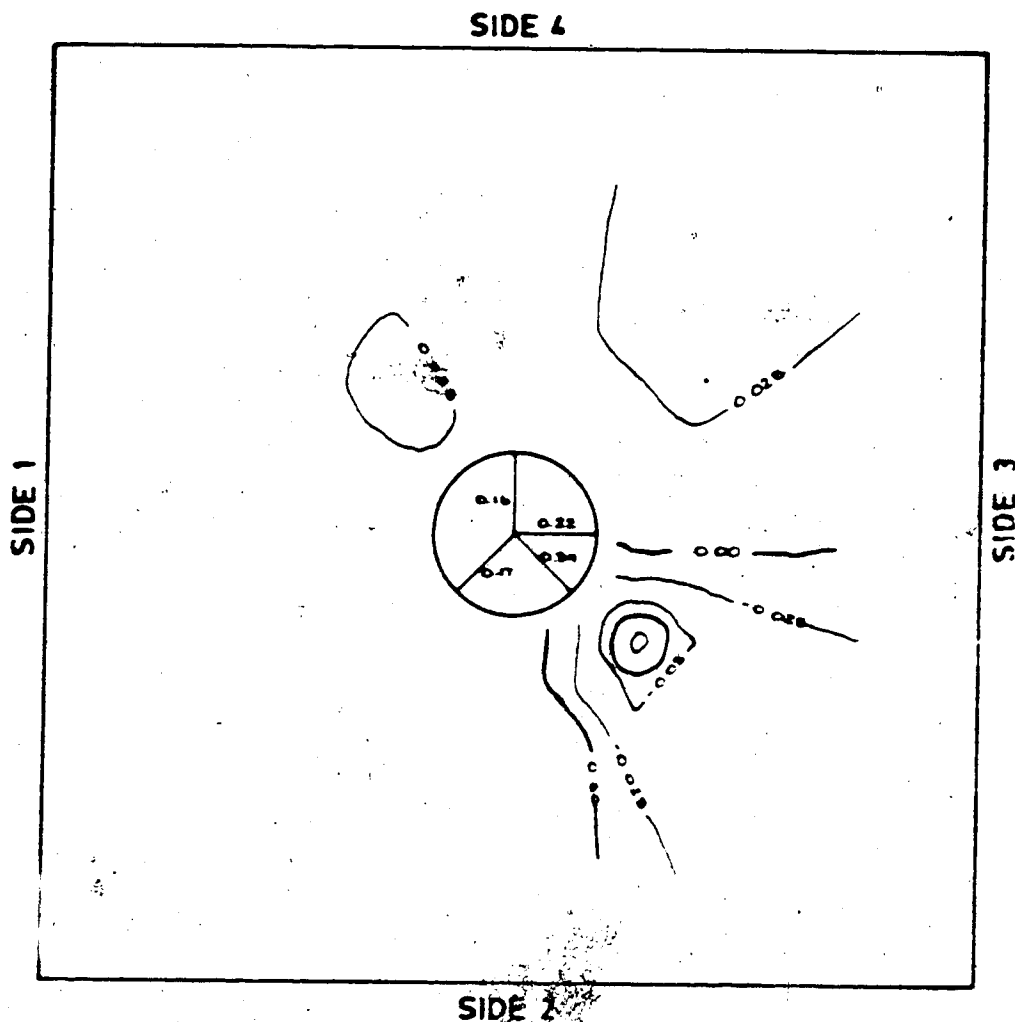


Figure 10.28 Creep Closure and Contours of Creep Strain - MC-7.13 at 12.5 MPa (t=20.0)

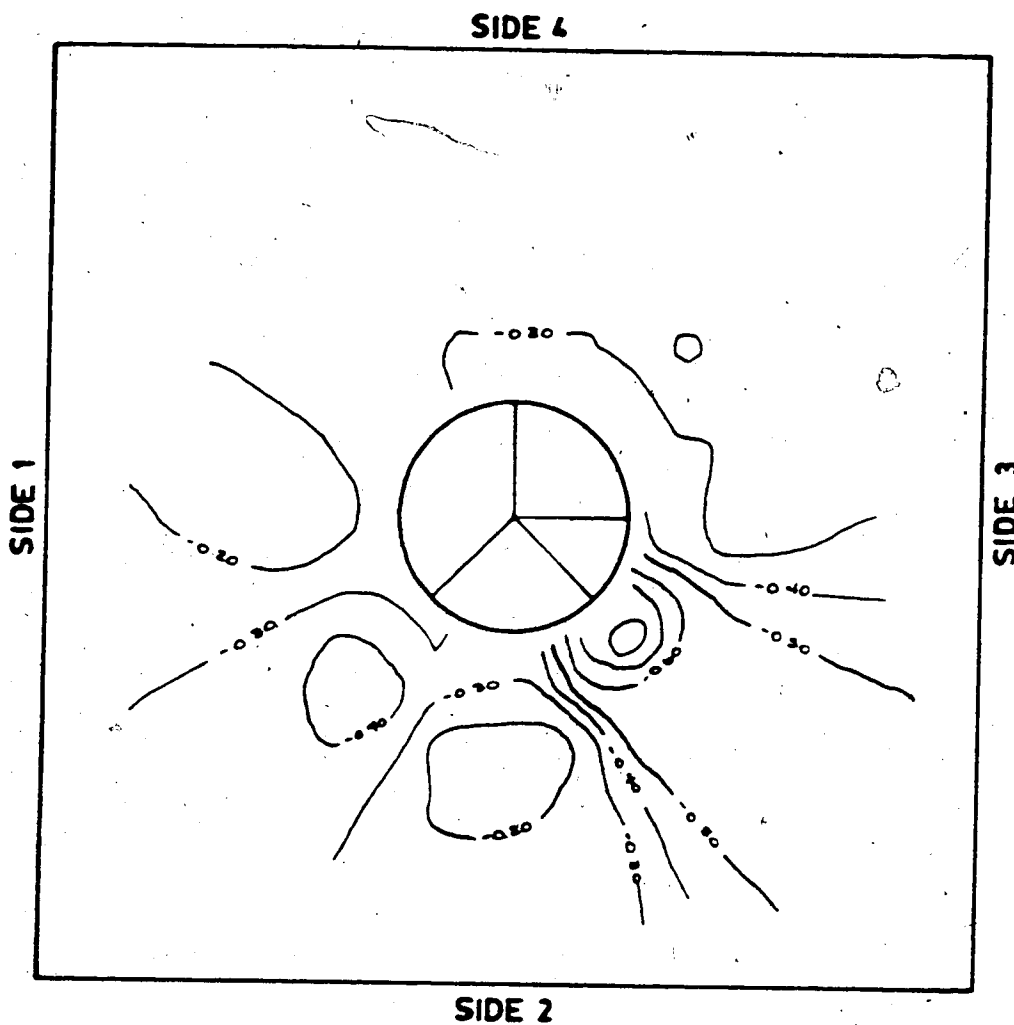


Figure 10.29 Creep Closure and Contours of Creep Strain -
MC-7.13 at 12.5 MPa (t=29.7)

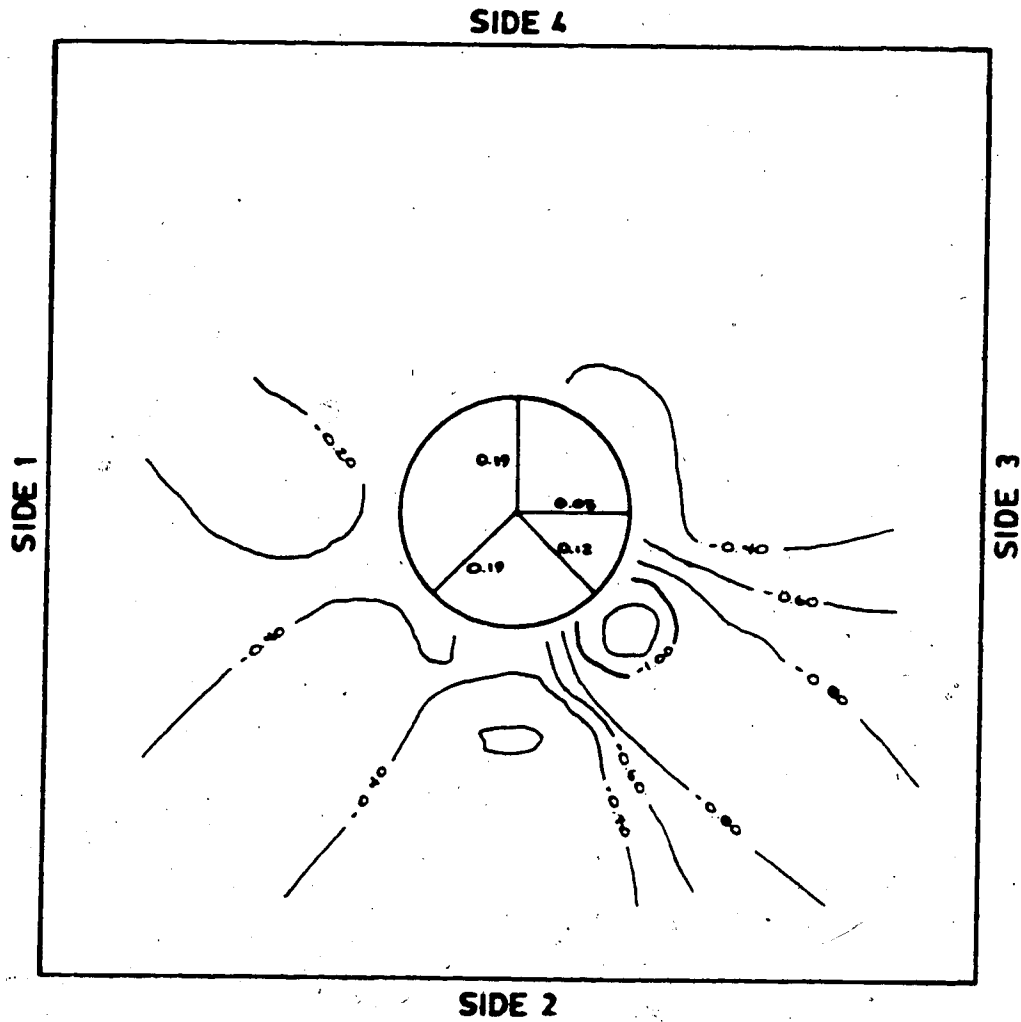


Figure 10.30 Creep Closure and Contours of Creep Strain -
MC-7.13 at 12.8 MPa (t=89.7)

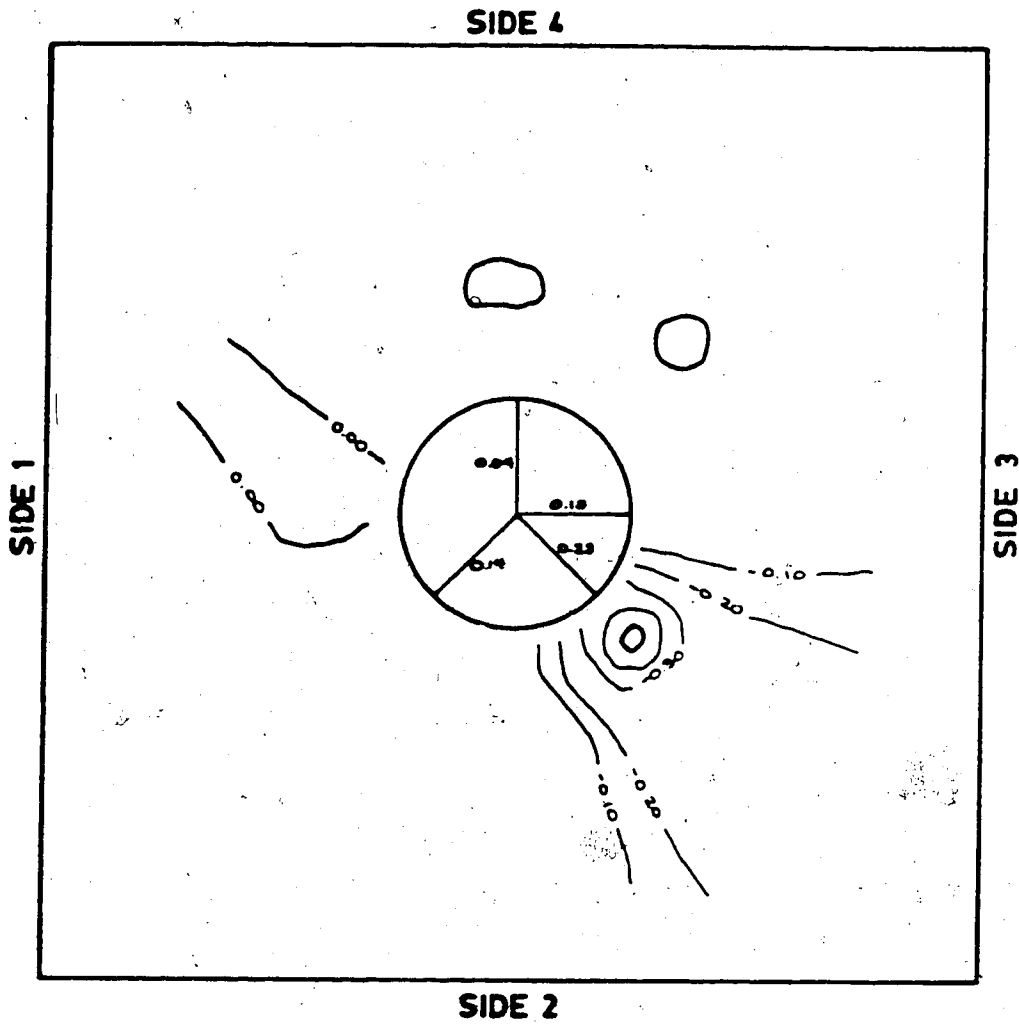


Figure 10.31 Creep Closure and Contours of Creep Strain -
MC-7.14 at 12.5 MPa

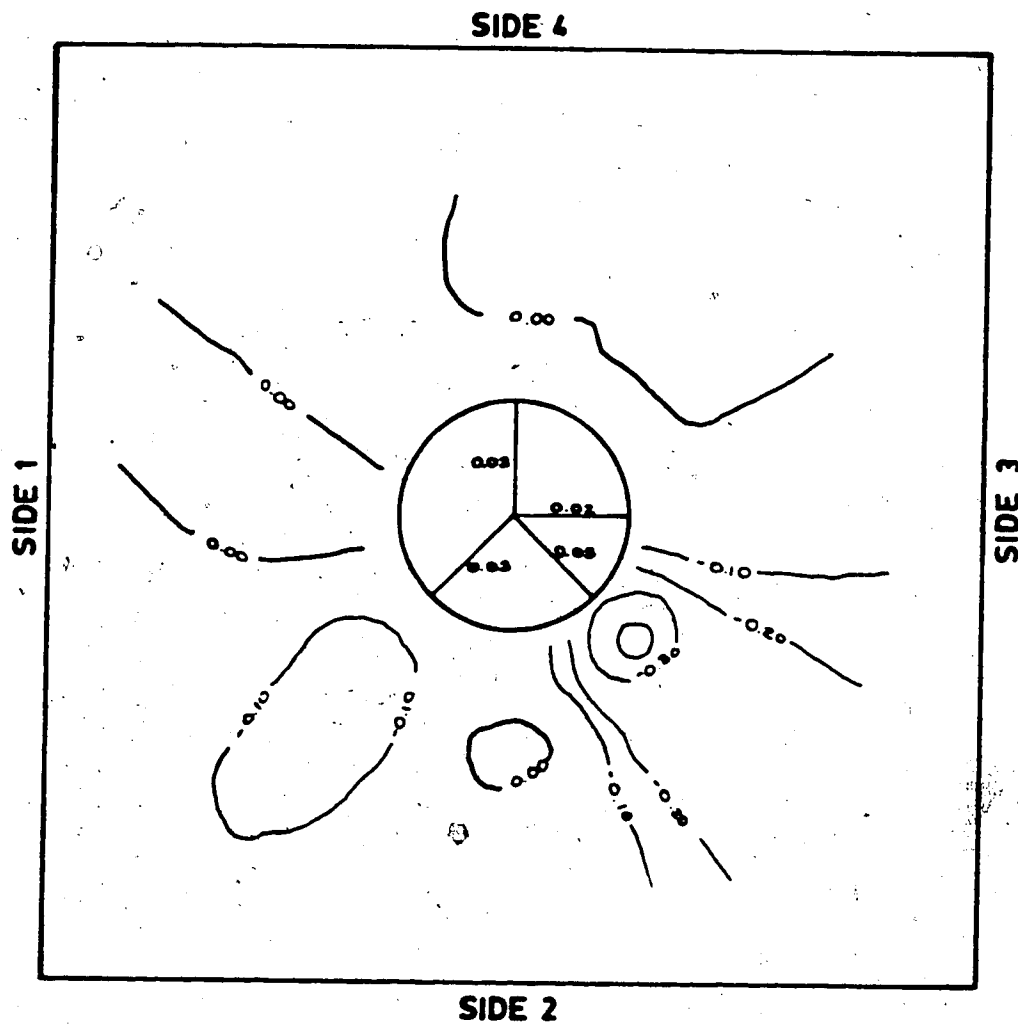


Figure 10.32 Creep Closure and Contours of Creep Strain - MC-7.15 at 7.5 MPa

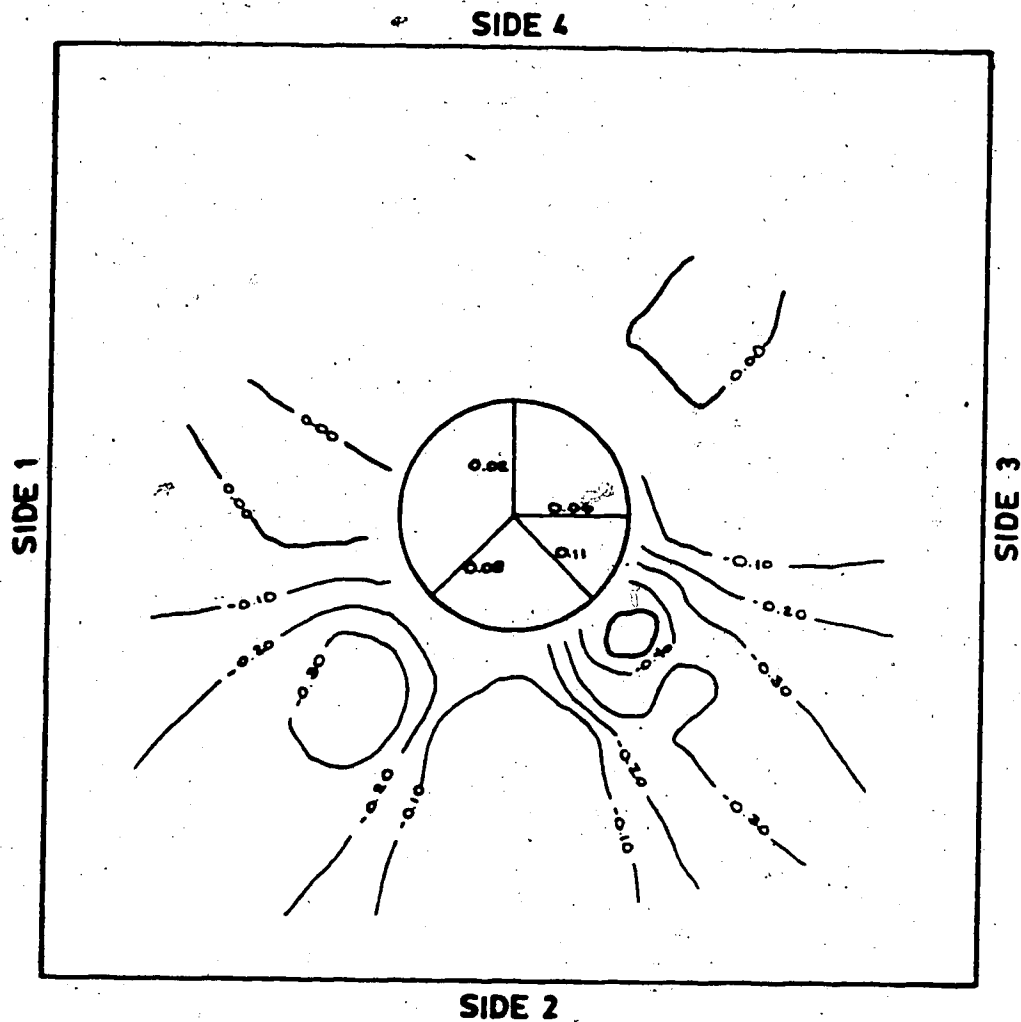


Figure 10.33 Creep Closure and Contours of Creep Strain -
MC-7.15 at 10.0 MPa

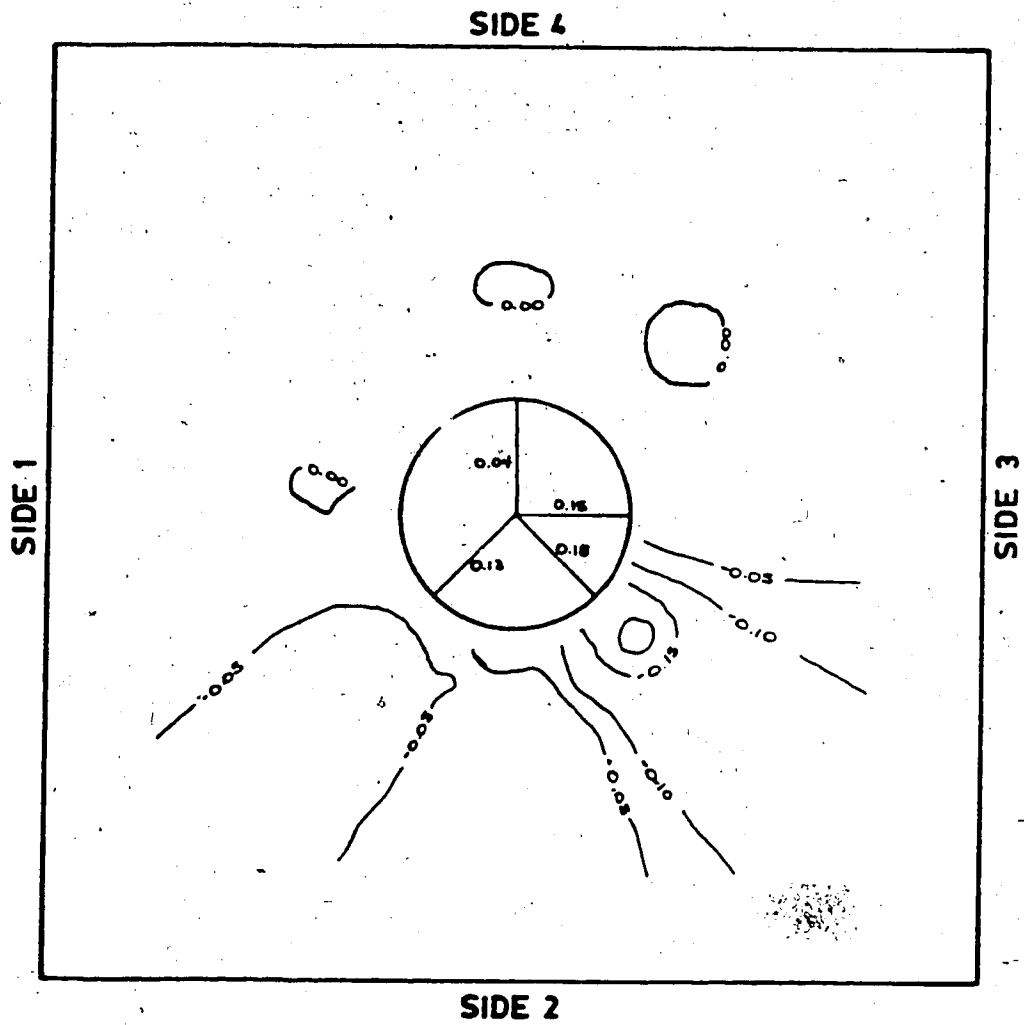


Figure 10.34 Creep Closure and Contours of Creep Strain - MC-7.15 at 12.5 MPa

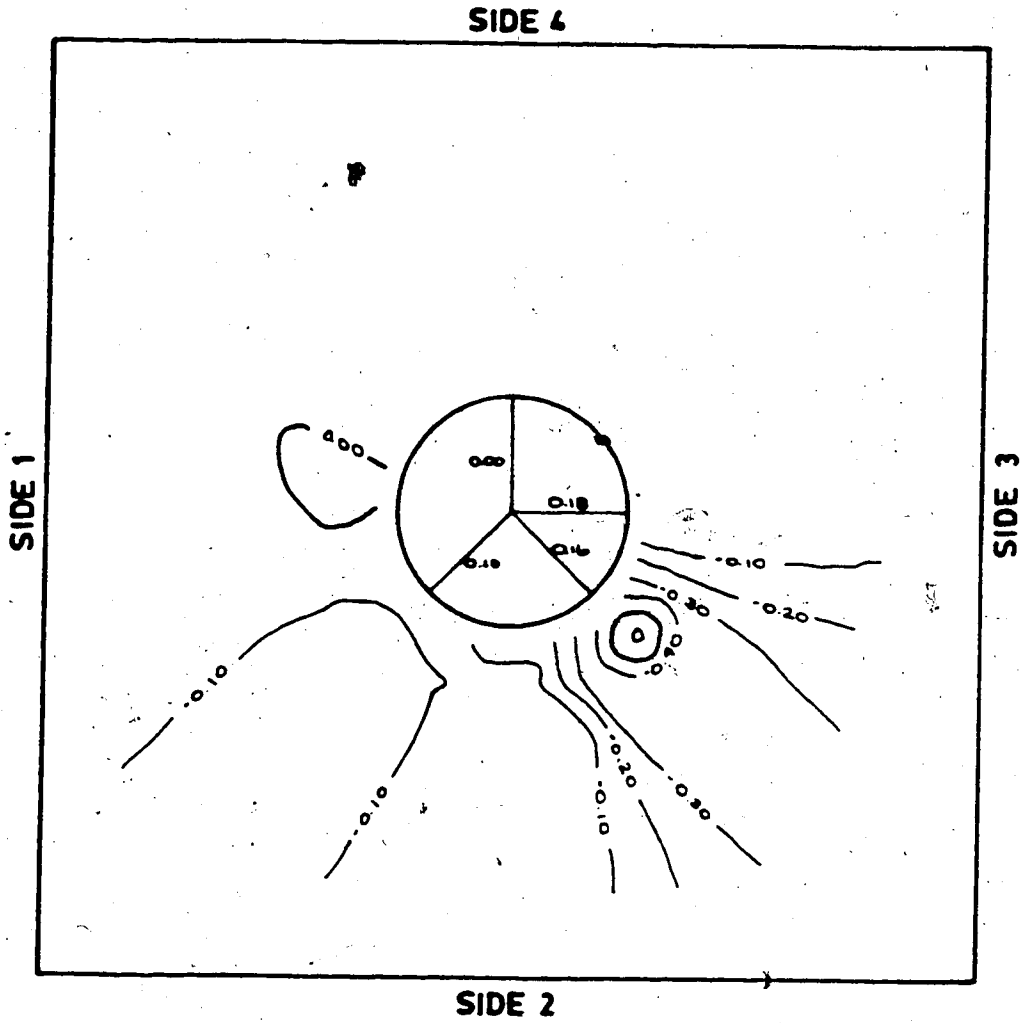


Figure 10.35 Creep Closure and Contours of Creep Strain - MC-7.15 at 14.0 MPa

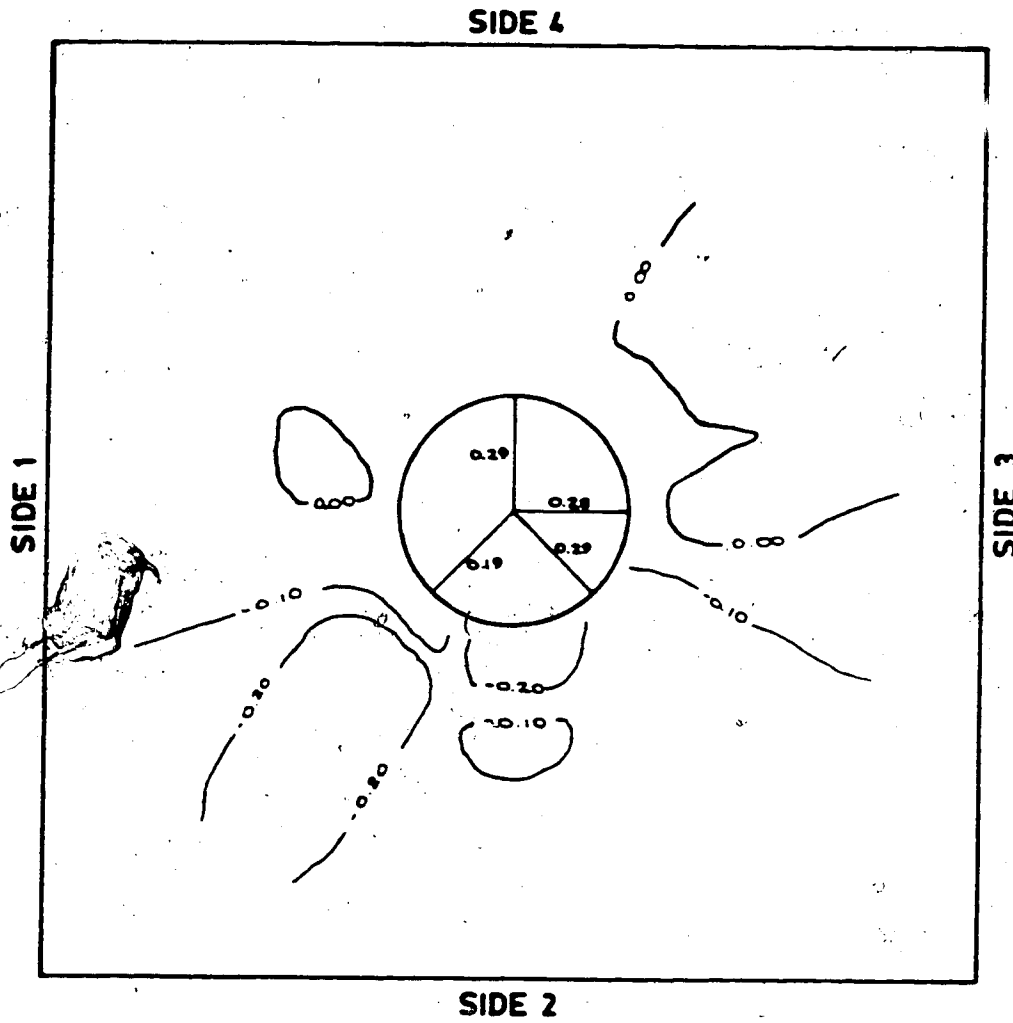


Figure 10.36 Creep Closure and Contours of Creep Strain - MC-7.16 at 12.5 MPa

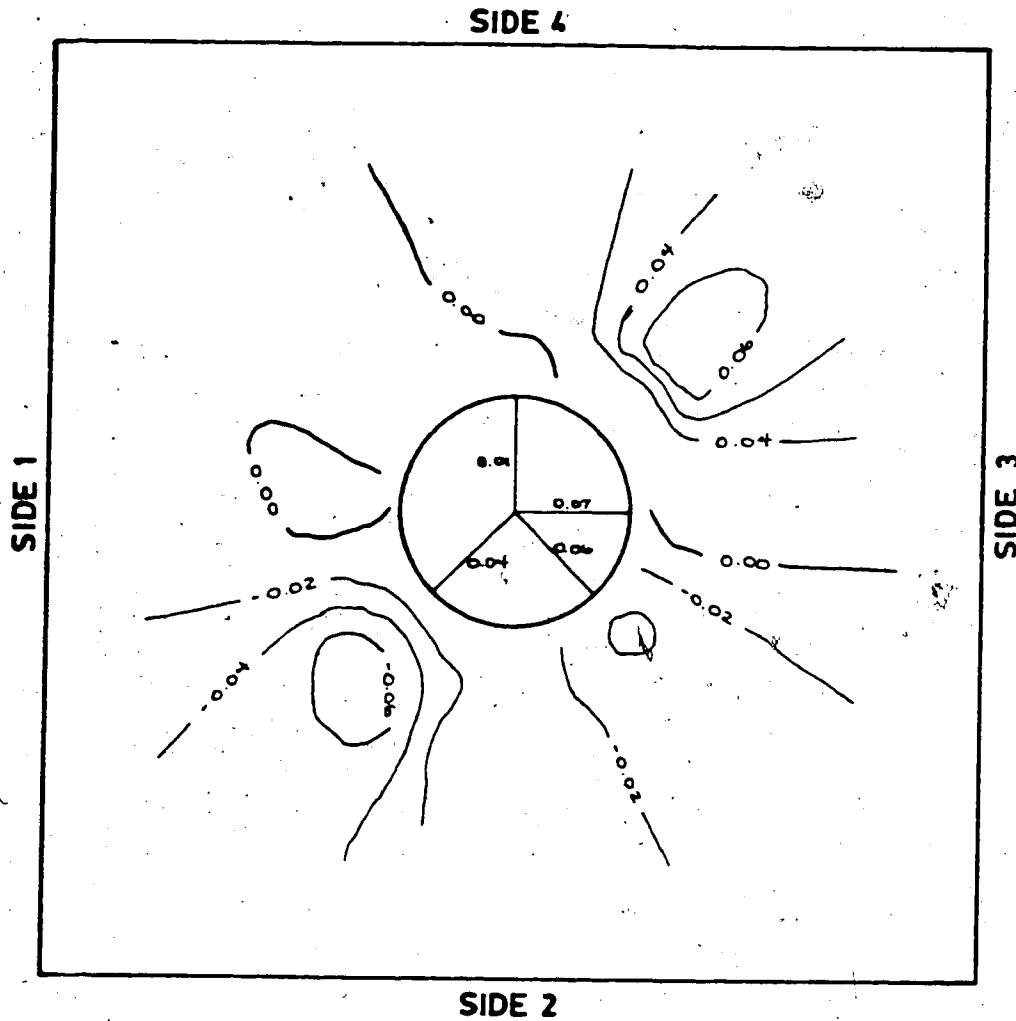


Figure 10.3 Creep Closure and Contours of Creep Strain -
MC-7.17 at 7.5 MPa

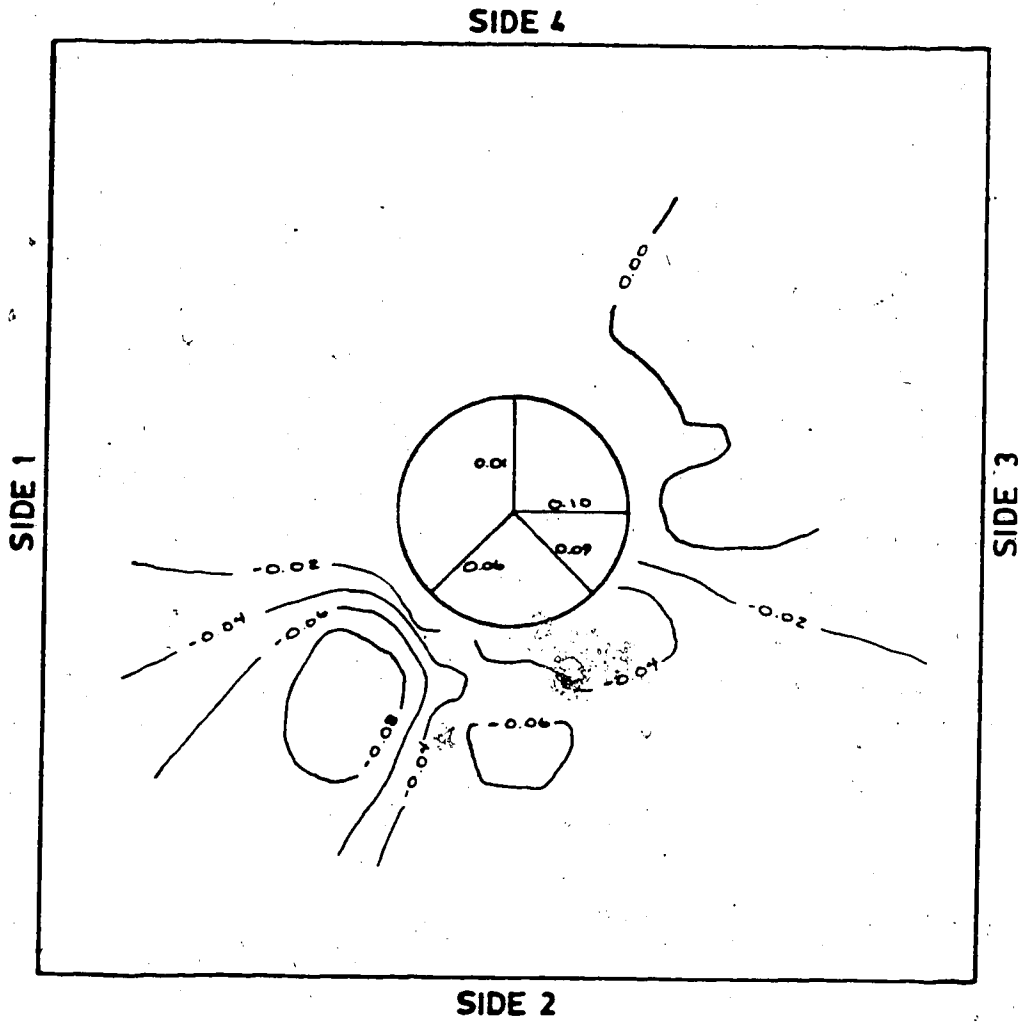


Figure 10.38 Creep Closure and Contours of Creep Strain - MC-7.17 at 10.0 MPa

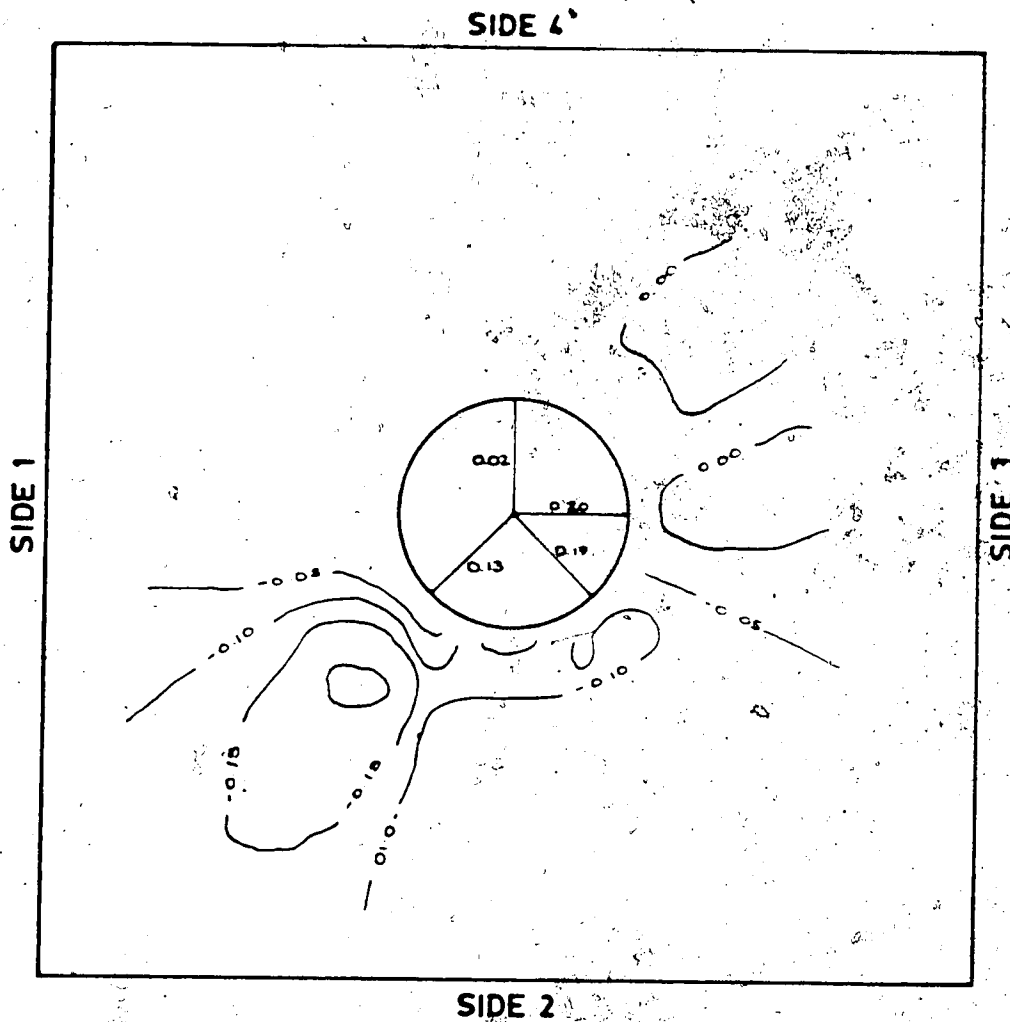


Figure 10.39 Creep Closure and Contours of Creep Strain - MC-7.17 at 12.5 MPa

11. APPENDIX D - DEVELOPMENT OF RADIAL STRAINS NEAR THE TUNNEL FACE - SAMPLE MC-7

The three sets of figures presented herein show the radial strain development around the advancing tunnel face for the conditions of initial excavation (Test MC-7.08) and subsequent widenings (Tests MC-7.10 and 7.13). The initial figure presented in each set shows the position of the advancing face as a function of time. The time at which the face arrives at a particular instrumentation station along the tunnel axis is given by the intersection of the advance curve and the dashed line corresponding to the desired station. The remaining figures in each set show the radial strains measured by the extensometers during each test. A plan view (to scale) of the extensometer positions is presented in the upper right corner of each figure. The time of face arrival and tunnel completion are noted on each figure (dashed lines).

The excavation of the 42 mm diameter tunnel (Test MC-7.08, Figure 1-1.1) was interrupted due to mechanical problems at Station 146 for a period of 0.3 hours. After this interruption the rate of advance was increased from the previous 0.026 m/hr to 0.102 m/hr (on average). Little extensional straining was observed until the tunnel was within 0.5 diameter of the instrumentation station. Typically the extensometers exhibited a rapid increase in extensional strain as the face advanced with a subsequent rapid decline. Virtually all straining was

complete within a diameter behind the face. This may be a result of the model's boundary conditions. Extensometers at Station 51 ($\theta=135^\circ$), Station 106 ($\theta=45^\circ$) and Station 156 ($\theta=45^\circ$) and Station 156 ($\theta=91^\circ$) exhibited straining much in excess of others at the same distance from the tunnel wall, however, the magnitudes of the strains were still very small (0.1%).

Widening of the excavation to a diameter of 108 mm (Test MC-7.10, Figure 11.9) was interrupted twice by mechanical problems. The first occurred at Station 146 for a period of 0.43 hours and the second at Station 170 for a period of 0.23 hours. The rate of advance, initially at 0.071 m/hr was increased to 0.984 m/hr after the second interruption. Strain patterns were similar to those observed in Test MC-7.08, however, extensional straining was generally not observed until the face was within 0.26 diameters of the instrumentation station. The distance over which the greater part of straining occurred (in terms of tunnel diameters) was much reduced. Strains greatly in excess of the average were observed in the 45° orientation and particularly in the 135° orientation.

Widening to a diameter of 152 mm (Test MC-7.13, Figure 11.17) was performed without interruption at a rate of 0.073 m/hr. Strain patterns were similar to those observed previously with continued higher than average straining in the 45° and 135° orientations. Some high strains were also observed in the 90° and 225° orientation close to the tunnel

1822

1822

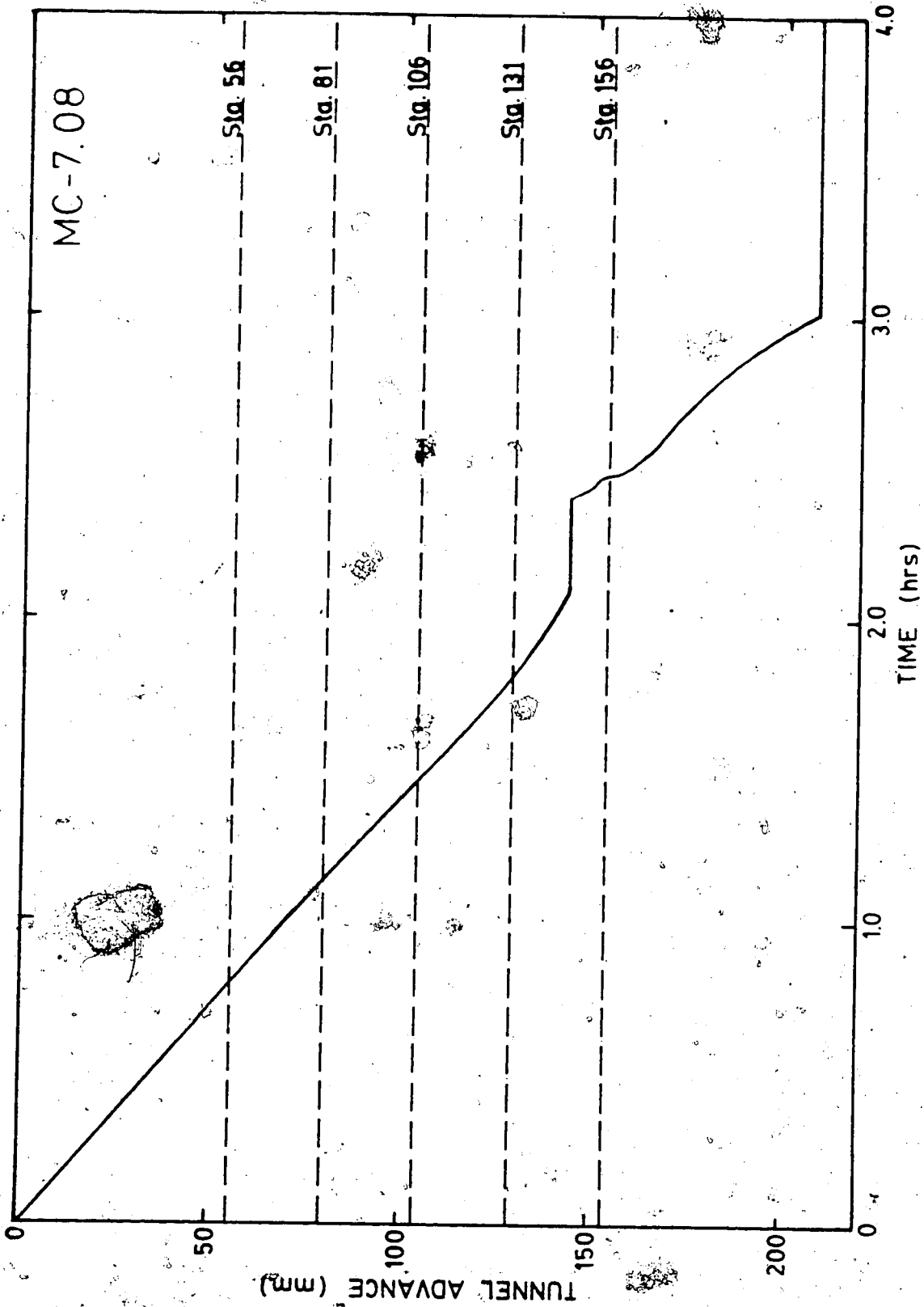


Figure 1.1 Tunnel Advance Test MC-7.08 Excavation

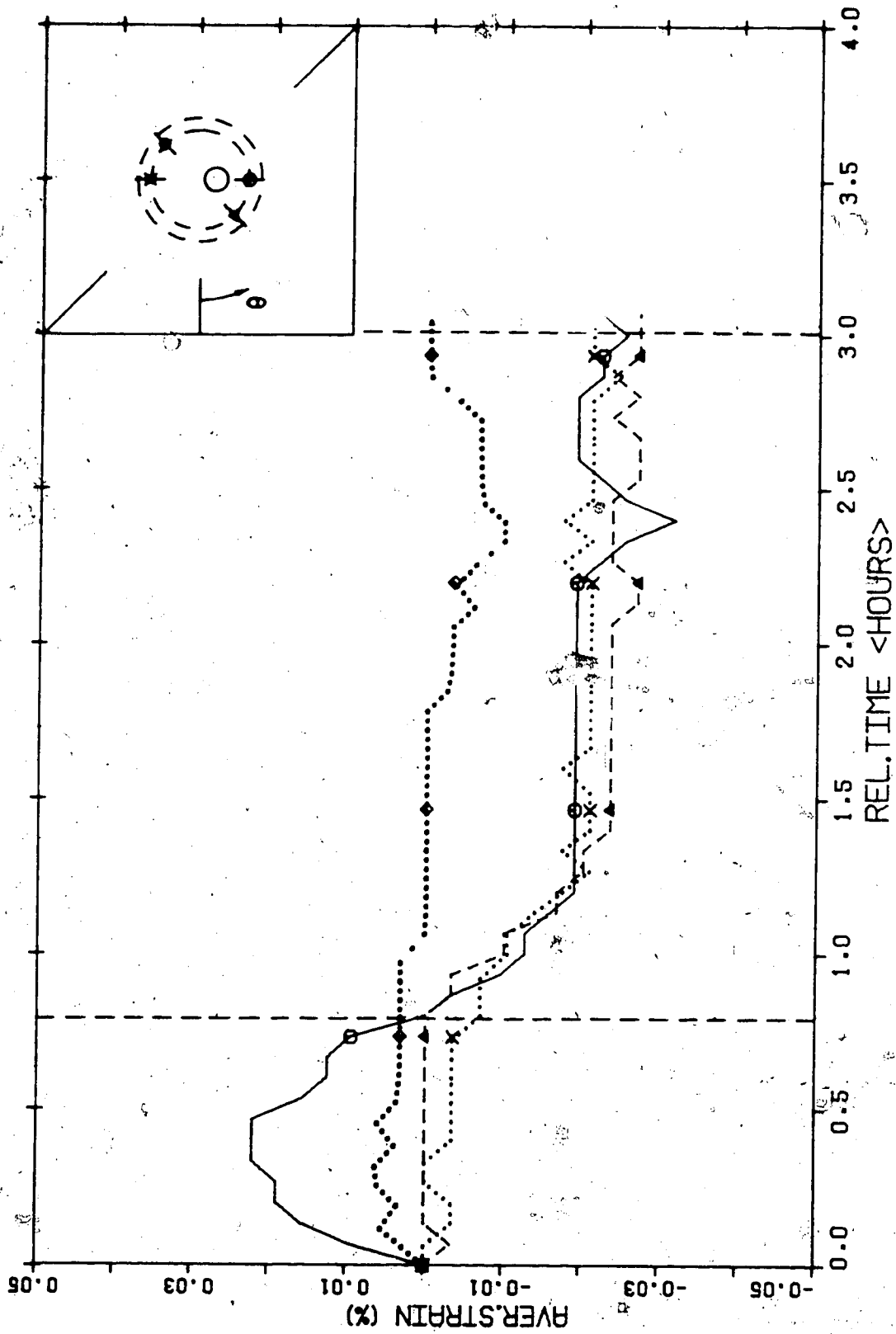


Figure 11.2 Development of Radial Strain - Test MC-7.08 Sta.

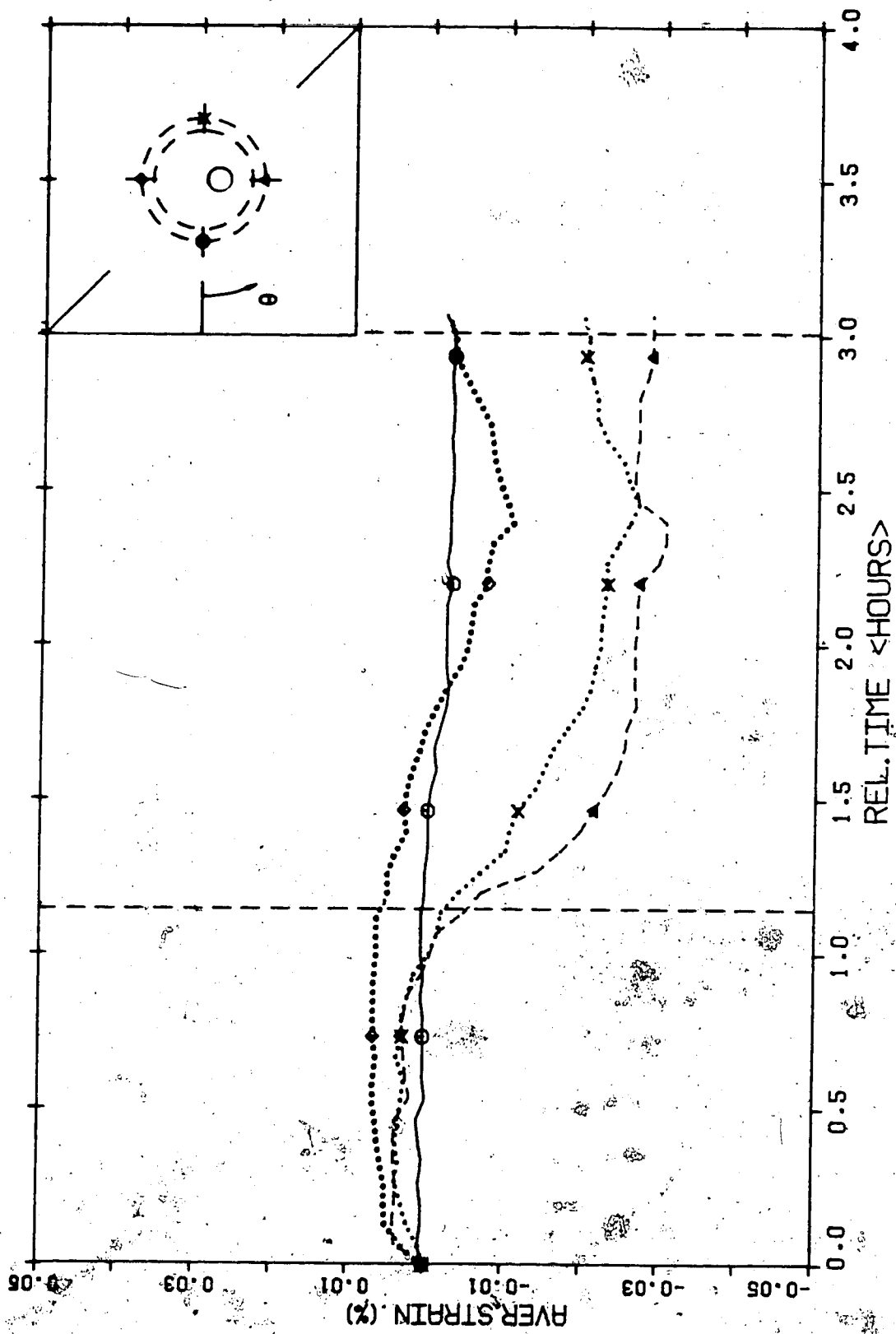


Figure 11.3 Development of Radial Strain - Test MC-7.08 Sta. 81 (parallel)

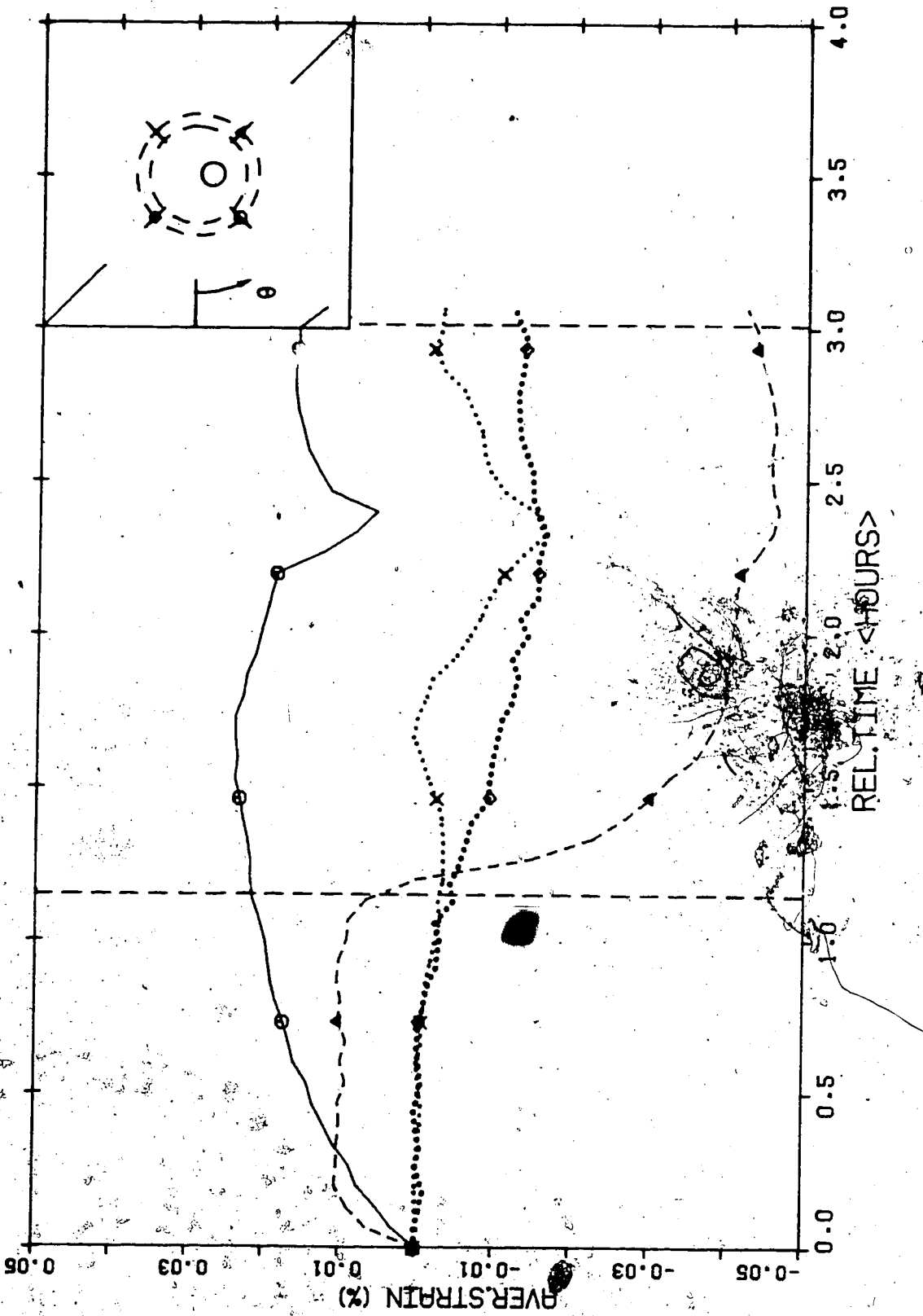


Figure 11.4 Development of Radial Strain - Test MC-7.08
Sta. 81 (45°)

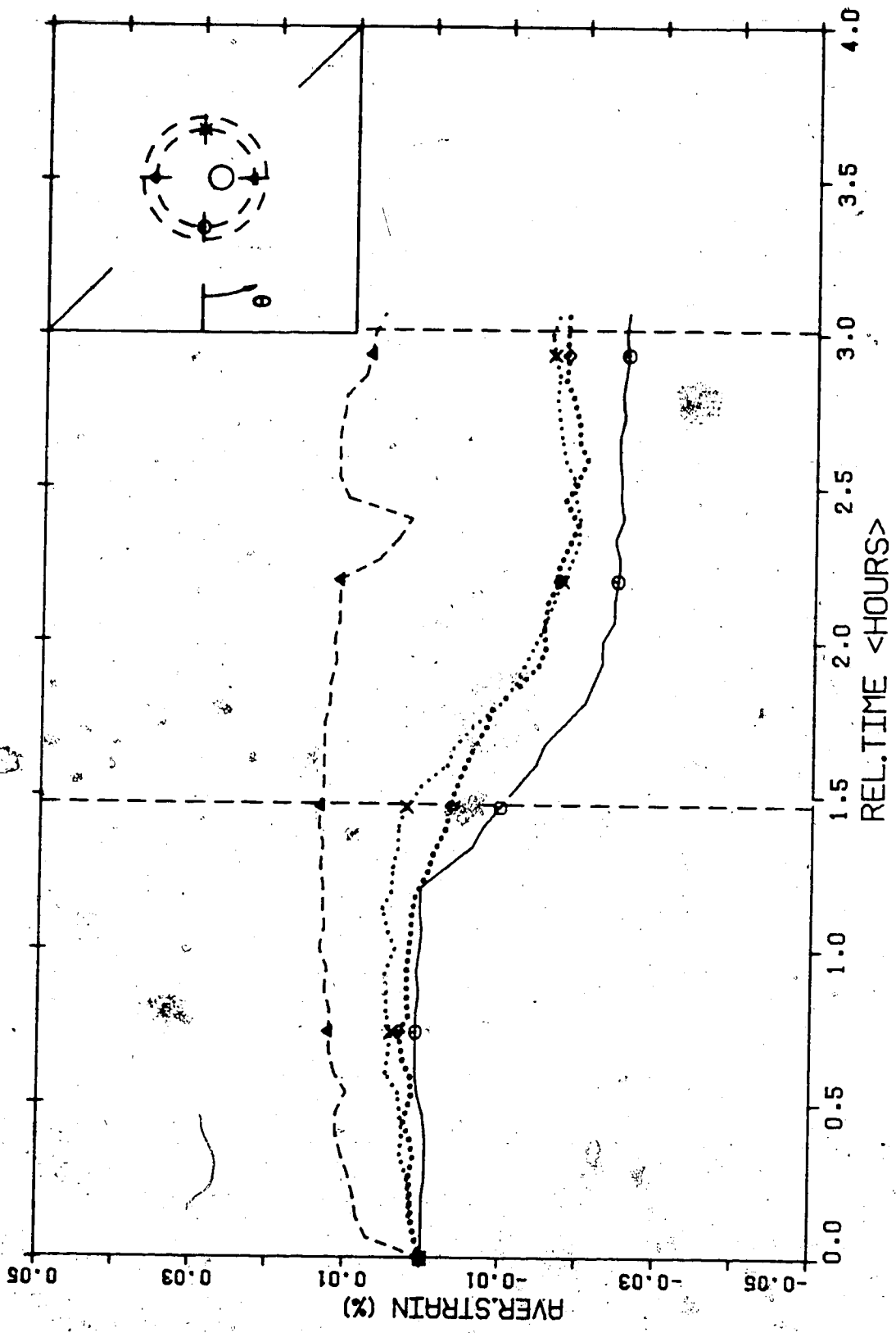


Figure 11.5 Development of Radial Strain - Test MC-7.08
Sta. 106 (parallel)

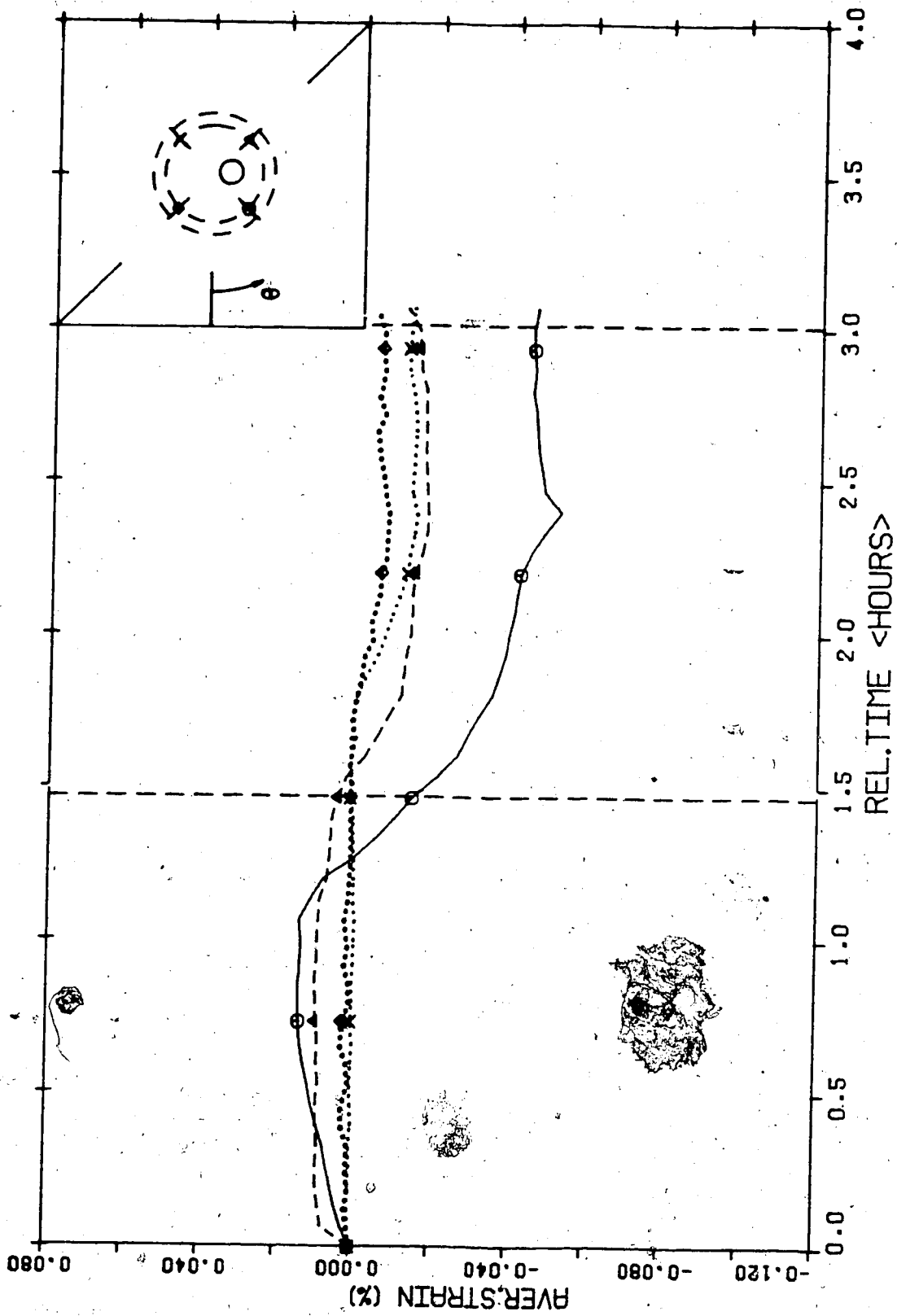


Figure 11.6 Development of Radial Strain - Test MC-7.08
Sta. 106 (45°)

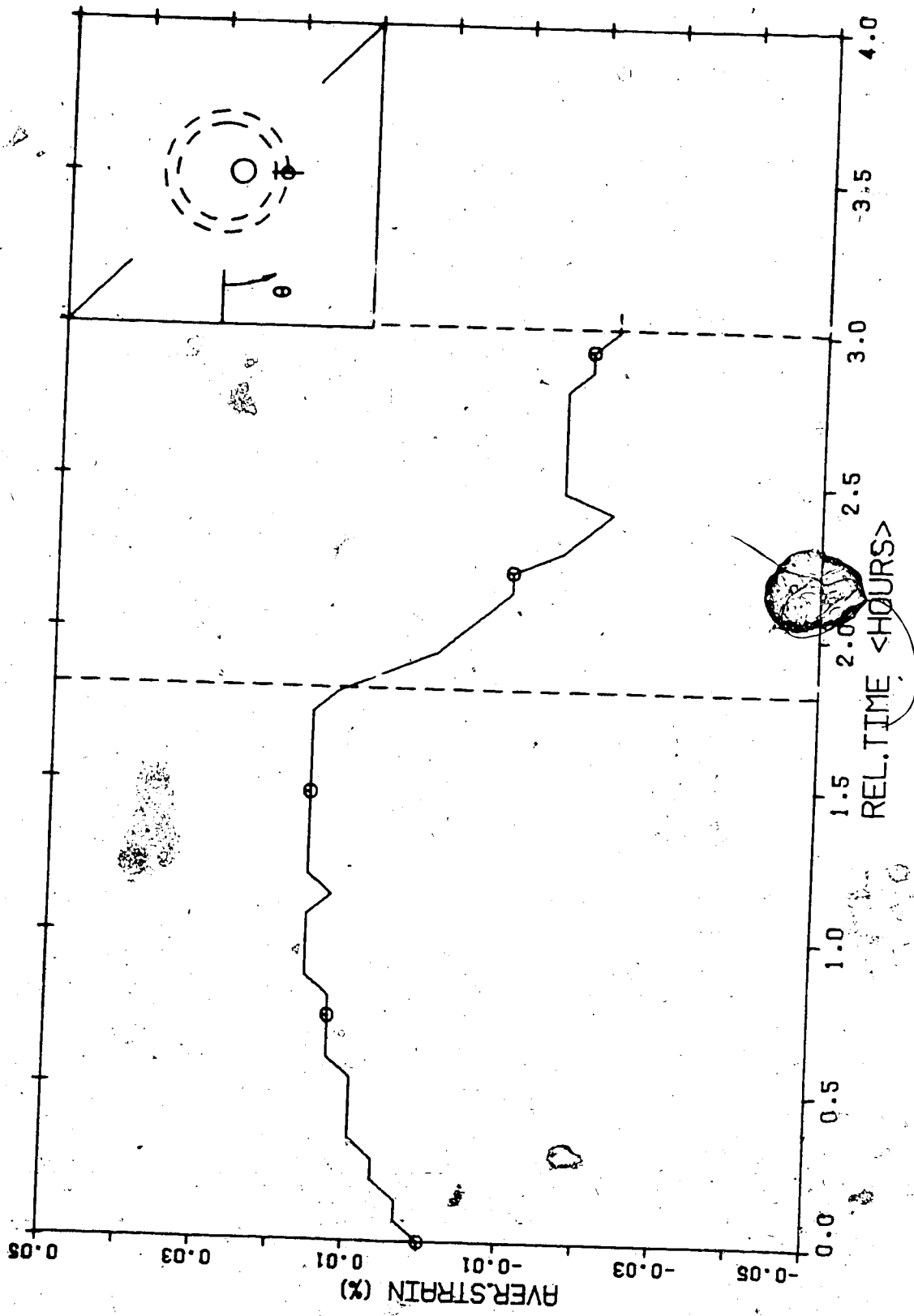


Figure 11.7 Development of Radial Strain - Test MC-7.08
Sta. 131

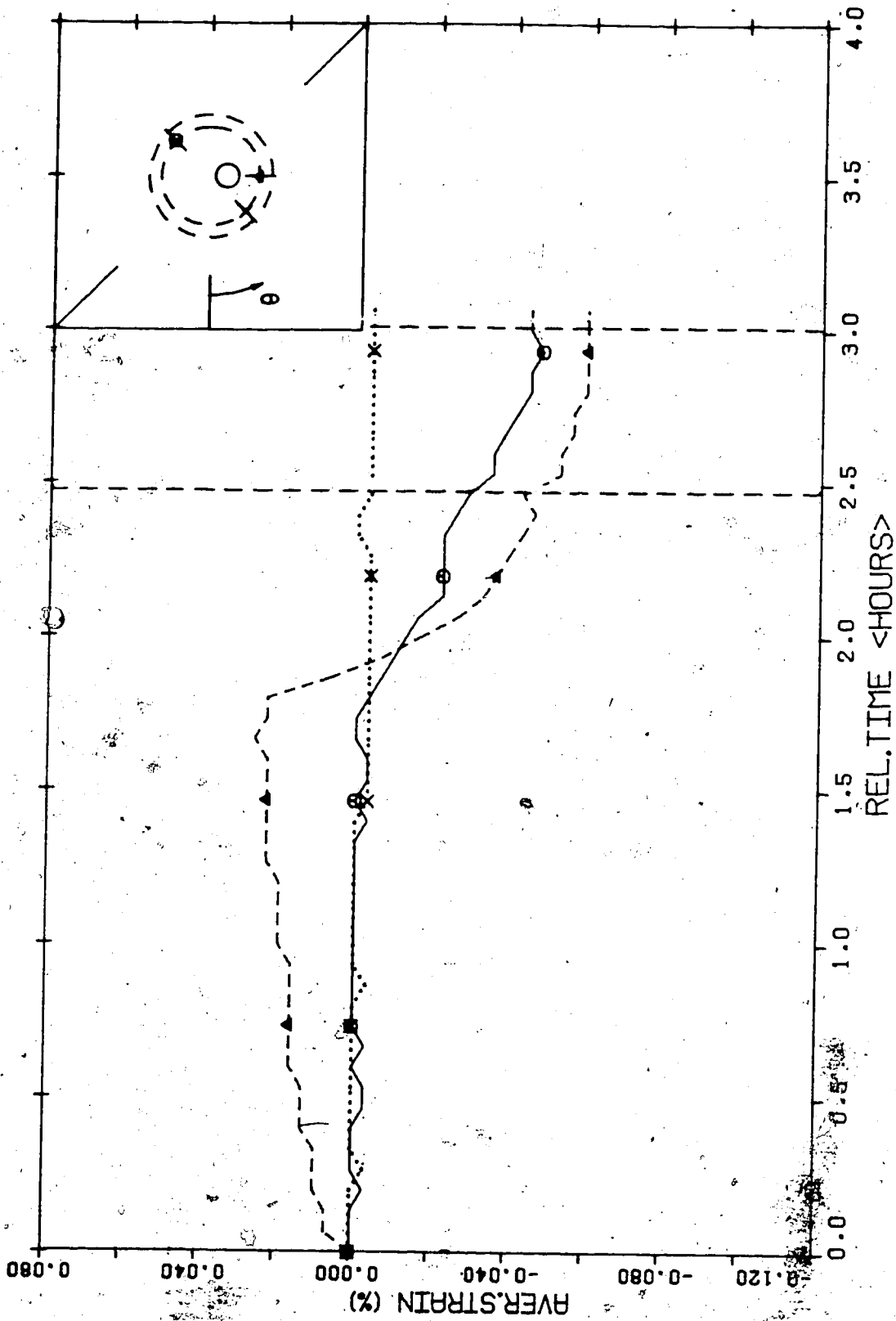


Figure 11.8 Development of Radial Strain - Test MC-7.08
Sta. 156

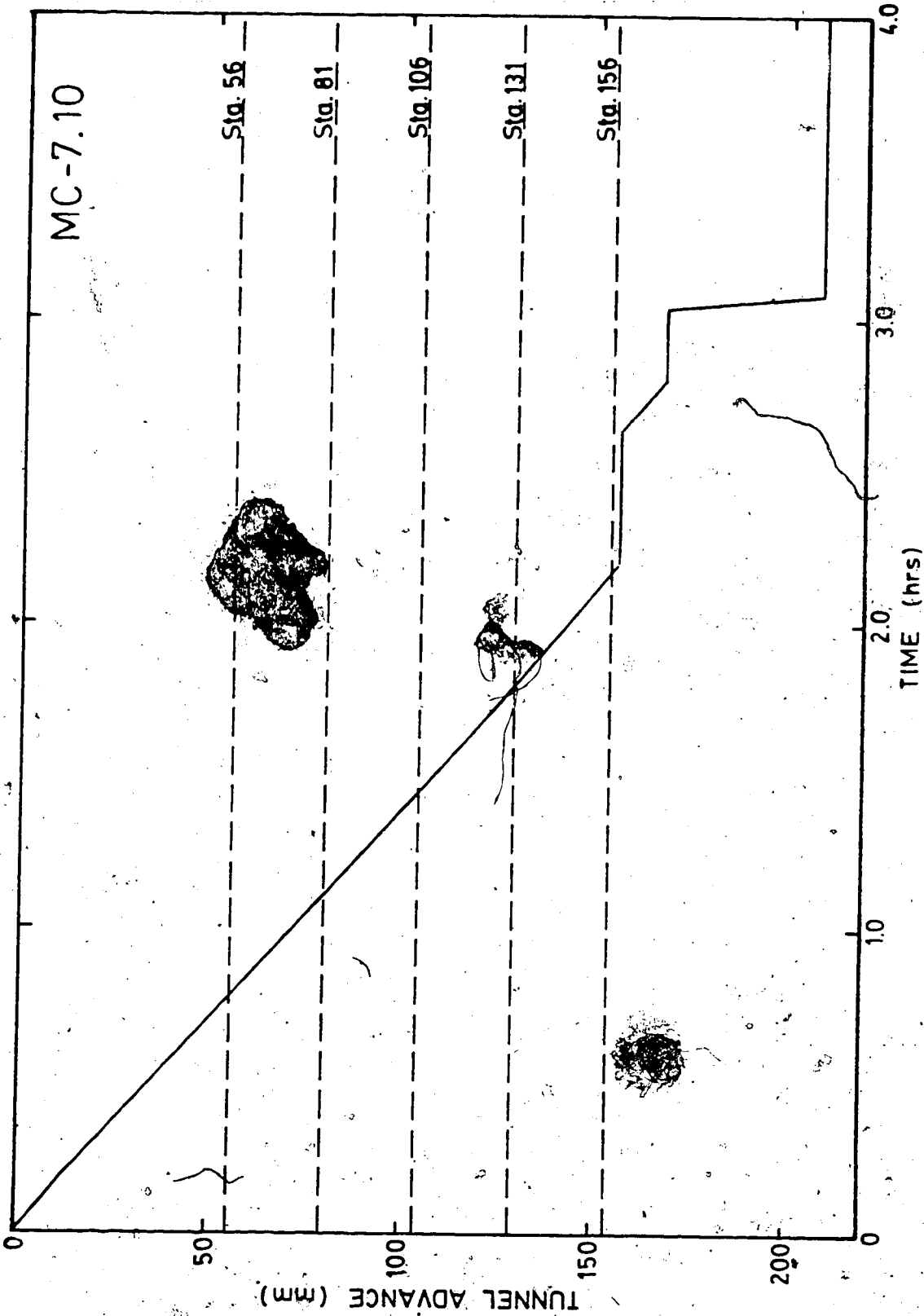


Figure 11.9 Tunnel Advance - Test MC-7.10, First Widening

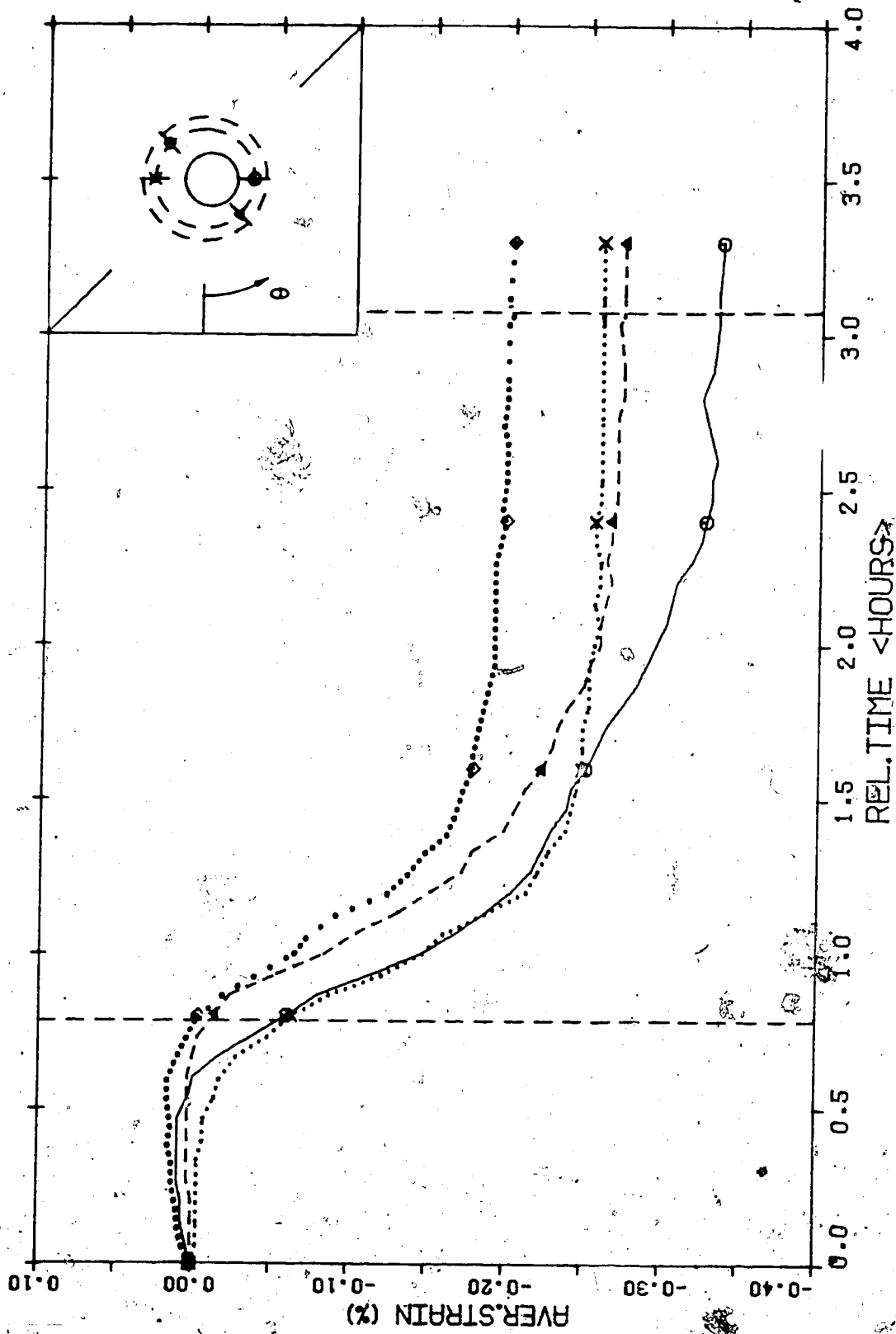


Figure 11.10 Development of Radial Strain - Test MC-7.10
Sta. 56

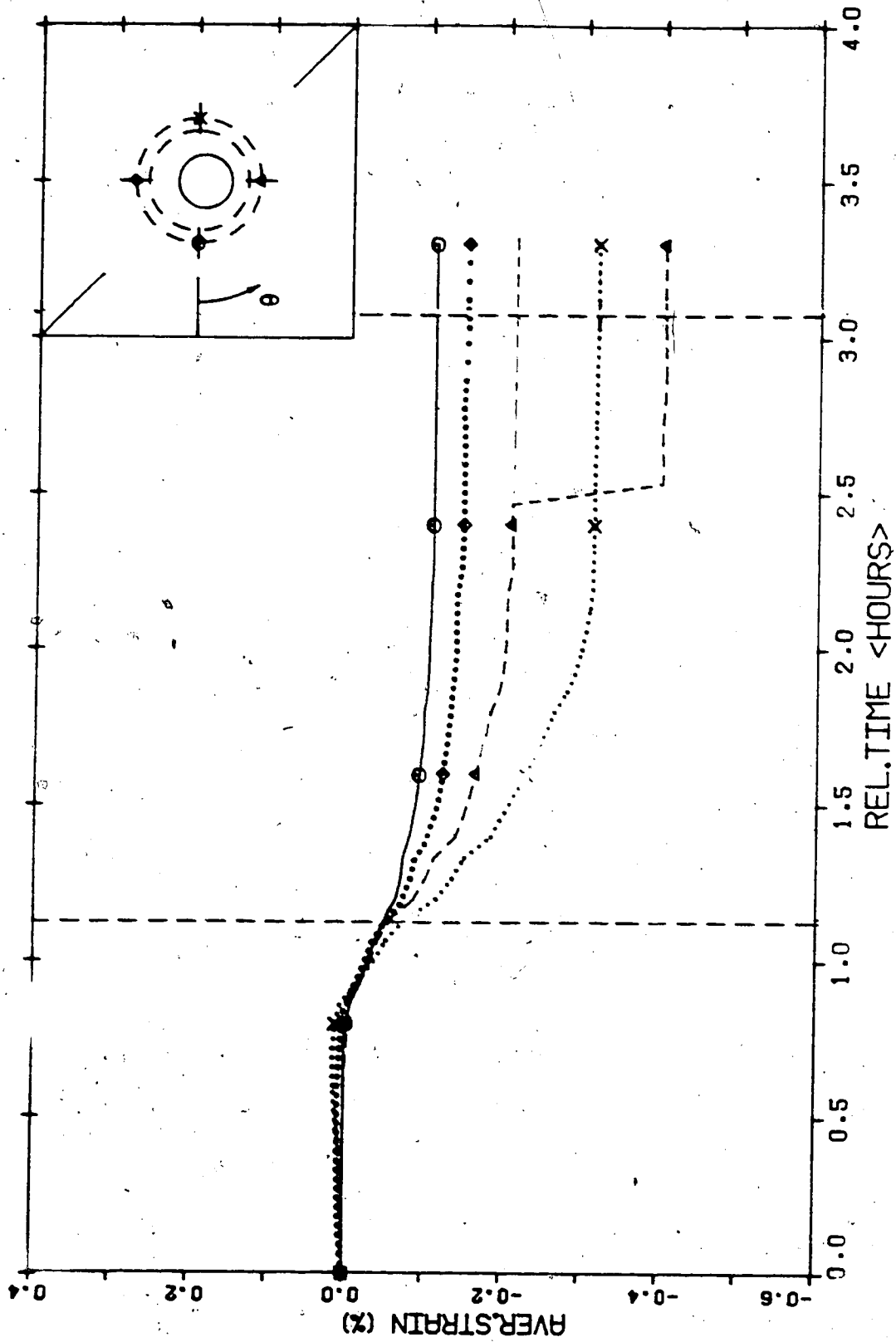


Figure 11.11 Development of Radial Strain - Test MC-7.10
Sta. 81 (parallel)

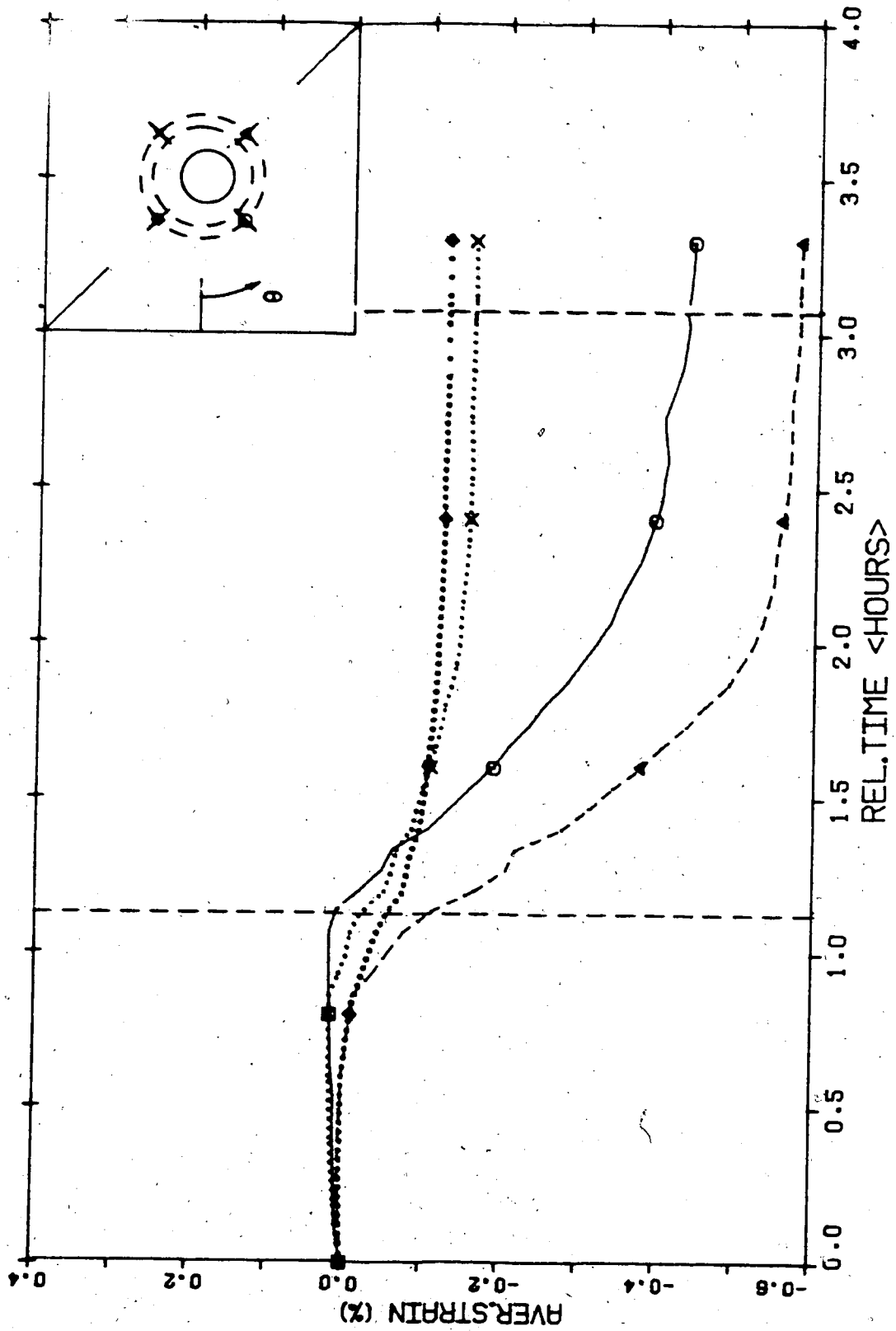


Figure 11.12 Development of Radial Strain - Test MC-7.10
Sta. 81 (45°)

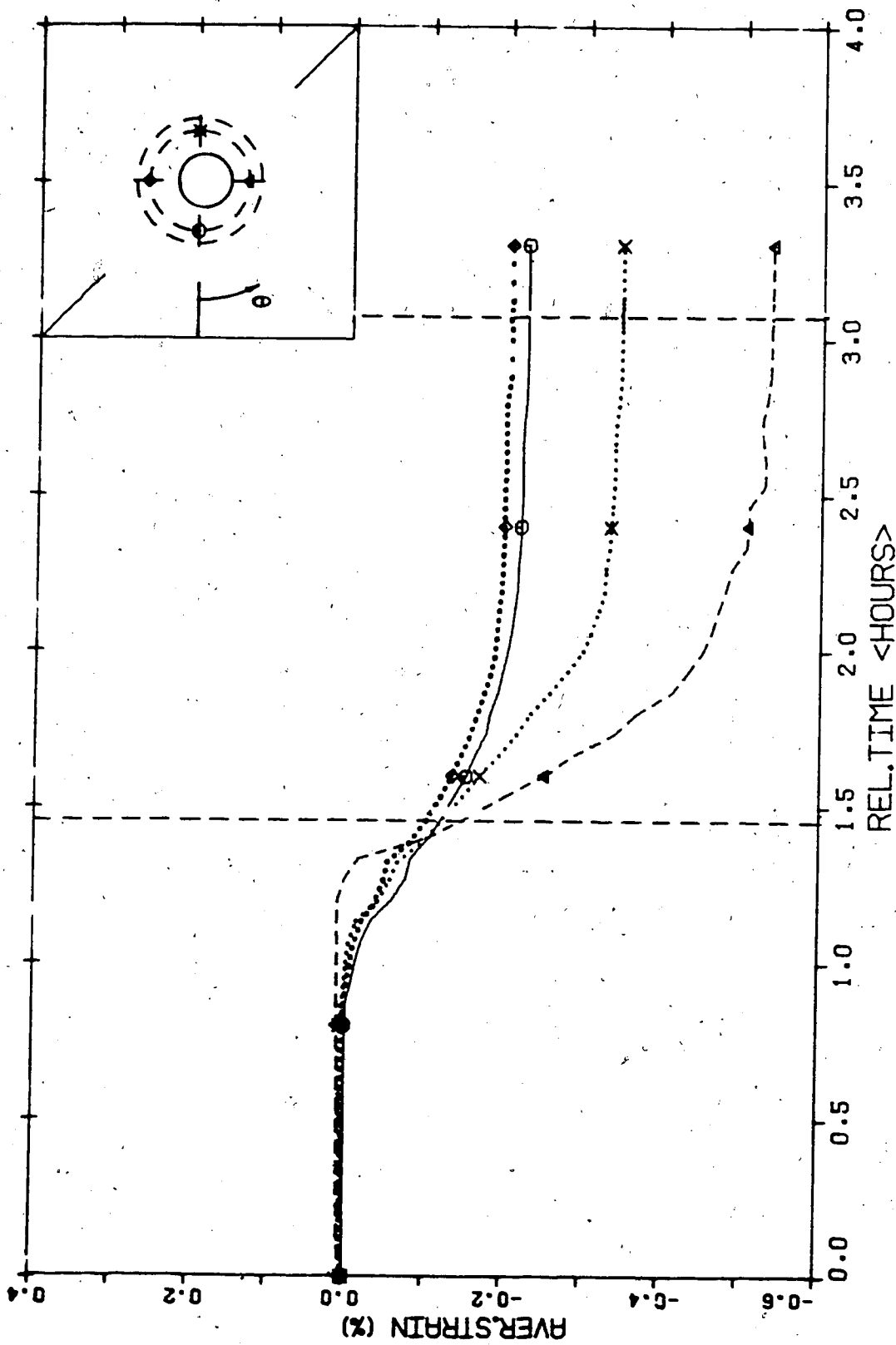


Figure 11.13 Development of Radial Strain - Test MC-7.10
Sta. 106 (parallel)

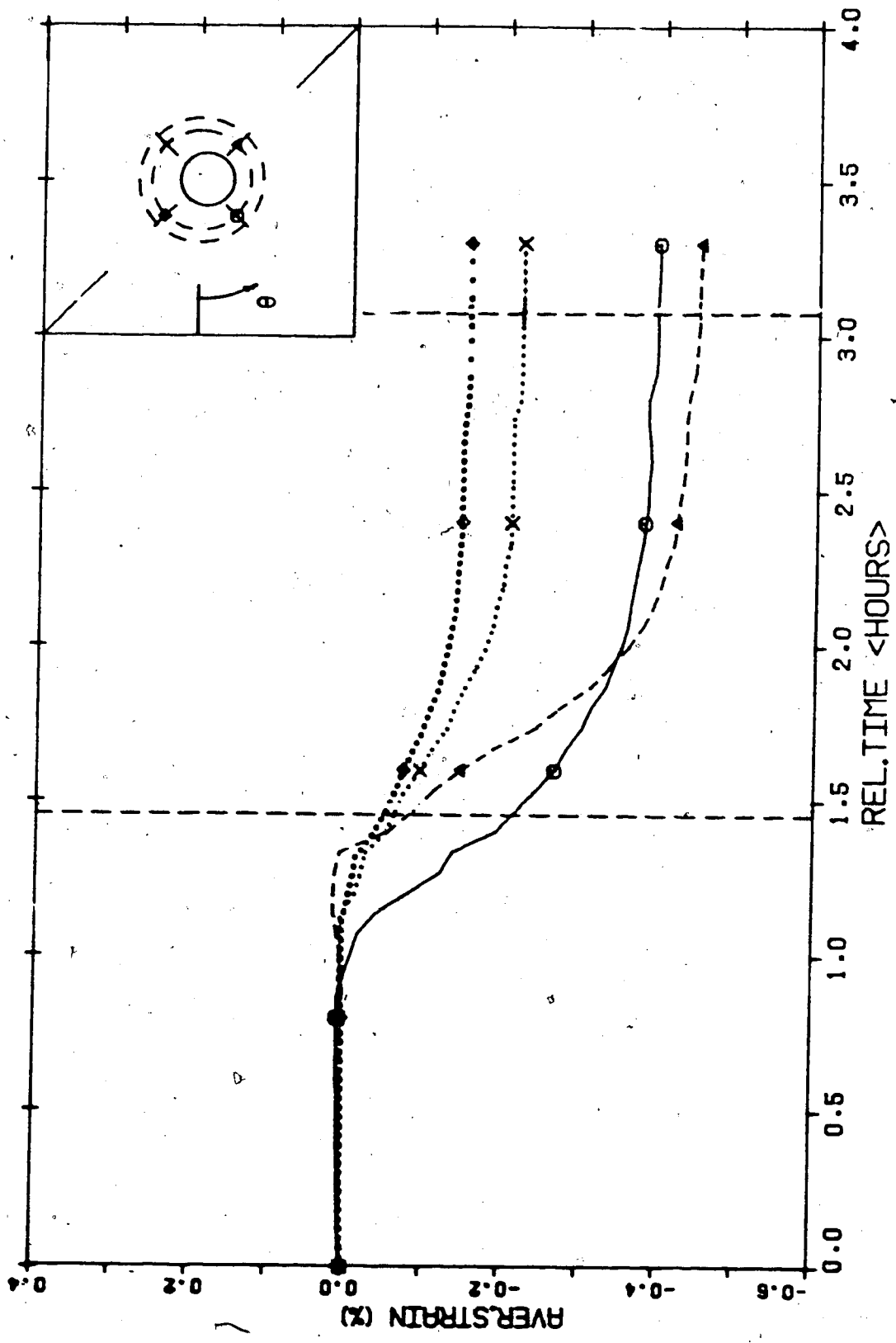


Figure 11.14 Development of Radial Strain - Test MC-7.10
Sta. 106 (45°)

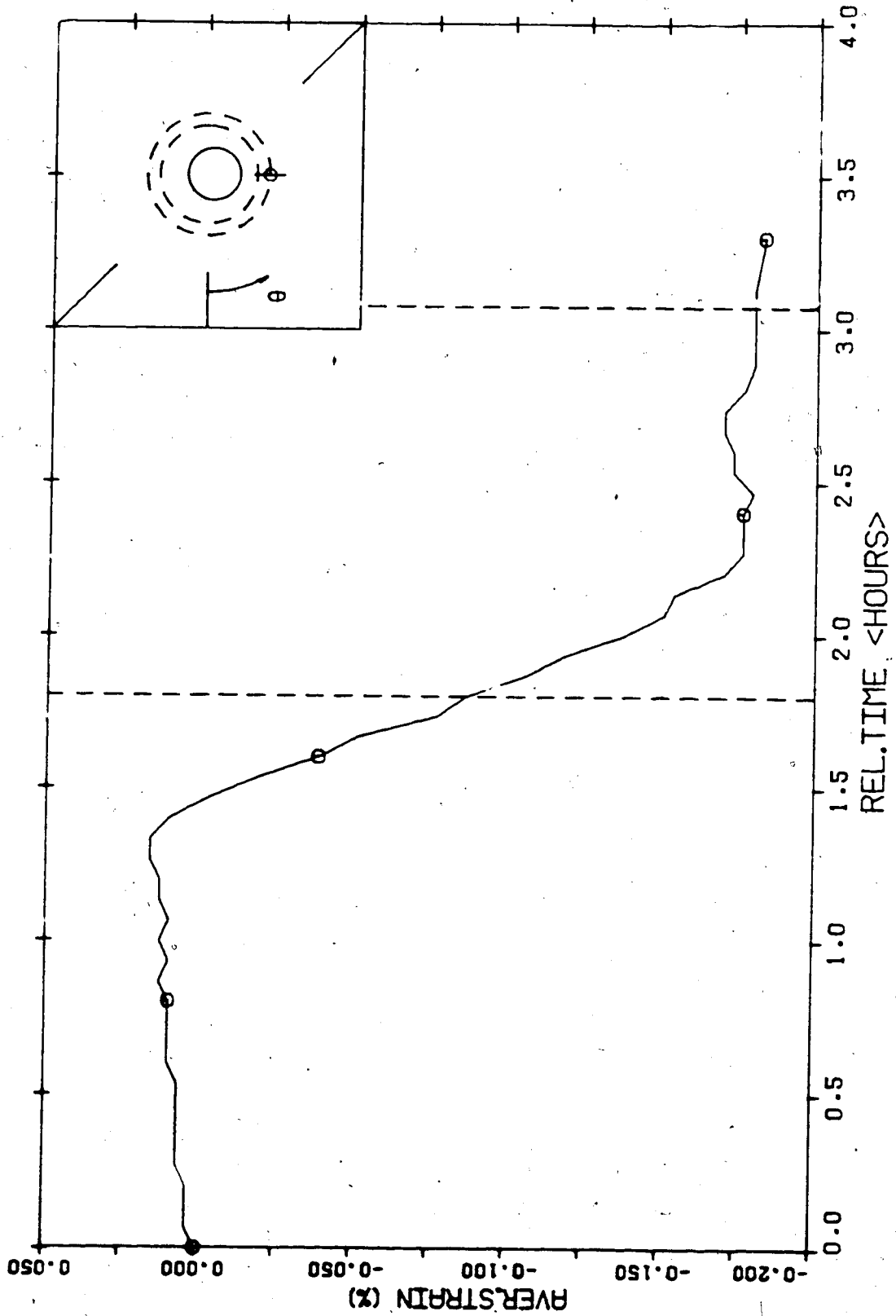


Figure 11.15 Development of Radial Strain - Test MC-7.10
Sta. 131

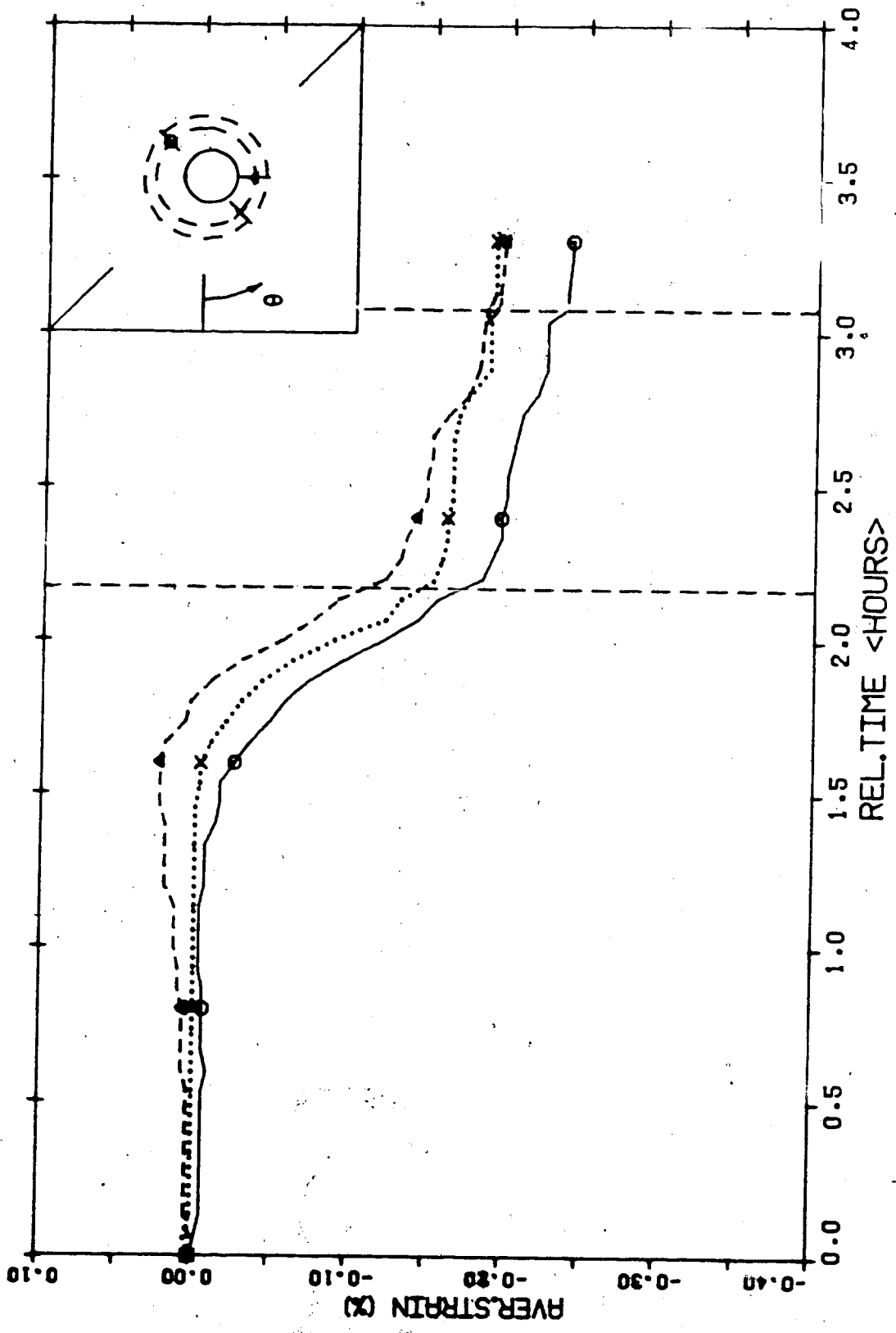


Figure 11.16 Development of Radial Strain - Test MC-7.10
Sta. 156

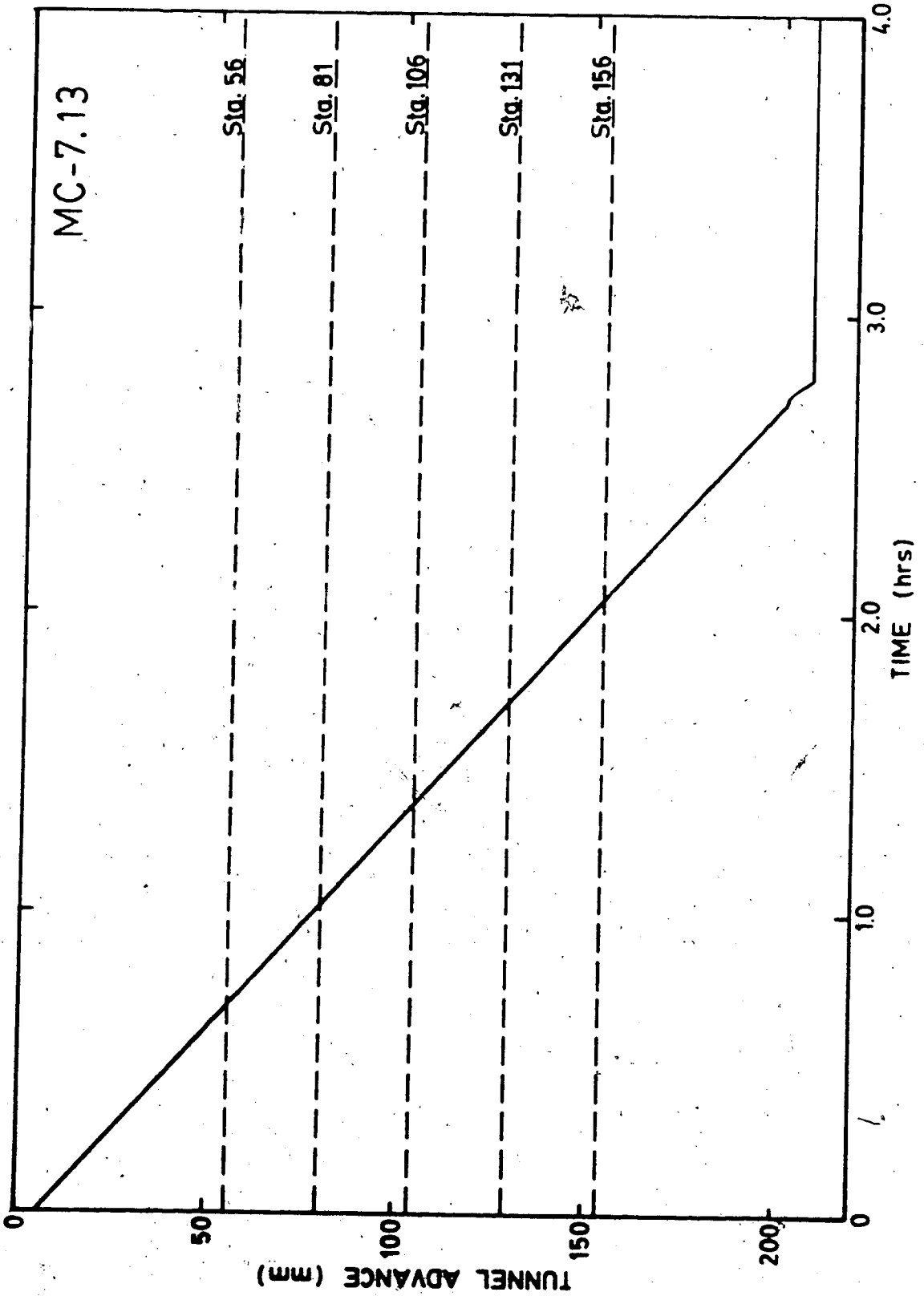


Figure 11.17 Tunnel Advance - Test MC-7.13, Final Widening

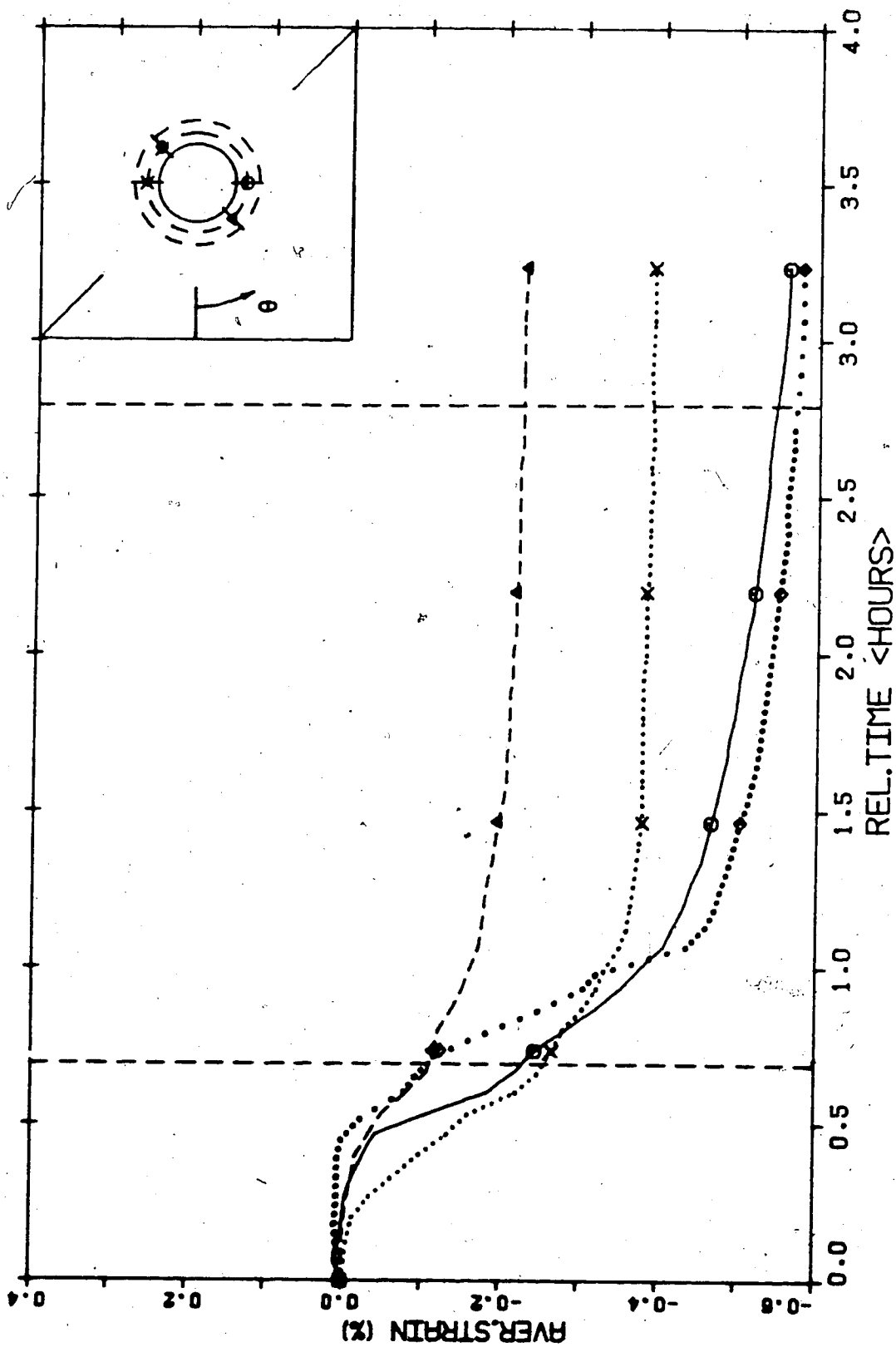


Figure 11.18 Development of Radial Strain - Test MC-7.13
Sta. 56

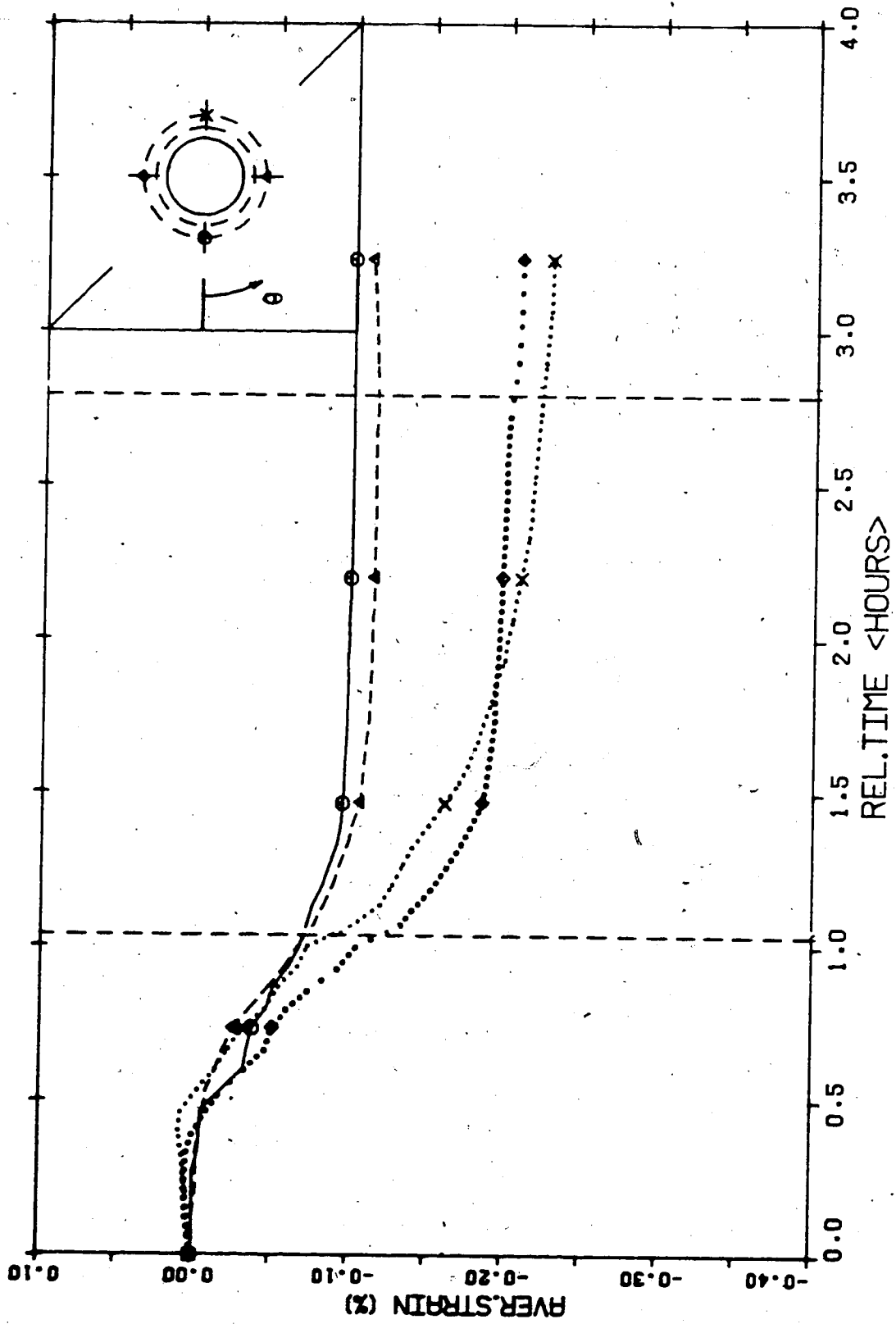


Figure 11.19 Development of Radial Strain - Test MC-7.13
Sta. 81 (parallel)

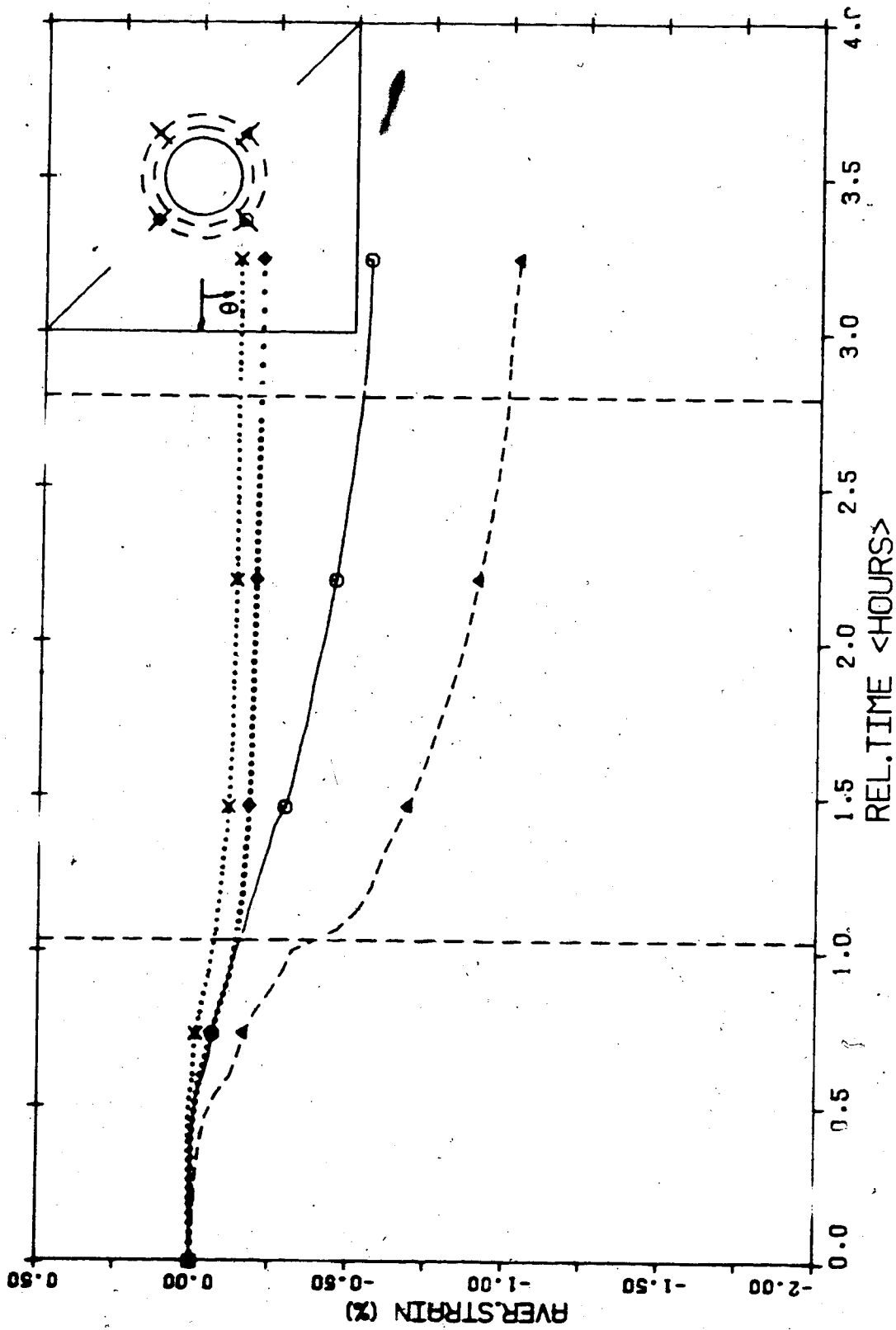


Figure 11.20 Development of Radial Strain - Test MC-7.13
Sta. 81 (45°)

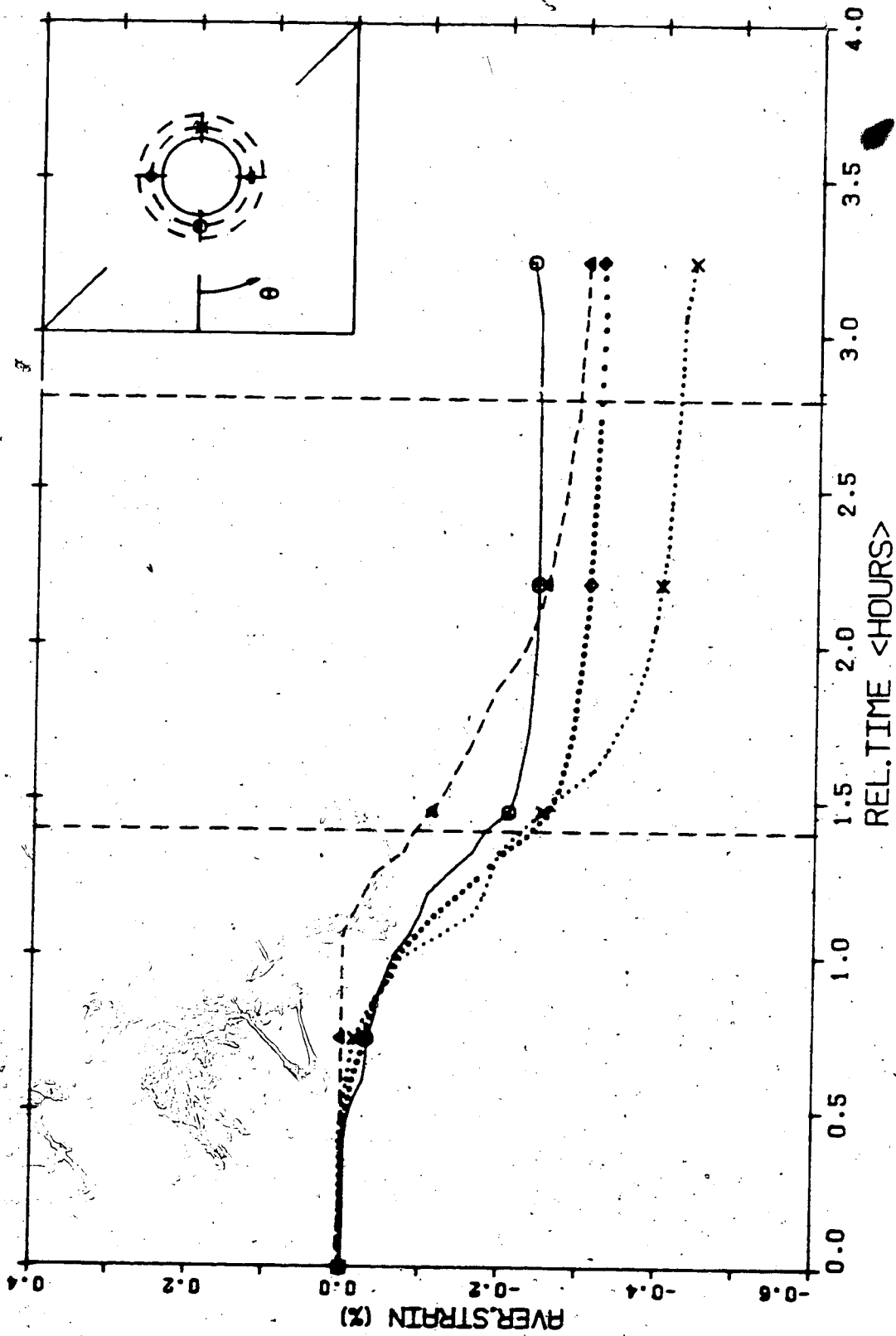


Figure 11.21 Development of Radial Strain - Test MC-7.13
Sta. 106 (parallel)

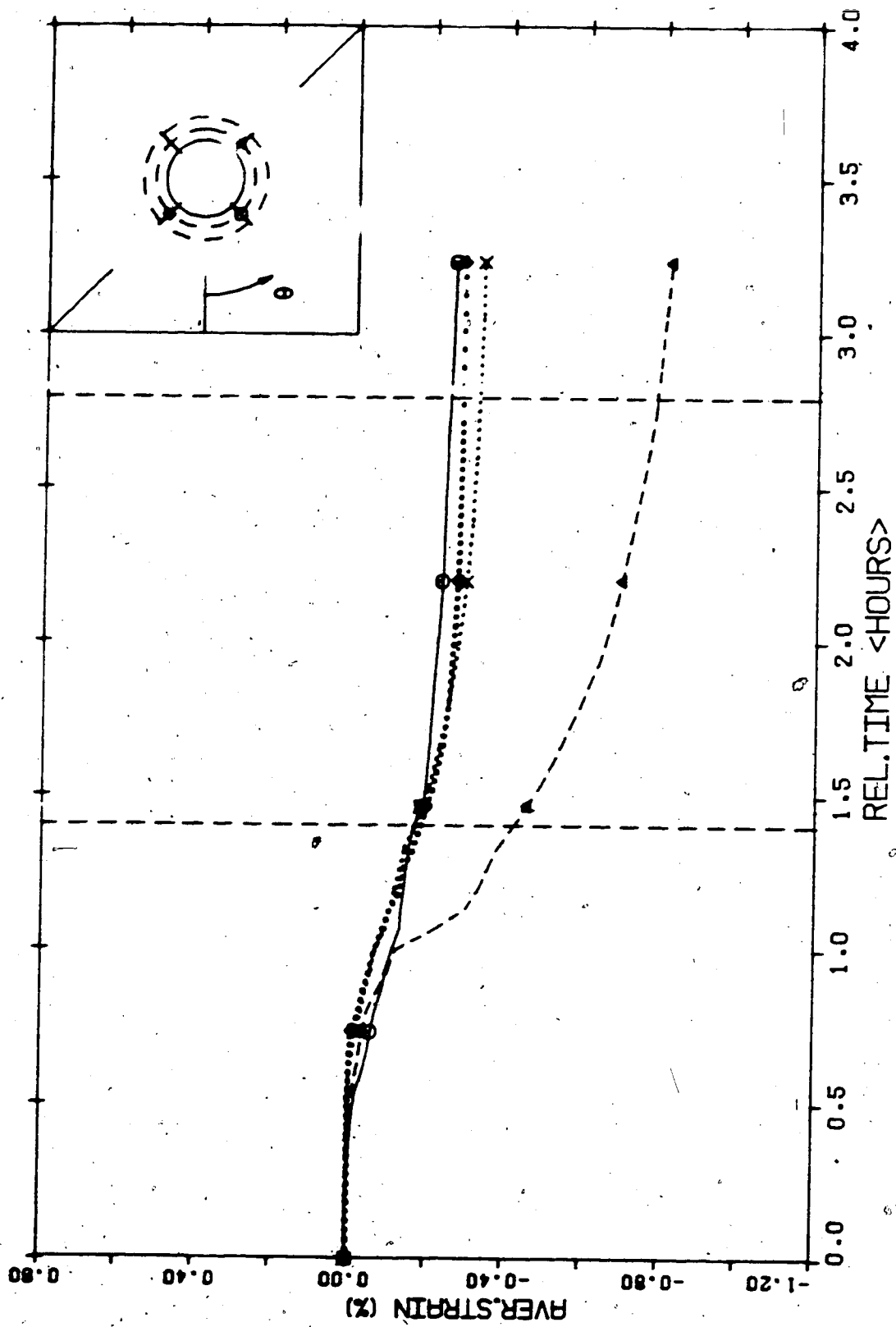


Figure 11.22 Development of Radial Strain - Test MC-7.13
Sta. 106 (45°)

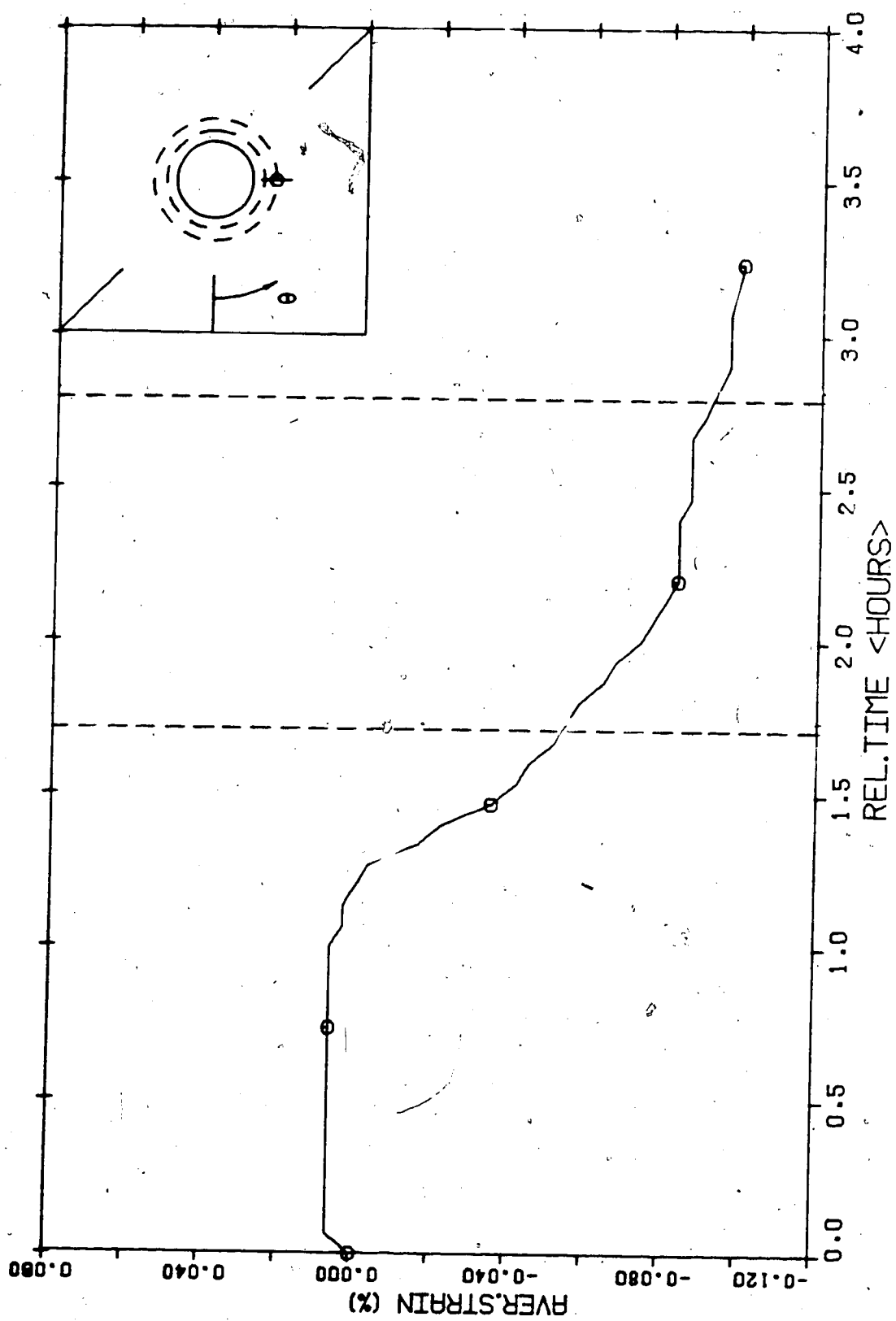


Figure 11.23 Development of Radial Strain - Test MC-7.13
Sta. 131

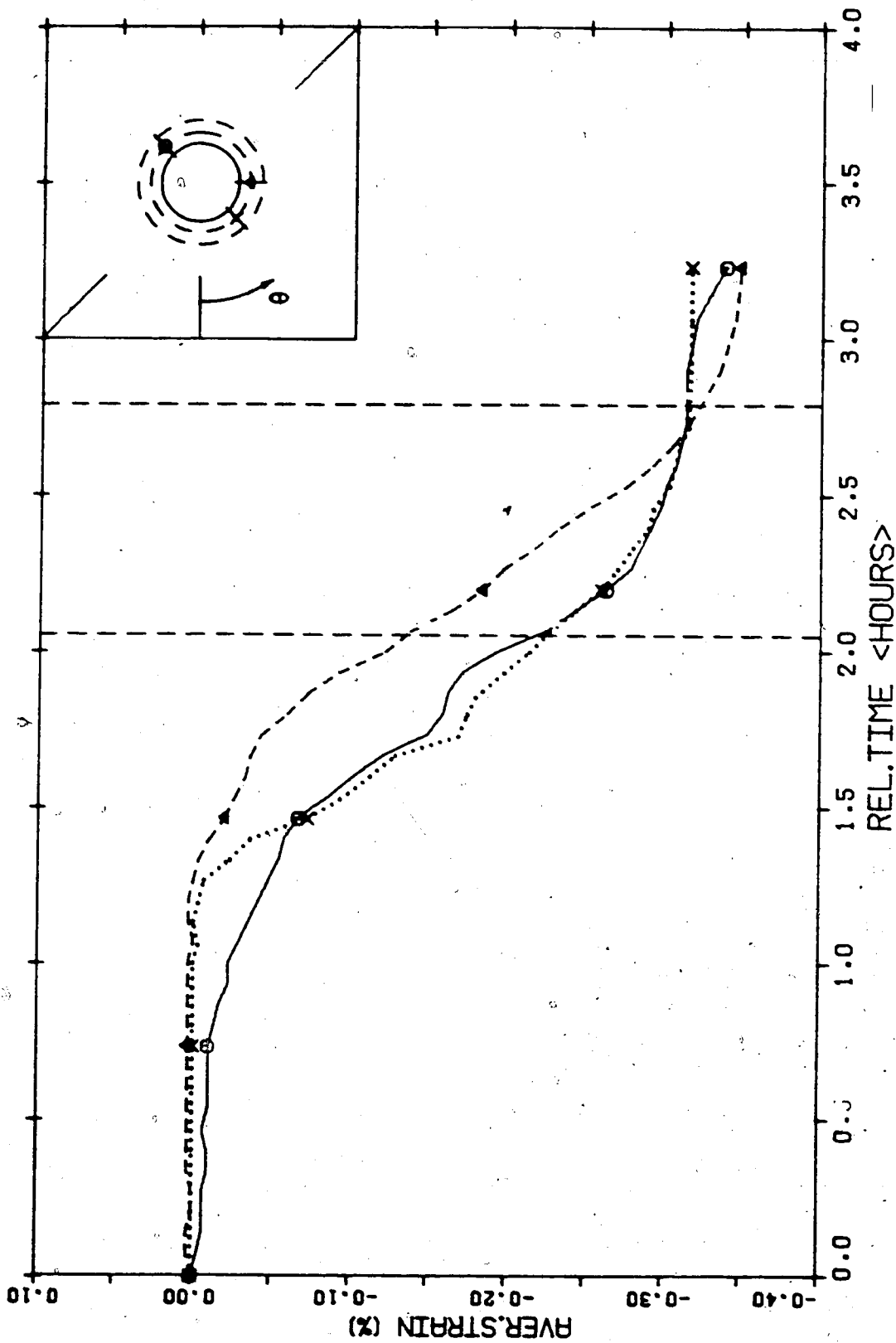


Figure 1.24 Development of Radial Strain - Test MC-7.13
Sta. 156